The use of machine vision to describe and evaluate froth phase behaviour and performance in mineral flotation systems

Sameer Harish Morar

Thesis Presented for the Degree of
DOCTOR OF PHILOSOPHY

Department of Chemical Engineering
UNIVERSITY OF CAPE TOWN

December 2010

Synopsis

Within froth flotation, it is widely acknowledged that froth stability affects flotation performance. As a result, it is expected that through the effective management of froth stability, it would be possible to both control and optimise a flotation cell and bank. However, for this to be possible, the relationships between the operating conditions, froth stability behaviour and flotation performance attributes need to be well understood. In addition, froth stability would need to be measured using a robust method suitable for on-line operation.

Within the literature, no robust methods are available to measure either the concentration of solids on the froth surface, or froth stability in a manner suitable for on-line operation. Thus, two novel non-intrusive machine vision measurements have been developed in this work to quantify these attributes. A measure for the solids loading on the froth surface was developed by measuring the roughness or texture of the segmented images of individual bubbles. A burst rate measurement was developed by identifying bursting bubbles on the froth surface through the comparison of consecutive segmented images. It was also shown that the burst rate could be used to obtain a measure of the air loss rate from the froth surface. The burst rate measurement is considered to relate directly to froth stability. The validity of the machine vision measurements were tested by comparing the effect of an operating condition on the machine vision measurement with the expected effect, based upon previous findings from the literature.

Froth stability encompasses a number of mechanisms, such as bubble coalescence causing an increase in bubble size, loss of interfacial surface area, detachment of particles, release of water and promotion of drainage. It is expected that operating variables will affect each of these factors differently, resulting in complex and inconsistent stability behaviour. Currently, no model exists that adequately describes the three-phase froth stability behaviour in terms of the effect of operating variables and internal mechanisms that occur within a froth.

In order to develop the understanding of the relationship between the effect of operating variables and the internal mechanisms affecting froth stability, real systems are required. Thus, two flotation systems, copper and platinum, were investigated where certain operating vari-

ables (air rate, froth height and frother concentration) were modified in a factorial experimental design to investigate the effect of the operating conditions on froth stability and flotation performance. This work required full circuit surveys across the rougher bank, with metallurgical samples and additional measurements taken at each set of operating conditions. In the copper system, nine different operating conditions were used in duplicate, while in the platinum system, fourteen operating conditions were used with one triplicate and one duplicate condition.

The two flotation systems chosen have different mineral hydrophobicities. The floatable minerals within the copper system were chalcopyrite and bornite, which tend to be highly hydrophobic. The floatable minerals within the platinum system were mostly pentlandite and pyrrhotite with some chalcopyrite, and tend to be of much lower hydrophobicity. The feed rates were 340 tonnes/hr and 4 tonnes/hr in the copper and platinum systems respectively. The head grades were 0.46% copper and 2.8 ppm platinum / 0.14 % nickel in the copper and platinum systems respectively.

Within each of these systems, two flotation rougher cells were chosen to study the change in the concentration of floatable solids within the pulp phase. The concentration of floatable solids available in the pulp phase decreases down the bank due to its removal from the system in the concentrate. The first rougher represented high floatable solids concentrations, while the third rougher represented low floatable solids concentrations.

Due to the difference in operating conditions, the data obtained from the first and third roughers from both the copper and platinum systems were not directly comparable. Thus, linear regression analysis was used to evaluate the relationship between the operating variables and froth surface descriptors and flotation performance factors across the different solids environments, allowing for the outputs from the linear regression analysis to be compared. The values considered, were the significance of the effect of the factors within the regression and the direction of the relationship (positive or negative). While it is widely acknowledged that the flotation process contains mechanisms that result in non-linear behaviour, linear regression was still chosen as an analysis tool, as it was judged robust enough over the range of operating variables tested to determine whether the direction that a factor is changed affects a system consistently.

Two sets of regression analysis were used. In the first, the effect of the operating variables (air rate, froth height and frother concentration) on the physical and dynamic froth stability factors (solids loading, bubble size, burst rate), froth transport rate (froth velocity) and flotation performance (solids recovery rate and concentrate grade) were investigated.

- Increased **air flow rate** was determined to be an important factor that destabilised the froth. This destabilisation was more significant in the first rougher, where higher concentrations of floatable solids were present and was reflected by a decrease in solids loading. This decrease in solids loading was attributed to either a decrease in solids loading on bubbles entering the froth, or an increase in the slurry drainage rate from the froth. The increased slurry drainage rate from the froth may have increased the rate of particle detachment and decreased the rate that detached particles re-attach in the lower levels of the froth. Either of these effects resulted in a reduction in the stability of the froth. The effect that air rate had on froth stability was diminished by a decrease in the concentration of floatable solids.

- The effect of **froth height** on the froth stability depended on the concentration of floatable solids available. At high solids concentrations, increased coalescence occurred when the froth height increased. As the interfacial surface area in the froth decreased from coalescence, the solids loading increased resulting in the armoured bubbles and the stabilisation of the froth closer to the surface, and larger bubble sizes were measured. Conversely, in the presence of a low concentration of floatable solids within the pulp, an increase in froth depth destabilised the froth due to no armouring occurring and increased bursting. As a result, only smaller bubbles were able to remain stable on the froth surface and the maximum height that the froth could attain was reduced. Thus, the two opposing effects observed were dependent on the concentration of floatable solids.

- The stabilising effect of **frother concentration** had only been shown to be significant in the presence of a low concentration of floatable solids within the pulp. However, counter-intuitively, increased frother concentration in the presence of high concentration of floatable solids destabilised the froth. This was attributed to an increase in water content in the lower regions of the froth facilitating more of the unattached floatable solids to drop back into the pulp. This decreased the re-attachment rate of these solids, resulting in froth destabilisation. Thus, the two opposing effects observed were dependent on the concentration of floatable solids.

These findings showed that the nature and concentration of floatable solids dictated the effects that operating variables had on the froth stability. Despite the air rate and froth depth having significant relationships to concentrate grade in the presence of high and low floatable solids conditions respectively, the relationships were not consistent across the changes in operating conditions made. No changes to operating variables were able to consistently affect the solids recovery rate across systems with different floatable solids hydrophobicity and concentration conditions. In addition, the relationship between solids recovery rate was not consistent with

the froth transport rate, as measured by the froth velocity. This finding implies that the machine vision froth surface measurements alone cannot be individually used to relate to flotation performance characteristics within an ore system with varying hydrophobicity and floatable solids concentrations.

The second set of regression analysis used tested the relationship between the measured stability factors (burst rate, solids loading, bubble size and frother concentration) and the froth transport rate (froth velocity) and flotation performance factors (solids recovery and concentrate grade). In contrast to the relationship between the operating variables and flotation performance, the stability factors related more consistently to the solids recovery behaviour. Within the highly hydrophobic system, the bubble size and solids loading strongly influenced the solids recovery, while in the low hydrophobicity system, the burst rate consistently influenced the solids recovery. However, under both these conditions, the effect of floatable solids concentration caused a reverse in the expected trend.

Thus, these results have demonstrated that the use of raw machine vision based froth surface descriptors and/or other measurements to control and optimise a flotation cell, or bank is not possible without the incorporation of an interpretation of froth structure, froth stability and internal froth mechanisms, and their relationships between each other. In addition, the results demonstrate that froth velocity alone cannot be utilised to reliably relate either solids recovery or grade across the range of operating variables investigated.

This research has extended the range of machine vision measurements available to monitor froth flotation processes and increased the understanding of the relationship between physical froth surface descriptors, froth phase stability and flotation performance. The findings show that better understanding of froth phase behaviour is required for the interpretation of the relationships between physical machine vision measurements and flotation performance. Thus, it is recommended that further research be focused on the development of an interpretive model that quantitatively relates machine vision measurements to internal froth phase mechanisms and froth phase performance that can be used for control and optimisation.

Declaration

I hereby certify that the work embodied in this thesis is the result of original research and has not been submitted for another degree at any other university of institution.

Sameer Harish Morar
December 2010

Statement of originality

The outcomes considered as original contributions from this research are:

1. Development of new machine vision measurements to measure solids loading on bubbles on the froth surface and the burst rate of bubbles on the froth surface.
2. Characterisation of the relationship between the novel froth surface descriptors and froth stability behaviour by identifying mechanisms responsible for either increasing or decreasing the solids loading on the froth surface and showing that solids loading and lamella size are the most significant factors affecting burst rate on the froth surface.
3. Identification of mechanisms to interpret the relationship between operating variables and froth surface descriptors that demonstrated the overriding effects of hydrophobic solids, in terms of air rate, froth height and frother concentration.
4. Demonstration of the complex relationship between operating variables and froth stability and the overriding effect of the floatable solids environment present on flotation performance.
5. Produced two data sets with extensive measurements available for further analysis.

Publications

Journal papers

Reddick, J., Hesketh, A., Morar, S., Bradshaw, D., 2009. *An evaluation of factors affecting the robustness of colour measurement and its potential to predict the grade of flotation concentrate.* Minerals Engineering, Vol 22, pp. 64–69

Barbian, N., Cilliers, J.J., Morar, S.H., Bradshaw, D.J., 2007. *Froth imaging, air recovery and bubble loading to describe flotation bank performance.* International Journal of Mineral Processing, Vol 84, pp. 81–88

Conference presentations

Morar, S.H., Bradshaw, D., Harris, M., 2008. *Assessment of stability down a flotation bank.* In: Proceedings of the XXIV International Mineral Processing Congress, Beijing, China.

Morar, S.H., Hatfield, D., Barbian, N., Bradshaw, D., Cilliers, J., Triffett, B., 2006. *A comparison of flotation froth stability measurements and their use in the prediction of concentrate grade.* In: Proceedings of the XXIII International Mineral Processing Congress. Istanbul, Turkey, pp. 937–945

Morar, S.H., Forbes, G., Heinrich, G., Bradshaw, D., King, D., Adair, B., Esdaile, L., 2005. *The use of a colour parameter in a machine vision system, SmartFroth, to evaluate copper flotation performance at Rio Tinto's Kennecott Utah Copper Concentrator.* In: Proceedings of the Centenary of Flotation Symposium. Brisbane, Australia

Patents

de Jager, G., Francis, J.J., Hatfield, D.P., Oostendorp, B.G., Bradshaw, D.J., Morar, S.H., Nicholls, F.C., Forbes, G.R., Heinrich, G.S., Markham, H.W., 2004. *A method and a control system for extracting valuable minerals from mined ore, "SmartFroth"*. Provisional application. Adams & Adams ref: V16402

de Jager, G., Hatfield, D., Bradshaw, D., Francis, J., Morar, S.H., 2005. *A method and a control system for extracting valuable materials from mined ore, "SmartFroth"*. South African Patent 2005/04232.

Acknowledgements

I would like to thank the following for their invaluable assistance, without whom thesis would not have been completed:

- My supervisors, Dee Bradshaw and Martin Harris for their support, guidance, encouragement and advice.
- Ray Shaw, Lucy Esdaile and Rio Tinto for the support of this project and allowing my involvement in the NorthParkes campaign. Rick Dunn and the NorthParkes mine staff for their assistance during the campaign. Jan Cilliers for permission to use this data-set in my research. In addition, the following colleagues who were also involved in the campaign: Brett Triffett, Esther Ventura-Medina, Nicolas Barbian, Katherine Hadler and Teing Lee.
- Sandy Lambert, Neville Plint and Anglo Platinum for the support of this project and the use of their pilot plant and ore for an experimental campaign. Alan Delany, Werner Louw, the Divisional Metallurgical Laboratory staff, Anglo Platinum Development Programme students, Gordon Forbes and Jules Kiteng for their assistance during the campaign. Senmin for providing reagents. Jenny Wiese and the Centre for Minerals Research laboratory staff for assistance in processing my samples.
- In addition to the colleagues mentioned above, the following individuals for their role in this work:
  - Megan Becker for assistance with proof reading.
  - Gerhard de Jager and Fred Nicolls for assistance with the development of machine vision measurements.
  - Tim Napier-Munn for advice on my experimental design.
  - Chris Anderson, Liza Burdukova, Douglas Hatfield, David Hatton and Stephen Neethling for the many illuminating discussions that have influenced my work.
- The South African National Research Foundation and Department of Labour for the award of my scarce-skills scholarship.
- Finally, my family and friends, and in particular, my parents and Catherine for their unwavering support, confidence and encouragement.

Contents

List of Figures

List of Tables

Glossary

Activator

A flotation reagent that enhances the adsorption of collector molecules onto mineral surfaces.

Air loss rate

The rate at which air is lost to the atmosphere from bubbles bursting on the froth surface.

Air/water interface

The interface separating air and water on the surface of a bubble or lamella.

Armouring

A mechanism by which the increase in packing density of solids loaded at the air/water interface on the bubble further stabilises the bubble.

Attached particle

A hydrophobic particle attached to the air/water interface on a bubble or lamella.

Attachment

The process involving a particle colliding and forming a stable aggregate between the particle and bubble or lamella.

Bubble surface noise amplitude

The average amplitude of the greyscale pixel variation in an image of a bubble surface on the froth surface.

Collector

A flotation reagent that selectively changes or enhances a mineral surface's hydrophobicity.

Concentrate

The high value product from a flotation cell, output from the froth phase by overflowing a collection launder.

Depressant

A flotation reagent that selectively aggregates and / or renders minerals non-floatable, so as to decrease the rate at which they become attached to bubbles in the pulp phase.

Detached particle

A floatable particle that has entered the froth phase attached to a bubble, which subsequently becomes detached, and is no longer attached to the air/water interface on a bubble or lamella.

Detachment

The process of an attached particle detaching from the air / water interface, on a bubble or lamella.

Drainage

The flow of water and entrained (non-floating and detached) solids due to gravity through the Plateau borders in the froth phase.

Entrainment

The entrapped, un-attached solids within the froth phase that include both non-floating and detached solids. The entrained solids usually reside in the Plateau borders, or drainage channels within the froth.

Floatability

The propensity for a mineral or particle to form a stable aggregate with a bubble in the pulp phase owing to the hydrophobicity of the minerals on the particle surface.

Floatable particles

Particles that contain enough hydrophobic minerals such that they are able to attach to the air / water interface on a bubble, and survive transport into the froth.

Flotation cell

A continuously stirred tank into which slurry, air and specific reagents are fed to effect the selective concentration of hydrophobic mineral species. Hydrophobic particles attach to bubbles in the pulp phase, and rise into a froth phase, which transports these and entrained particles out of the cell into a collection launder.

Flotation reagent

A chemical that facilitates and enhances the performance of the flotation process.

Foam

A two-phase cellular structure made up from a liquid and air comprising of thin films (lamellae) and drainage channels (Plateau borders), separating the air voids within the structure.

Froth

A three-phase cellular structure made up from a liquid slurry and air, containing particles entrained and attached at the air / water interface and comprising of thin films (lamellae) and drainage channels (Plateau borders), separating the air voids within the structure.

Froth depth

The height between the pulp-froth interface and the froth surface.

Froth phase

The region within a flotation cell in which the froth forms.

Froth stability

The propensity for a froth resist breakdown due to coalescence and bursting on the froth surface owing to processes such as lamella thinning, water drainage and random perturbations.

Froth surface descriptor

A *machine vision* based measurement that characterises a property or aspect of the froth surface, or its appearance.

Frother

A surface active flotation reagent that facilitates the formation and stabilisation of a foam or froth.

Grade

The percentage of a specific mineral or element within a sample from a stream entering or exiting the process.

Highlight

The bright reflection of light in an image, typically saturated owing to the dynamic range of the camera. A highlight is typically present on each bubble in a picture of a well illuminated froth surface.

Image analysis

The analysis of digital images to extract useful information.

Induction time

The time taken between a particle that has collided with a bubble to attach to the bubble.

Lamella

The thin film of liquid that separates two voids within a foam or froth.

Machine vision

The use and application of image analysis to solve a physical problem.

Ore

The extracted rocks from the ground that contain valuable minerals or elements which can be economically extracted using an industrial process.

Plateau border

Channels within the structure of a foam or froth, which connect three lamellae containing liquid or slurry.

Pulp

A relatively homogeneous mixture of fine particles ($<200\mu$m), small ($<$2mm) gas bubbles and a solution consisting of water and flotation reagents.

Pulp phase

The region within a flotation cell in which the pulp exists, below the froth phase.

Recovery

The percentage of a component within the feed to the flotation cell that is reports to the flotation concentrate.

Recovery rate

The mass flow rate of a particular species recovered to the concentrate stream.

Sauter mean bubble diameter

The bubble diameter of a bubble that would have the same average volume to surface area ratio of a distribution of bubbles.

Slurry

A fluidised mixture of liquid and solid particles.

Solids loading

The concentration of solids per unit surface area at the air/water interface on a bubble or lamella.

Superficial gas velocity

The effective velocity of gas through the pulp phase, determined by measuring the volumetric gas flow rate per unit area.

Tails

The low grade slurry stream exiting a flotation cell.

Valuable minerals

Minerals within the ore which have economic importance, around which the process is focused on concentrating or extracting.

Chapter 1.

Introduction

Froth flotation is a three-phase physico-chemical separation process that takes place in two zones, the pulp and the froth. It is widely recognised as a complex process, due to the range of sub-processes and interactions within the system.

In the pulp phase the rate of bubble-particle attachment governs the process. As a result, the number and size of bubbles and particle size, concentration and surface properties are of critical importance. The air rate and frother concentration determine the number and size of bubbles in the pulp. The ore characteristics and grinding environment determine the particle size and surface properties. Flotation reagents, such as collectors, modify the surface properties to increase the selectivity of valuable mineral recovery relative to unwanted gangue recovery.

Particles report to the froth phase by two mechanisms. The first is the selective recovery of hydrophobic particles by true flotation. This occurs as a result of particles colliding and attaching to the surface of bubbles as they rise into the froth phase. The second is unselective recovery by entrainment. Entrainment is the mechanism by which suspended particles within the pulp get trapped within the froth and remain unattached to the air/water interface. It is mainly dependent on particle size, although particle density and shape can also affect the process.

A number of processes occur within the froth that cause or influence the breakdown of the froth. The rate of froth breakdown is often colloquially referred to as the froth stability. The processes related to the froth breakdown also modify the selectivity of mineral recovery in the froth phase. Stable froths promote a high rate of recovery and poor selectivity owing to the recovery of a higher concentration of entrained material. Conversely, unstable froths result

in lower rates of recovery and good selectivity owing to lower transport and higher drainage rates.

Conditions vary in flotation circuits owing to variations within the feed caused by the natural variability of the ore and variability in upstream processes. These variations typically affect attributes such as the mineral liberation, particle hydrophobicity, size distribution and the concentration of valuable and active gangue species within the flotation feed to a particular cell. These variations affect both the pulp and froth phase performance.

The effect of individual attributes on froth stability, such as particle hydrophobicity and surfactant properties, are reasonably well understood. However, the interactions between the particle properties, internal froth mechanisms and their contribution to froth stability and flotation performance have not been clearly established.

Current physical froth stability measures (columns and impedance sensors) are impractical for the purpose of providing a continuous on-line froth stability measurement, owing to their intrusive nature. The non-intrusive nature of machine vision makes it an attractive technology that has the potential to measure key aspects of the froth that relate to flotation performance, such as froth stability. However, current machine vision based stability measurements measure properties of consecutive images such as the correlation or disparity between the two images. These measures are able to robustly measure stability changes in conditions where the froth structure is similar over narrow ranges of conditions. However, they are not robust enough to deal with the effect of changing conditions causing froths that have a significant structural variation.

Machine vision techniques can measure other physical, textural and chromatic attributes of the froth surface (froth surface descriptors). However, froth velocity is the only machine vision measurement used within industrial systems to control the solids recovery rate. Previous authors have empirically linked a wider range of measurements to flotation performance, however, none of these relationships have been shown to be robust over a wide range of operating conditions. This is aggravated by poorly understood relationships between the currently available measurements and processes within the froth. Alternatively, the current measurements may be inappropriate for describing processes occurring within the froth.

Thus, the overall objective of this work was to further develop the understanding of the mechanisms that change froth stability behaviour, and develop more appropriate non-intrusive machine vision measurements that relate to froth behaviour, including stability.

This work investigates the effect of changes in operating variables on these new and previously established machine vision measurements and measured flotation performance at two different bank locations (roughers 1 and 3) for two different flotation systems (copper and platinum). The different bank locations represent changes in floatable solid concentration within the pulp phase, while the different flotation systems represent differing floatable particle hydrophobicity.

Currently, due to a lack of adequate measures and the appropriate understanding of froth stability factors it is not possible to control the process to a specified selectivity or recovery target automatically. The control of the froth phase requires two components. Firstly, an understanding of how the operating conditions affect the behaviour and stability of the froth and their relationship to flotation performance. Secondly, the froth stability needs to be robustly measured using an appropriate technique. This thesis addresses both the development of new measures and the understanding of froth phase mechanisms affecting flotation performance. The outcomes from this work are a vital step towards the development of a robust control system for a flotation cell.

1.1. Scope of this thesis

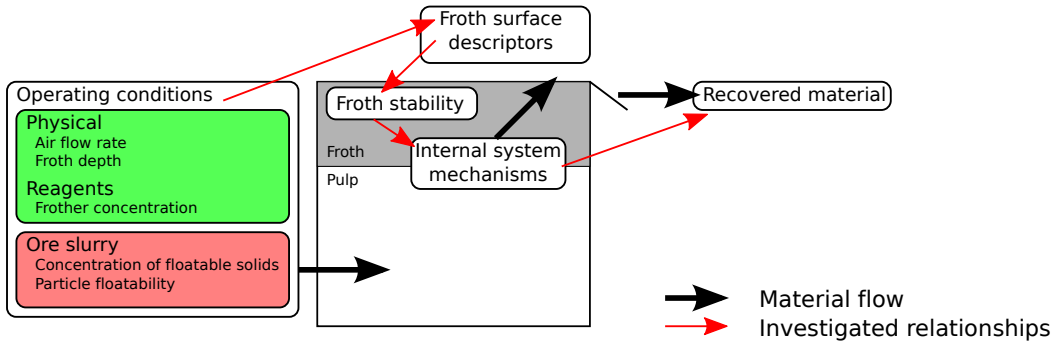

Figure 1.1.: Schematic illustrating the variables investigated in the scope of this thesis.

The scope of this work is schematically represented in figure 1.1. A number of varying inputs enter the flotation system. Typically, variation in the ore slurry results in variations in the internal system mechanisms. The mechanisms affect the recovered material by modifying the froth stability behaviour. To counteract changes in ore slurry affecting the internal froth mechanisms and maintain consistent operation, the relationships between the operating variables and internal system mechanisms need to be known.

The operating conditions in the flotation system considered in this thesis are the air flow rate, froth depth, frother concentration, as well as concentration of floatable solids within the pulp phase, the particle floatability, and within a limited scope, frother type and the presence of an activator. The operating variables investigated relate to those modified in routine flotation cell operation.

Mechanisms internal to the flotation system determine the amount and grade of material recovered to the concentrate (flotation performance). They affect froth stability and result in visual changes to the froth surface. The internal mechanisms considered include the particle attachment rate within the pulp, the entrapment and entrainment of non-floatable material near the pulp-froth interface, the amount of coalescence, liquid drainage and particle detachment and re-attachment occurring within the froth.

Thus, this work investigates the effects that the input operating conditions have on the internal system mechanisms which result in the measured flotation performance and the related changes measured on the froth surface.

The following froth surface descriptors were used: solids loading, bubble burst rate, bubble size and froth velocity towards the launder. These were considered as appropriate indicators of both the physical and dynamic characteristics of froth behaviour.

Thus, this project has the following objectives:

1. To develop machine vision measurements that obtain more appropriate froth surface descriptors which relate to specific physical froth characteristics, such as:

    a) Solids loading

    b) Froth stability

2. To test the sensitivity of machine vision measurements in measuring expected changes on the froth surface from changes in operating variables within a flotation system when the solids environment changes.

3. To determine the extent to which the operating variable effect on the froth surface behaviour and froth stability is consistent across a range of operating conditions within a single flotation cell when the solids environment changes.

4. To investigate the relationship between the froth stability and flotation performance across a range of operating conditions within a single flotation cell when the solids environment changes.

The changes in solids environment considered in this work were floatable particle hydrophobicity, through the use of two different ore systems and floatable solids concentration, through the use of two different cells in a flotation rougher bank.

The operating variables investigated in this work relate to those modified in routine flotation cell operation. Thus, other variables also considered important, such as energy input into the flotation cell, variation in feed rate and pulp properties such as density, particle size distribution, pH and reduction potential (Eh) are outside the scope of investigation.

The key themes within this work revolve around determining the effect that operating variables have on the froth phase and the identification of significant and dominating mechanisms across different operating conditions. This understanding is required before a model of the froth phase can be developed. Thus, the modelling of the froth phase is outside the scope of this thesis. In addition, while a future objective may require the development of a control system, a model of the froth phase would be required to achieve this objective. Thus, the development of a control system is also outside the scope of this thesis.

1.2. Structure and layout of thesis

Chapter 2 details the background to the flotation process and contains a review of work performed with respect to the understanding of the relationship between froth stability and flotation performance and the development and use of machine vision in froth flotation.

Chapter 3 provides a description of the experiments performed in each flotation system (copper and platinum), along with the operating conditions changed and details on the measurements and samples taken.

Chapter 4 describes the development of the two new machine vision measurements proposed within the objectives. This includes the testing of these measurements using the data obtained from the experiments described in chapter 3.

Chapter 5 analyses and discusses the data collected from the systems described in the experimental chapter. The correlation between the froth surface descriptors and expected observations, determined from the literature, was used to test the performance of the froth surface descriptors. The effect of operating conditions on froth stability and flotation performance is investigated. An analysis evaluating the dominant mechanistic effects relating the observed froth stability behaviour to flotation performance is performed. In addition, the suitability and potential for the use of machine vision measurements for flotation control is discussed.

Chapter 6 details key conclusions drawn from this work and makes recommendations for future work.

Chapter 2.

Literature review

To address the objectives set out in chapter 1, it is necessary to review previous research with respect to the relationship of froth stability to flotation performance and the use of machine vision in flotation control systems.

Thus, this chapter addresses the following topics:

- An introduction to froth flotation describing the background of the industrial use of flotation for mineral separation.
- A review of the research into the fundamental mechanistic processes that occur within flotation. Emphasis is placed on studies investigating the effect of solid and solution factors on froth stabilisation within a single cell and down a flotation bank.
- A review of the development and application of machine vision technology to the monitoring and control of froth flotation processes.

2.1. Background to froth flotation

Froth flotation is a physico-chemical separation, or concentration process, used to extract valuable material from unwanted waste material (gangue) or separate valuable minerals from each other. Flotation selectively exploits differences in the surface properties between minerals. The primary property exploited is the hydrophobicity associated with different mineral surfaces.

The differences in properties are only exploitable on exposed mineral surfaces. The ore is ground into fine particles to increase the mineral composition per particle and increase the mineral surface exposure.

2.1.1. Grinding circuit

Typically, a series of crushing devices reduces the particle size of mined ore to produce a suitable feed to the flotation grinding circuit. In the grinding circuit, milling devices break up the particles to a desired particle size distribution. The desired particle size distribution varies across ore type and is dependent on ore mineralogical properties such as hardness and mineral liberation. Typically, milling circuits are operated to produce feed where 80% of the material passes a size below between 50 and 100 μm. The primary purpose of the grinding circuit is to liberate the minerals and provide clean mineral surfaces for the flotation process.

Water is added to the ore in the primary mill to create a slurry. This facilitates the transport of particles around the grinding and flotation circuits.

Grinding circuits often operate as a closed circuit with a classification device recycling over-sized particles back to a grinding device allowing the under-sized particles to proceed to the flotation circuit.

The classification devices most commonly used are hydro-cyclones and wet screens. Hydro-cyclones are advantageous because they allow a higher throughput of slurry, are cheaper and require less maintenance than a screen, however, their separation efficiency is worse than a screen. Figure 2.1 illustrates a simple grinding circuit configuration.

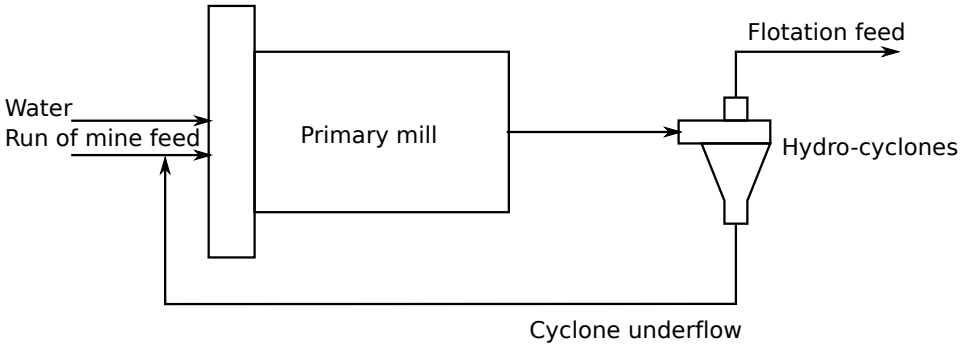

Figure 2.1.: Simple closed grinding circuit featuring a primary mill and hydro-cyclones.

It is not uncommon to have multiple mills, hydro-cyclones and screens set up within a single grinding circuit.

2.1.2. Flotation circuit

Once the slurry exits the grinding circuit, it enters a conditioning tank where added reagents react with the particles within the slurry. After conditioning, the slurry enters the first flotation cell. A flotation cell is an agitated tank, driven by an electric motor, containing an input for air in the form of a sparger and has a baffle configuration to create a specific intensity and distribution of turbulence. A flotation cell has two outputs, a launder for the collection of froth containing valuable minerals and an exit valve for the tail slurry. Within the flotation cell, two physical regions exist; a pulp phase and a froth phase.

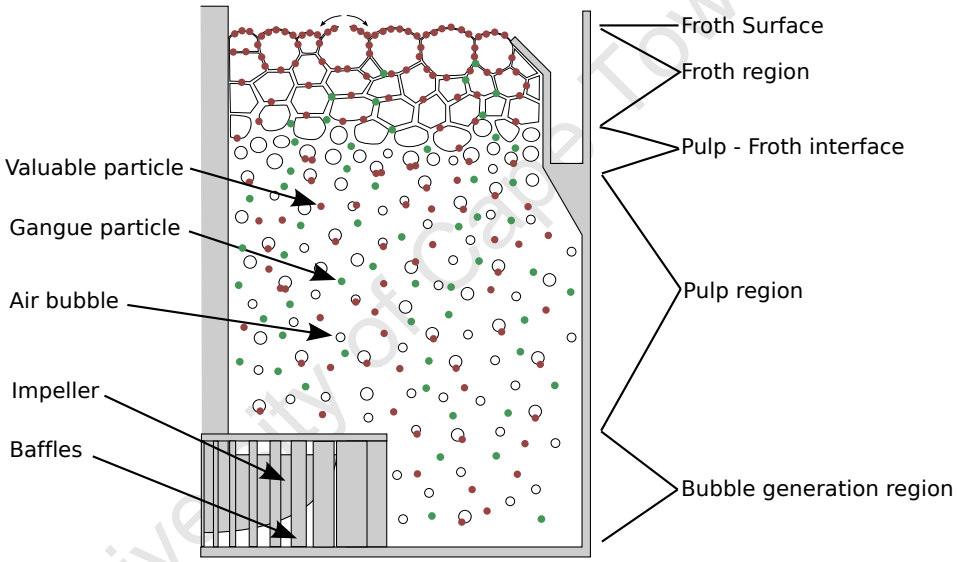

Figure 2.2.: An illustration of a cross-section through a flotation cell, showing the impeller on the left and the launder on the right. Red particles represent floatable hydrophobic, valuable minerals and green particles represent the non-floatable, hydrophilic gangue.

Within the pulp phase, the flotation cell disperses the air effectively via agitation to promote bubble-particle collisions. When a particle with exposed hydrophobic minerals collides with a bubble, it may attach to a bubble and rise through the flotation cell to reach the pulp-froth interface and enter the froth phase.

Due to the presence of frothing reagents (frothers), the air bubbles form a froth layer on top of the pulp. The role of the froth phase is to selectively transport the valuable particles towards and into a collection launder. Bubbles at the pulp-froth interface trap, or entrain, non-floatable gangue into the spaces between the bubbles. The extent to which these particles reach the froth surface and are recovered to the concentrate determines the purity or grade of the concentrate. Figure 2.2 shows a cross-section through a flotation cell that illustrates these regions.

The control of the feed flow rate into and tail flow rate out of the flotation cell maintains a specific froth depth, which is typically measured using a level sensor.

It is generally understood that at shallow froth depths, the recovery of entrained material to the concentrate increases, resulting in lower concentrate grades. In the case of a high froth depth, the entrained material has a greater chance of draining out of the froth, resulting in higher concentrate grades.

The chemical reagents used within the flotation process are of critical importance. They typically manipulate surface properties of particles and create stable bubbles. Four main types of reagents are used, each for a specific purpose, although some reagents may have a dual purpose.

- **Collectors**
  Collectors are surface active chemicals which selectively render the surface of minerals hydrophobic. This enables particles that contain these minerals to attach to bubbles.

  The most widely used collectors in the recovery of sulphide minerals belong to the following general chemical families: monothiophosphates, dithiophosphates, thionocarbamates, thioureas, alkyl-xanthate esters, xanthogen formates, mercaptobenzothiazole and xanthates (Day, 2002).

- **Frothers**
  Frothers, as applied to flotation, are a class of hetero-polar surface active molecules which enable the formation of a wet foam, or, in the presence of solids, froth.

  Many frother types exist, of which the most common can be classified as alcohols, alkoxy-type frothers or polyglycol-type frothers (Laskowski, 1998). Frother manufacturers typically tailor a proprietary blend of different frothers for a particular application.

  Frothers play three important roles within the flotation process:

  – Frothers influence the bubble size distribution in the turbulent region near an impeller or an air sparger. They also prevent existing bubbles from either breaking up into smaller bubbles, or coalescing with each other (Finch and Dobby, 1990).

  – Frothers may interact with collector molecules, both in solution and at the point of bubble-particle collision. A reduction in the necessary induction time for a particle to attach to a bubble has been attributed to this role of frother (Hadler *et al.*, 2005, Leja and Schulman, 1954).

  - Frothers facilitate both the formation and stabilisation of a froth due to their adsorption at the air/water interface. Frothers cause viscous effects that inhibit bubble-bubble contact (Klassen and Makroussov, 1963). Within the froth, these viscous effects retard slurry drainage and thus lamella thinning. This slows down processes such as lamella rupture, bubble coalescence and bubble bursting (Kitchener and Cooper, 1959). Low frother dosages tend to form a froth that is brittle and breaks down quickly, with high amounts of slurry draining out of the froth. In contrast, high frother dosage can result in a stable froth, where the amount of slurry drainage occurring in minimised, resulting in lower concentrate grades due to the increased recovery of entrained material.

- **Activators**
  Under certain conditions, an activator enhances collector adsorption. However, it is of critical importance not to cause inadvertent activation of gangue, as collector adsorption to gangue is detrimental to the process performance.

- **Depressants**
  Within some ores, gangue minerals may be naturally floatable. Depressants selectively aggregate and/or render these minerals non-floatable, so as to prevent them from becoming attached to bubbles within the pulp phase.

Specific reagents are usually chosen based upon the ore type and operational goals. Flotation performance is typically evaluated by the extent to which the separation is complete (recovery) and selective (grade).

Figure 2.3.: Three flotation banks in an industrial flotation plant.

Typically, flotation is performed using flotation banks. These are collections of flotation cells in series that operate to achieve specific goals. Figure 2.3 shows three flotation banks in an industrial plant. Three classes of flotation banks exist; roughers, scavengers and cleaners. Each of these banks operate with a specific objective:

- **Rougher banks**
  Rougher banks operate to maximise the recovery of the floatable material to the concentrate. The concentrate and tails from the rougher bank are usually fed to the cleaner and scavenger banks respectively.

- **Scavenger banks**
  Scavenger banks operate to minimize the amount of valuable material lost to the final tails. The tails from the scavenger bank is usually the final tails, which after thickening is disposed of in a tailings dam.

- **Cleaner banks**
  The concentrate produced from the cleaner banks is usually the final concentrate product. Thus, the cleaner banks operate to achieve a specified grade of valuable material and ensure that the concentration of any undesirable material is below specified maximum acceptable limits. It is not uncommon that multiple cleaner stages are used to meet final grade targets.

Figure 2.4 is a flow sheet that shows a simple flotation circuit configuration.

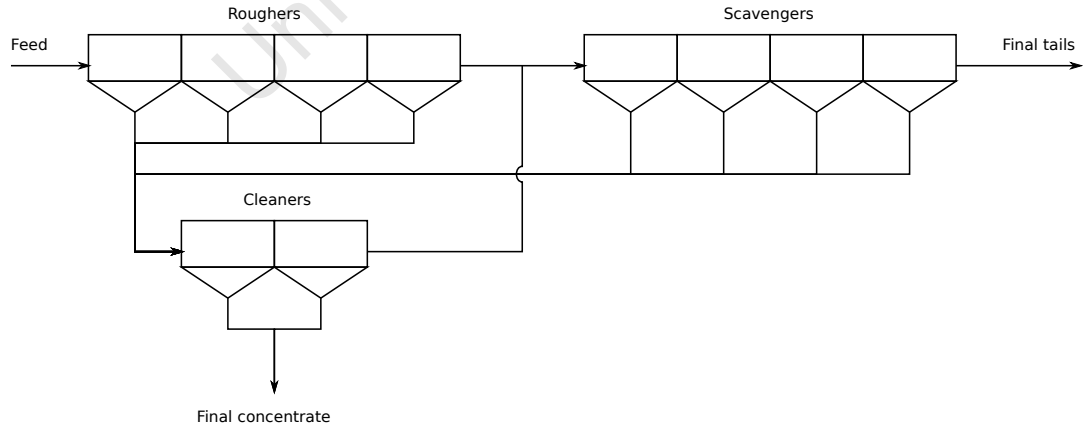

Figure 2.4.: A simple flotation circuit showing rougher, scavenger and cleaner banks.

2.2. Flotation fundamentals

A number of studies performed investigate the fundamental processes that occur within froth flotation. The research described here is split between the pulp and froth phase.

2.2.1. Pulp phase

The kinetic behaviour of the mineral particles in the pulp phase has been studied extensively (Dai *et al.*, 2000). The main kinetic drivers of the attachment of particles to bubbles are ore type, particle size distribution and the number of and size distribution of the bubbles within the pulp.

The processes upstream of flotation, described in section 2.1.1, determine the particle size and concentration entering the flotation circuit. The next section discusses the behaviour of these particles in the pulp phase.

The understanding of processes within the pulp phase is important as the pulp phase feeds the froth phase. Obtaining good performance in the pulp phase is essential to maintaining efficient flotation performance, as a poorly performing pulp phase will result in a decrease in floatable material recovered to the concentrate.

Particle behaviour

Flotation exploits the hydrophobicity of mineral surfaces to achieve an effective separation. Hydrophobicity is typically measured using the contact angle at the point of three phase contact between a mineral surface, water and air. A high contact angle between the water and the mineral surface indicates a low wettability, or high hydrophobicity, whereas a low contact angle indicates a high degree of wettability, or a low hydrophobicity. A mineral particle is floatable if it can successfully attach to an air bubble and rise out of the pulp phase.

By considering that intermolecular attractions independently contribute to surface tension, Fowkes (1964) used the dispersion force contribution to calculate the work of adhesion between phases. This allowed the determination of precise interfacial tensions and contact angles between phases.

Schuhmann (1942) and Sutherland (1948) developed models to determine the flotation rate based upon a collision theory between particles and bubbles. They established that the key

factors influencing flotation rate are the probability of collision between particle and bubble and the probability of adhesion of the particle to the bubble after the collision. This concept was further extended to include a probability that the particle remained attached, as a stable bubble-particle aggregate. Thus, within the pulp, key factors of bubble-particle interaction are the: collision probability, induction time and stability of the attached particle. The induction time is the time taken for a particle that has collided with a bubble to attach to the bubble. Nguyen *et al.* (1998) and Dai *et al.* (2000) performed a comprehensive review of models based upon these concepts.

The collision probability is influenced by two main factors. The first is the number, size and velocity of the bubbles, while the second is the particle size, shape and concentration.

Laskowski (1974) performed a study which demonstrated that under different concentrations of surface active reagents, the induction time required for bubble-particle attachment varied. This finding shows that collectors improve kinetics of the bubble-particle attachment process.

Bradshaw and O'Connor (1996) measured bubble loading as a function of particle size and showed that there was an increase in the number of particles attached per bubble as a function of particle size. Yoon and Luttrell (1989) developed a fundamental collision model, validated within a coal system. Their results agree with the findings of Bradshaw and O'Connor and later work (Phan *et al.*, 2003, Yoon, 2000). Schulze (1977) determined that an upper particle size limit exists, above which floatability does not increase. This is due to a combination of factors, where bubbles rise more slowly due to particle weight and larger particles have a lower attachment stability, which makes them more susceptible to detachment. Thus, an optimum particle size exists with which maximum attachment occurs within the pulp.

Laskowski (1986) showed that more highly hydrophobic particles, modified by changing solution pH, resulted in higher concentrate yields, illustrating the important role that hydrophobicity plays in the attachment and recovery of material. Laskowski *et al.* (1991) performed a thermodynamic study of the energy of attachment between particles and bubbles which explain these results. They showed that more hydrophobic particles have a lower energy barrier to bubble-particle attachment, reducing the induction time for attachment and increasing the attachment stability within the pulp, resulting in a higher inherent floatability. The results of an investigation performed by Koh *et al.* (2009) show that in addition to hydrophobicity, particle shape also plays a role in determining a particle's floatability.

Seaman *et al.* (2005) showed that selective recovery of floatable particles from the pulp into the froth occurs at the pulp-froth interface. Their results, obtained from a number of froth recovery measurement techniques, showed that higher recoveries of finer particles into the

froth occur. This indicates that the energy required for particle detachment increases with particle size.

The extensive research performed on particle recovery in the pulp indicates that the measurement of solids recovered in the pulp, or entering the froth is important in evaluating the pulp phase performance. Thus, researchers have developed devices to measure solids loading in the pulp phase.

In laboratory systems, Hallimond tubes were classically used to perform particle floatability studies. However, Bradshaw and O'Connor (1996) developed a more reliable laboratory based device, the CUT micro-flotation cell, to measure the particle floatability and bubble loading under different conditions.

In industrial systems, Seaman *et al.* (2004) and Yianatos *et al.* (2008) developed devices to measure the concentration and type of solid particles attached to bubbles at any point within the pulp phase. This measurement is important as it decouples the mass transfer within flotation between the pulp and froth phases. This enables the measurement of froth recovery and provides further insight into the kinetic behaviour of particle attachment within the pulp phase.

Currently, the instruments developed for use in industrial cells are at a 'proof of concept' state and show varying degrees of success at obtaining reliable in-pulp bubble loading measurements.

Based upon the findings from the work reviewed, the behavior of particles within the pulp is such that the size of both particles and bubbles influence the probability of a bubble-particle collision. The hydrophobicity of the particle influences the time taken for a stable bubble-particle aggregate to form. The likelihood that the aggregate will remain stable and rise into the froth is dependent on both the hydrophobicity and size of the particle.

Despite the significant progress made towards measuring the type and quantity of attached particles entering the froth phase within an industrial cell, to date, no commercially available instruments are available that perform this measurement reliably.

Bubble formation and behaviour in the pulp

The bubbles generated within the flotation cell are dependent on air flow rate, surfactant concentration, slurry characteristics, physical cell geometry (sparger, impeller, baffle configuration, etc.) and energy input. The formation and behaviour of bubbles within the pulp is

important, as the number and size of the bubbles within the pulp affect the probability of bubble-particle collision.

Previously, the main factor determining bubble size considered was surface tension. However, Sweet *et al.* (1997) showed that significant variation in bubble size occurred over an insignificant change in surface tension. Subsequently, Comley (2001) and Grau and Laskowski (2006) show that the dynamics of frother adsorption control pulp bubble size.

Laskowski *et al.* (2003) showed that a critical coalescence concentration (CCC) of frother exists, above which, no further coalescence between bubbles in the generation zone occurs. This is of particular significance, since above this frother concentration, the pulp bubble size distribution in the system is most consistent and at its smallest. Frother type and system geometry determine the minimum bubble size, however, gas rate does vary bubble size (Nesset *et al.*, 2005). The CCC of frother has been shown to be system independent. Currently, while it is clear that the frother prevents further break up and coalescence of the generated bubbles, the fundamental explanation for this observation is not well understood.

The velocity at which bubbles rise has also been the subject of much study. This is important in flotation, as the behaviour of bubbles rising within the pulp influences the gas holdup and stability of attached particles within a flotation cell (Fuerstenau and Wayman, 1958). The gas holdup influences the amount of collision between bubbles and particles within the pulp phase. Models proposed by Levich (1962), Sam *et al.* (1996) and Zhang and Fan (2003) attempt to explain the bubble rise velocity, however, these models do not adequately explain the effect of frother on the bubble rise velocity (Navarra *et al.*, 2009).

Yoon and Luttrell (1989) developed a collision model which showed that the probability of collision between bubbles and particles decreases as bubble size increases, validated by collecting particles within a coal system.

The bubble size and superficial gas velocity are parameters used to calculate the bubble surface area flux (Finch and Dobby, 1990). The bubble surface area flux is inversely proportional to the bubble size. Gorain *et al.* (1997) showed that the bubble surface area flux is linearly related to the overall (pulp) flotation rate constant.

Nesset *et al.* (2005) and Cappuccitti and Nesset (2009) performed extensive surveys to characterise the effect of operating conditions on gas dispersion in flotation cells across a number of industrial flotation applications. Their findings related changes in the bubble size distribution to the concentration of frother and have shown that both bubble size and bubble surface area

flux increases with superficial gas velocity. They also determine a relationship between gas holdup and two-phase froth height across a number of different frothers.

Based upon this research, the measurement of the hydrodynamic properties of the pulp phase is important to characterise pulp phase performance. As a result, a number of researchers have developed devices to measure the superficial gas velocity, gas holdup and bubble size distribution within the pulp phase in flotation cells.

Gomez *et al.* (2003) developed a gas holdup sensor for flotation systems based on the conductivity difference between the slurry and pulp phase. This device consists of a open tube that measures the pulp phase conductivity and a siphon tube, through which no bubbles are able to enter, which measures the slurry conductivity. The difference between the conductivity measurements relates to the gas holdup (Fan, 1989).

Gorain *et al.* (1996) developed a superficial gas velocity measurement device. This device consisted of a perspex tube, filled up with water and closed off to the atmosphere. The superficial gas velocity is measured by inserting the device into the pulp phase and measuring the rate at which the water level drops, due to the collected air rising up from the pulp phase. Torrealba-Vargas *et al.* (2004) have developed an on-line, continuous instrument, based upon the above principles, but measuring the air rate through the use of a pressure sensor.

Randall *et al.* (1989) developed a bubble sizing instrument that measured the length and velocity of bubbles captured into a capillary tube using an optical detector. This method works well in both laboratory and industrial systems, despite some bias in the fine and coarse sizes, which has also been observed in commercial apparatus presently used. However this method is less practical in industrial systems. Grau and Heiskanen (2002) and Hernandez-Aguilar and Finch (2005) developed instruments based upon the capture of bubbles within the pulp and used image analysis to determine their size as the bubbles flow past a transparent viewing plate. The device developed by Hernandez-Aguilar and Finch (2005) utilized an inclined viewing plate, while the other did not.

A signals processing company, StoneThree, has developed an industrialised bubble sizing instrument and superficial gas velocity measurement device (Taute and Mc Clelland, 2006), based upon principles from the devices developed by Gorain *et al.* (1996), Grau and Heiskanen (2002) and Hernandez-Aguilar and Finch (2005). This instrument, was used to collect data for this thesis and is described in more detail in section 3.2.

Based upon the findings from the work reviewed, bubble generation is a complex process which is poorly understood. However, due to the importance of bubble size within the process,

gas dispersion within a flotation cell has been extensively studied. Conditions where either smaller bubbles are formed, or a large gas holdup occurs tend to result in more bubble-particle collisions and an enhanced flotation rate.

The concentration of surface-active agents (frothers) reduces the generated bubbles size to a minimum at the CCC, above which no further bubble size reduction takes place.

2.2.2. Froth phase

The froth phase consists of a foam like structure with solid particles attached at the air/solution interface and entrained within the solution.

The froth phase performance is generally attributed to the effect of the froth stability. This encompasses the behaviour of the froth with respect to bubble coalescence and its ability to transport solid and liquid to the launder.

The understanding of the froth phase within flotation is important, owing to the role that froth stability has on froth phase performance. Furthermore, active management of the froth phase has the potential to control and optimise the flotation performance.

Froth structure

Bubbles enter the froth at the base of the froth phase and are either spherical, or slightly deformed. The extent of deformation depends on the size of the bubble and surface tension at the air/solution interface. Generally, large bubbles ($> 1.0\ mm$) deform readily, while smaller bubbles are able to retain a spherical shape.

The bubbles at the pulp-froth interface generally pack using optimal packing, such as hexagonal close packing when the bubbles are of similar sizes in mono-disperse systems. As layers of bubbles accumulate, water drains from between the bubbles and polyhedral structures develop.

The slurry drainage from the froth occurs due to gravitational and viscous dissipation forces opposing capillary forces and causes thin films to form between bubbles. Channels called Plateau borders connect the thin films. A single Plateau border connects three films and four adjacent Plateau borders connect at a vertex. Further development of the froth takes place due to energy minimisation at the air/solution interface, resulting in the minimisation of the size of the thin films brought about from the surface tension.

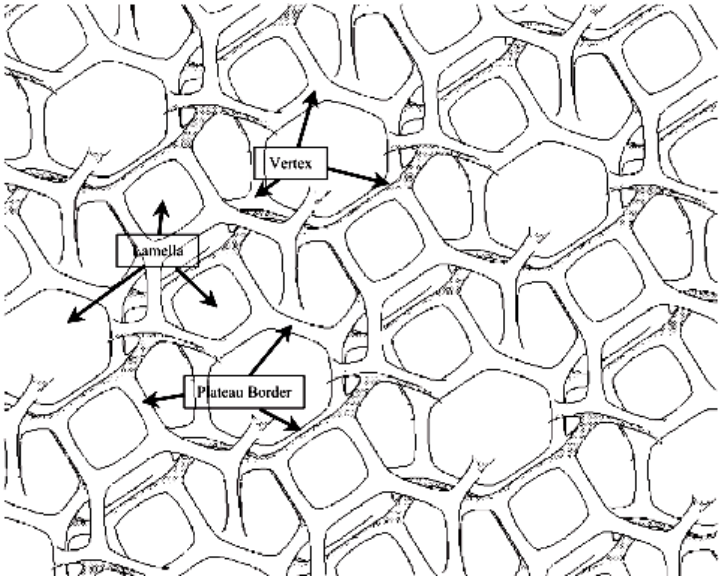

Figure 2.5.: A portion of Kelvin foam from Neethling and Cilliers (2003), illustrating froth structural components, such as lamellae, Plateau borders and vertices.

The form of the resulting polyhedral structure, as proposed by Lord Kelvin, consists of packed tetradecahedra (Figure 2.5). Weaire and Phelan (1994) more recently showed that a structure of alternating dodecahedra and tetradecahedra, is more efficient and optimal when packing bubbles of equal volume.

Energy minimisation and random disturbances brought upon by the interactions of solid particles and solution chemistry may cause film rupture between two polyhedral bubble structures to occur. This results in the joining of the two bubbles (coalescence) to create a single larger bubble. Factors affecting coalescence and thus froth stability are further discussed.

Froth stability

Froth stability affects both the flotation recovery and selectivity. Stable froths tend to entrain a significant concentration of gangue material, which sometimes causes a drop in concentrate grade. Conversely, less stable froths tend to break down and cause the entrained material to drain out of the froth, increasing the grade, but in doing so, decreasing the froth recovery. Thus, froth stability is a key parameter that influences flotation performance (Hatfield, 2006, Subrahmanyam and Forssberg, 1988, Ventura-Medina *et al.*, 2003). A flotation froth, described as meta-stable (Harris, 1982), needs sufficient robustness to support particles, survive transport to the launder and break down easily.

Froth stability is generally influenced by two factors; the attached solid particles on the froth bubbles and the solution chemistry. A number of studies performed quantify the effect of each of these factors on froth stability separately; however, little work performed investigates the interaction of these effects.

The nature of the research performed on froth stability is on two phase foams (in the absence of solid particles) and three-phases froths (with solid particles present), as described in the next sections.

Two-phase foam stability

The mechanisms relating to froth stability are inadequately understood (Bikerman, 1973, Kitchener and Cooper, 1959). A number of interactions exist which tend to disrupt foams and increase the rate of film failure, potentially leading to the foam's collapse. These include liquid drainage, bubble motion, bubble deformation and differential pressure between bubbles. The significance of these interactions depend on the properties of the solution and the physical conditions under which the foam forms.

Bikerman (1973) has reviewed a number of measurements proposed to measure foam stability. Malysa *et al.* (1981) developed a foamability measurement called retention time (rt). The foam retention time is a static column measurement based upon the establishment of an equilibrium foam. A constant air rate (u_g) feeds the column which results in an equilibrium foam that occupies a measured volume (V_g). The retention time is the gradient of the relationship between the volume of the foam and the air rate feeding the foam, as shown in figure 2.6.

$$rt = \frac{\Delta V_g}{\Delta u_g} \tag{2.1}$$

Studies utilising this methodology have established that the observed behaviour with respect to retention time is similar to that shown in figure 2.6 across a number of different surfactant types. Typically, the gas rate for a given surfactant concentration (C) determines the volume of the foam and an increase in concentration tends to result in the foam occupying a larger volume.

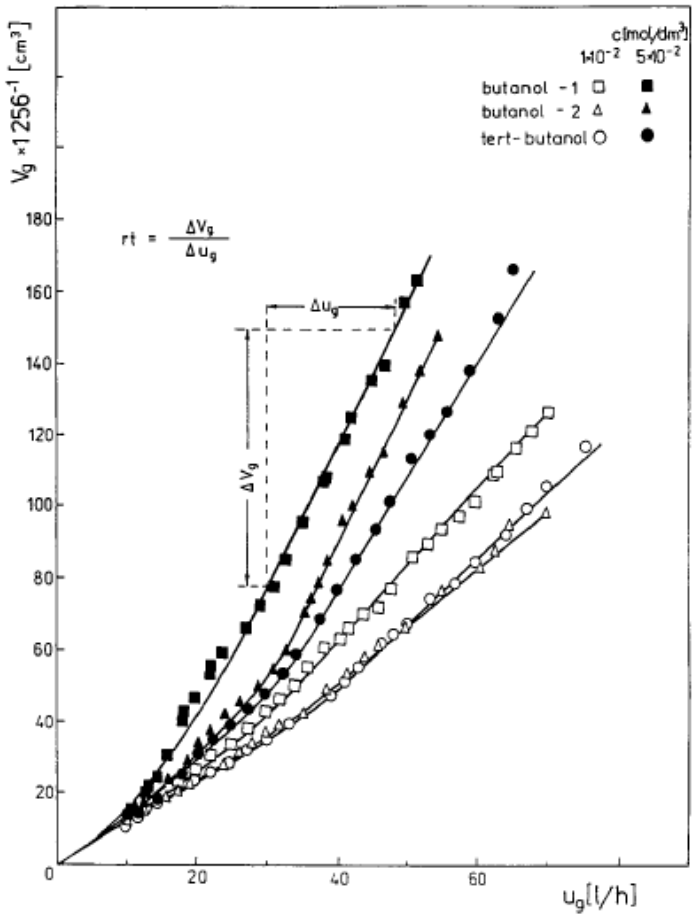

Figure 2.6.: Dependence of the total gas volume (V_g) in the system (solution + foam) on the gas flow (u_g) for aqueous solutions of Butanol-1, Butanol-2 and *tert*-Butanol (Jachimska *et al.*, 1995).

Figure 2.7 shows the dependence of frother concentration on the foam retention time. It is evident from figure 2.7 that retention time typically increases with surfactant concentration and approaches a constant value at higher levels of surfactant concentration.

A dynamic foamability index (DFI), was also proposed by Malysa *et al.* (1981, 1978), which relates the above-mentioned change of retention time with surfactant concentration, as shown in figure 2.7. The DFI is the gradient of the retention time versus surfactant concentration where the concentration is close to zero.

$$DFI = \left(\frac{\delta rt}{\delta C}\right)_{C \to 0} \tag{2.2}$$

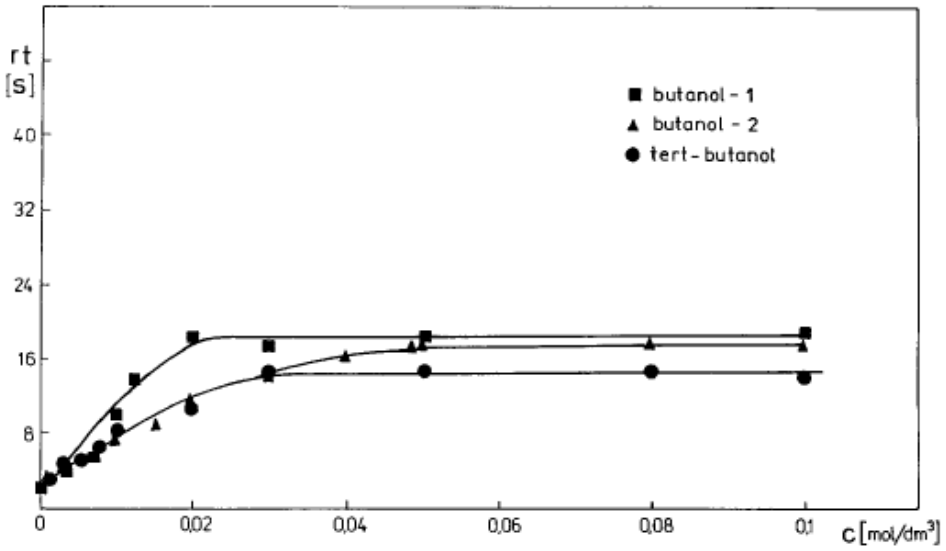

Figure 2.7.: Dependence of the retention time (rt) on the concentration (C) of Butanol-1, Butanol-2 and *tert*-Butanol (Jachimska *et al.*, 1995).

The net effect of the surfactant molecules at the air/water interface is to lower the surface tension (Kitchener and Cooper, 1959), however, evidence has shown that significant DFI change occurs at concentrations where the surface tension does not decrease significantly (Sweet *et al.*, 1997). A mechanism that explains this effect is that frothers restrict the motion of water molecules and add drag at the interface because of weak hydrogen bonding forces which results in the impeding of slurry drainage within the froth phase (Gelinas *et al.*, 2005).

Frothers have typically been described qualitatively as 'powerful' or 'selective'. Laskowski *et al.* (2003) proposed the use of a comparison between the CCC and DFI to quantitatively classify frothers in terms of their strength and selectivity. In addition, Melo and Laskowski (2005) showed that the flotation rate constant for the recovery of water correlates well with CCC and DFI data. Cappuccitti and Nesset (2009) developed an alternative method to classify the strength of frothers based upon the relationship between the equilibrium two-phase foam height and the gas holdup in the pulp. This approach attempts to distinguish pulp phase (gas holdup) from froth phase (froth height) effects of frother, which the other measures combine.

Models developed also show that is possible to characterise the mechanisms relating to the break down of foams, such as fluid viscosity, bubble motion, bubble deformation and differential pressure between bubbles and predict parameters such as foam rise profiles, liquid content profiles and slurry drainage rates (Neethling and Cilliers, 2003, Neethling *et al.*, 2003, Stevenson, 2007).

Three-phase foam (froth) stability

In addition to surfactants within the solution, solid particles also affect the froth stability characteristics within a froth (three-phase foam). The effects of attached particles on froth stability are well known, but not well understood. Particle hydrophobicity, state of aggregation, bubble loading, particle size and shape are all known to affect froth stability.

A number of authors show that increasing the hydrophobicity of valuable particles increases the stabilising effect of particles on the froth. However, once a 'critical' hydrophobicity is reached, highly hydrophobic particles start to destabilise the froth (Ata *et al.*, 2003, Gaudin, 1957, Johansson and Pugh, 1992, Schwarz, 2004, Schwarz and Grano, 2005). This mechanism occurs owing to different particle surface properties, such as roughness or homogeneity (Koh *et al.*, 2009) and from film effects, such as film thickness or the Marangoni effect (Pugh, 1996).

Lamella coverage, or bubble loading, increases froth stability due to the increased viscosity of the bubble film to form a tightly bound 'armoured' hydrophobic layer which impedes liquid drainage (Hatfield, 2006, Pugh, 1996, Subrahmanyam and Forssberg, 1988).

Dippenaar (1982a,b) and Aveyard *et al.* (1994) showed that hydrophobicity and lamella coverage interact such that particles of similar hydrophobicity have different effects on froth stability depending on the extent of coverage of the bubble surface.

Despite a number of laboratory studies characterising the particle effect on froth stability, little work performed investigates the effect of operating variables such as drivers of froth stability.

Barbian *et al.* (2005) performed an experiment to determine the froth surface rise rate as a measure of froth stability within a three-phase froth flotation system. They used a square column (0.3×0.3 m) placed in the flotation cell such that the bottom of the column reached the pulp phase. The froth rose within the column until it reached a maximum 'equilibrium' height (H_{max}), while its rise rate was recorded.

Figure 2.8 shows the froth volume at 'equilibrium' with froth height at three air rates and two different frother concentrations. This plot is analogous to that shown in figure 2.6, determined by Malysa *et al.* (1981) for a two-phase foam.

Figure 2.8 shows that as the air rate increases, froth equilibrium height reaches a maximum, after which a further increase in the air rate destabilises the froth, resulting in a lower maximum 'equilibrium' height. Further work by Hadler and Cilliers (2009) equated this peak in equilibrium froth height to froth stability. They related the peak to a condition under which improved valuable material recovery and grade occurred.

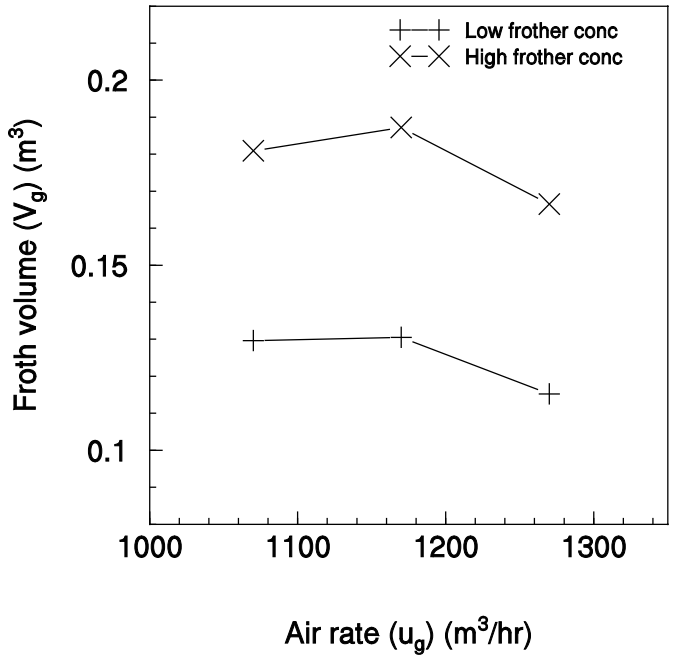

Figure 2.8.: Dependence of the total froth volume (solution, solids + air) on the gas flow (u_g) in a copper flotation system. Data obtained from Barbian *et al.* (2005).

Aktas *et al.* (2008) used the dynamic stability measurement developed by Barbian *et al.* (2005) to investigate the effect of grinding conditions and conditioning time on froth stability. Their results showed that finer particles resulted in higher froth stability and an increase in the conditioning time caused a decrease in the froth stability. The conditioning time result was attributed to an effect of collector adsorption onto the sulphide minerals. As time increased, the collector adsorbed onto low grade, low hydrophobicity material, which when floated resulted in froth destabilisation.

Zanin *et al.* (2009) performed a study on two copper plants, where they used a column based device to measure the in-situ froth half-life. When inserted into a flotation cell, the froth developed until it reached an equilibrium height. The froth half-life was determined from the froth collapse rate which was measured after closing a valve at the base of the column. In addition to the measurement of the froth half-life, in one of their systems they measured the frother deportment down the bank. Their results showed a decrease of 9 % in frother concentration within the pulp phase down the bank. They fitted a semi-empirical model relating froth half-life and bubble size to the concentration of hydrophobic solids present within the froth. Their findings illustrated the important role that solids play in froth stabilisation and showed that froth recovery correlated to froth stability.

Based upon results from research into the stability behaviour of flotation froths, it is clear that the solid particles affect froth stability more strongly than the solution factors. In addition, froth stability encompasses a number of mechanisms, such as the increase of bubble size, loss of surface area, detachment of particles and release of water promoting drainage. A number of these and potentially other factors may interfere with the solids particles available and thus lead to complex stability behaviour across different operating conditions. As a result, a robust froth model has not been developed thus far.

It has been conclusively shown within the literature that froth stability affects the froth phase flotation performance. Therefore, a number of froth stability measurement techniques have been developed.

Bikerman (1973) proposed a simple, dynamic method to determine stability of two-phase foams using the rise rate of a foam within an open column. Barbian *et al.* (2005) adapted Bikerman's method to mineral flotation froths. The main difference between Barbian *et al.* and Bikerman's methods is that the equilibrium height of two-phase foams increases when air rate increases. However, the equilibrium height of a flotation froth increases and then decreases as air rate increases.

Measurements are taken by inserting a column into a flotation cell, such that the base of the column is located below the pulp-froth interface. The rise rate is measured and fitted to the following expression by observing the motion of the froth surface within the column. The maximum height that the froth reaches and equilibrates at (H_{max}) is measured, while τ is fitted.

$$H(t) = H_{max} \cdot \left(1 - e^{\frac{-t}{\tau}}\right) \tag{2.3}$$

A stable fraction (β) can be determined as a function of height using the rise velocity of the froth surface, where A is the column cross-sectional area and Q is the air flow rate into the cell.

$$\beta(H) = \frac{\delta H(t)}{\delta t}\frac{A}{Q} = \frac{(H_{max} - H(t))}{\tau}\frac{A}{Q} \tag{2.4}$$

The mechanism driving this column based method is the air loss on the froth surface. As the air loss on the froth surface increases, the rise rate of the froth decreases until the amount of air entering the column is equal to the amount of air exiting the froth at the froth surface. Froth height stabilises at its maximum height at this point.

Zanin *et al.* (2009) also developed a column based measure for determining froth stability, however, their approach measures the break down rate of a developed froth to determine its half-life.

Hu *et al.* (2009) developed a froth stability measurement by measuring the electrical impedance spectrum between two electrodes to obtain a stability index. The results from a laboratory based study showed an inverse relationship between the stability index and product yield.

Another approach to stability measurement, proposed by Ventura-Medina *et al.* (2003), measures the fraction of air lost on the froth surface. This method, described in the next section, relates to froth transport more directly as a flotation system consists of an expanding froth.

In addition, Hyotyniemi *et al.* (2000) and Hatfield (2006) developed machine vision based stability measurements, described in more detail in section 2.3.1 and in appendix C.2.3.

A number of froth stability measurement devices have been proposed. However, most of these measurements are intrusive and thus unsuitable for prolonged industrial use owing to the abrasive environment within a flotation cell. The exception are the machine vision measurements, discussed further in section 2.3.2.

Particle behaviour

Based upon the research performed on the factors affecting froth stability, it is clear that the particles play a dominating role. However, additional complexity arises given that particles within a froth are mobile and the distribution of attached particles changes due to processes such as particle attachment and detachment in the froth.

Results from a study performed by Falutsu and Dobby (1989) indicated that froth recovery was not strongly froth dependent, which suggested that particle re-attachment or negligible detachment occurs within the froth. These observations are also consistent with the view that detachment of particles occurs at the pulp-froth interface. van Deventer *et al.* (2004), by developing a model for the percentage of apparent detached material showed that the pulp-froth interface plays a significant role in the upgrading action of flotation. Seaman *et al.* (2005) showed that the transport of material across this region is selective.

However, the detachment of particles is not only limited to the region of the pulp-froth interface. Ata (2009) has shown that particle detachment occurs between two coalescing bubbles. Factors that affected the rate of detachment were particle size and collector concentration. The detachment of particles was attributed to the kinetic energy from lamella oscillations on the resultant bubbles transferring to the particle and overcoming the inertia and energy of attachment between the particle and the interface. These oscillations are likely dampened in the presence of frother. Honaker and Ozsever (2003) and Honaker *et al.* (2006) have performed studies that further suggest that detachment from coalescence within the froth occurs selectively, with the less hydrophobic particles detaching more readily.

Thus, based upon the observations of detachment occurring within the bulk of the froth phase, to account for the observations made by Falutsu and Dobby, attachment or re-attachment of particles occurs in froth phase.

Ross (1997) proposed a model to describe the attachment of hydrophobic draining particles to rising bubbles in a flotation froth. His model predicts that higher rates of attachment occurs in deep froths with low solids loadings and under pulp conditions where the gas holdup is high. Neethling and Cilliers (2002) proposed that the rate of solids re-attachment within a froth is low, as the air/water interfacial area in the Plateau borders is small and likely to be saturated.

Thus, particle detachment must occur both at the pulp-froth interface and through the froth phase, in varying proportions. In addition, authors have proposed that a low amount of re-attachment occurs under conditions where the solids loading is low. However, the loading on bubbles entering the froth is low and increases through the froth phase. Therefore, particle re-attachment may occur at high rates in the lower regions of the froth.

Froth transport

The flux of bubbles and attached particles flowing through the pulp 'feeds' the froth at the pulp-froth interface. As discussed previously, cell design and operating conditions such as frother concentration and air flow rate into the cell influence the bubble surface area flux. Particle floatability and flotation rate constant (dependent on the bubble surface area flux) determine the attached particle flux entering the froth.

Of critical importance, however, is the ability of the froth to transport the minerals through the froth phase towards the froth surface and over the launder. This 'feed' to the froth provides the driving force for the expansive transport of froth from the pulp-froth interface to the laun-

der. A stable froth is efficiently transported; and as the stability decreases, the transport rate decreases.

An important contribution to the froth transport is the bubble surface area flux recovered to the concentrate. This factor is strongly influenced by the size of bubbles on the froth surface and the rate at which they travel to the launder.

The rate at which the froth travels to the launder is influenced by the the amount of air recovered over the launder, or not lost by bursting at the froth surface, relative to the amount of air fed into the cell. The air recovery is thus related to froth recovery and is a function of operating conditions such as air flow into the cell, froth depth and both solution and solid froth stability factors.

Murphy *et al.* (1996) developed a numerical model of bubble trajectories, by developing stream lines of bubble flow through froth. Their results illustrate the effect of air recovery on the froth surface velocity profile, where a low air recovery results in a low velocity profile and a high air recovery with a velocity profile where bubbles far from the launder have a high velocity in the direction of the launder. It is worth noting, that within the machine vision literature, no work performed shows a measured velocity profile on the froth surface. Rather, authors have focused on an average velocity of the froth near the launder (Zheng *et al.*, 2004, Zheng and Knopjes, 2004).

The air recovery can be determined by measuring the volume of the froth overflowing the launder using the height of the froth at the weir and measuring the froth velocity using image processing (Ventura-Medina *et al.*, 2003, Woodburn *et al.*, 1994). This method works well for systems where the flow over the weir is consistent, as the height of the froth measurement can be subject to a large variation in a low mass-pull, surging system.

Froth transport, however, can be considered as an extension to froth stability, as at the extremes, froth transport is entirely dependent on froth stability. In a highly unstable froth, where all of the air entering the froth escapes to the atmosphere, the froth will not move towards the launder. In the opposite case, where no air escapes to the atmosphere, the air rate entering the froth phase defines the froth transport rate. However, in the intermediate region, the amount of air lost to the atmosphere due to bubble bursting will relate to the froth transport rate, however, the froth transport rate is an aggregate of the entire froth stability across the flotation cell. Thus, froth transport is not necessarily sensitive to reflect a wide range in froth stability behaviour.

Froth recovery

The primary function of the froth phase is to selectively recover solid material from the pulp to the concentrate. Material recovered to the concentrate occurs by two mechanisms; true flotation and entrainment.

Wilson and Stratton-Crawley (1991) and Finch and Dobby (1990) define froth recovery as the fraction of solids entering the froth attached to bubbles that get recovered to the concentrate. Froth recovery is useful for modelling and evaluating froth phase performance, as it represents a first order kinetic rate, separating the froth and collection zone.

The material recovered by true flotation enters the froth attached to bubbles and is then carried up towards the top of the froth. A proportion of the attached material that enters the froth detaches through its transport to the concentrate. Some of this material drops out of the froth due to slurry drainage, while the remainder is either re-attached to the air/water interface or gets recovered within the entrained material (Honaker and Ozsever, 2003, Honaker *et al.*, 2006, Seaman *et al.*, 2006).

Material recovered by entrainment is material that has non-selectively entered the froth with the water. Estimation of the entrained material recovered is widely established (Johnson *et al.*, 1974, Savassi *et al.*, 1998). Particle size determines the entrainability of material and the amount of entrained material recovered to the concentrate is closely related to the amount of water recovered to the concentrate.

It is possible to determine the proportion of material recovered by true flotation to the concentrate by discounting the entrained proportion of the concentrate stream. However, it is difficult and non-trivial to determine the amount of solids entering the froth by true flotation (Seaman *et al.*, 2004, Yianatos *et al.*, 2008), as discussed in section 2.2.1. Thus, indirect techniques are able to determine froth recovery (Alexander *et al.*, 2003, Feteris *et al.*, 1987, Savassi *et al.*, 1997, Vera *et al.*, 1999). However, none of these methods are practical or suitable to determine a measure for froth recovery during routine operation.

2.3. The use of machine vision in flotation

Machine vision has been long considered as a technology that can assist flotation control and optimisation, as it is non-intrusive and can determine high frequency measurements. The underlying assumption is that given that operators are able to judge flotation performance vi-

sually, machine vision can augment or remove the 'human element' associated with a flotation operator's judgement, which is subjective, and inconsistent across different individuals. In addition, operators are unable to consistently monitor all of the flotation cells within an industrial plant.

2.3.1. Algorithm development

The fields of image analysis and machine vision are relatively new. The application of this technology has been dependent upon the increase in processing power of personal computers.

The field of image analysis is the use of computer algorithms to extract information out of computer images. A number of these algorithms have become standard and are available as components within different image processing applications and platforms.

Machine vision, however, is the use of image analysis to solve a physical problem. Machine vision is a diverse field, with many applications in many industries, where each particular problem requires an individual customised solution.

Machine vision typically consists of hardware and software components. From a hardware perspective, systems are designed to be robust and reliable within their industrial setting. They typically incorporate a video camera, a lighting setup, a computer system and the means of communication between each component. Appendix C.1 describes the hardware systems used within this thesis.

The software component is a set of machine vision algorithms, each of which consists of a combination of both well known and custom purposed image analysis algorithms. Thus, a certain degree of variability in performance of machine vision algorithms occurs across different individual implementations.

Froth colour

Typically, the output of video cameras consist of images in red, green and blue (RGB) fields, which combine to provide a representation of the true colour in the image. The RGB colour space, however, does not account for the intensity of luminosity independently. Other colour models developed are able to describe chromacity independent of intensity.

The two main colour models used are Hue, Saturation, Value (HSV) or Hue, Saturation, Intensity (HSI) and the CIE Lab (LAB) colour space. The objective of the HSV and HSI colour

spaces is to represent relative colour relationships more accurately than RGB. The objective of the LAB colour space is to represent colour relationships similarly to that of the human eye.

A number of authors have cited the use of colour measurements within their work. Cipriano *et al.* (1997), Hargrave and Hall (1997), Moolman *et al.* (1994) and Hatonen *et al.* (1999) performed measurements using the RGB colour space. In addition to the RGB colour space, Bonifazi *et al.* (2000a,b), Guarini *et al.* (1995), Hyotyniemi *et al.* (2000) and Bonifazi *et al.* (2002) also performed measurements using the HSI and / or HSV colour spaces In addition to the RGB and HSI and HSV colour spaces, de Jager *et al.* (2004), Heinrich (2003), Morar *et al.* (2005) and Reddick *et al.* (2009) performed measurements using the CIE Lab colour space. These authors made colour measurements within controlled lighting environments and relative to a colour calibration object that was visible within the video frame to minimize the effect of lighting variation on the measured colour.

Froth surface bubble size distribution

The froth surface bubble size distribution provides an indication of the froth structure near the surface and the extent to which coalescence has occurred within the froth. A method to measure the bubble size distribution on the froth surface is to measure the cross-sectional area that each bubble lamella occupies.

The froth surface consists of curved lamella, commonly assumed to represent the bubble size below the froth surface. Lighting interacts with this froth surface in such a way that a higher intensity of light reflects towards the camera at the point in the curved surface that is normal to the mid-point between the camera and the light source. The intensity then decreases from that point on the bubble to the bubble boundary, where it meets adjacent bubbles. Thus, this intensity variation is often used as a basis for segmentation of individual bubbles on the froth surface.

Guarini *et al.* (1995) pre-processed the images using a low pass filter and contrast stretch and then performed a bubble segmentation using a gradient based method to find the minima in the gray-level map. Fitting ellipses to the resultant segmentation areas approximate the final bubble areas.

Nguyen (1998), Nguyen and Thornton (1995) and Holtham and Nguyen (2002) performed textural analysis on the froth surface to measure a texture spectrum. One of the parameters from this texture spectrum, termed *MID_TU* showed a correlation with bubble size.

Sweet *et al.* (2000), Wright (1997) and Francis (2001) developed a real-time segmentation method for froths, using the watershed segmentation technique (Vincent, 1992, 1993, Vincent and Soille, 1991). This method used the identification of markers, given by the highlights determined from a homotopic transform, used as a starting point for the watershed segmentation (Appendix C.2.2).

The watershed algorithm on its own performs well under conditions where the froth surface bubble size distribution is near mono-disperse. It however, does not perform well over widely differing bubble size conditions, where large and small bubbles are present, resulting in either over-segmentation of large bubbles, or the under-segmentation of regions containing smaller bubbles (Forbes and de Jager, 2004).

Forbes and de Jager (2004) developed a method which uses the classification of segmented regions into classes of individual or groups of bubbles, using the contrast measure from the grey-scale co-occurrence matrix of each bubble to improve the watershed performance under conditions where large and small bubbles exist within the same image (Appendix C.2.2).

Hyotyniemi *et al.* (2000) performed research into the measurement of bubble characteristics, such as aspect ratio, bubble perimeter and bubble roundness. Ventura-Medina and Cilliers (1999) performed work using the average specific surface area of bubbles on the froth surface. The specific surface area is equivalent to the surface area per unit volume.

Bonifazi *et al.* (2002) developed a method to fit a three dimensional model to a froth surface. The method segments the froth using the watershed technique, fits ellipses to the segmented regions and reconstructs a froth surface based upon the placement of these ellipses.

Louw (2009) investigated the use of shape from shading and combined images from two camera sources to determine point correspondence and obtain a three dimensional froth reconstruction.

Wang and Neethling (2007) investigated the relationship between the apparent and actual size of bubbles on the froth surface. Their work concluded that the perception of a froth with a uniform froth surface bubble size is that it has a wide bubble size distribution. However, this effect decreased as the actual bubble size distribution became more distributed. In addition, they developed a model that provided a correction factor to correct the perceived bubble size distribution to the actual bubble size distribution.

Froth velocity

The velocity of the froth travelling towards the launder is an important measurement, as it provides an indication of the froth recovery rate. This measurement is useful to combine with other information to calculate an estimate of factors such as the volumetric recovery of froth, or on its own to establish whether a flotation cell is operating within a specified range.

Francis (2001), Francis and de Jager (1998) and Sweet *et al.* (2000) developed an algorithm to measure froth velocity by tracking the motion of segmented bubbles, determined using the watershed segmentation, across a number of frames.

Hatfield (2006), Hyotyniemi *et al.* (2000) and de Jager *et al.* (2005) measured froth velocity using a cross-correlation between two consecutive images and determined the displacement of the correlation peak.

Holtham and Nguyen (2002) utilised a pixel tracing algorithm to measure froth velocity. This method tracks pixel movement across consecutive frames, where the minimum difference of the sum of squares of the intensity values determines the average displacement between two frames. This method, performed in the real domain, is similar to the cross-correlation method, performed in the Fourier domain.

Froth stability

As discussed in section 2.2.2, froth stability is an important factor in determining the froth phase selectivity and performance. There is therefore strong motivation to develop measures of froth stability that are practical and robust.

Hyotyniemi *et al.* (2000) developed a froth stability measurement, termed the bubble collapse rate, based upon the disparity occurring above a specified threshold between two consecutive, aligned images. The image alignment performed used the cross correlation technique, or a single block match to determine the displacement between the two images.

Hatfield (2006) and de Jager *et al.* (2005) modified this method and introduced the use of the normalized cross-correlation peak as a stability measurement. This is equivalent to determining the correlation coefficient for two images, where a perfect correlation is equal to 1.0 and represents high froth stability, with a decreases in correlation coefficient as the froth stability decreases.

All of these outputs from these machine vision algorithms, represent the difference, or similarity between consecutive images. The interpretation of these image comparison measurements may be difficult, since the measurements do not directly relate a physical property of the froth. In addition, these outputs are unlikely to be comparable across the different froth structural conditions that can occur owing to changes in operating conditions within a flotation cell.

Froth texture

The froth surface appearance can vary across operating conditions. Each appearance has a characteristic signature, or 'state', often determined by factors such as the size, shape or translucency of bubbles.

Froth state measurement refers to the identification and monitoring of the visual state of the froth. This is potentially beneficial, as these systems can identify froth states that result in poor performance and implement corrective action.

Holtham and Nguyen (2002) utilised a technique based upon gray scale co-occurrence matricies (Haralick, 1979), for each RGB image field to create a texture spectrum and determine a texture unit (TU) number. The texture unit numbers determined were then correlated to physical froth parameters, such as *MID_TU* to bubble size.

Forbes (2007) and Forbes and de Jager (2004) developed methods to classify froth images into classes using texture based methods. They defined froth texture as a relationship to the froth surface bubble size distribution and identified that certain froths exhibit dynamic bubble size distributions. Using Fourier ring and texture spectrum based measures they were able to classify froth images. In addition, they determined that under certain conditions, dynamic froth textures exist, whereby a single frame does not capture the froth class, as the texture signature changes across frames. This method utilised frequently occurring bubble size distributions to separate froth classes.

All of the machine vision measurements described above measure either abstract or physical properties of the froth. They are often termed as 'froth surface descriptors'. However, these measures are not metallurgical measures and thus are not measures of froth phase performance. Thus, machine vision measures need to be combined with each other, or with other physical factors or operating variable inputs to determine useful performance measures that can evaluate the flotation performance.

2.3.2. Machine vision use in performance measurement

A number of performance measurements exist that are useful in the control and operation of a flotation bank. The most important ones are generally considered to be the concentrate solids recovery rate and concentrate grade and recovery of valuable mineral or metal. Previous authors have attempted to predict these values based upon the use of froth surface descriptors derived from machine vision systems.

Concentrate grade measurement

The measurement of the concentrate grade is important within flotation, as most flotation operations operate to a target grade performance, based upon the requirements of downstream processes. Concentrates below the target grade may be uneconomical to process, and subject to penalty fees, whilst the cost of concentrates above the target grade are lower recoveries.

Generally, within routine flotation operation, samples are obtained on a shift basis and take a number of hours to process. On-line instruments do exist to measure grade, however, these instruments are expensive to maintain and may have low sample frequencies. Thus, should a disturbance occur that shifts the process away from the target grade, corrective action may only be possible hours after the disturbance. Hence, a cheap, reliable, non-intrusive alternative is attractive.

Hargrave and Hall (1997) investigated the use of colour measurement in tin flotation. They showed that a parameter defined as relative redness, derived from the RGB colour space, related to the grade of tin in the concentrate. They went further to show that the colour parameter gave a poor concentrate flow rate prediction. Relative redness was used, due to the presence of hematite (Fe_2O_3), a mineral which turns red when ground up due to the presence of ferric iron, within the concentrate.

Hatonen *et al.* (1999) used partial least squares regression to develop a model to measure flotation grade. The parameters used were a bubble stability measurement, froth velocity and the mean, standard deviation, skewness and kurtosis of each of the red, green and blue colour components measured by their machine vision system. They showed that these five variables were able to explain 66 % of the variation in zinc grade.

Hyotyniemi *et al.* (2000) showed results where a froth stability measurement provided a linear correlation with zinc concentration in the rougher tails. However, the froth stability measurement also showed an inverse correlation with the incoming zinc grade. In addition, they

showed that the copper sulphate concentration had an inverse correlation with their stability and transparency measurements.

Bonifazi *et al.* (2000a,b, 2002) investigated a copper, lead and zinc ore using the RGB, HSV and HSI colour spaces. Under the conditions investigated, they showed that a relationship existed between zinc grade and saturation and hue and that this relationship improved with the inclusion of the froth structural parameter, average bubble aspect ratio. The bubble aspect ratio is the ratio between the major and minor axis of an ellipse equivalent to the bubble. They also showed that when considering 3D fractal measurements and reagent dosages, a relationship between zinc grade and 3D fractal dimension, average grey intensity and the depressant dosage existed. Furthermore, they described relationships between copper grade with the average value and the standard deviation of the hue in the HSI colour space. A relationship between lead grade and 3D fractal dimension, the standard deviation of the value parameter in the HSV colour space and depressant dosage was also shown. A relationship between MgO grade and hue, the hue standard deviation and the 3D fractal dimension was also shown.

All of the authors above-mentioned did not discuss the effect of lighting on colour measurement. They often incorporate both, luminosity parameters and parameters which are affected by luminosity within their models, which are likely to be problematic across ambient lighting changes, especially changes between day and night. Only under exceptional circumstances, such as where large colour differences between minerals exist (e.g. hematite flotation systems), this may not be a problem.

Heinrich (2003) indicated that there is a statistically significant relationship between the chromatic colour components and grade of a pyrite/chalcopyrite flotation froth system, however, further research by Morar *et al.* (2005) indicated that more accurate grade predictions were obtained when parameters, such as velocity and stability were used in conjunction with colour.

Reddick *et al.* (2009) highlight the importance of the consideration of luminosity within colour measurements and demonstrate that under controlled conditions, and using the luminosity decoupled colour space, CIE Lab, luminosity variations between night and day still overpower the subtle changes seen across large grade variations within a pyrite / chalcopyrite system. In addition they show that the colour relationship between chalcopyrite and the gangue minerals is complex, requiring additional parameters to discern between the minerals.

Morar *et al.* (2005, 2006) and Barbian *et al.* (2007) showed that froth stability measurements in combination with froth velocity can used to predict concentrate grade on two different copper circuits. They concluded that the froth stability was related to the concentration of attached

material within their system, whilst the velocity related to the concentration of entrained material recovered.

Runge *et al.* (2007) show that a 'collapse rate' parameter in conjunction with froth velocity can be used to predict concentrate grade in a copper circuit.

Forbes (2007) performed work to classify and identify froth classes, based upon the froth surface bubble size distribution. It was also then shown that the froth class, in addition to froth velocity and bubble size measurements can be used to predict concentrate grade.

Mass flow measurement

Mass flow, or mass recovery, measurements indicate the rate of solids recovery to the concentrate. This measurement is important, as it relates to the recovery of the desired mineral species and it enables easy identification of areas of a circuit that perform sub-optimally.

Sweet (2000) performed work that showed the potential for the use of machine vision measurements to determine the mass flow rate of solids recovered to the concentrate.

Hatfield and Bradshaw (2003) showed that the watershed based velocity measure is best for slow moving froths, where sub-pixel accuracy is desirable. They also showed that it is possible to predict the concentrate mass flow rate using froth velocity measurements.

Gorain (2005) performed work on lead and zinc flotation circuits. It was shown that superficial gas velocity within the cell followed a linear relationship with the froth velocity. It was also shown that the froth velocity was linearly related to the lead and zinc concentrate grade.

Air recovery measurement

Ventura-Medina *et al.* (2003) developed a method of determining the recovery of air to the concentrate. Assuming that the velocity profile (streamlines) of the froth flowing over the lip is constant (flat), the measurement of the froth velocity and height over which the froth flows into the launder determines the volumetric flow-rate of the froth. This measurement was then determined relative to the amount of air input into the flotation cell to determine the fractional recovery to the launder.

All of the flotation performance measurements determined using machine vision measures use empirical relationships, with the exception of the air recovery measurement. However, the air

recovery measurement requires an accurate measure of the amount of air entering the flotation cell and a measure of the height of the froth flowing above the launder lip.

The use of empirical measures have shown to be unreliable, as acknowledged by Gorain (2005) and are often only valid under a small range in operating conditions in situations where the froth structure and appearance does not change by a large amount.

2.3.3. Machine vision use in flotation control

As the use of machine vision to determine froth surface descriptors is non-intrusive, and can operate constantly, it is appealing to utilise this technology to control the flotation process.

Cipriano *et al.* (1997) describes a system to supervise flotation cells through the use of machine vision. The system measures the colour (RGB and HSI), bubble size, bubble shape, bubble density, froth velocity and froth stability and uses a rule based system for control. Although they did not present any results they indicated that the system is able to identify anomalous operating states.

Hyotyniemi *et al.* (2000) developed a rule based control system, which controlled the copper sulphate addition to a zinc flotation bank. Within their system, the copper sulphate activates the zinc minerals, resulting in higher zinc floatability. Their scheme implemented actions to either increase ($+$) or decrease ($-$) the copper sulphate (activator) addition rate. The measurements that they used were measures for froth thickness, or mobility, froth stability, zinc content obtained from correlations to colour measurements and bubble transparency.

Table 2.1.: Rule based control system implemented by Hyotyniemi *et al.* (2000)

Ranking	Condition	Action
1	IF *froth thickness* $<$ *lower limit*	$-$
2	IF *instability* OR *bubble transparency* $<$ *lower limit*	$-$
3	IF *zinc content in rougher tailing* $>$ *upper limit*	$+$
4	IF *zinc content in scavenger tailing* $>$ *upper limit*	$+$
5	IF *froth thickness* $>$ *upper limit*	$+$
6	IF *instability* OR *bubble transparency* OR *bubble size* $>$ *upper limit*	$+$
7	ELSE	$-$

Their results indicated that the system was able to control plant operation, however, no results published shows performance gains other than a mention that the system minimised froth collapse situations.

Gorain (2005) developed a three level approach to controlling a flotation circuit. The first level was the identification of the optimum range of cell operating conditions in individual cells. The second level was the identification of optimum bank operating profiles and the final level was the control of cell operating conditions and bank gas dispersion profile. The third level consisted of the use of machine vision measurements, where the manipulation of the air flow rate controlled to a froth velocity set-point. This method has been shown to work well on ores that are consistent. The relationship between froth velocity and solids recovery rate changes with ore type and feed rate. Thus, this method is unable to optimize performance, and only maintains operation within a specified operating regime.

Supomo *et al.* (2008) described a control system to control a flotation bank to a froth velocity set point by modifying the froth depth. A decreasing velocity set point profile (inverse exponential) down the bank was used owing to the exponential nature of the flotation kinetic response curve. Their results indicated an increase in recovery by 1.0 % at a 1.1 % Cu feed. Additional benefits cited were an increase in stability in their regrind circuit.

Within industry, the froth velocity measurement is used extensively as a control parameter. Typically, a velocity set-point is controlled to by manipulating air rate and/or froth depth. This is usually performed under the assumption that the froth velocity relates to the solids recovery rate. However, this is not true under conditions where the froth structure changes, which would occur when the amount of floatable solids present in the feed changes. Currently, the use of more complex control and optimisation systems is not common within industry.

2.4. Summary from the literature survey

2.4.1. Froth stability

It is widely recognised that froth stability is a key driver of flotation selectivity and recovery. However, owing to the non-linearity of mechanisms occurring within the froth as well as the dominant mechanistic effects changing across different conditions, it is not well understood. Not enough research has been performed into the affect of operating variables on froth stability behaviour and its relationship to flotation performance.

Extensive work has been performed in two-phase foam systems to characterise the effect of surfactants on bubble size, foam stability and water recovery. This work has shown that stability within a two-phase froth is well characterised by the nature and concentration of the surfactant, along with the air rate. It is clear that the understanding of mechanisms that relate to two-phase foam stability is relatively well understood and authors have demonstrated models that are able to predict factors such as liquid content and water recovery under different conditions.

However, the understanding of three-phase froths is much less advanced.

Studies on the effect of solids hydrophobicity have shown that not only can solid particles stabilize the froth, high loadings and highly hydrophobic solids can override the effect of solution stabilising effects within the froth. Therefore, two-phase foam stability work is inadequate as a means of understanding froth stability behaviour, as solution effects are easily overwhelmed by solid effects.

Within a three-phase, industrial system, a number of froth stability measurement devices have been developed. Many of these measurement devices are intrusive, such as the column or electrical impedance measurements. Due to the abrasive environment within a flotation cell, intrusive measurement devices are not desirable. Currently, the only available non-intrusive stability measurements are based upon machine vision. However, current machine vision stability measures are not directly related to physical froth properties. Rather, the measurements only infer stability behaviour from image similarity based properties. Thus, a better froth stability measurement is required. Visually, froth stability is indicated by the rate, or proportion of bursting bubbles, or lamellae on the froth surface. As machine vision systems are able to measure the size of the bubbles on the froth surface, they may be able to identify bursting bubbles and thus measure the rate that they burst directly.

Froth stability encompasses a number of mechanisms, such as the increase of bubble size, loss of surface area, detachment of particles, release of water and promotion of drainage. In addition, each of these mechanisms are likely to have a different effect on flotation performance and under different conditions, each of these mechanisms may be affected differently. Owing to the large dominance of solid effects on froth stability, little is known about the distribution of solids through the froth, particularly in reference to detachment and attachment processes occurring within the froth phase. Thus, understanding the relationship between stability and these mechanisms is key to understanding the effect of operating variables on froth stability, and froth stability on flotation performance.

Currently no model exists that adequately describes three-phase froth stability behaviour in terms of the effect of operating variables and the internal mechanisms that occur within a froth. Factors such as the solution and solid effects on froth stability are known. However their relative effect on the above-mentioned mechanisms across different operating conditions is unclear.

In many flotation feeds, the hydrophobicity and concentration of the hydrophobic material change owing to the heterogeneity of natural ores and variability in upstream processes. In addition, the concentration of hydrophobic solids present usually decreases through a flotation bank. One of the biggest challenges in managing flotation banks and circuits is dealing with ore variability. Thus, understanding the froth stability and performance behaviour across different floatable solids concentrations and levels of hydrophobicity is essential.

2.4.2. The use of machine vision in industrial flotation systems

In order to effectively manage a flotation system, performance measurements are essential. Currently, a number of measurement techniques exist, however, many of these are intrusive to the process. As the internal environment in flotation cells is harsh due to the highly abrasive slurry, non-intrusive measures are desirable. Machine vision has the potential to provide non-intrusive flotation performance measures.

Currently, all relationships developed between machine vision measurements and flotation performance characteristics within the literature have been based upon empirical correlations.

Colour based measurements have been shown to be unreliable due to the inability to control the lighting conditions (Reddick *et al.*, 2009). They are likely to fail unless the colour variations that are required to be identified are large, which is not the case in the majority of ore systems.

The following general trends have been demonstrated to hold under normal operating conditions within the literature:

- Froth velocity is proportional to solids recovery
- Froth velocity is inversely proportional to concentrate grade
- Superficial gas velocity, or air flow rate, is proportional to froth velocity
- More coalescence occurs on the froth surface in the presence of lower grade material.

However, these relationships are not universal and have not been established over time and with changes in feed and operating conditions.

The value of using empirical relationships have been shown within a flotation control strategy, however, these empirical relationships limit the ability to which these strategies can be used to optimize flotation bank or circuit operation, as these relationships change with the feed to the flotation circuit, as acknowledged by Gorain (2005).

Within the literature, it has been widely acknowledged that flotation performance is related to froth stability. Thus, non-intrusive measurements of froth stability are desirable, as they may provide a more robust method of automated flotation bank control and optimisation.

Current machine vision based stability measurements use algorithms where stability information is inferred from image based properties, such as either a measure of the difference, or a measure of correlation between two consecutive video frames. These stability measurements do not relate to a physical property manifested by stability behaviour, such as bubble bursting events, bubble size change, or any other property relating to the collapse rate of the froth. Thus, these machine vision measurements are empirical descriptors of stability behaviour, and machine vision measurements that relate directly to stability behaviour, drivers of stability behavior or mechanisms affected by froth stability are required to capture the following properties:

- The concentration of solid particles on bubble films reaching the froth surface.
- The failure rate of bubbles or lamella films on the froth surface (burst rate).
- The rate at which air is lost through the froth surface.

Thus, this thesis aims to address the following objectives:

1. To develop machine vision measurements that obtain more appropriate froth surface descriptors which relate to specific physical froth characteristics, such as:

   a) Solids loading

   b) Froth stability

2. To test the sensitivity of machine vision measurements in measuring expected changes on the froth surface from changes in operating variables within a flotation system when the solids environment changes.

3. To determine the extent to which the operating variable effect on the froth surface behaviour and froth stability is consistent across a range of operating conditions within a single flotation cell when the solids environment changes.

4. To investigate the relationship between the froth stability and flotation performance across a range of operating conditions within a single flotation cell when the solids environment changes.

Chapter 3.

Experimental methodology

This chapter presents the details of the experimental work carried out in this thesis.

The data used in this work is from two sets of experiments. The first data set obtained was from an experimental campaign performed at Northparkes Mine, New South Wales, Australia, which is a copper mine that processes an ore containing bornite and chalcopyrite. The second data set obtained was from a pilot plant study using a platinum group metal ore sampled from the Merensky reef in the Bushveld complex. Both of these experimental campaigns consist of plant surveys performed under different operating conditions where metallurgical samples were taken from a number of streams. In addition, a number of non-metallurgical measurements were obtained. These include machine vision measurements, in-pulp bubble size, superficial gas velocity and the solids loading on the froth surface bubbles.

3.1. Measurement of froth surface descriptors

The SmartFroth machine vision system was used to perform froth surface descriptor measurements. SmartFroth (de Jager *et al.*, 2004, 2005, Forbes and de Jager, 2006, Sweet *et al.*, 2000), developed at the University of Cape Town, is a research tool for froth flotation.

SmartFroth utilises well known image processing techniques for the characterisation of bubbles on the froth surface to provide a measure of froth surface bubble size distribution, bubble velocity, bubble stability, surface texture and colour.

Within this thesis, SmartFroth was primarily used to determine the froth surface bubble size distribution and the froth surface velocity, as described in appendix C. Two new algorithms de-

veloped measure the solids loading on the froth surface and the burst rate on the froth surface, as described in chapter 4.

3.2. In-pulp bubble size and superficial gas velocity measurements

In-pulp bubble sizing was performed using the Anglo Platinum bubble sizer (APBS; Taute and Mc Clelland, 2006). This instrument was also used to measure the superficial gas velocity.

The Anglo Platinum bubble sizer is a commercially available bubble sizer designed using the principles used in similar instruments developed at McGill University (Chen *et al.*, 2002, Hernandez-Aguilar and Finch, 2005) and Helsinki University of Technology (Grau and Heiskanen, 2002).

The APBS consists of a reservoir of water, closed to the atmosphere. Bubbles from the pulp get captured and rise up a pipe inserted into the pulp phase, displacing the water in the reservoir. The rising bubbles pass an inclined viewing plane where they get photographed.

The bubble images are then analysed using image processing software to determine the bubble size distribution.

Bubbles observed within the viewing chamber are not the same size as they were in the pulp due to the change in hydrostatic pressure between the pulp phase and the viewing chamber. Thus, the bubble size measurements require a pressure correction to determine the actual bubble size within the pulp.

The APBS was also used to measure the superficial gas velocity which is performed by measuring the rate that the water level drops within the reservoir. The superficial gas velocity is calculated by accounting for the change in cross-sectional area between the reservoir and down pipe, and the pressure drop within the system.

The change in cross-sectional area between the reservoir and the down pipe is accounted for using equation 3.1.

$$J_{g,1} = J_{g,0} \cdot \frac{D_e^2}{D_i^2} \tag{3.1}$$

$J_{g,0}$ is the measured velocity of the air / water interface in the reservoir, D_i is the internal diameter of the reservoir and D_e is the opening diameter at the end of the down pipe.

The sperficial gas velocity measurement is corrected to determine its value at the point where the bubbles enter the down pipe by accounting for the change pressure using equation 3.2.

$$J_g = J_{g,1} \cdot \frac{P_{atm} + \rho_p \cdot g \cdot H_p(1-\varepsilon_g) - \rho_w \cdot g \cdot H_w(1-\varepsilon_g)}{P_{atm} + \rho_p \cdot g \cdot H_p \cdot (1-\varepsilon_g)} \tag{3.2}$$

P_{atm} is atmospheric pressure, ρ_p is the pulp density excluding bubbles, ρ_w is the water density, H_p is the distance from the pulp-froth interface to the end of the down pipe, g is the gravitational factor and ε_g is the gas hold-up in the pulp.

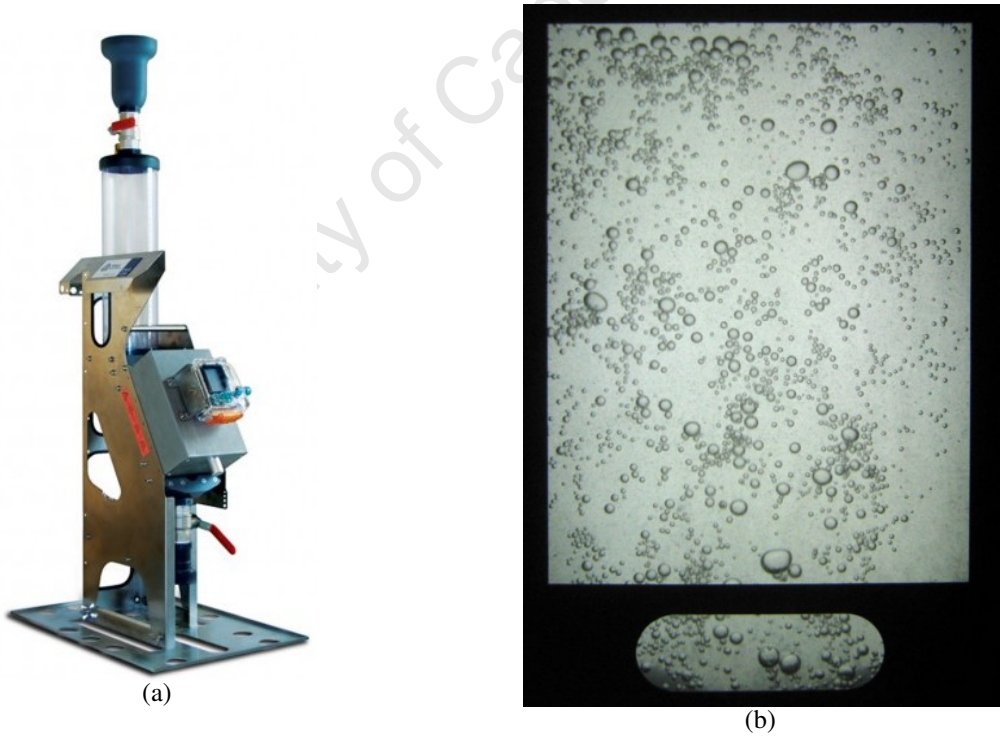

(a) (b)

Figure 3.1.: (a) Anglo Platinum bubble sizer. (b) Image of bubbles captured from the Anglo Platinum bubble sizer (Source: http://www.stonethree.com).

3.3. Solids loading on froth surface

The amount of solids attached on bubbles at the froth surface (solids loading) is of particular interest, as this is likely to be a key parameter in a model based froth optimisation strategy. The solids loading and the surface area flux recovered to the flotation concentrate relates to the attached component of the solids recovered.

Sadr-Kazemi and Cilliers (2000) developed a gravimetric method for determining the amount of water and solids present within a bubble lamellae. This method involves touching a glass microscope slide to a single bubble on the froth surface, causing the bubble to burst and the solid particles and water from the lamella to adhere to the slide surface, as shown in figure 3.2. The slide, which is pre-weighed is then weighed wet and dry, to an accuracy of 0.1 mg.

Due to the small amount of water present over a relatively larger surface area, evaporation adversely affects the accuracy of the wet weight measurement.

Figure 3.2.: A solids loading sample taken using the gravimetric method by sampling with a microscope slide.

The area covered by the bubble on the slide was measured from a photograph of the slide. Using these measurements, the bubble film thickness and solids loading was calculated.

In this thesis, this measurement was used to test the effectiveness of a proposed method to determine the solids loading on the froth surface using machine vision (Section 4.1) and investigate the relationship between froth stability and solids loading under different operating conditions (Chapter 5).

3.4. Copper ore (industrial plant)

This study was performed on a rougher bank at Northparkes Mine, New South Wales, Australia, which produces a copper concentrate. The main copper containing minerals present in the ore are bornite (Cu_5FeS_4) and chalcopyrite ($CuFeS_2$). The scope of this experimental work was to collect measurements of the flotation bank performance at a specified air rate, froth depth and frother dosage conditions.

Figure 3.3.: Rougher bank (Module 2) at Northparkes showing the first cell in the foreground.

The first four cells in the rougher bank, which are rectangular and measure 2.66 $\times$ 3.34 m, were used (Figure 3.3). The cells are force aerated and were designed such that every two cells share the same air feed. The flow rate to each cell pair was controlled to a set point. The air split ratio between each pair of cells is adjusted manually, and not automatically controlled. Superficial gas velocity measurements were carried out to determine the split ratio between the cell pairs. The split calculated between cells 1 and 2 was 30 and 38% respectively, while the split between cells 3 and 4 was 40 and 46% respectively. In each case, the remainder was determined to be lost from the pair of cells into the next cell by reconciling the superficial gas velocity measurements with the air flow measurement to the pair of cells.

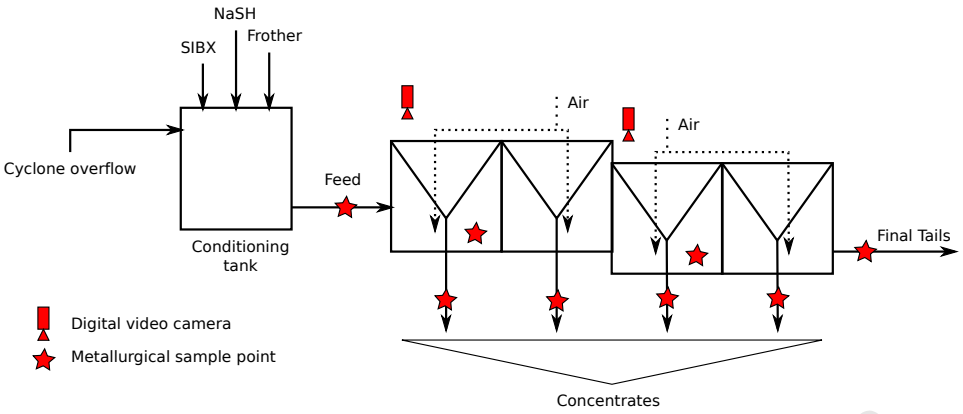

Figure 3.4.: Northparkes rougher bank configuration (Module 2) showing the location of the video cameras and metallurgical sample points.

The pulp level was controlled to a level set point, which could be modified to alter the froth depth.

The reagents were added in a conditioning tank. No extra addition points were used in the four cells sampled. The variations in reagent addition rates were performed by changing the reagent flow rate into this conditioning tank.

The feed conditions were kept constant through all of the experiments. The feed was maintained at a 340 $\pm$ 10 tonnes/hr flow rate with a solids content of 33.7 $\pm$ 0.5 % by mass. The feed copper grade was 0.46 $\pm$ 0.02 % by mass. The particle size was approximately 65 % passing 75 μm. (The errors stated represent the 95 % confidence limits.)

3.4.1. Samples and measurements

Samples were taken from various positions from the rougher bank, as illustrated in figure 3.4. Composite samples were taken of the feed to the bank, concentrate and tails from each cell over a period of 90 minutes for each experiment. The samples were filtered and dried, then analysed for % solids, copper, sulphur and silica content.

Samples taken from the feed and concentrate were obtained using sample cutters, while the sample obtained from the tailings was obtained using an air actuated in-pulp sampler. The feed rate to the bank was measured using a timed sample.

In addition, samples containing the solids on the bubble lamella on the froth surface were taken using the gravimetric method, as described in section 3.3. Water content was not mea-

sured, as the evaporation rate was high and the length of time that passed between sampling and weighing the microscope slides would have resulted in high measurement errors. Three samples were taken, from which an average solids loading was determined, for each cell at each experimental condition.

Image data of the froth was captured on each cell in the bank using digital video cameras, illuminated by 500 watt halogen lights, mounted to observe the froth prior to it overflowing into the launder. The cameras were placed in equivalent positions over each cell to minimise the effect of the variation in the superficial gas velocity within the cell and baffle and wall effects on the behaviour of the froth surface across the cell. Under steady state conditions, the froth surface was recorded for 20 minutes for each experimental condition for off-line image processing. It was assumed that a steaty state condition was reached after an hour of consistent operation with no operating variable changes made to the milling, classification and flotation plant sections.

The image data from the videos were processed using SmartFroth. The image processing algorithms were used to output measurements of the bubble size distribution and froth velocity, as described in more detail in appendix C.2 and solids loading and surface air loss as described in chapter 4. The average values and standard deviation of these measurements were calculated from the data.

The height of the froth overflowing the weir was measured six times, using a tape measure to obtain three measurements at two positions along the length of the weir for each cell at each experimental condition. The 95% confidence margin of error from these measurements varied between 10 and 39% of the mean values for the conditions tested. This measurement was used with the froth velocity and length of the weir to determine the volumetric flow rate of the froth into the launder.

The superficial gas velocity measurements were taken at three points in each cell using a superficial gas velocity probe, developed at the Julius Kruttschnitt Mineral Research Centre, University of Queensland, and described by Gorain *et al.* (1996). These data were averaged to determine an average superficial gas velocity for the cell. This data was also used to determine the air split to each of the paired cells.

3.4.2. Experimental conditions

The variables manipulated during the study were air flow rate, froth depth and frother dosage. The frother used in this work was Interfroth 68, which is a weak alcohol based frother. A total of nine conditions were surveyed as shown in table 3.1.

Table 3.1.: Operating variables tested with the copper ore

	Frother addition (ml/min)	Froth depth (mm)	J_g (Cell 1) (cm/s)	J_g (Cell 3) (cm/s)
Low froth depth Low frother concentration	100	155	1.03 1.10 1.17	1.26 1.48 1.61
High froth depth Low frother concentration	100	200	1.03 1.10 1.17	1.26 1.48 1.61
High froth depth High frother concentration	140	200	1.03 1.10 1.17	1.26 1.48 1.61

3.5. Platinum ore (pilot plant)

This study was performed at the Anglo Platinum Divisional Metallurgical Laboratories pilot plant. The scope of this experimental work was to collect measurements of the flotation bank performance for a wide range of froth structure variations caused by changes in frother type, frother dosage, froth depth and activator addition.

Figure 3.5.: The pilot plant rougher bank showing the first five cells, with the first cell in the foreground.

The study was performed using a pilot scale rougher bank (Figure 3.5), as the range in variation of the conditions tested could have had significant negative consequences if they were tested on a production system.

The ore used in this study was a platinum bearing ore, from the Merensky reef of the Bushveld complex. Merensky reef is feldspathic pyroxenite and shows a large variation in mineralogy, both on a small and large scale. It also contains talc which is a problematic gangue mineral. The PGM's are finely disseminated and associated in solid solution with the sulphide minerals which are predominantly pentlandite, chalcopyrite and pyrrhotite.

The ore was blended to provide a uniform feed throughout the overall campaign and each test.

The ore was milled in a pilot scale ball mill in a closed circuit with the screen underflow feeding a rougher bank consisting of six 400 L flotation cells. The screen cut size was 80 μm.

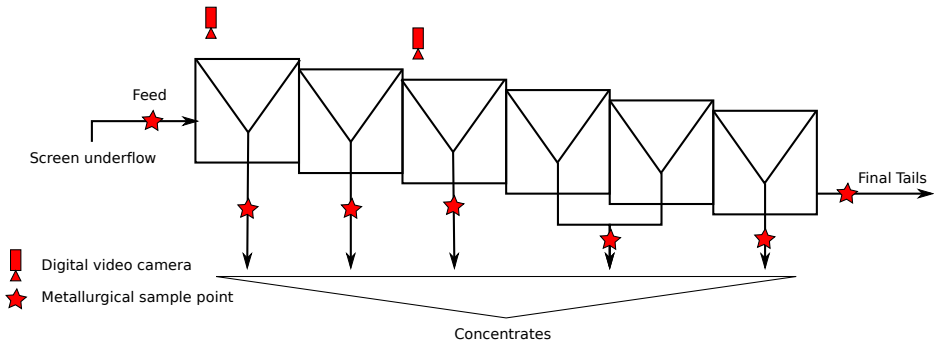

Figure 3.6.: Pilot plant rougher bank configuration, showing the location of the video cameras and metallurgical sample points.

The collectors used were sodium isobutyl xanthate (SIBX) and Sascol 61, which is a co-collector produced by Sasol that consists mostly of dithiophosphate (DTP). The frothers used were XP 200 and XP 250, which are polyproplyene glycol methyl ether frothers manufactured by Senmin, with an average molecular mass of 200 and 250 g/mol respectively. In addition, some experiments were performed using $CuSO_4$ as an activator, which is common practice in normal plant operation for this ore.

The feed conditions were kept constant through all of the experiments. The feed was maintained at a 3.94 ± 0.11 tonnes/hr flow rate with a solids content of 33.7 ± 0.5 % by mass. The feed platinum and nickel grade was about 2.83 ± 0.29 ppm and 0.140 ± 0.009 % respectively. (The errors stated represent the 95 % confidence limits.)

3.5.1. Samples and measurements

Samples were taken from various positions from the rougher bank, as illustrated in figure 3.6. Composite samples were taken of the bank feed, concentrate and tails, over a period of 60 minutes for each experiment. The concentrate samples for cells 4 and 5 were combined. The sample points described above are shown in figure 3.6. All of the samples collected were filtered and dried, then analysed for % solids, platinum, palladium, copper, nickel, magnesium and aluminium by Anglo Research Laboratories. In addition, the flow rate of the bank feed, concentrate and tails was measured using a bucket and stopwatch.

Bubble loading samples were taken using the gravimetric method, as described in section 3.3. Water content was not measured, as the evaporation rate was high and the length of time that passed between sampling and weighing the microscope slides would have resulted in high

measurement errors. Either four or five samples were taken, from which the average and standard deviation of the solids loading was determined, for each cell at each experimental condition.

Image data of the froth was captured on the 1^{st} and 3^{rd} cells using industrialised video cameras, illuminated by 200 watt halogen lights, mounted to observe the froth before it overflowed into the launder. The cameras were placed in equivalent positions in each cell to minimise the effect of the variation in the superficial gas velocity and cell baffle and wall effects on the behaviour of the froth surface across the cell. Under steady state conditions, the froth surface was recorded for 20 minutes for each experimental condition for off-line image processing.

The image data from the videos were processed using SmartFroth. The image processing algorithms were used to output measurements of the bubble size distribution and froth velocity, as described in more detail in appendix C.2 and solids loading and surface air loss as described in chapter 4. The averages values and standard deviation of these measurements were calculated for the 20 minute period.

Pulp bubble size and superficial gas velocity measurements were taken on the 1^{st} and 3^{rd} cells at each condition using the Anglo Platinum bubble sizer, as described in section 3.2.

3.5.2. Experimental conditions

A two level factorial experimental design was performed with XP 250 frother. The full two level factorial for XP 200 was not completed owing to operating problems during the campaign.

In the factorial design, the two manipulated parameters were the frother concentration, from 20 g/t (low) to 60 g/t (high) and froth depth. The froth depth set points on the first rougher were taken as 25% (low) or 75% (high) of the maximum froth height achievable ($\mathrm{H_{max,fdpth}}$), where mass is just recovered at the maximum air flow rate to the cell. The froth heights in roughers 2-6 were changed over smaller ranges, as these changes were subject to the stability of the froth in each cell, which decreased down the bank.

Consistent operation of the bank was achieved by manually manipulating the air flow rate to obtain a solids mass recovery of 1.5 % in the first rougher cell and 0.75 % as compared to the feed rate for each subsequent cell down the rougher bank for each test. However, this was not possible in cell 6 at the low frother concentration, due to the mass recovery decreasing

Table 3.2.: Operating variables tested with the platinum ore

Frother type	Frother concentration (g/t)	Froth depth (frac. of $H_{max,fdpth}$)	Copper sulphate
XP 200	60	0.75	N
		0.25	Y
			N
	40	0.50	Y
	20	0.25	Y
			N
XP 250	60	0.75	Y
			N
		0.25	Y
			N
	20	0.75	Y
			N
		0.25	Y
			N

significantly. The use of consistent mass recovery profile as an operating goal across each test condition was chosen for two reasons; it ensured bank operability at each test condition and full-scale plants operate banks based upon set mass recovery profiles down a bank. Full-scale plants however tend to operate with an exponentially decaying mass recovery profile. This was not used in this case for two reasons. Firstly, to simplify the experimental protocol, and secondly as the objective of this work was to study the effects of operating variables on performance, and not optimize the operating variables, running the plant using a more optimum profile was not deemed necessary.

Chapter 4.

New machine vision measurements

The first objective of this project is the development of machine vision measurements to obtain more appropriate froth surface descriptors that relate to physical froth surface descriptors, such as solids loading and froth stability. The second objective relates to testing the effectiveness and sensitivity of machine vision measurements.

Thus, this chapter introduces two new machine vision measurements for the analysis of the froth surface within mineral flotation. It also details the machine vision algorithms and evaluates and discusses the potential for using these new measurements to determine specific froth phase performance characteristics.

The first proposed machine vision measurement measures solids loading on individual bubbles on the froth surface. This measure determines a measure of the surface 'roughness' of individual bubbles in images of the froth surface. The second proposed machine vision measurement is a measure of the rate at which bubbles burst on the froth surface. This measure uses an algorithm that identifies bursting bubbles.

4.1. Measurement of solids loading

The concentration of solids that reach the froth surface in combination with froth structural and transport factors determines the mass of solids recovered to the concentrate per unit time. The principal froth structural factor that governs this is the froth surface area per unit volume. The principal factors that govern the froth transport rate, reflected by the froth velocity, are the air flow rate into the flotation cell and the air loss rate on the froth surface. The bubble size

distribution on the froth surface reflects the surface area per unit volume of the froth near the launder.

However, the solids recovery rate also requires a measurement of the mass of solids associated per unit area of froth, comprised of two components; attached solids and entrained solids. Attached solids occur on the bubble lamellae and are hydrophobic, while the entrained solids occur within the Plateau borders and consist of a combination of non-floatable and floatable (detached) solid particles. As the floatable particles attached to the lamellae are visible on the froth surface, it should be possible to measure their loading.

The solids loading measured gravimetrically, as proposed Sadr-Kazemi and Cilliers (2000) and reviewed in section 3.3, may be subject to high variation and has limitations. This measurement technique may attract sample bias, as larger bubbles are easier to sample than smaller bubbles. In addition, this measurement, performed manually, has a long turnaround time, making it unsuitable for use in on-line control.

However, the visual textural appearance of bubbles on the froth surface tends to indicate a level of solids loading, where lightly loaded bubbles appear transparent, while heavily loaded bubbles are opaque. Thus, it should be possible, by measuring textural aspects of the images of bubbles, to infer the solids loading on the froth surface. In addition, it is possible to measure solids loading as a function of bubble size by considering the image segmentation outputs. Thus, the variation in the solids loading with bubble size may provide insight into the extent to which solids detach as smaller bubbles coalesce to form larger bubbles.

Under different conditions, bubbles on the froth surface vary from appearing transparent to opaque, depending on the concentration of solids attached to the bubbles.

Bubbles tend to appear transparent under conditions of low solids loading and appear opaque with high solids loading conditions. A large textural difference occurs between these two conditions, where the transparent bubbles appear to have a rough texture, due to the visibility of bubbles below the froth surface, while the opaque bubbles appeal to have a smooth texture.

Hypothesis 4.1
Therefore, it is hypothesised that a measure characterising the roughness of surface on bubbles in images of the froth correlate to solids loading on the froth surface.

On the froth surface, two coalescence mechanisms have been identified; coalescence between adjacent bubbles, both with lamellae visible on the froth surface, or coalescence between a single bubble on the froth surface and a bubble that exists wholly-below the froth surface.

In the case of the former mechanism, a single larger lamellae forms when the two surface lamellae become joined. In the latter, the froth surface lamellae expands due to the increased air within the resultant bubble.

These two coalescence mechanisms affect the solids loading on the lamella on the exposed froth surface differently. When two adjacent bubbles coalesce, two exposed lamellae join to become one lamella, resulting in a decrease in surface area. Thus the solids loading on the surface lamella should increase. When a bubble on the froth surface coalesces with a bubble below the froth surface, the exposed lamella grows in size, while no solids are added to it. Thus, the solids loading will decrease.

Hypothesis 4.2
Therefore, it is hypothesised that an on-line measurement that relates to solids loading is able to distinguish changes to the loading based upon the coalescence mechanism.

4.1.1. Behaviour of attached solids on the froth surface

The concentration of solids attached to bubbles on the froth surface affects the appearance of the froth surface. When more solids are present on the surface of a bubble, the surface is more clearly defined, whereas a low solids loading results in transparent or translucent bubbles, or bubbles with 'windows'. Furthermore, in heavily loaded bubbles, when solids on the bubble surface are tightly packed together, the bubbles appear smoother, as the bubble reflects incident light more uniformly.

Figure 4.1 shows grey level scan-lines, sampled across the centre of bubbles, for bubbles with a high and low solids loading in the platinum and copper systems. It is apparent that the more heavily loaded bubbles have a smoother bubble surface, with less variation, than the bubbles with a low solids loading.

Coalescence effect on froth surface solids loading

When a film or lamella separating two bubbles ruptures, the two bubbles coalesce to become a single bubble. A fraction of the solids attached to the ruptured lamella will remain attached to the resulting bubble with the remainder of the solids detaching from the bubble. Due to this coalescence event, the surface area to bubble volume ratio decreases, resulting in a net increase in solids concentration, or loading on that particular bubble.

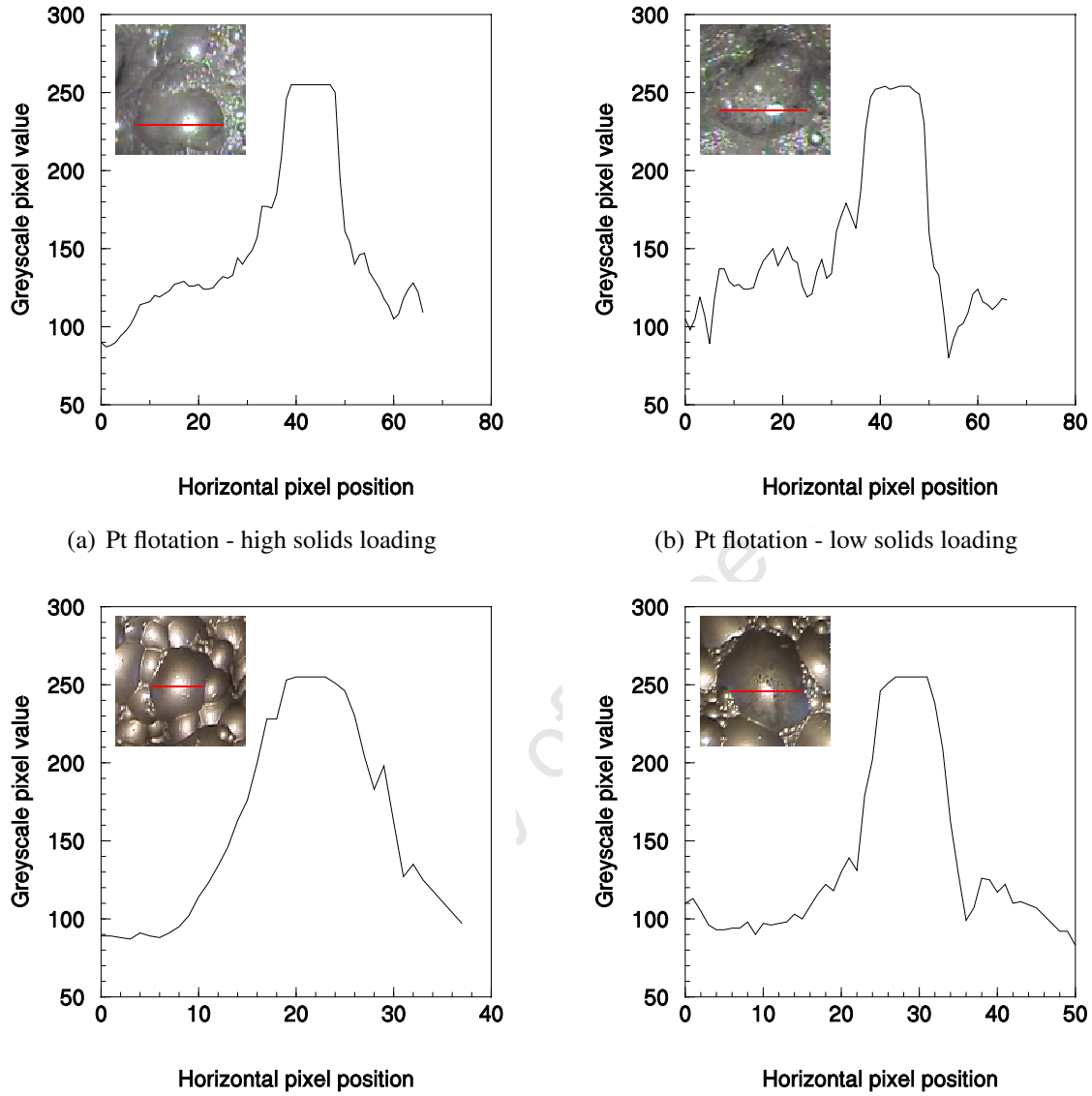

(a) Pt flotation - high solids loading

(b) Pt flotation - low solids loading

(c) Cu flotation - high solids loading

(d) Cu flotation - low solids loading

Figure 4.1.: A comparison of greyscale pixel values according to solids loading for the two industrial ores tested. The horizontal scan-lines taken intersect through the highlight of similar sized bubbles with different solid loadings.

Within the context of the froth surface, this process occurs and is evident, as shown in figure 4.2(a), where two adjacent bubbles coalesce. This process typically results in an increase in loading on the froth surface lamella due to the concentration of the solids as the surface area to volume ratio decreases. Figure 4.2(a) shows scan lines of the greyscale pixel value across a bubble as it coalesced with an adjacent bubble. The variation on the froth surface remains low before, during and after the coalescence event.

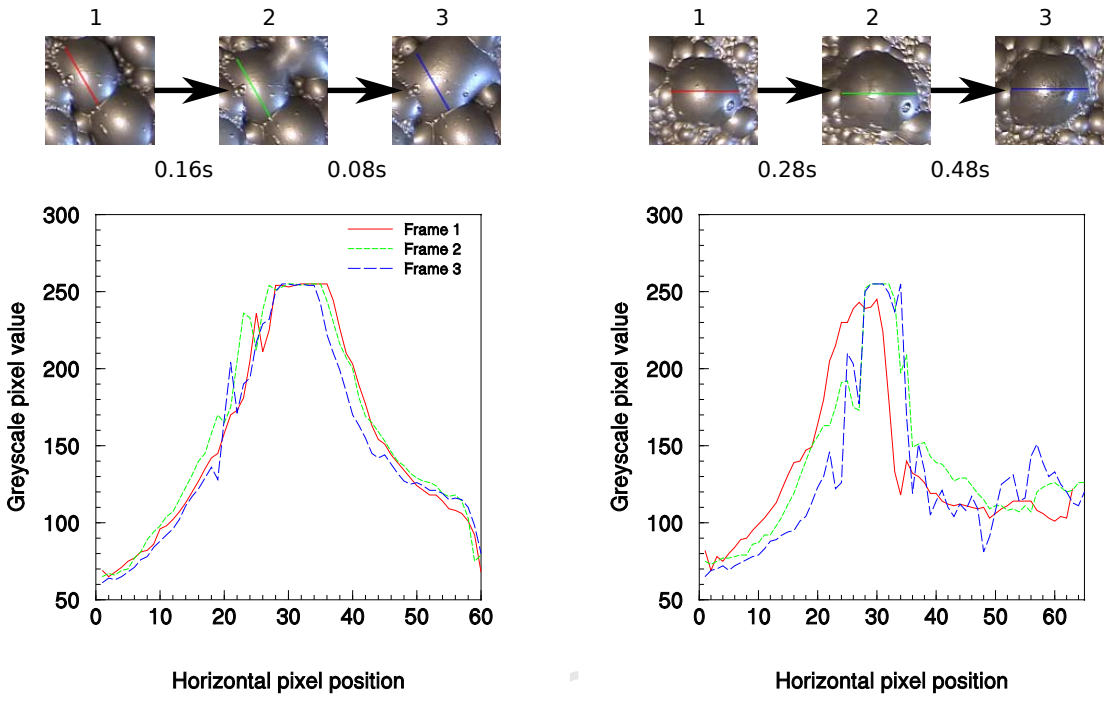

(a) Bubble loading increasing

(b) Bubble loading decreasing

Figure 4.2.: A series of three images showing scan lines across the surface of a bubble when coalescence occurs (a) with an adjacent bubble on the surface and (b) with an adjacent bubble below the froth surface.

However, an additional coalescence effect observed on the froth surface affects the solids loading on the froth surface lamellae. If the bubble on the froth surface coalesces with an adjacent bubble below the bubble on the froth surface, no extra particles get added to the top lamellae, whilst the added air decreases the surface area to bubble volume ratio. However, while the overall surface area to bubble volume ratio decreases, the size of the lamella on the top surface of the bubble increases, resulting in the loading on the top surface of the bubble decreasing, as indicated by the textural change in figure 4.2(b). Figure 4.2(b) shows that the variation on the froth surface increased as the bubble size increased due to coalescence with bubbles below the surface.

On the froth surface, the larger bubbles present have formed from more coalescence events than the smaller bubbles present. Given the existence of coalescence mechanisms which may increase or decrease the solids loading on the froth surface lamella, the solids loading on the froth surface will change as a function of bubble size. In addition, bubbles which have undergone more coalescence events are likely to have a higher variance in solids loading.

The bubbles on the froth surface have evolved from the bubbles entering the pulp. Thus, the loading on these bubbles also relates to the bubble loading on the bubbles entering the froth. As bubbles coalesce through the froth phase, a fraction of the attached material at the air/water interface will become detached, due to the decreasing interfacial area through the froth. This fraction detached may change, and is likely related to the amount of loading on the bubble.

4.1.2. Proposed solids loading measurement

A machine vision method to estimate solids loading on the froth surface is proposed. This machine vision method measures the high frequency variation on the bubble surface, which infers a measurement of solids loading.

Figure 4.3 illustrates structural components of an image which contains high frequency variation. Figure 4.3(a) is shown as a three-dimensional structural map utilising each grey-scale pixel value to represent height in 4.3(b). Figure 4.3(c), is the three-dimensional structural map of the image after it has undergone low-pass filtering, or image smoothing. This height map shows the low frequency information contained within the image, which, to some extent mirrors froth structural features.

The unfiltered three-dimensional structural map of figure 4.3(a) is shown in figure 4.3(b). This illustrates the presence of variation on the surface of the structure, which corresponds to bubbles shown in figure 4.3(c). The majority of the large spikes present within this structure are due to the highlights present on each bubble.

An image processing algorithm can exploit the above-mentioned properties of the bubble surface. It is possible to remove the low frequency variation within the images, which represents the bubbles and froth structure, to measure the observed high frequency variation.

This image processing algorithm makes use of the top-hat, or rolling ball filter (Ritter and Wilson, 2001). This is a widely used morphological transform is analogous to rolling a sphere under the image, where the surface generated from the top of the rolling ball, based on the motion of the centre of the ball is subtracted from the original image. Figure 4.4 illustrates this process. This filter is commonly used to remove low frequency variation within images, whilst preserving the high frequency variation. The only parameter that adjusts this filter is the radius of the sphere.

Figure 4.5 shows the result of the top-hat transform as applied to figure 4.3(a). The high peaks in this output correspond to the highlights and borders of the smaller bubbles. The larger

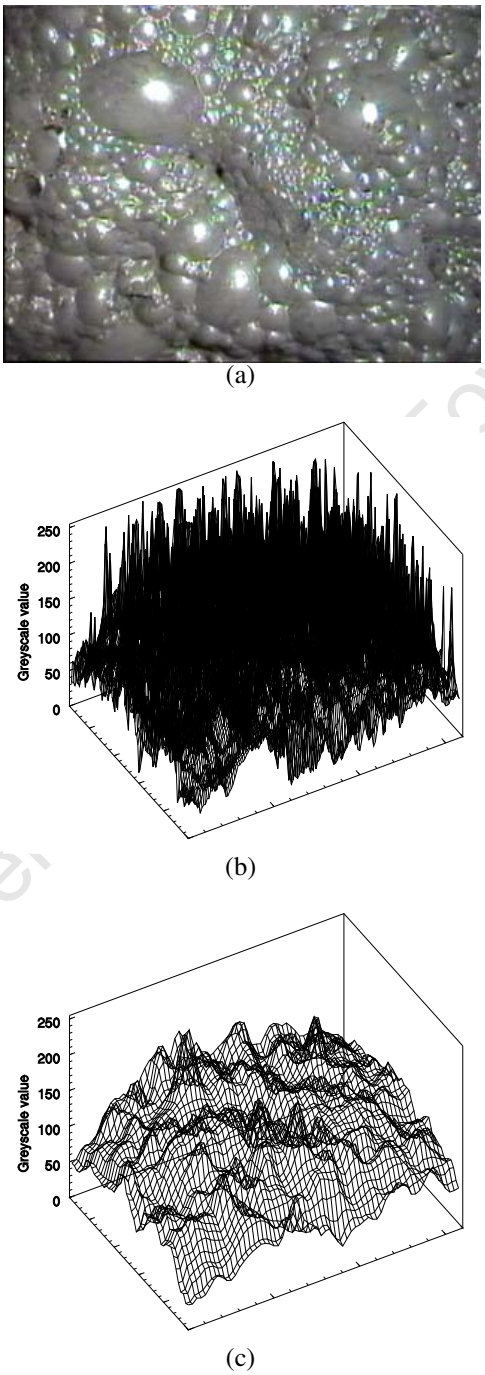

Figure 4.3.: An image of a froth surface (a) shown as a grey-scale height map before (b) and after (c) image smoothing.

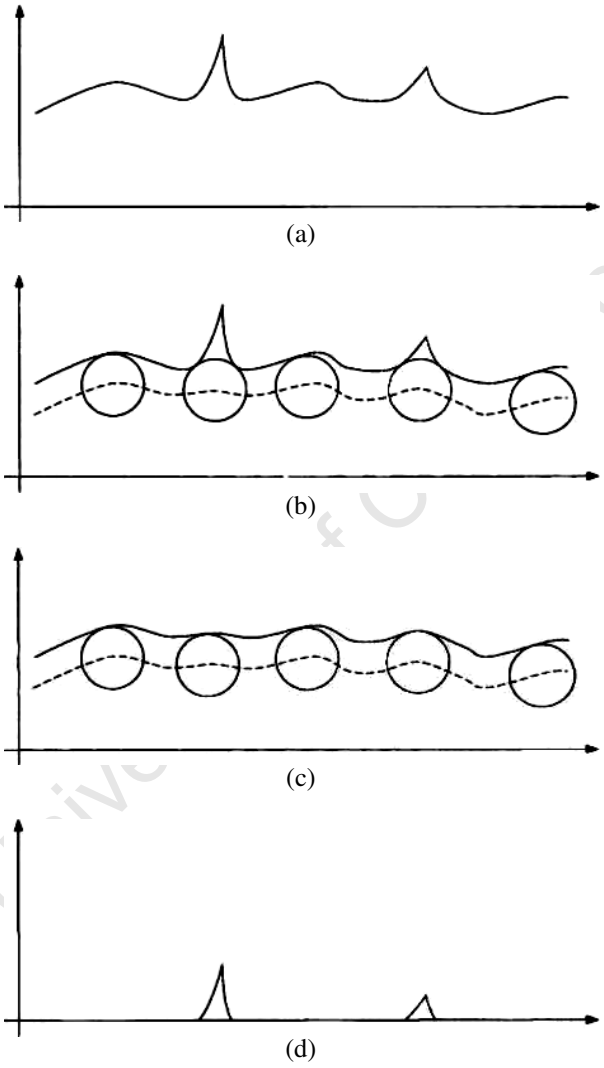

Figure 4.4.: The rolling ball algorithm. (a) The original signal, (b) the surface determined from the centre of the rolling ball, (c) the surface determined from the top of the rolling ball and (d), the result of the algorithm, determined by subtracting (c) from the original signal in (a). (illustration from Ritter and Wilson (2001))

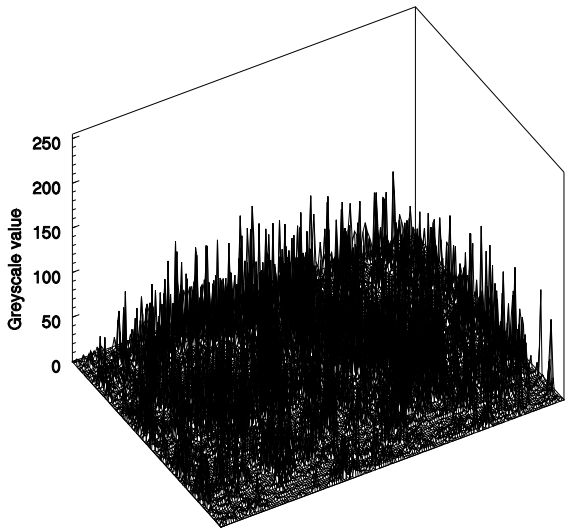

Figure 4.5.: The effect of the rolling ball, or top-hat algorithm applied to figure 4.3(a)

bubbles are not represented, as the rolling ball is able to enter the highlights within the larger bubbles.

The spikes present due to highlights on the bubble surface do not represent variation on the bubble surface due to solids loading, as the dynamic range of the camera saturates the image at these points. Thus, the removal of these areas can be performed using a cut-off threshold.

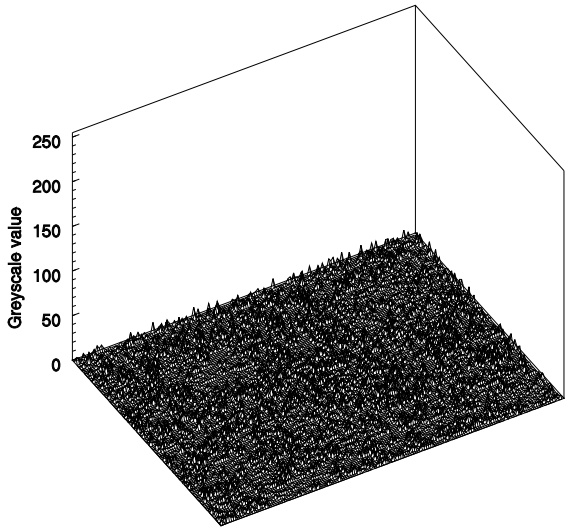

Figure 4.6.: The effect of the rolling ball, or top-hat algorithm and a cut-off threshold applied to figure 4.3(a)

Figure 4.6 shows the result of the cut-off threshold applied to the output from the top-hat transform, in figure 4.5. It exposes the surface variation on the bubble, which is hypothesised to correspond to solids loading on the bubble surface.

The output from the cut-off threshold can be segmented using the output from the watershed segmentation (Appendix C.2.2) to determine the variation on each individually segmented bubble. Thus, it is possible to determine this new measurement as a function of bubble size.

The bubble size distribution is determined using a histogram of the cumulative cross-sectional area of the bubbles on the froth surface. The average value and standard deviation from this new measurement can be determined for each histogram bin by averaging the variation on each bubble that falls within each histogram bin.

The algorithm to perform this measurement (Figure 4.7) is:

1. Apply a white top-hat of radius, r, transform to a grey scale froth image.
2. Apply a threshold, t, to the output from (1.) to create a cut-off mask.
3. Incorporate the output from (2.) with the watershed segmentation output to determine the average intensity of the image for each segmented region.

Based upon the above algorithm, this method requires two input parameters. The top-hat radius, r, and cut-off threshold value, t. These input parameters relate directly to image grey level values. Hence, these values require calibration for a particular system configuration. The calibration would account for any variation in the dynamic range due to camera exposure and different sized field of views.

This measure utilises the variation on the surface of bubble and can therefore be more accurately termed as the *average bubble surface noise amplitude* (BSNA). This proposed method addresses the implementation of the measure of froth surface roughness mentioned in hypothesis 4.1.

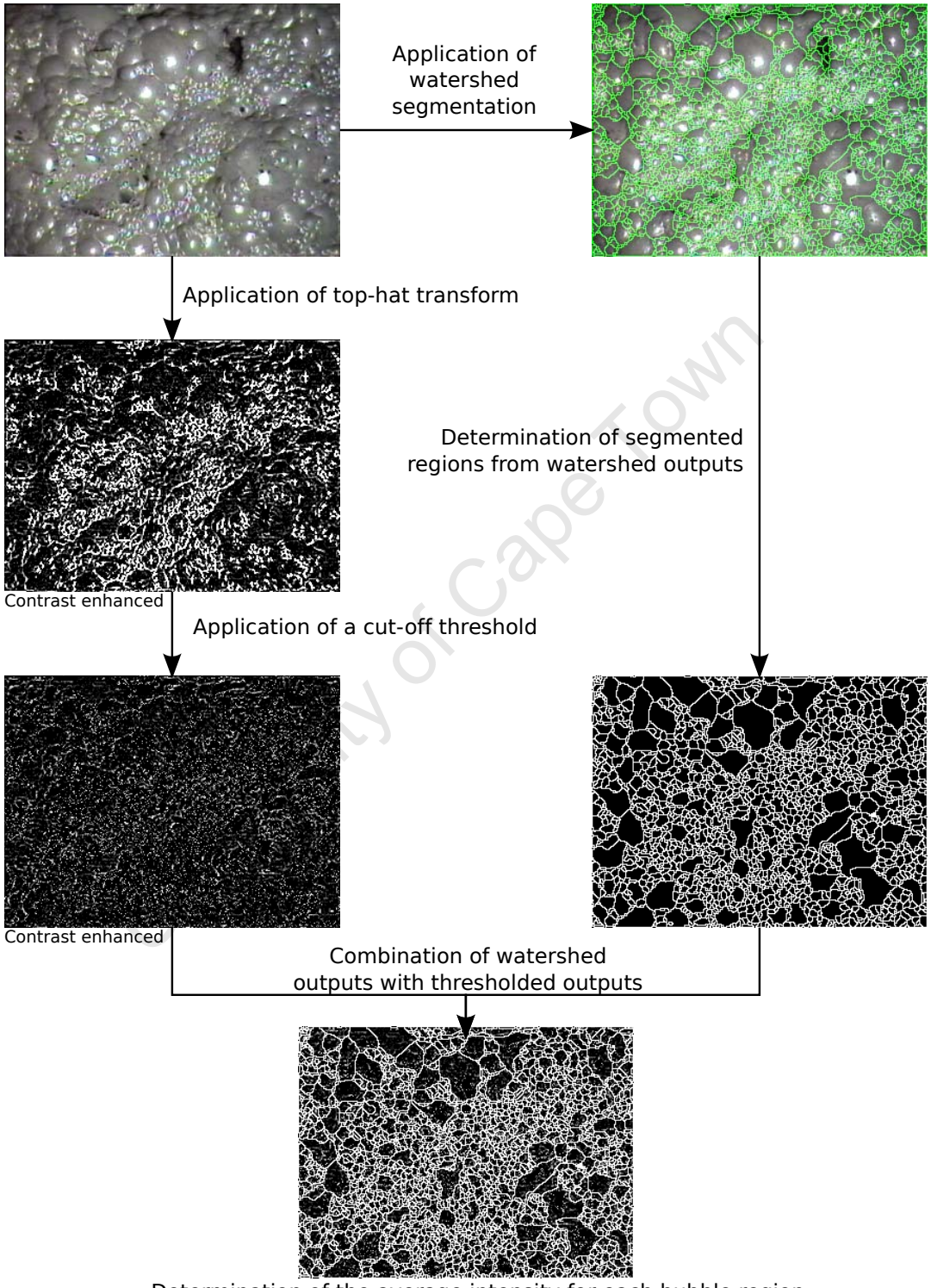

Figure 4.7.: Illustration of the algorithm used to determine the bubble surface noise amplitude on the froth surface.

4.1.3. Solids loading measurement results

This proposed solids loading measurement method has been applied to videos from different to characterise the behaviour of the measurement.

The results from the first cell at one operating condition on each of the two experimental systems are presented here. The conditions in the copper system were high froth depth, high air rate and high frother concentration, and in the platinum system were high froth depth, high air rate and a high concentration of the XP250 frother.

Figure 4.8 shows the results of the bubble surface noise amplitude measurement on each bubble in a single frame determined as a function of bubble size.

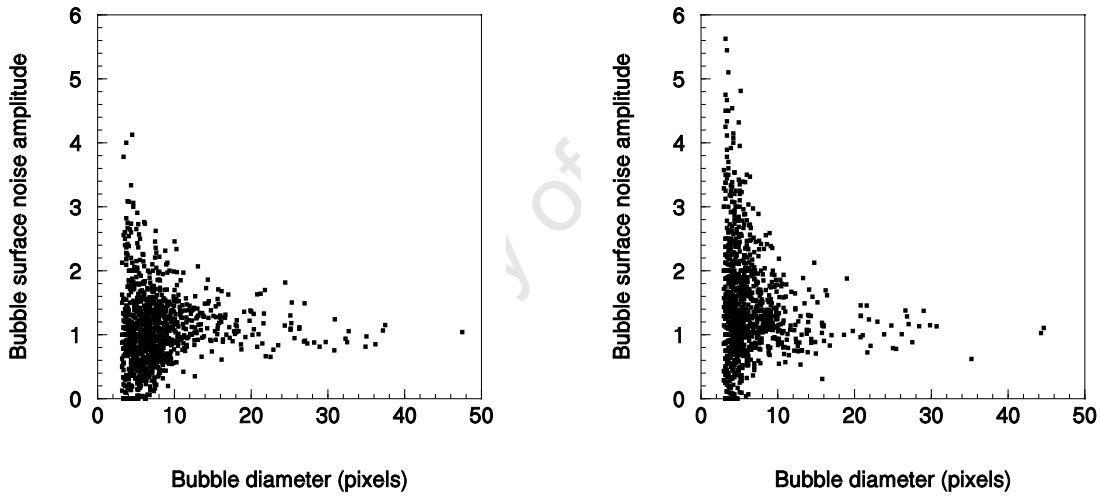

(a) Copper (b) Platinum

Figure 4.8.: Bubble surface noise amplitude results versus bubble size for a single video frame in each experimental system.

Figure 4.8 shows that typically, a large variation in the BSNA measurement occurs at lower bubble sizes, which decreases with larger bubbles.

The data in figure 4.8 can be binned into decile[1] increments based upon the cumulative bubble size distribution. The cumulative bubble size distribution has been calculated on a bubble cross-sectional area basis, where as the bubble size increases, the number of bubbles sampled per bin decreases by square power law. Thus, an error analysis needs to be performed to

[1]Cumulative size distribution *deciles* are the 10% increments in the size distribution.

ensure that the confidence of the bubble surface noise amplitude measurements remain within the same order of magnitude as bubble size increases. This has been performed in figure 4.9.

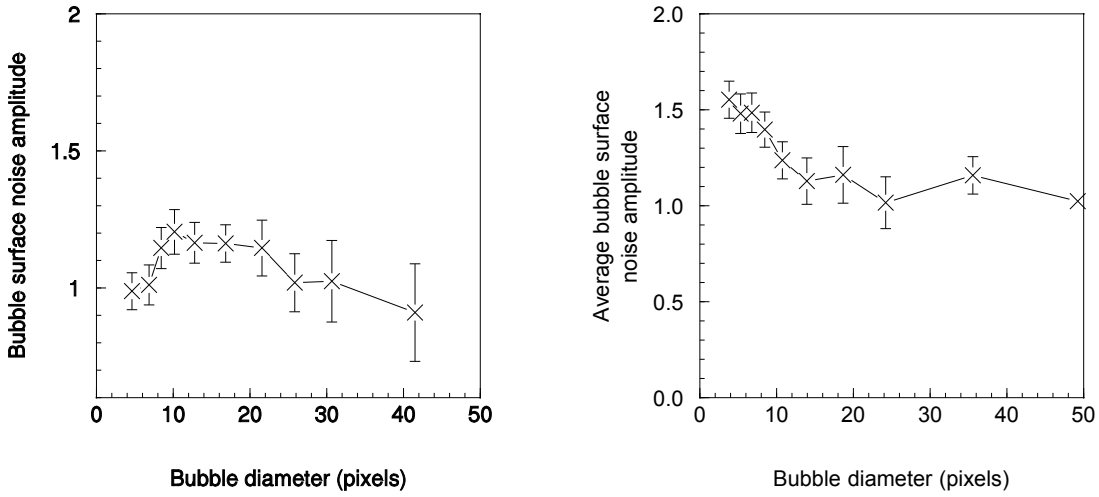

(a) Copper (b) Platinum

Figure 4.9.: The bubble surface noise amplitude versus bubble size for each bubble size distribution decile for a single video frame in each experimental system (error bars denote the 95 % confidence limits).

Due to the number of bubbles sampled within each decile, the 95 % confidence interval of these measurements increase with bubble size in the case of the copper system, while they decrease in the case of the platinum system.

The trend also shows that under these operating conditions, in the copper system the smaller bubbles have a lower bubble surface noise amplitude which increases and then decreases again at larger bubble sizes, while the bubble surface noise amplitude decreases and then remains constant in the platinum system.

It is possible to obtain these measurements for consecutive frames, as shown for three different bubble size distribution deciles in figures 4.10 and 4.11. The average value for each decile does vary, with a large variation observed at the higher bubble size distribution deciles. This variation is, however, partially due to a variation in the bubble size of the decile interval.

Figure 4.12 shows the 95 % confidence interval for measurements using four consecutive frames, decreasing the margin of error. Typically, SmartFroth processes between three to five frames every two seconds to produce a single data point in time. Averaging this measurement over time would further improve the confidence interval.

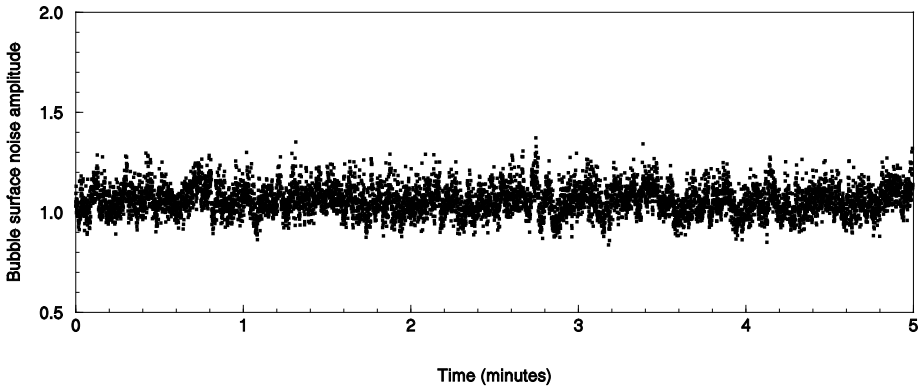

(a)

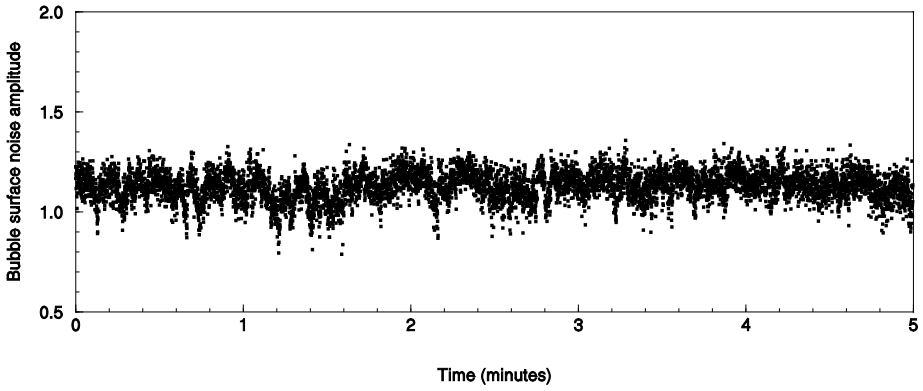

(b)

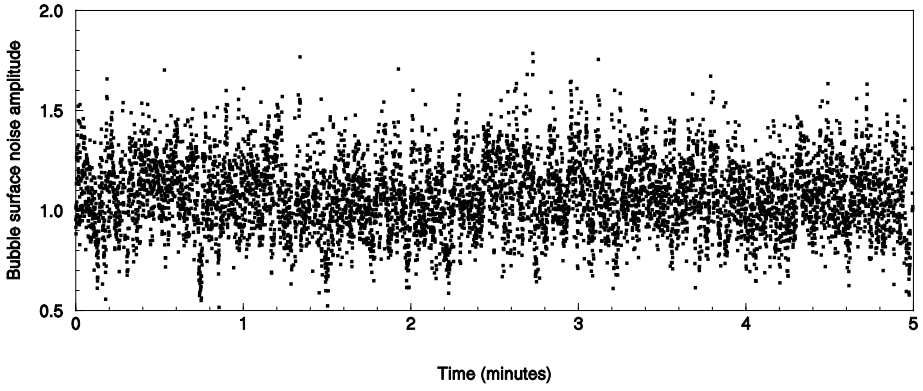

(c)

Figure 4.10.: Variation of the average bubble surface noise amplitude for (a) 10–20 %, (b) 50–60 % and (c) 90–100 % bubble size distribution deciles over five minutes (7500 frames) in one condition in the copper system.

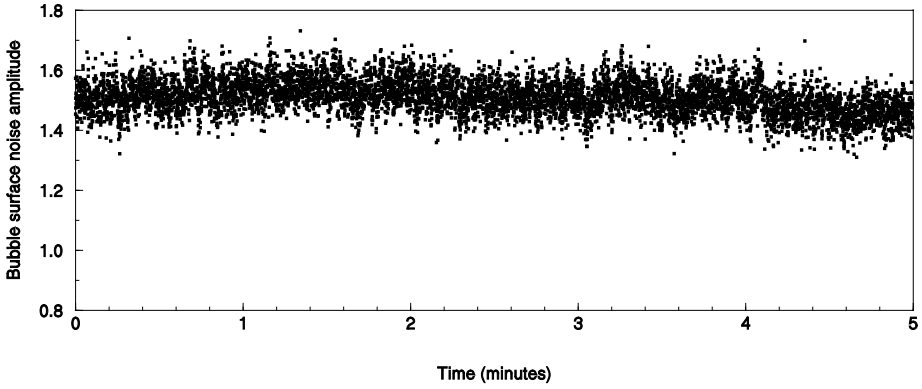

(a)

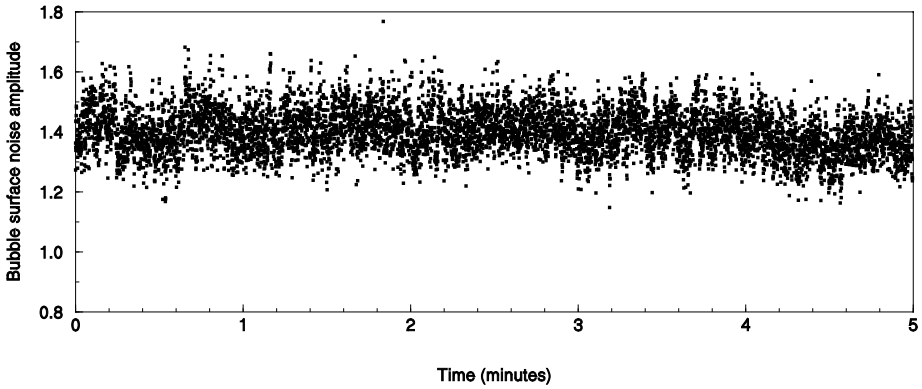

(b)

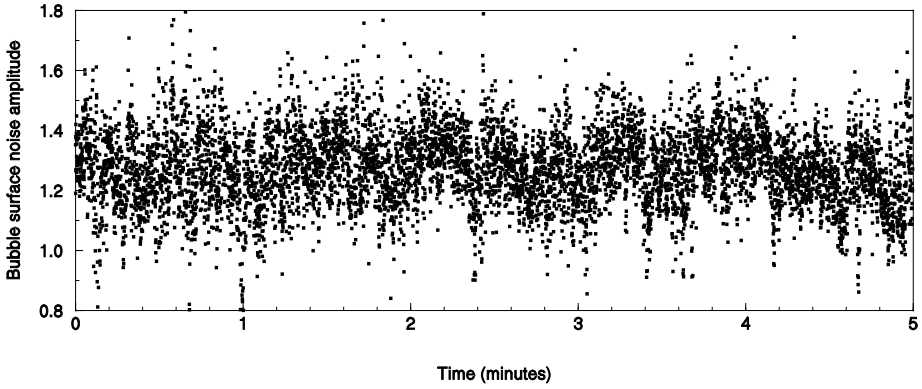

(c)

Figure 4.11.: Variation of the average bubble surface noise amplitude for (a) 10–20 %, (b) 50–60 % and (c) 90–100 % bubble size distribution deciles over five minutes (7500 frames) in one condition in platinum system.

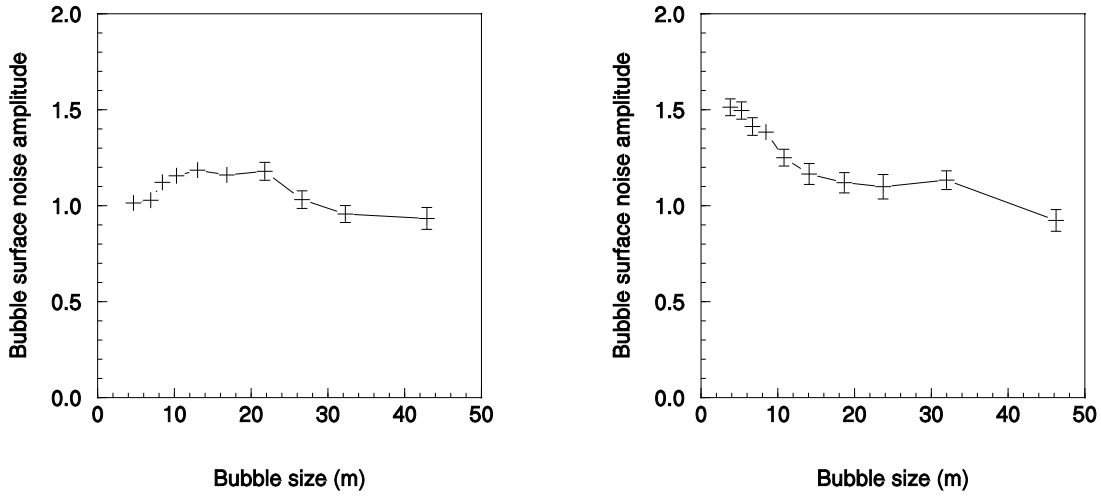

(a) Copper (b) Platinum

Figure 4.12.: The 95% confidence interval for the bubble surface noise amplitude measurement using four frames of data in one condition on each experimental system.

The results of the measurements shown support hypothesis 4.1 and shows that bubble loading, as interpreted by this measure, varies as a function of bubble size.

Visual assessment of solids loading measurement

Hypothesis 4.1 asserts that solids loading on the froth surface affects the visual appearance of bubbles on the froth surface. In addition, this effect has been linked to the texture of the froth surface in terms of roughness. In this section, the effectiveness of the bubble surface noise amplitude measurement is visually assessed with respect to appearance of the bubble surface.

Figure 4.13 shows images of individual bubbles grouped by their bubble surface noise amplitude value. Figure 4.13 shows that bubbles with low BSNA values appear to have a more uniform surface, whereas bubbles with higher BSNA values look like they have more imperfections on the bubble surface. In the majority of cases, these imperfections occur due to the bubble on the surface being translucent, through which the structure of the bubbles below the bubble on the surface is apparent.

These results suggest that the froth surface roughness measurement (BSNA) is able to differentiate between bubbles that are uniformly coated and opaque, from bubbles that are more sparsely coated and translucent, thus providing support for the first part of hypothesis 4.1.

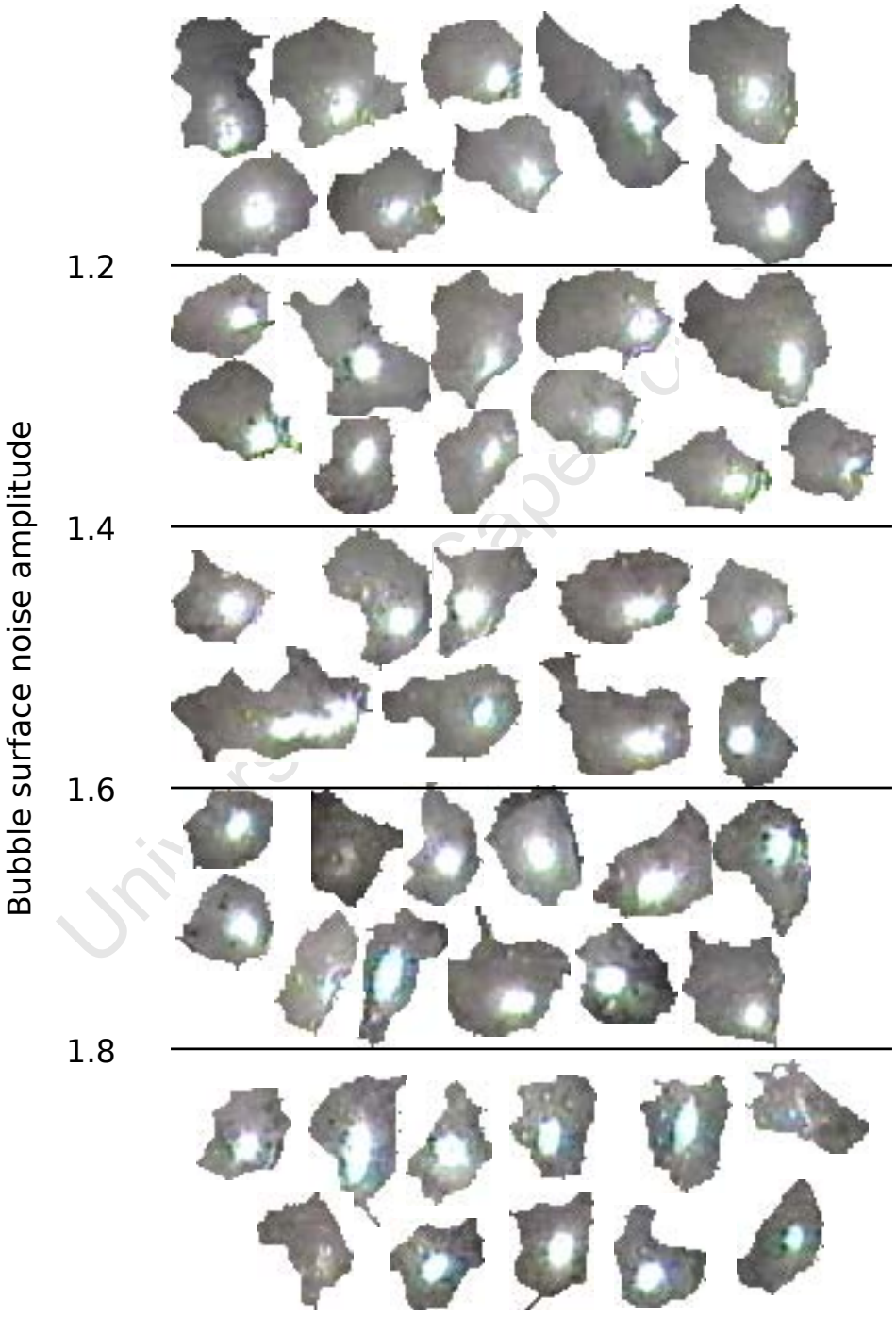

Figure 4.13.: Individual bubbles grouped by their bubble surface noise amplitude values.

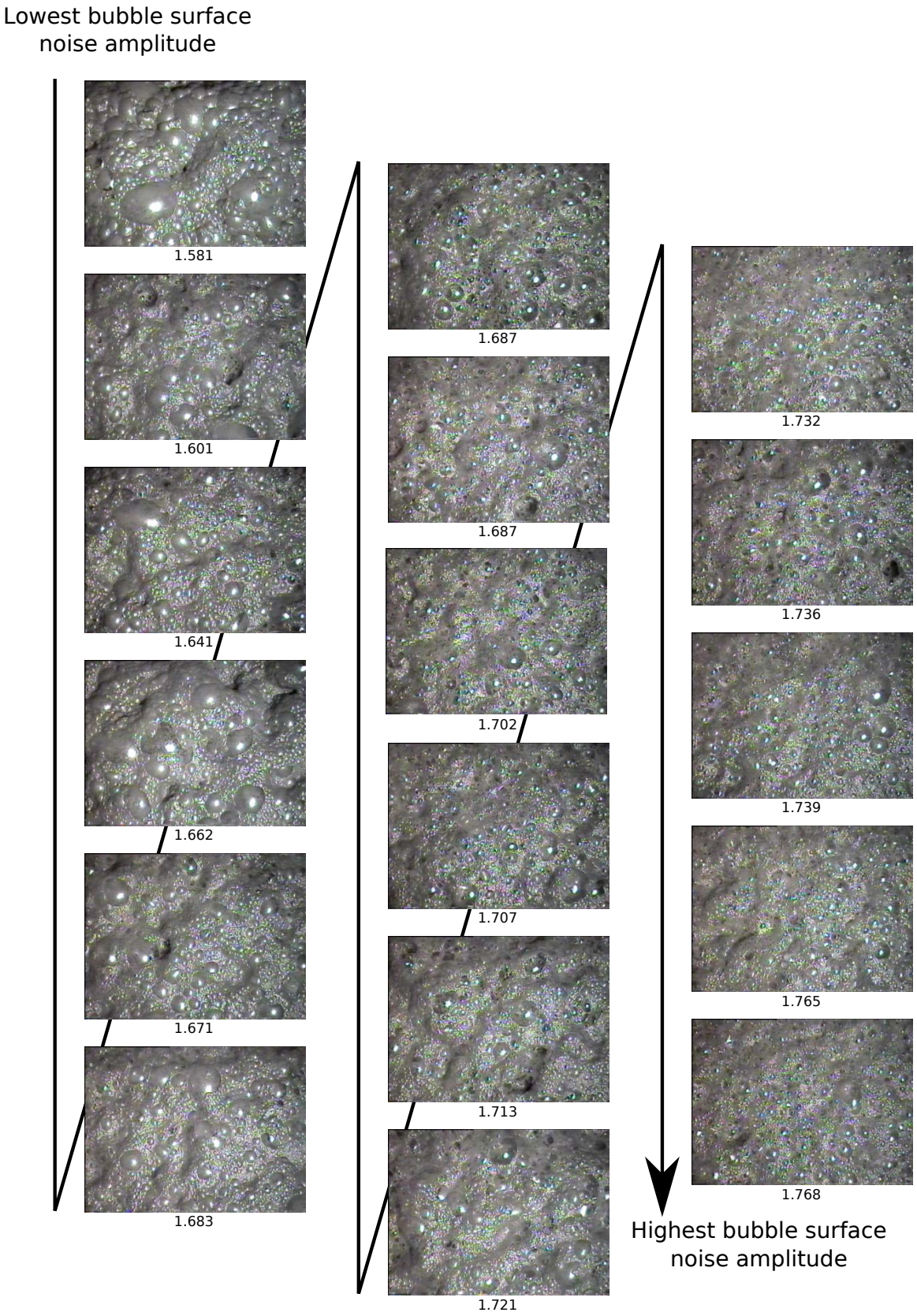

Figure 4.14.: The froth surface appearance across different operating conditions, arranged from the lowest bubble surface noise amplitude to the highest bubble surface noise amplitude.

In terms of the entire froth surface, the average BSNA value of all the bubbles within a frame can be determined. Figure 4.14 shows images of the froth surface which arranged in order of lowest to highest BSNA, across different operating conditions. Generally, the average bubble size decreases as the bubble surface noise amplitude increases. This is expected, as bubble coalescence drives an increase in solids loading as the bubble size increases.

Hypothesis 4.2 asserts that bubble loading and thus, assuming hypotheses 4.1 is true, froth surface roughness is modified in different ways by the two identified froth surface coalescence mechanisms. In order to confirm that the bubble surface noise amplitude measurement is able to detect differences between the two mechanisms governing solids loading on the froth surface, as identified in section 4.1.1, bubbles undergoing these two mechanisms of coalescence have been analysed across a number of frames before and after both of the coalescence mechanisms have occurred, as shown in figures 4.15 and 4.17.

Figures 4.15(a) and 4.16(a) show series of consecutive images, where two bubbles (red and green markers) coalesce with each other to form a resulting bubble (black marker). Figures 4.15(b) and 4.16(b) show the variation of the average bubble surface noise amplitude and the variation in bubble size for the bubbles in this series of frames. The coalescence between the two adjacent bubbles result in a bubble which has a lower bubble surface noise amplitude measurement than the average value between the two coalescing bubble. This is in line with the expectation that as the bubble loading increases, the bubble surface appears smoother, as bubbles below the froth surface are not visible.

Figures 4.17(a) and 4.18(a) show series of images of bubbles changing size due to coalescence with bubbles below the froth surface. Figures 4.17(b) and 4.18(b) shows the variation of the average bubble surface noise amplitude and the variation in bubble size for the bubbles in these frame series. As the bubble's size increases, the bubble surface noise amplitude measurement of that bubble's surface increases, which is in line with the expectation that the bubble loading decreases, causing a greater amount of variation on the bubble surface. Thus, it has been shown that the average bubble surface noise amplitude measurement is sensitive to the two identified surface coalescence mechanisms, providing support for hypothesis 4.2.

The analysis shows that the bubble surface noise amplitude varies between frames where no significant event has occurred. This occurs owing to variations in the quality of the footage obtained. Well focused sharp images tend to produce higher bubble surface noise amplitude values than images which suffer from blurring due to either motion, or poor camera focus. The analysis of sufficient images to obtain a robust average of the response mitigates this effect.

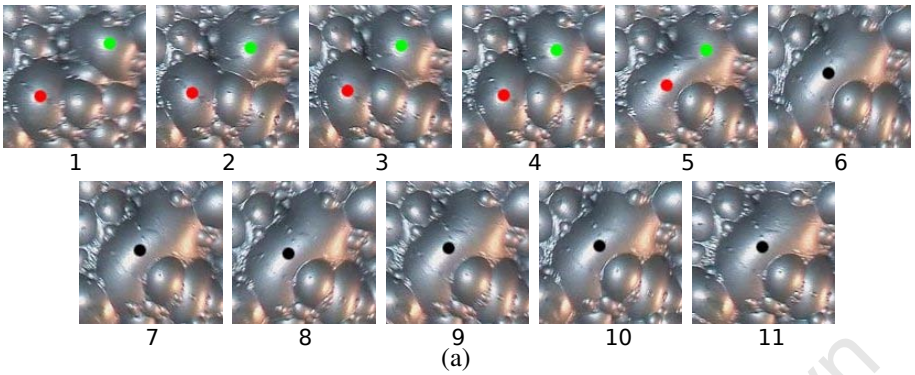

(a)

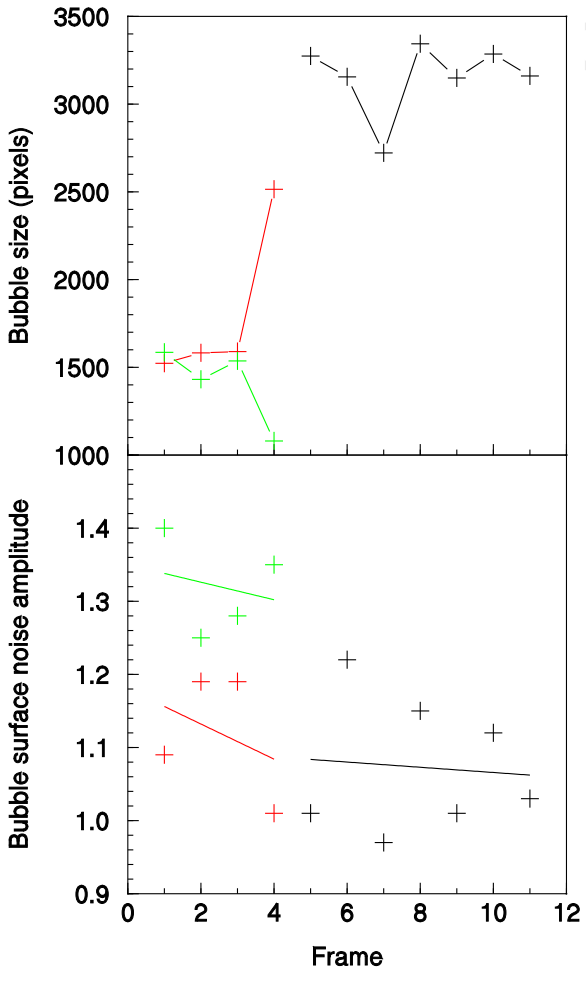

(b)

Figure 4.15.: A series of consecutive frames (a), where two adjacent bubbles on the surface (red, green) coalesced with each other to form a final bubble (black) and the measured bubble surface noise amplitude and bubble size (b), corresponding to the series of consecutive frames.

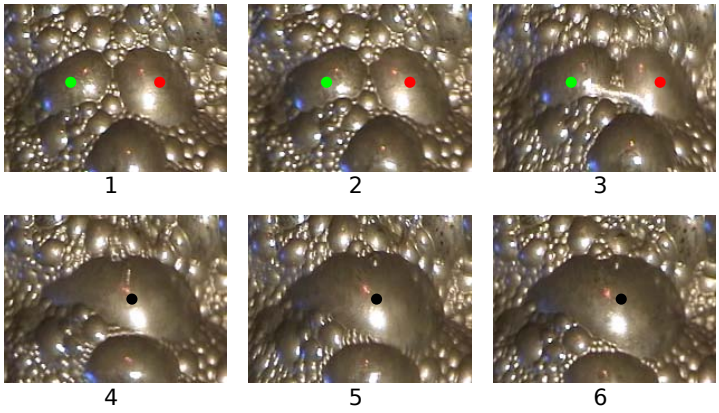

(a)

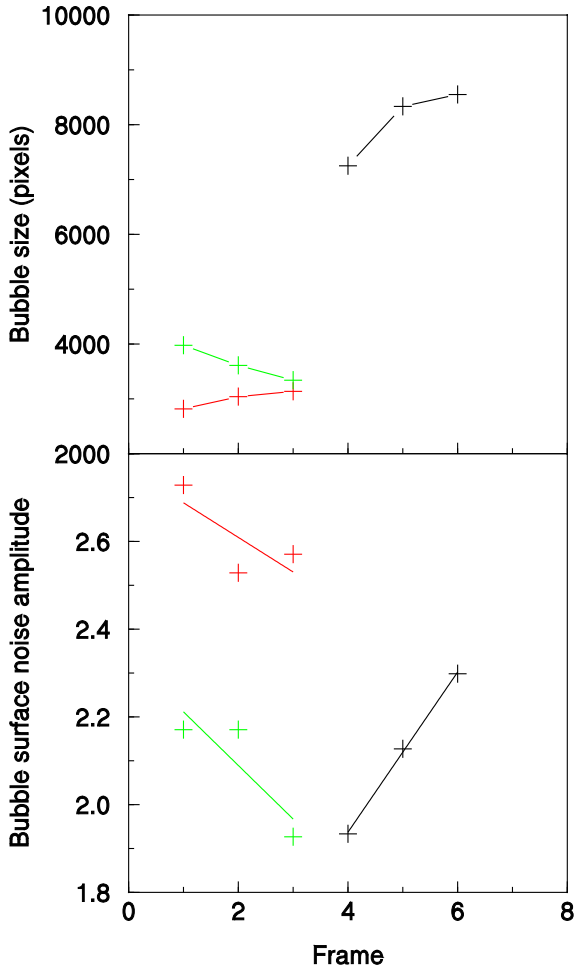

(b)

Figure 4.16.: A series of consecutive frames (a), where two adjacent bubbles on the surface (red, green) coalesced with each other to form a final bubble (black) and the measured bubble surface noise amplitude and bubble size (b), corresponding to the series of consecutive frames.

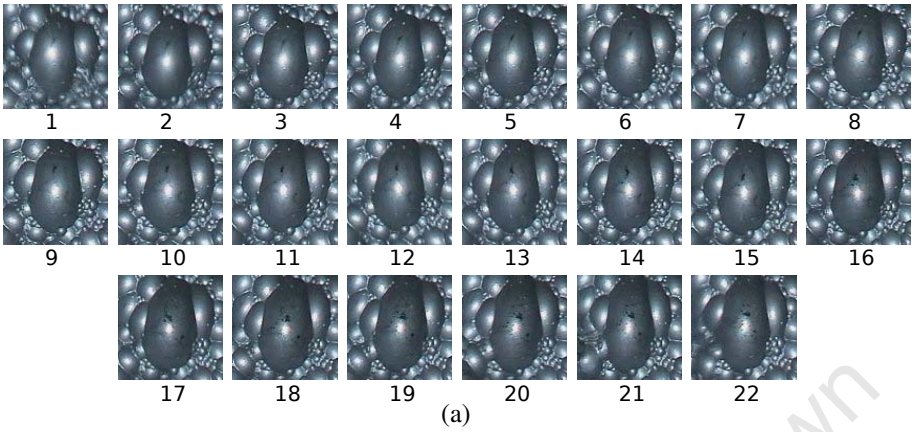

(a)

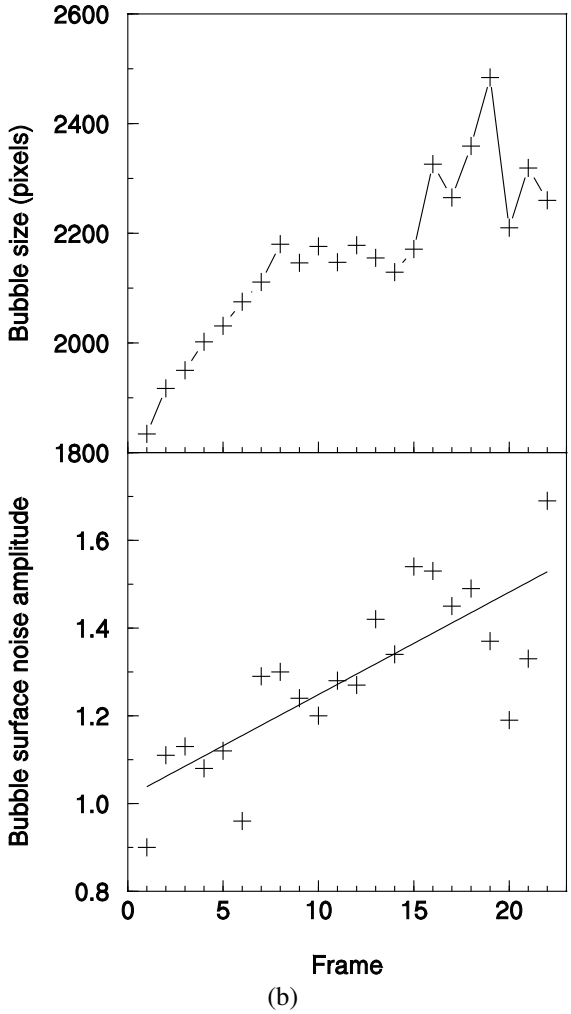

(b)

Figure 4.17.: A series of consecutive frames (a), where the bubble on the froth surface expanded due to coalescence with bubbles below it, and the bubble surface noise amplitude and bubble size (b), corresponding to the series of consecutive frames.

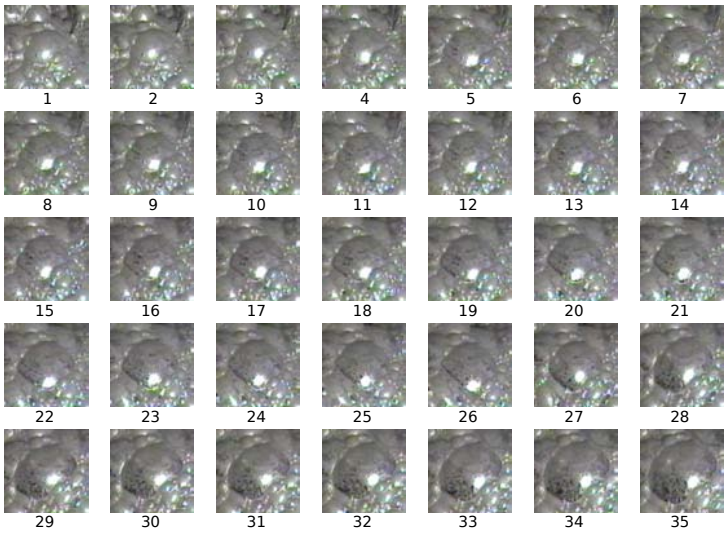

(a)

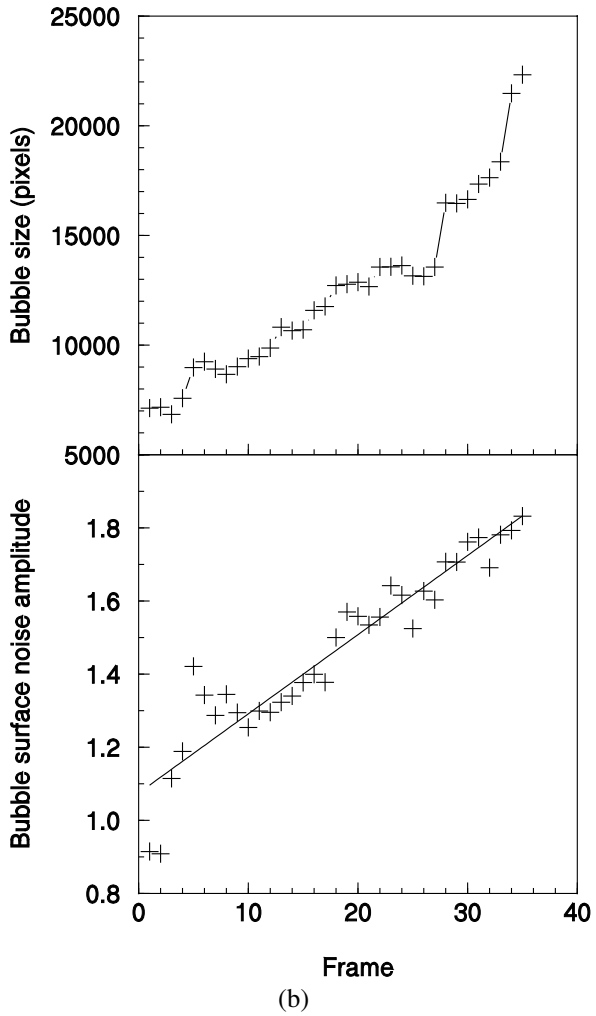

(b)

Figure 4.18.: A series of consecutive frames (a), where the bubble on the froth surface expanded due to coalescence with bubbles below it, and the bubble surface noise amplitude and bubble size (b), corresponding to the series of consecutive frames.

4.1.4. A comparison of solids loading measurements

The gravimetric method (Sadr-Kazemi and Cilliers (2000)) described in section 3.3 has been used for comparison. This measurement is easy to perform and is robust in systems that have homogeneous froth surface bubble size distribution, low surface burst rates and bubbles of larger than average size. However, on systems that exhibit either high amounts of bubble bursting, a wide range of froth surface bubble size distributions or smaller bubble sizes, the gravimetric based solids loading measurement becomes difficult to perform.

Within these problematic systems, measurements are subject to human bias, towards underestimating solids loading. This occurs due to the tendency to sample less frequent, but larger bubbles that have grown due to coalescence below the froth surface as described in section 4.1.1. This mechanism only occurs on the froth surface. Typically, conventional coalescence within the froth, results in an increase in solids loading with bubble size. As such, a wider range of bubble loading occurred at larger bubble sizes, as observed by the increase in variability with bubble size for the upper end of the bubble size distribution in figures 4.10 and 4.11. The larger bubble sizes are more easily sampled and thus attract sample bias.

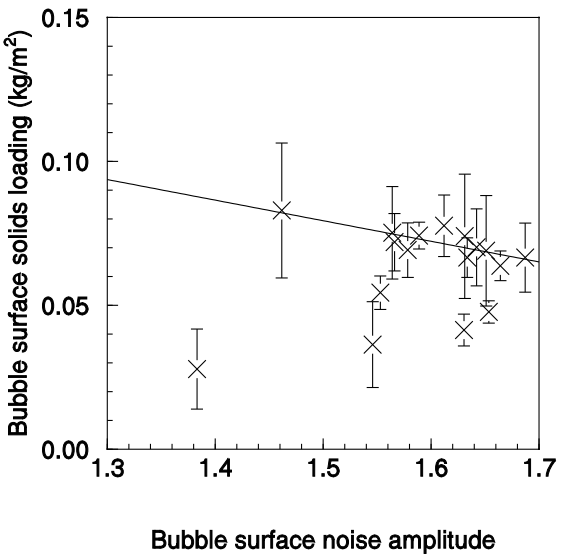

Figure 4.19.: Measured bubble loading versus average bubble surface noise amplitude across the top three deciles of the bubble size distribution (the error bars represent the 95 % confidence intervals).

Figure 4.19 shows the measured bubble loading, using the gravimetric technique versus the average bubble surface noise amplitude. Four or five samples were taken using the gravimet-

ric technique, whereas 7500 consecutive frames were sampled using the bubble surface noise amplitude measurement. The top three bubble size distribution deciles were used to determine the average bubble surface noise amplitude, which account for the bias towards larger bubbles from the samples taken using the gravimetric technique. The results shown in figure 4.19, show that the majority of the BSNA measurements correlate with the solids loading measurements. However, some outliers are present.

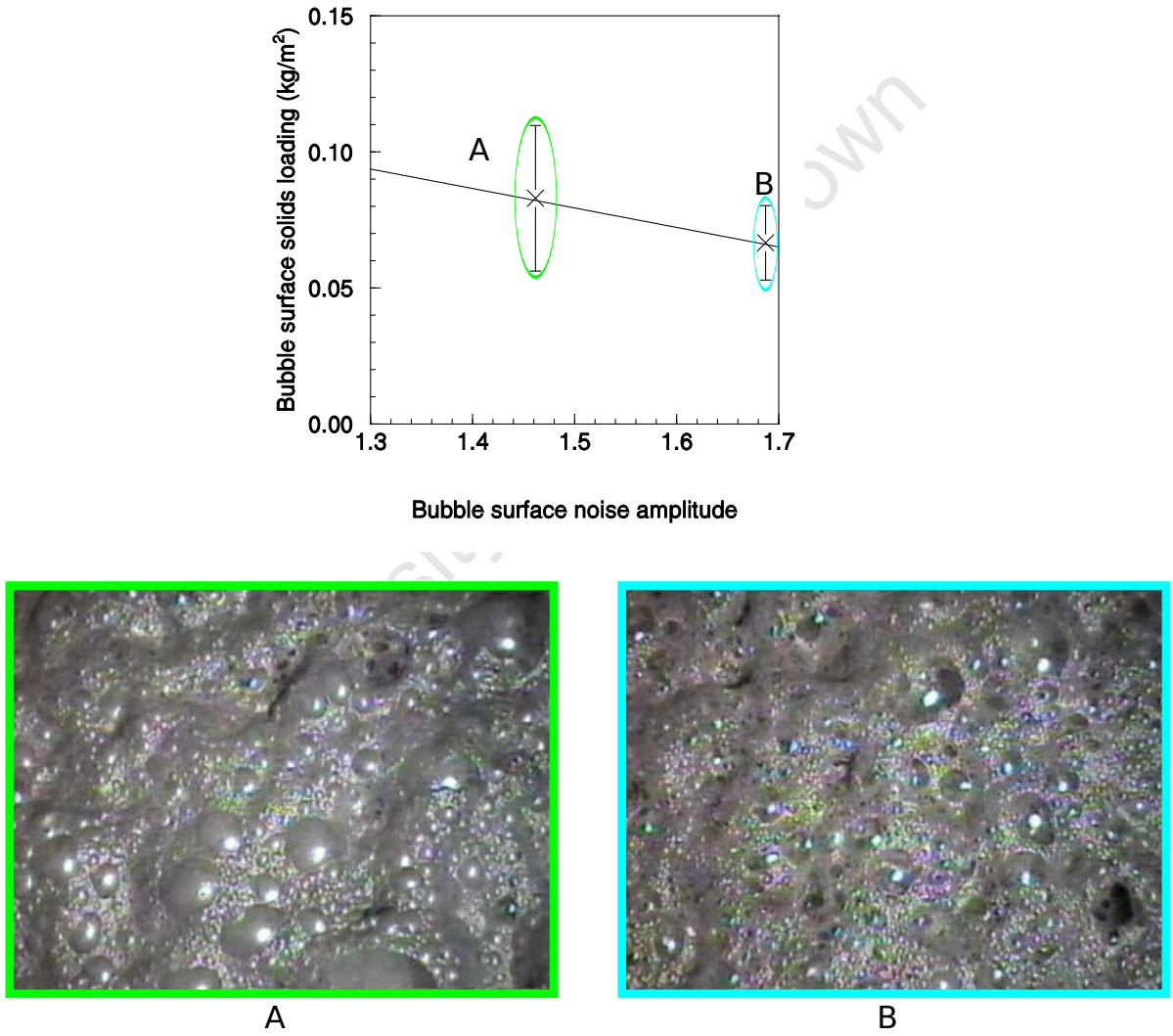

Figure 4.20.: A visual comparison between measured solids loaded and the average bubble surface noise amplitude for two of the conditions shown in figure 4.19.

Figures 4.20 and 4.21 both show a visual comparison between extreme points from figure 4.19 and the typical appearance of the froth surface under those operating conditions. Figure 4.20 shows that, as expected, image A appears less translucent than image B, from which a higher inferred solids loading has a lower average BSNA measurement. However, figure 4.21 shows

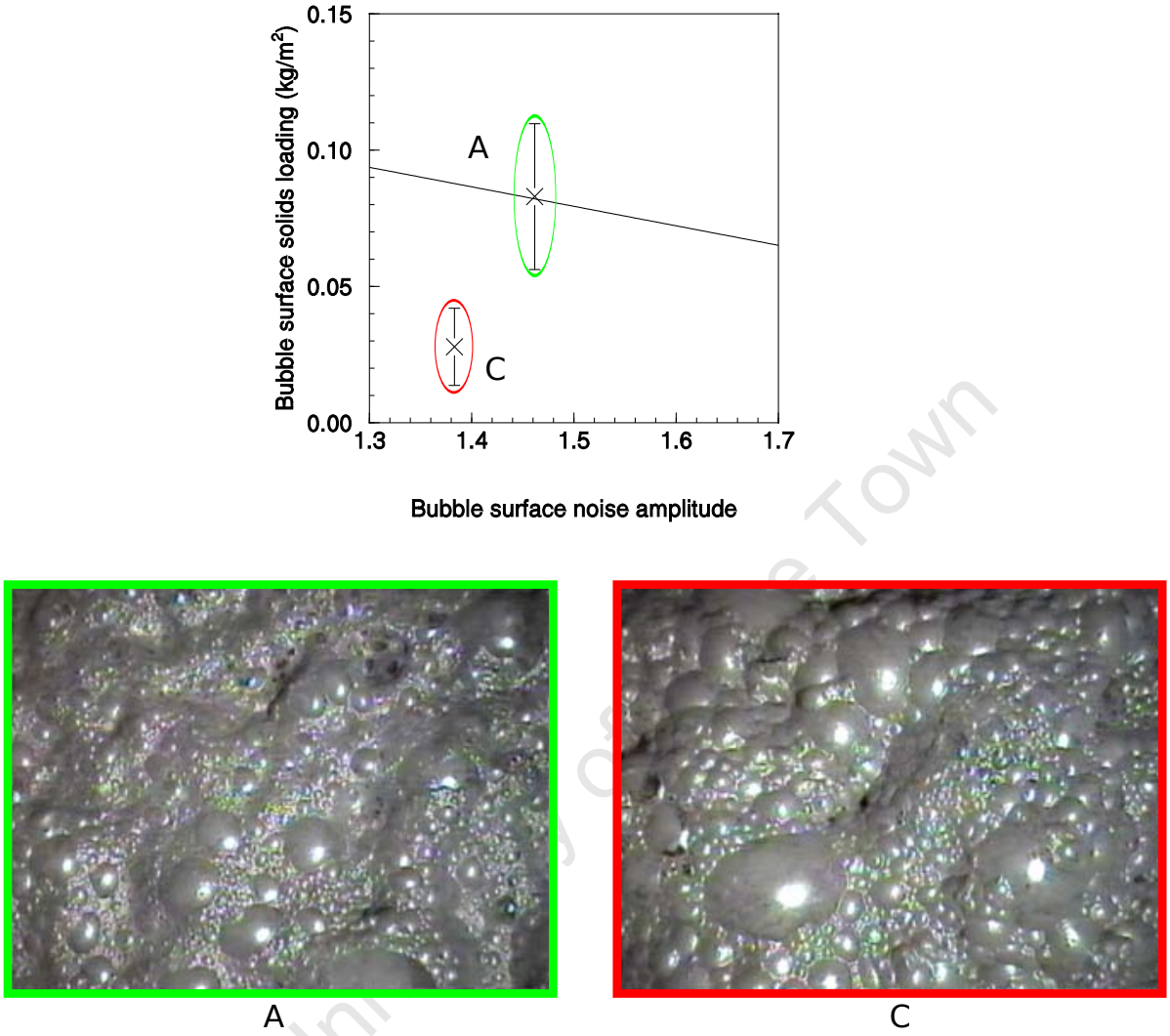

Figure 4.21.: A visual comparison between measured solids loaded and the average bubble surface noise amplitude for two conditions shown in figure 4.19.

that the measured solids loading for image C is less than that of image A, where both visual and the BSNA measurement suggest a higher bubble loading. Thus, it is possible that the specific bubbles sampled using the gravimetric method had undergone coalescence with bubbles below the froth surface, resulting in a lower solids loadings for those specific samples. As the bubble surface noise amplitude varies over a wider range at larger bubble sizes, as shown in figures 4.10 and 4.11, these lower points have most likely been subject to measurement bias. This bias occurred as result of sampling larger bubble lamellae that have had their solids loading decreased due to coalescence with bubbles below the froth surface.

The above-mentioned figures have trend lines plotted through the points that are not considered to be outliers. The outlier points can be visually confirmed to have similar solids loadings as the points vertically above them, as illustrated in figures 4.14 and 4.21.

These results show that as the bubble size increases, the accuracy of the gravimetric measurement decreases, although variable precision is evident across the conditions. A visual assessment of the froth surface and corresponding bubble surface noise amplitude measurement shows that the measurement is able to quantify the qualitative judgement, obtained visually, of the solids loading on bubbles on the froth surface. Thus, these results further provide support for hypotheses 4.1 and 4.2.

4.1.5. Calibration of the solids loading measurement

From the comparison between the machine vision and gravimetric solids loading measurements, a calibration can be determined by excluding the under-estimated loadings determined from the gravimetric method. In order to obtain a good relationship between the solids loading measured using the gravimetric technique and the average bubble surface noise amplitude, the input parameters for the machine vision method need to be calibrated.

Due to the nature of top-hat algorithm, a change in the top-hat radius will affect the resulting amplitude of the high frequency signal output proportionally to the change in top-hat radius. As the amplitude of the high frequency signal output changes, the cut-off threshold needs adjustment. Thus, a relationship exists between the top-hat radius and cut-off threshold.

This relationship between parameters is determined by performing a comparison between the gravimetric solids loading measurements and the average bubble surface noise amplitude, measured for different top-hat radii and cut-off threshold values.

Video footage obtained at each condition was analysed to obtain the average bubble surface noise amplitude measurement using a combination of top-hat radius and cut-off threshold values across a specified range. The results from this analysis were tested using an F-test for goodness of fit, and the F statistic value for each condition tested has been plotted in figure 4.22.

These results show an optimum relationship between the top-hat radius and cut-off threshold, which is shown in figure 4.23. This relationship is an approximate linear relationship between the top-hat radius and cut-off threshold value exists to obtain an optimal correlation between solids loading and the average bubble surface noise amplitude.

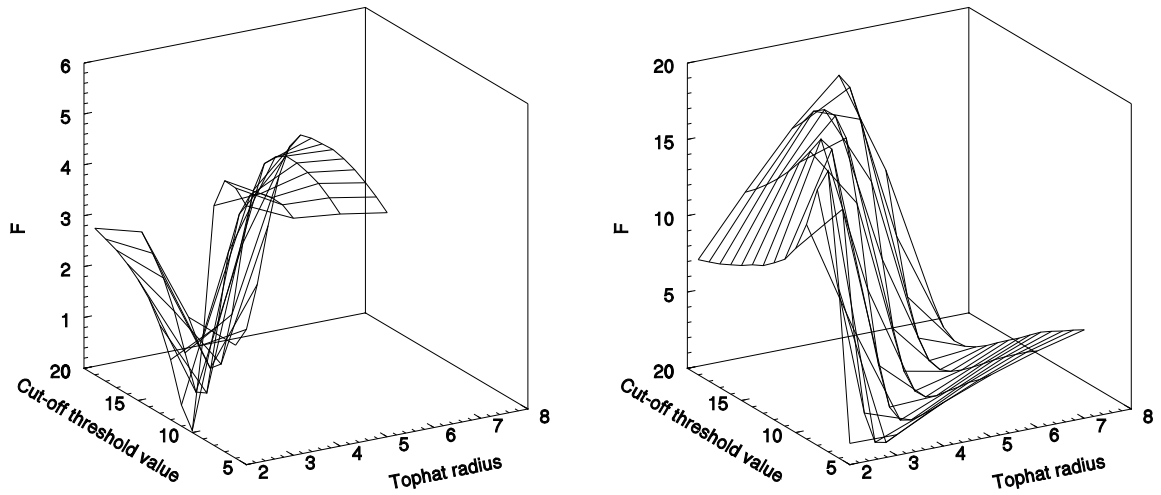

(a) Copper (b) Platinum

Figure 4.22.: The results from the F-test for goodness of fit, determined when using different values of top-hat radius and cut-off threshold, when comparing the average bubble surface noise amplitude measurement with solids loading measurements obtained by the gravimetric technique.

As the top-hat radius is increased, the relationship between solids loading and the average bubble surface noise amplitude, as shown in figure 4.24 tends to flatten out horizontally. Thus, lower values for the top-hat radius and corresponding cut-off threshold values, read from figure 4.23 are preferred.

Due to the nature of this measurement, it is expected that the quality and sensitivity of the data will increase with higher resolution images. Currently, SmartFroth uses a resolution of 320 $\times$ 240 pixels per image (constrained by computational speed limitations) for viewing froth areas. Typically the width of the field of view occurs anywhere between 10–50cm. Thus, one pixel can represent anywhere from 1.6mm to 0.3mm.

Since this measure is a factor of image resolution, the noise amplitude will increase for lower camera focal lengths. Thus, on a typical plant, where camera focal length decreases down the bank (because bubble size typically decreases down the bank), a calibration is required for each cell, individually. However, it is expected that for a given ore ground to a specific target particle size distribution, a robust relationship between the bubble surface noise amplitude and solids loading can be obtained for different focal lengths.

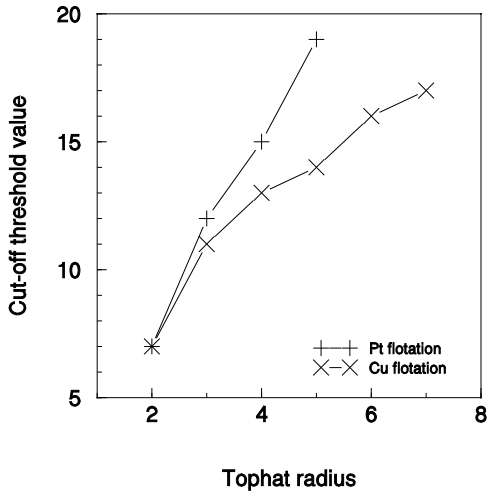

Figure 4.23.: Threshold and top-hat radius values, which maximize the F statistic obtained when comparing the average bubble surface noise amplitude measurement with the solids loading measurement obtained by the gravimetric technique.

In the case of larger millimeter to pixel ratios, this method may show large variability between single images. The analysis of sufficient images to obtain a robust measurement minimises this effect.

Figure 4.24 shows the resultant calibration curve for the platinum and copper systems once the appropriate top-hat radius and cut-off threshold values for each system was determined.

The top three decile measurements determine the average bubble surface noise amplitude measurement, as the solids loading measurement using the bias in the gravimetric method is towards larger bubbles.

Thus it is possible, assuming a linear relationship between the calibration curve for the top three bubble size decile range, to extrapolate across all the bubble size deciles to determine the bubble solids loading as a function of bubble size, as shown in figure 4.25.

The results in figure 4.25 correspond to the results analysed in figure 4.9. However, instead of calculating the solids loading for a single frame of data, this was performed across five minutes of video footage. The copper results correspond well, where the solids loading decreases and then increases with bubble size, while in the case of the platinum results, the solids loading increase with bubble size is slight.

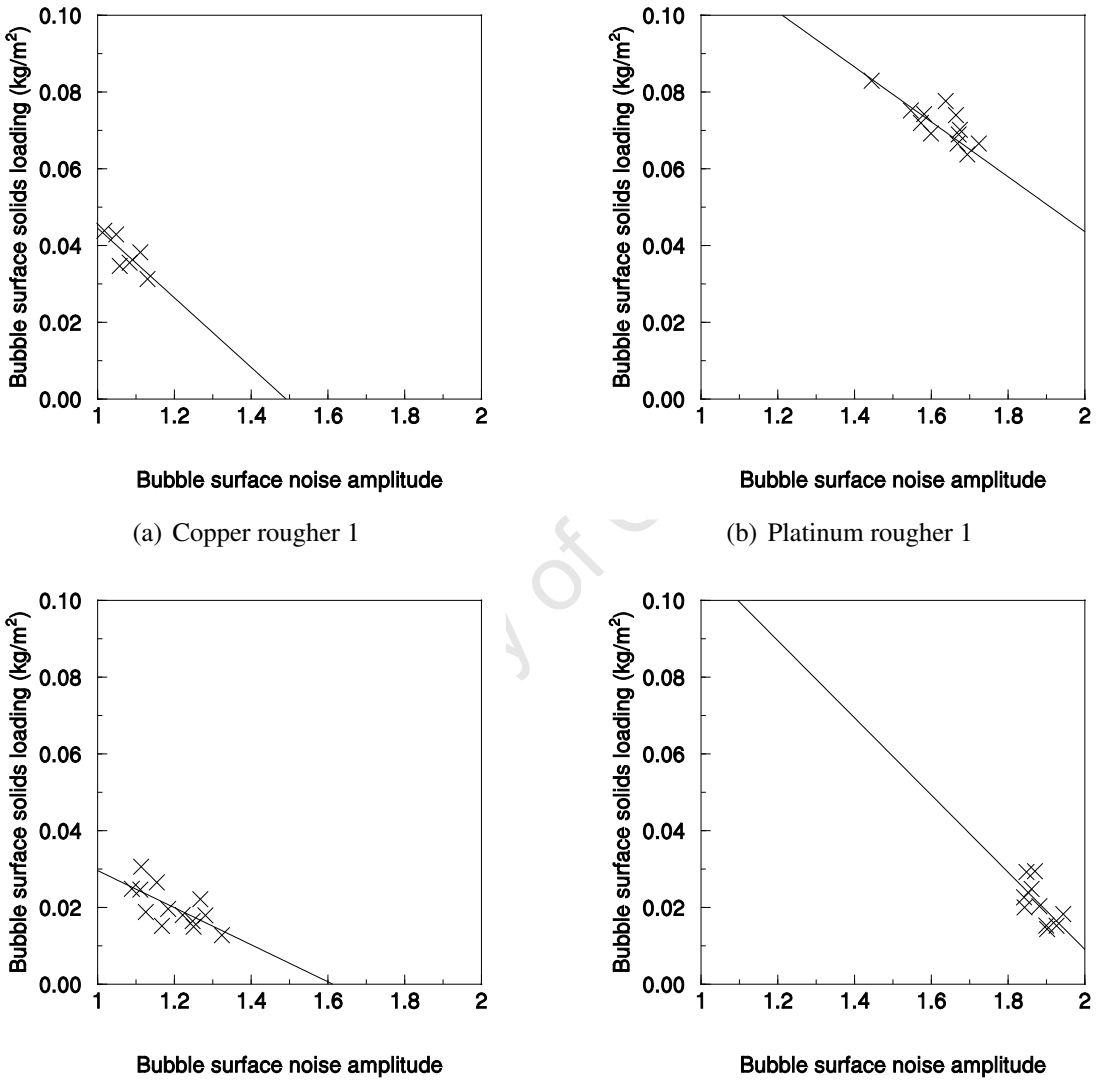

(a) Copper rougher 1

(b) Platinum rougher 1

(c) Copper rougher 3

(d) Platinum rougher 3

Figure 4.24.: Measured bubble loading versus average bubble surface noise amplitude for samples across the top three bubble size distribution deciles. This figure excludes the outliers similar to those shown in figure 4.19.

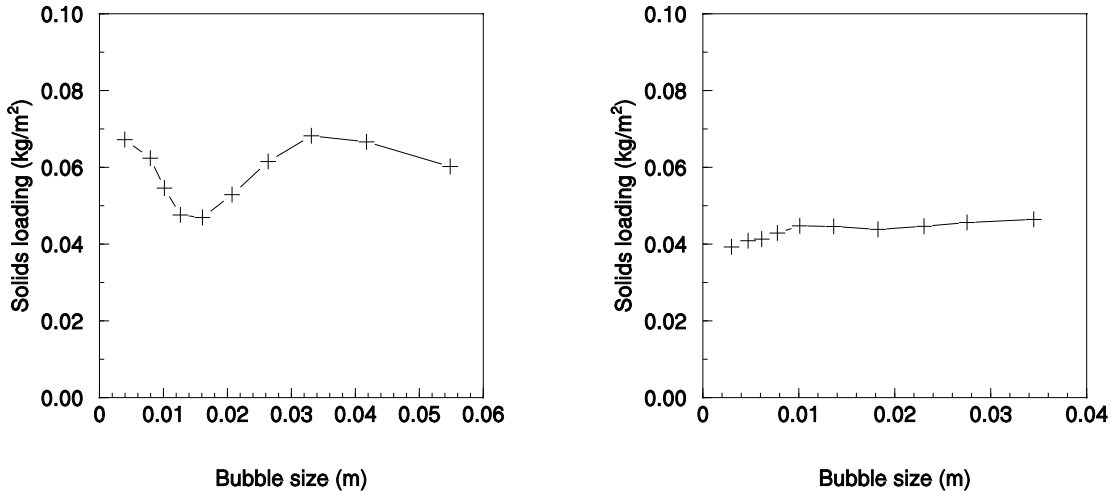

(a) Copper (b) Platinum

Figure 4.25.: Measured solids loading versus bubble size, calibrated from the bubble surface noise amplitude measurement.

The results presented thus far support the hypotheses presented at the start of this chapter. Evidence that the froth surface appearance relates to the solids loading on the froth surface is shown and a measure of this appearance characteristic has been developed.

4.1.6. Combining solids loading and other measurements

The proposed solids loading measurement, combined with additional measures can be used to estimate of a number of useful flotation performance indicators.

For example, the solids loading may be an important factor in the estimation of solids recovery to the concentrate. However, solids loading only provides information for one of the solid components recovered to the concentrate; the others being detached and entrained solids. Also, the use of a solids loading measurement assumes that solids loading on the lamellae below the froth surface is similar to that on the froth surface. However, it is likely that the froth surface loading is higher than the froth below the surface due to additional solids re-attaching from bubbles that burst in the top few layers of froth.

Froth structural, froth transport and solids loading factors all relate to the overall solids recovery to the concentrate. The key froth structural factor that affects solids recovery is the surface area available. The available surface area is inversely related to bubble size, where

froths consisting of small bubbles have large surface areas. The key froth transport factor is the rate at which the froth flows into the launder, typically measured using the froth velocity. In addition, it is expected that the solids loading near the froth surface will indicate the mass of solids associated per unit surface area near the froth surface. Thus, the solids recovery to the concentrate ($M_{s,conc}$) is proportional to the froth velocity (v) and solids loading (Γ_s) and inversely proportional to the froth overflow Sauter mean bubble size ($d_{32,fs}$).

$$M_{s,conc} \propto \frac{v \cdot \Gamma_s}{d_{32,fs}} \tag{4.1}$$

Equation 4.1 shows that the solids recovery rate of attached material to the concentrate is directly related to froth velocity, solids loading and bubble size.

Hypothesis 4.3
Thus, it is hypothesised that a solids loading measurement on the froth surface will improve the prediction of the overall solids recovery rate using velocity and bubble size measurements.

Chapter 3 describes the solids recovery measurements taken in the two experimental systems. It is possible to test the effectiveness of the addition of the novel machine vision based solids loading measurement to the above relationship by performing a regression analysis.

The four data sets chosen to test the effectiveness of the new machine vision measurements represent four ore conditions with different concentrations of floatable solids and floatable particle hydrophobicities. The four data sets chosen were the first and third roughers from the copper and platinum data sets referred to in chapter 3. The floatable minerals in the copper system were highly hydrophobic, while the floatable minerals in the platinum system were of low hydrophobicity. The floatable solids concentration is high in the first cell and much lower in the third cell of a rougher bank.

Within each of these systems, the solids recovery rate to the concentrate was measured by collecting timed samples that were dried and weighed. SmartFroth measured the velocity, bubble size distribution and solids loading on the froth surface. Additional solids loading measurements were taken using the gravimetric method.

The experimental procedure and measurements taken for each of the above-mentioned data sets are described in chapter 3. The raw data from these measurements which are also used in the following analysis are presented in appendix A.

The effect of the proposed solids loading measurement was investigated by performing a regression analysis to empirically model the solids recovery. The extent to which solids loading improved the solids recovery estimation was investigated by performing subsequent regression analyses where the inverse bubble size and solids loading measurements were added to the velocity measurement. In addition, the effect of the gravimetric solids loading measurement was also investigated. The results from this regression analysis are presented in appendix B.1.

Figure 4.26 shows the results of a regression model to measure solids recovery using the velocity and bubble size with and without the machine vision and gravimetric solids loading measurements. The results show that some relationships are evident between these factors and the solids recovery. However, it is clear that the differences between the model relationships are subtle, and it is difficult to discern any measure of improvement that the solids loading measurement has on the relationship between the model and the actual measurement.

Table 4.1.: The significance of an F-test for goodness of fit (measured in percent) from the modelled versus measured solids recovery relationship when the bubble size and machine vision and gravimetric solids loading measurements were subsequently added to velocity in the regression model.

	Velocity	**Velocity, Bubble size**	**Velocity, Bubble size Solids loading (MV)**	**Velocity, Bubble size Solids loading (GV)**
Copper rougher 1	76.9	99.4	99.8	99.4
Copper rougher 3	90.2	87.9	80.7	83.1
Platinum rougher 1	91.2	98.7	96.7	99.3
Platinum rougher 3	84.1	95.4	93.7	92.9

Table 4.1 show results from the F-test for goodness of fit for the regression analysis performed. The data reported is the significance of F, measured in percent ($100(1-p)$). These results show the extent to which the addition of the bubble size and solids loading measurements to the froth velocity improve the determination of the rate of solids recovery to the concentrate.

These results show that the froth velocity relates poorly to the solids recovery to the concentrate across the range of conditions tested. However, the addition of the froth surface bubble size tends to improve the relationship significantly (with the exception copper rougher 3). The added bubble size improved the relationship by increasing the significance of the fit of the regression model by up to 22 %.

However, the addition of the solids loading measurements only allowed for a marginal improvement in some cases, and a decrease in the model fit in other cases.

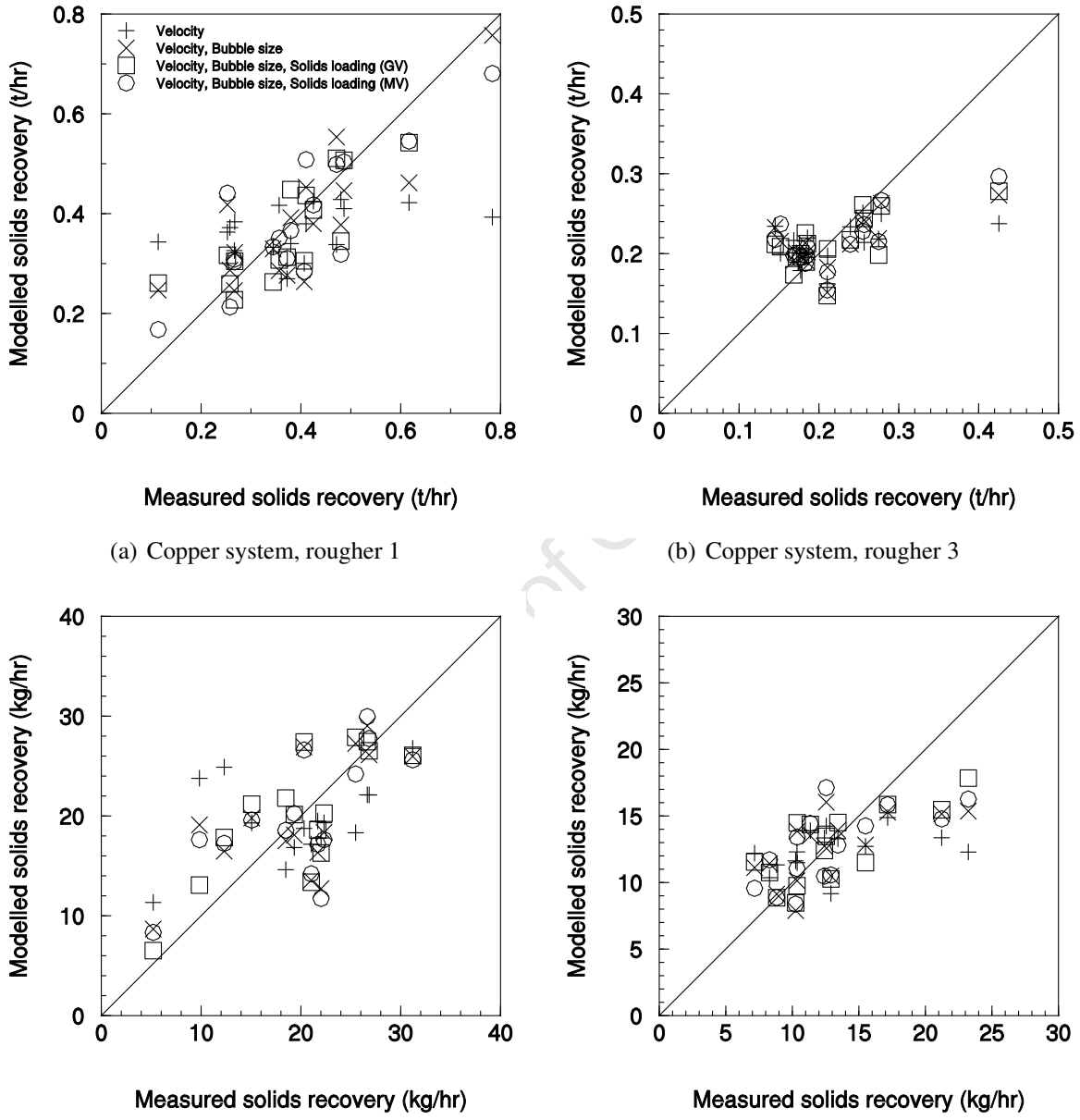

(a) Copper system, rougher 1

(b) Copper system, rougher 3

(c) Platinum system, rougher 1

(d) Platinum system, rougher 3

Figure 4.26.: Measured solids recovered versus modelled solids recovered, as determined from a regression using velocity and the bubble size inputs, with and without the machine vision and gravimetric solids loading measurements.

In the copper rougher 1 system, the consideration of the solids loading improves the relationship between velocity and bubble size to solids recovery. Under this condition, the observed variation in the machine vision solids loading measurement correlated with the rate of solids recovered to the concentrate and this component and the bubble size were significant contributors to the overall relationship in the regression model. This was not true for any conditions where the solids loading showed an insignificant benefit.

Comparing the effect of the machine vision solids loading measurement with the gravimetric solids loading measurement shows that the two measures performed differently to each other.

These results show that the measurement of solids loading on the froth surface only sometimes partly accounts for changes in the mass flow of solids to the concentrate, disproving hypothesis 4.3. In addition, the solids loading appears much less significant than either the velocity or bubble size factors. This is explained by the proportion of entrained material recovered to the concentrate changing across the different conditions. The amount of entrained material present is a strong function of froth structure, and is reflected in the change in bubble size.

In addition, assumptions that are made by equation 4.1 may not hold true under a wide range of operating conditions. The main assumption that this equation makes is that each parameter is constant across the excess froth height that overflows the weir. Thus, the velocity profile of the froth needs to be flat, the solids loading on bubbles below the surface need to be similar to those on the surface and the measured froth surface bubble size would need to be representative of the froth layers below the surface that get recovered.

4.2. Measurement of the burst rate

Within conventional flotation cells, air enters the cell near the impeller, where the shearing forces surrounding the impeller region break up the air into small bubbles. The air then passes through the pulp phase as bubbles, to which particles may attach upon collision. Under certain conditions, these bubbles may also coalesce upon collision with each other. However, the frother reagent present minimises this effect.

The bubbles enter the froth phase at the pulp-froth interface and move up through the froth, owing to froth expansion, driven by the addition of bubbles at the pulp-froth interface. At the froth surface, the froth flows towards the collection launder as a result of the froth expansion and due to a pressure buildup either at the centre of the cell, or along any constrained wall or side of the flotation cell.

Both froth structural and transport factors define the mass of material (water + solids) recovered to the concentrate. The principal froth structural factor affecting mass recovery is froth surface area per unit volume, while the principal transport factor is the volume of froth recovered, influenced by the air flow rate into the flotation cell and the rate of air loss on the froth surface.

The air flow rate into the flotation cell and the rate of air loss on the froth surface determines the volumetric recovery of froth. The air flow rate into the flotation cell is often known and is sometimes manipulated for control purposes in forced air flotation cells.

Ventura-Medina *et al.* (2003) proposed a method to approximate the amount of air recovered to the concentrate through the measurement of the froth volume recovered to the concentrate. However, this approach does not measure the absolute amount of air recovered, as it includes the water and solids recovered with the froth. Using this approach it is possible to measure the air recovery rate to the concentrate.

By combining volumetric recovery of froth to the concentrate with a measure of air fed into the flotation cell and accounting for the rate of air loss to the tailings, one can estimate the proportion of air lost on the froth surface.

Within this thesis, a proposed method to measure the direct air loss from the froth surface near the launder incorporates the comparison of consecutive frames of segmented bubbles to identify bursting bubbles and an estimation of air loss by estimating the volume of the bursting bubbles.

The watershed segmentation algorithm is used to segment an image into regions that represent bubble lamellae on the froth surface.

Hypothesis 4.4
Thus, it is hypothesised that by comparing segmentation results of subsequent frames it is possible to detect bursting bubbles.

Should be possible to detect the rate of bubble burst events, it should be possible, by estimating the volume of air contained within bursting bubbles, to determine a measure of the rate of air loss from the froth surface.

Bubbles burst on the froth surface as a result of destabilised surface lamellae and thus, the rate at which this occurs relates to the overall stability of the froth.

It is widely accepted that the concentration of attached solids present within a froth tends to stabilise the froth. Thus, that bubbles that are less stable, which burst on the froth surface may do so owing to lower concentrations of attached solids.

Hypothesis 4.5
Thus, it is hypothesised that the measured solids loading on bubbles that are about to burst will be lower than the average solids loading on the froth surface.

As bubbles increase in size, they become less stable, due to the interfacial forces required to maintain the bubble lamellae as the surface area to volume ratio decreases.

Given that the image regions determined by the watershed segmentation represent the size of bubbles on the froth surface, it is possible to determine the fraction of bubbles that burst as a function of bubble size.

Hypothesis 4.6
Thus, it is hypothesised that a higher fraction of larger bubbles present on the froth surface will burst, when compared to smaller bubbles.

4.2.1. Behaviour of air on froth surface

On the froth surface, three distinct mechanisms occur which result in the loss of air.

- **Surface film or lamella bursting**
  This is the most common mechanism for air loss on the froth surface. The lamella on the froth surface ruptures, exposing bubbles below it. This occurs due to film drainage, resulting in either thinner films or film expansion which leads to the lowering of solids coverage.

- **Froth 'Boiling'**
  Froths comprised of smaller bubbles that contain a high liquid content are prone to froth boiling. Larger bubbles entering the froth, or developing within the froth, due to their higher buoyancy, race through the froth and burst on the froth surface. Typically, this occurs repeatedly at the same point in the froth, as subsequent bubbles follow paths of least resistance.

- **Froth collapse**
  This effect has similar characteristics to the 'boiling' condition. It occurs when the mass of the froth near the froth surface collapses the froth structure below it, resulting in significant air loss through the froth surface.

The surface lamella bursting condition occurs most commonly within a wide range of froth conditions and is easily observable. Typically, the froth surface lamella rupture exposes smaller bubbles below the burst bubble.

Both the boiling and froth collapse conditions only occur under specific conditions. The boiling occurs in froths depleted of solids and at air rates above the designed operating range of a cell. The froth collapse condition typically occurs in heavily mineralised froths that are well drained and brittle.

In the case of the boiling froths, the only noticeable feature is an area of the froth where a 'hole' develops that continuously releases air. A greater visual impact occurs for the froth collapse condition, as a region of froth undergoes a disturbance when a froth collapse event occurs. However, it is difficult to observe the precise location where air loss occurs.

In both the boiling and collapsing froth cases, there is almost no indication of the quantity of air lost. Therefore, it may not be possible to use a visual means to measure air loss as a result of these two mechanisms. However, the size of a bubble that subsequently bursts on the surface indicates the amount of air lost due to the burst event.

4.2.2. Proposed burst rate measurement

The machine vision method developed to identify bursting bubbles on the froth surface compares the image segmentation outputs of consecutive images to detect burst bubbles.

This algorithm compares segmented regions between consecutive frames and identifies regions which have 'broken' into smaller regions. In the context of a segmented image of a froth surface, the algorithm identifies bubbles which burst and expose smaller bubbles underneath. In addition, an approximation of the volume of gas released from the burst bubble event can be determined. This information can be used to determine the volumetric flow rate per cross-sectional area of air escaping the region of froth surface analysed.

This method uses the output from the watershed froth segmentation and froth stability algorithm, as described in section 2.3, from consecutive images to determine the volumetric gas flow rate per unit area, or superficial gas velocity, of air leaving the froth surface.

The watershed segmentation algorithm, as described in appendix C.2.2, outputs a labelled image, which denotes each segmented region. These regions are not aligned in consecutive frames owing to the displacement caused by the motion of the froth. A single block match can determine this displacement, similarly to the froth stability algorithm (Appendix C.2.3). The measured displacement is used to extract two aligned sub-images from the consecutive labelled images output from the watershed segmentation.

Each segmented region in the current frame is mapped to corresponding or overlapping segmented regions in the consecutive frame. Within the context of consecutive segmented froth images, larger bubbles that overlap smaller bubbles in consecutive frames are identified.

The centroid of the bubble under consideration in the current frame and overlapping regions in the consecutive frame is determined. A region of interest is determined relative to the current bubble under consideration based on its radius and cross-sectional sphericity. All of the centroids in the overlapping regions identified in the consecutive frame which are within the region of interest are subsequently determined.

Thus, a bubble remains in the current frame which is either the same bubble in the consecutive frame, or a group of other bubbles which were beneath a burst bubble.

An additional criteria is imposed upon this result to determine if a coalescence event has occurred. The ratio of the average area of the identified regions in the consecutive frame to the area of the region under consideration in the current frame is compared to a threshold value.

Bubbles from the first frame, identified to have coalesced are subsequently approximated as volumes of air. These volumes are based upon an ellipse, fitted to the bubble's shape, which is rotated around the longer axis.

This process can be performed over a range of consecutive images and an average loss of bubble volume per unit cross-sectional area of the cell to the atmosphere can be determined.

The algorithm used to perform this measurement and illustrated in figure 4.27 is:

1. Segment consecutive images in a video sequence using the watershed technique.
2. Determine the displacement between the consecutive images using a single block match.
3. Align the labeled image outputs from the watershed segmentation with one other.
4. Determine the centroid of each region in both of the output images.
5. Determine the intersection of bubbles between consecutive frames.
6. For each bubble in the first frame:
    - Determine whether the centroids of the bubbles in the second frame are within a radius, r, specified relative to the size of the selected bubble in the first frame.
    - If the ratio of the bubble size from the first frame to the average area of the intersecting bubbles is greater than a threshold, t, the selected bubble in the first frame has burst.
        - Fit an ellipse around the selected bubble in the first frame.
        - Rotate the ellipse around its long axis to approximate the volume of the selected bubble in the first frame

The above-mentioned algorithm requires two input parameters. The fraction of equivalent circular area which determines the search radius, r, and the threshold bubble area to average bubble area ratio, t.

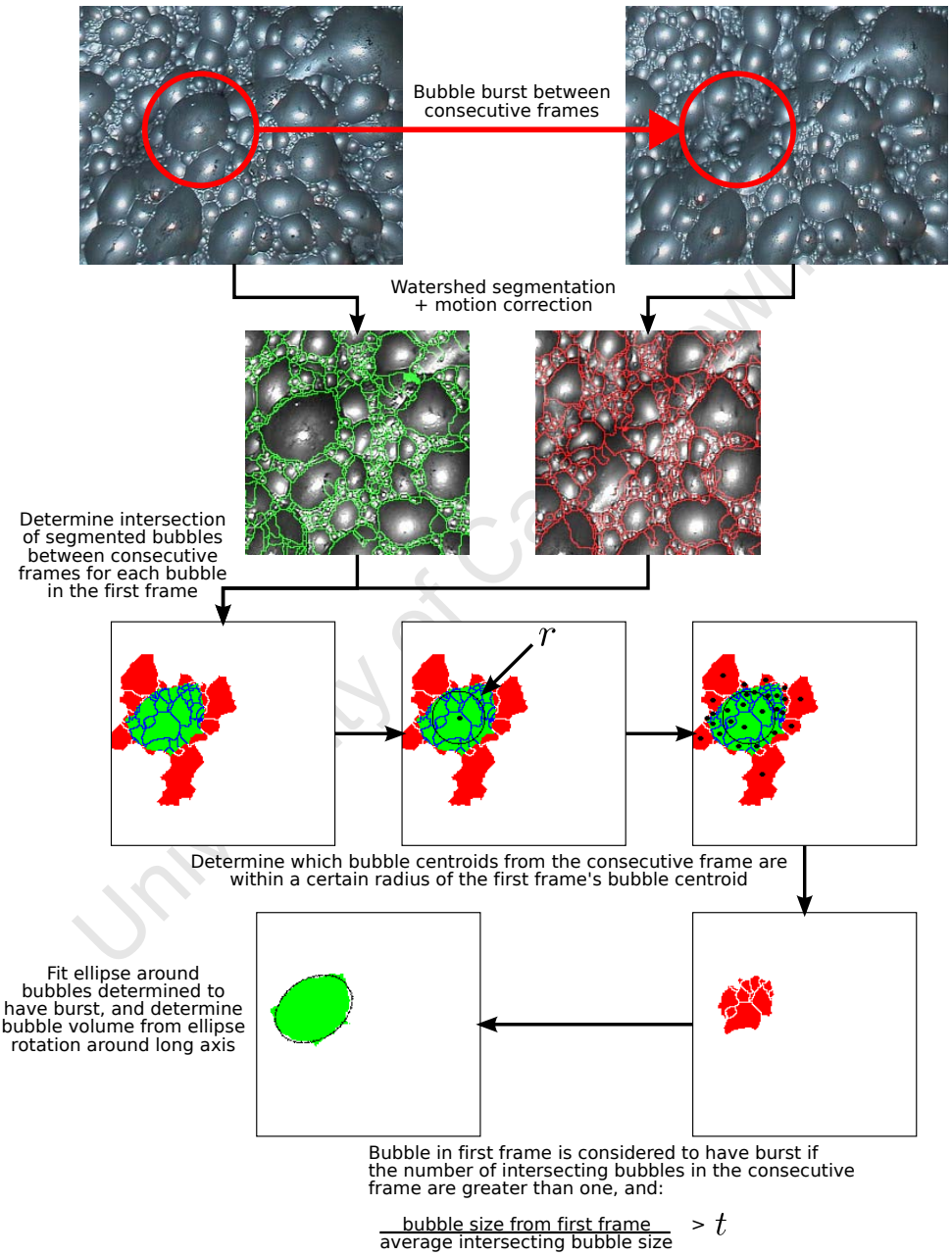

Figure 4.27.: Flow-sheet illustrating the algorithm used to detect the burst bubble and determine the volume of air lost due to a bubble burst event on the froth surface.

4.2.3. Burst rate measurement results

The results of the air loss measurement for a series of frames determined over time is shown in figure 4.28.

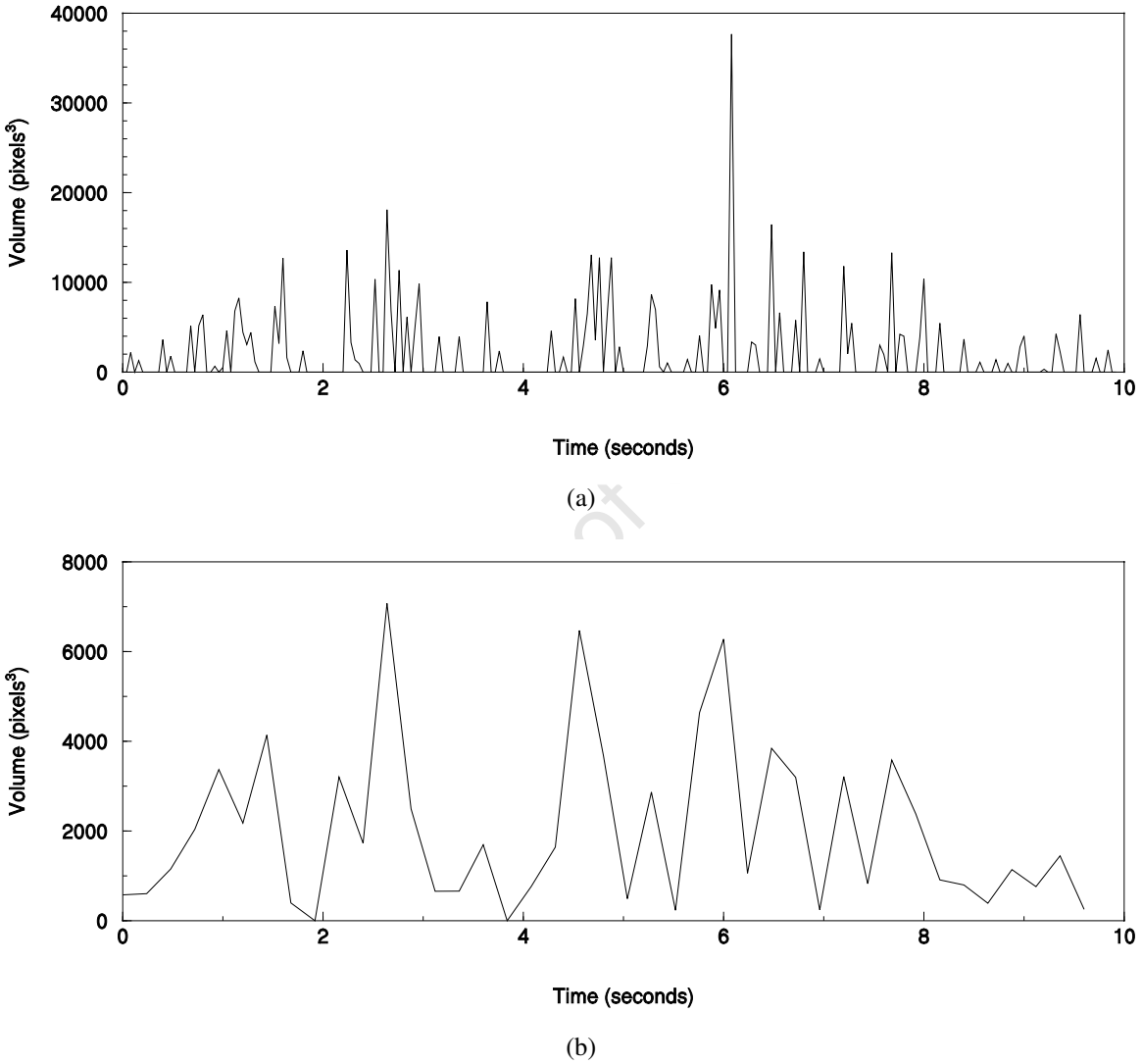

Figure 4.28.: Measurement of air lost through the froth surface for (a) individual frames and (b) the averaged every five frames.

Figure 4.28(a) shows that considerable variability in this measurement is observed. This is due to bubble bursting events occurring at discrete points in time that occur at non-regular intervals. Figure 4.28(b) shows the same data, where each point consists of an average of five frames. It is apparent that the air loss on the froth surface follows a non-uniform cyclic

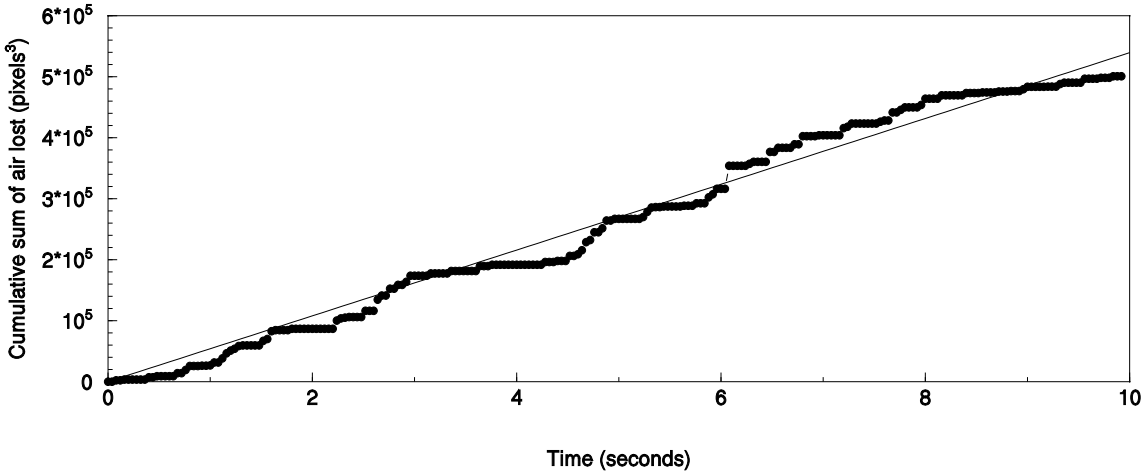

Figure 4.29.: Cumulative sum of measured air loss through the froth surface.

pattern. As a result, it may be more appropriate to analyse this data using the cumulative sum of the air lost on the froth surface.

Figure 4.29 shows the cumulative sum of the measured air loss on the froth surface. These results show that the cumulative sum of the air loss increases at a steady rate, with some minor deviation from the fitted trend. This deviation is due to the irregular number and size of bursting bubbles per frame and the average gradient relates to the average volume of air lost per unit time.

The standard error of the linear regression gradient through the cumulative sum versus time measurement is easily determined. This measurement incorporates the variance in the bubble burst events on the froth surface and the measurement error. The standard deviation of the linear regression gradient in figure 4.29 is 11% of the measured gradient. SmartFroth typically operates by sampling four frame pairs every two seconds. Thus, this system would only be able to detect a 10.7 % change at 95 % confidence every two seconds. After a minute of sampling, this system would be able to detect a 2 % change at 95 % confidence.

Measurement validation

This measurement was validated using a comparison of the algorithm's output to manually segmented images of bursting bubbles. These manually segmented images were used in the same way that the algorithm determines the volume of air lost. Thus, this validation tests the

ability of the algorithm to detect burst bubbles and the accuracy of the segmentation of these bubbles.

Images from both the copper and platinum froth systems were tested. Within both systems, video clips of 10 seconds in duration were selected. Each sample video was taken in the first rougher. The manual segmentation was performed by 'painting' the area occupied by each burst bubble onto an image overlaid on the froth. The volume of air released from the bursting bubble is approximated by subsequently fitting an ellipse to the painted area and rotating the ellipse around its long axis, which is the same method that the algorithm uses.

A comparison of the identification of a burst bubble using manual segmentation and the algorithm, for a single burst event, is shown in figure 4.30.

Figure 4.30(a) shows that a bubble has burst in the second frame. Thus, this bubble is manually segmented, as shown in figure 4.30(b). The corresponding bubble region from the segmentation algorithm is shown in figure 4.30(c).

Using these two measurements on a series of images, the volume of air lost, as determined by the algorithm, can be compared to a more accurate measurement of the volume of air lost over time. This comparison can be use to validate the use of the algorithm as a relative measure and calibrate it to an absolute value.

Figure 4.31(a) shows that the volume of air lost determined by the algorithm is less than that determined manually. However, the intensity in the figure increases in regions where the manual segmentation increases. This is illustrated in figure 4.31(b), which shows a correspondence in the automatic and manually segmented measures.

As in the case of the automatic measurement, the manual measurement can be represented using the cumulative sum. A comparison of the standard deviation between the manual and calibrated automatic measurements shows that the variance in the manual measurement, which represents the variance in the actual bubble burst rate, is less than that in the automatic measurement, with an error of 6% and 11% respectively. Thus, the difference in variance between the two measurements, which can be attributed to measurement error, is 5%.

As the standard deviation is less in the manual measurement, it follows that the number of samples required to determine the gradient of the cumulative sum versus sample number, and thus a calibration factor, at 95 % confidence is less than that of the automatic measurement.

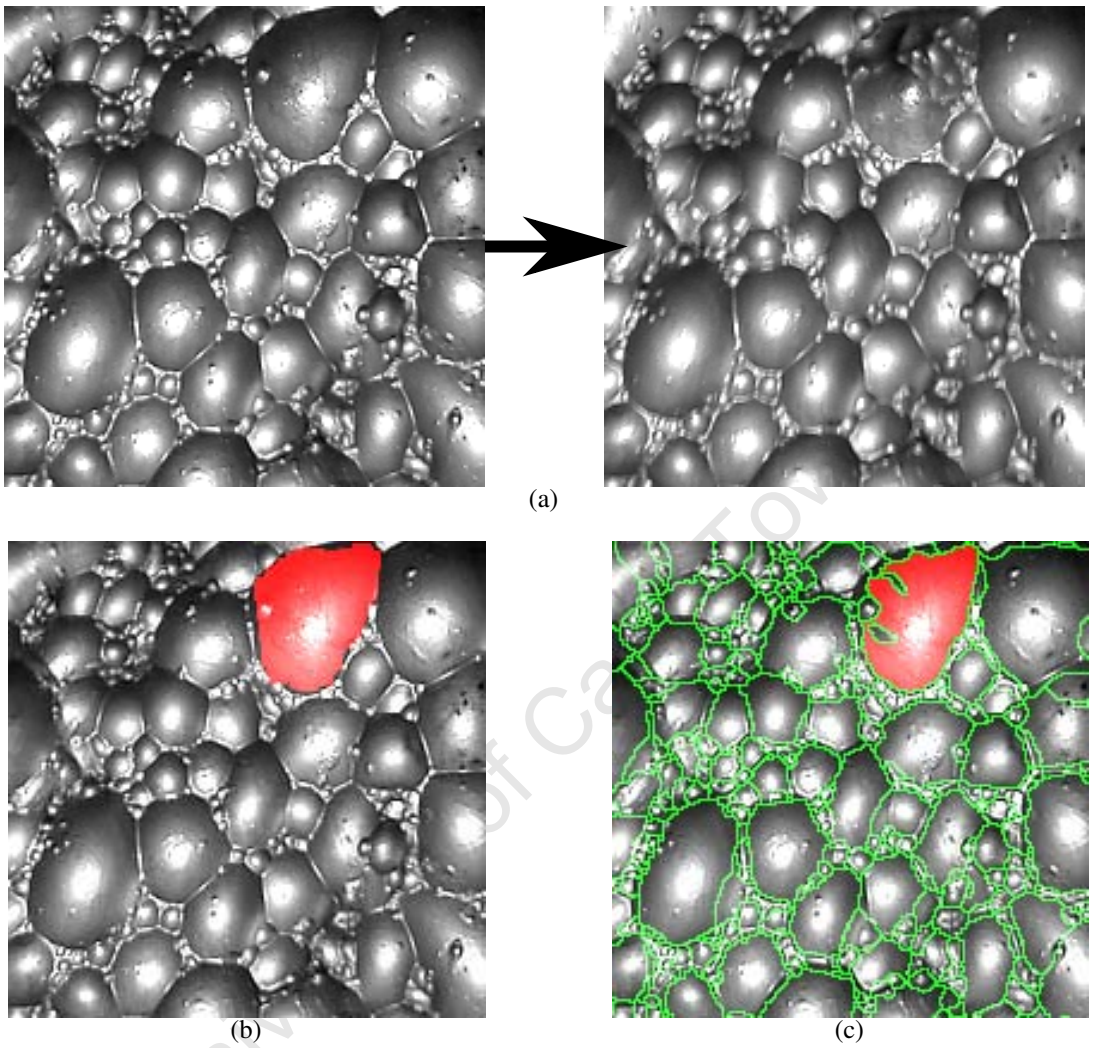

Figure 4.30.: An example of a bubble bursting in two consecutive frames shown in (a), where the burst bubble has been identified in (b) by manual segmentation and (c) using the automatic air loss algorithm (in a copper froth).

Figure 4.32 shows the relationship between the cumulative sum of the automatic measurement and the manual measurement. The automatic method under-estimates the amount of air lost through the froth surface.

The results of this comparison across all of the tested conditions are shown in figure 4.33, where the average rate of air loss across the ten second clips is determined using the automatic algorithm and manually segmented measures.

Examination of figures 4.31, 4.32 and 4.33 shows an element of bias exists between the manually and automatically segmented regions. This bias may be caused by a few factors.

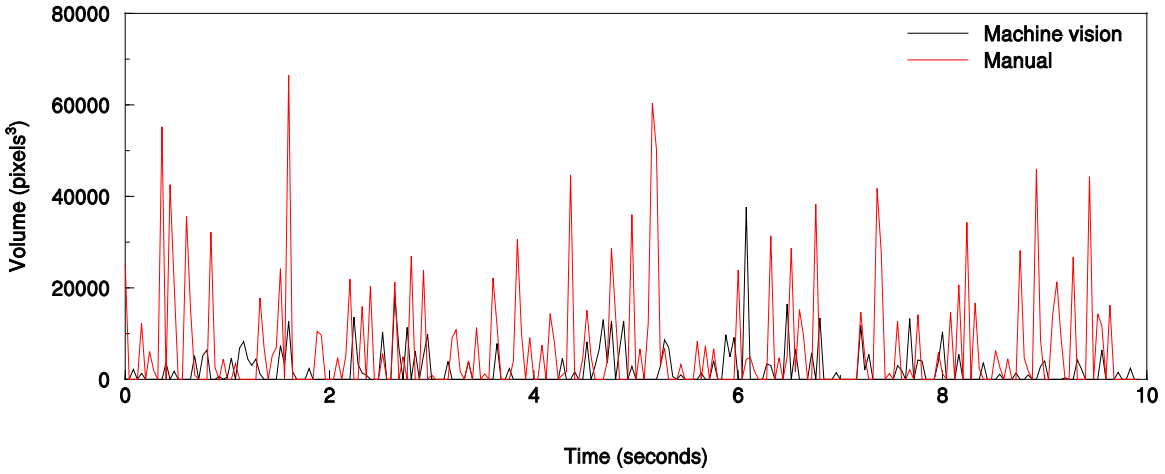

(a)

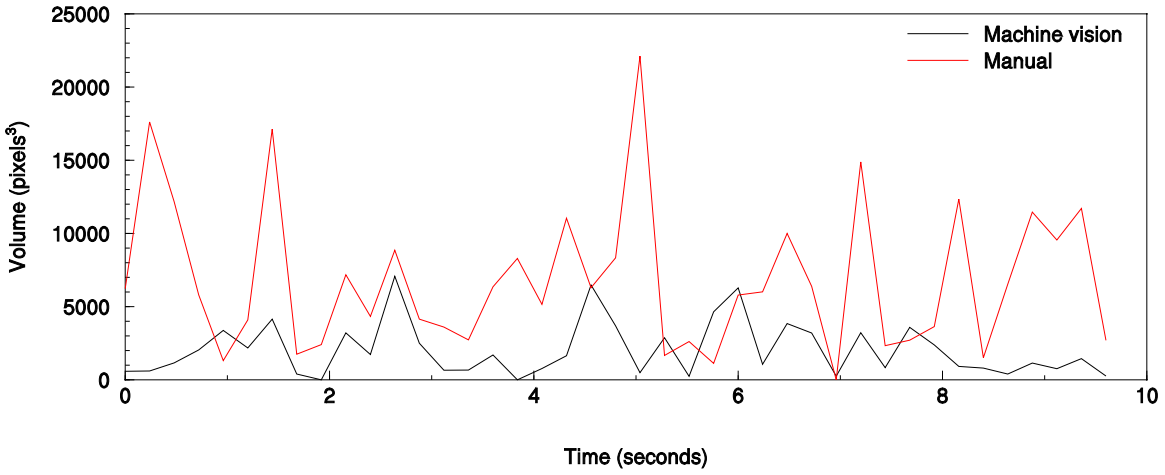

(b)

Figure 4.31.: A comparison between the automatic and manual measurement of air lost through the froth surface for (a) individual frames and (b) averaged every five frames.

Firstly, regions may be over-segmented. Larger bubbles are prone to over-segmentation at their boundary, which may be as a result of a filtering artifact, due to the low-pass filter currently implemented in pre-processing, before the segmentation algorithm. With larger bubbles, the segmentation line in the current watershed algorithm tends to be on the inside of the bubble's border, thus resulting in a smaller elliptical fit for the bubble. The significance of this effect on bubble volume increases with bubble size.

This phenomenon can be observed in figure 4.34, where the burst bubble can be observed to have been over segmented in the darker shadowed regions of the bubble.

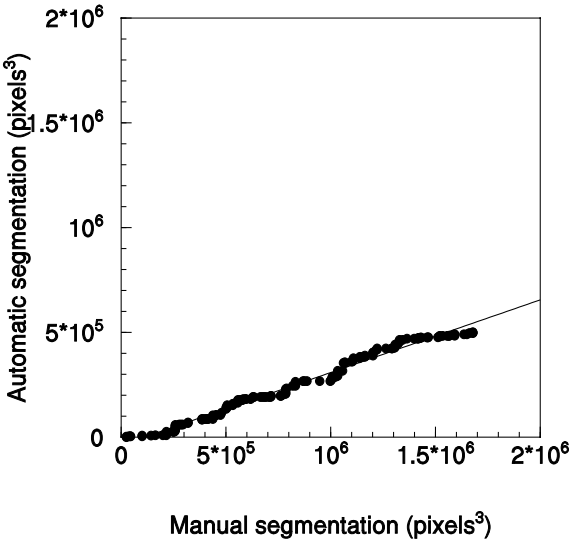

Figure 4.32.: Cumulative sum of air lost as determined using the automatic versus manual measurement

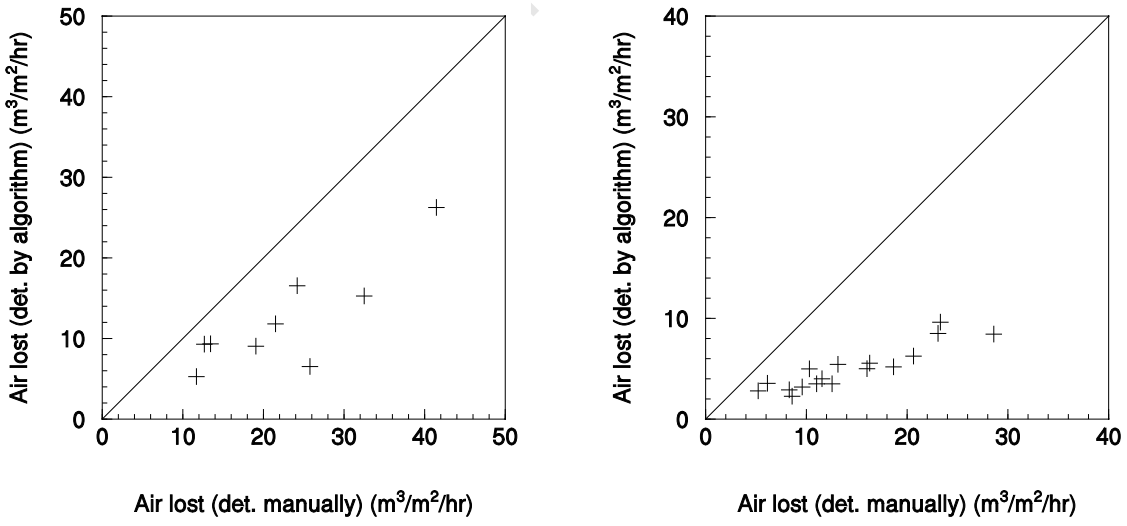

(a) Copper froth

(b) Platinum froth

Figure 4.33.: Comparison between the air loss measurements determined by the automatic algorithm and as determined by manually segmented images for (a) copper and (b) platinum froth data set.

Secondly, larger bubbles are prone to over-segmentation. However, this may occur due to an uneven surface lamella, or multiple highlights, which tend to occur further apart on larger bubbles. Here, the segmentation may result in a single bubble being segmented into two

regions, where both of these regions are identified as having ‘burst’. In this case, the total volume of air lost determined from these regions would be lower than if the bubble had been correctly segmented into a single region.

This phenomenon can be observed in figure 4.34, where the burst bubble can be observed to be over-segmented into four distinct regions.

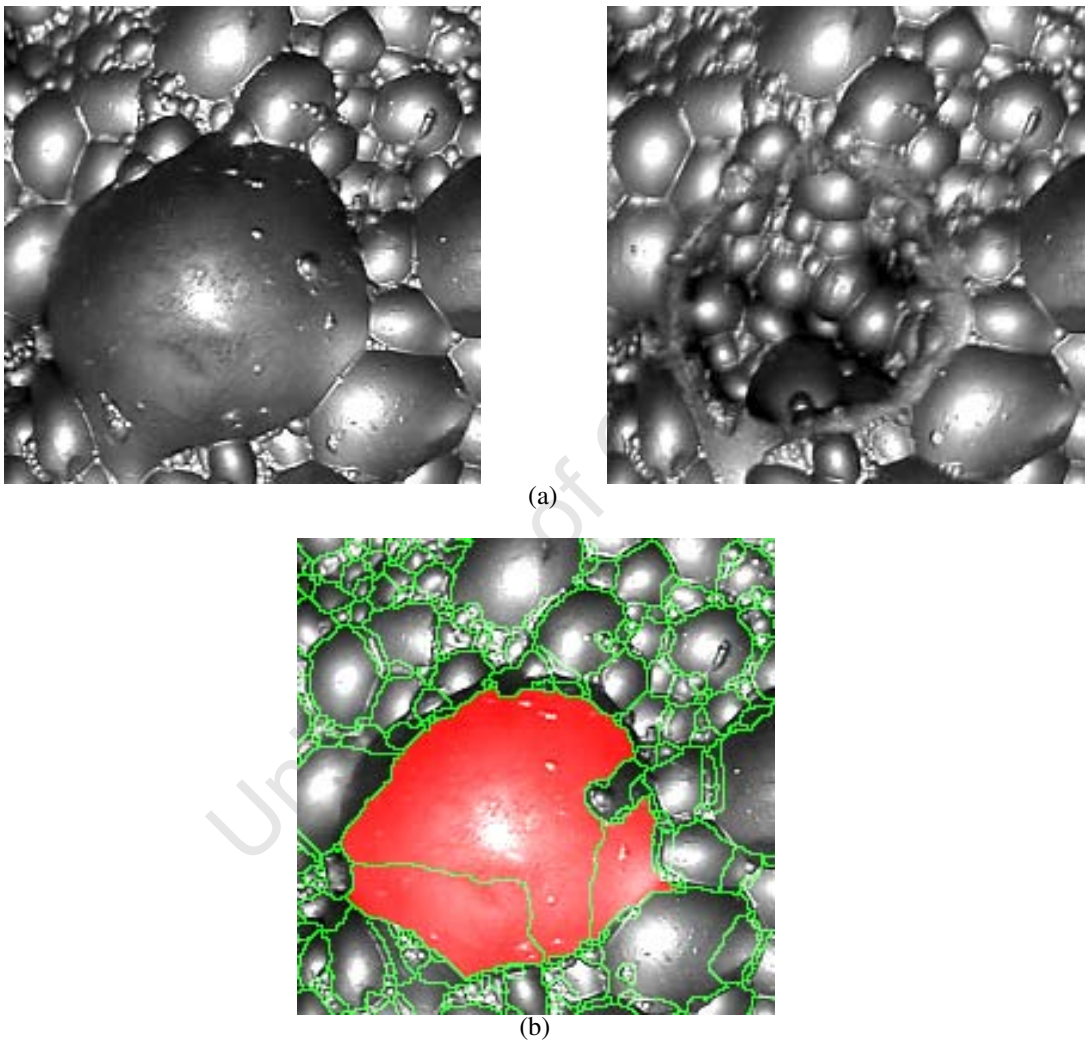

Figure 4.34.: An example burst bubble (a) showing over segmentation along the top border and into multiple regions (b), both leading to an under-estimation of the amount of air lost.

Another factor that may result in a measurement error may be due to the mis-identification of a burst bubble, due to the over-segmentation of the bubble in a consecutive frame. However, this would lead to an over-estimation in the amount of air lost, which is not determined to be the cases in figure 4.33. This problem can be mitigated by a comparison of the current frame’s segmentation with the previous and future frames after its consecutive frame. This was

implemented in the measurement of air loss through the use of the algorithm. This resulted in the minimisation of the scenario where an over-estimation of the air lost is possible.

The bias due to the mechanisms described above have been shown to be consistent across all of the different conditions investigated. Based upon this evidence, the bias can be corrected and accounted for under these conditions and within these systems. Figure 4.37 shows the air loss measurements where the measurement bias has been determined and corrected for using a comparison of the automatic algorithm with the manually segmented images. In addition, the error associated with the measurement of each sample can be determined.

As the measurement bias appears to be consistent across the different conditions tested, a single calibration factor can be determined that is independent of operating conditions to determine an absolute measurement of air loss on the froth surface, supporting hypothesis 4.4.

Under the tested conditions, the bias was corrected using a linear regression through the manual and automatic measurements shown in figure 4.33.

Figures 4.35 and 4.36 show the effect of the calibration on the output illustrated in figure 4.31(b). Some correspondence is noted between the air loss peaks determined from the two methods, with some cases where burst bubbles were not identified and some which were mis-identified. The cumulative sum of air lost shows good correspondence between the two segmentation methods.

Figure 4.37 shows the effect of calibration on the results illustrated in figure 4.33.

4.2.4. Investigation of the effect of bubble size

As the air loss algorithm requires the use of segmented images, the size of each burst bubble is known. Thus, using the average total number of bubbles in each bubble size distribution decile and the average number of bubbles burst in each bubble size distribution decile, the fraction of coalescence for each bubble size distribution decile can be determined, as shown in figure 4.38. This measurement is related to the probability that a bubble of a certain size will coalesce. As expected, the measurement shows an increase in probability with bubble size, supporting hypothesis 4.6. Furthermore, the relationship between the measured volume of air lost and the burst rate and froth bubble size can be investigated.

A linear regression was performed to model the amount of air lost through the froth surface from the burst rate and the bubble size measurements. In this case, the 80th percentile bubble size ($d_{b,p80}$) was used to account for the fact that the majority of bursting bubbles tend to be

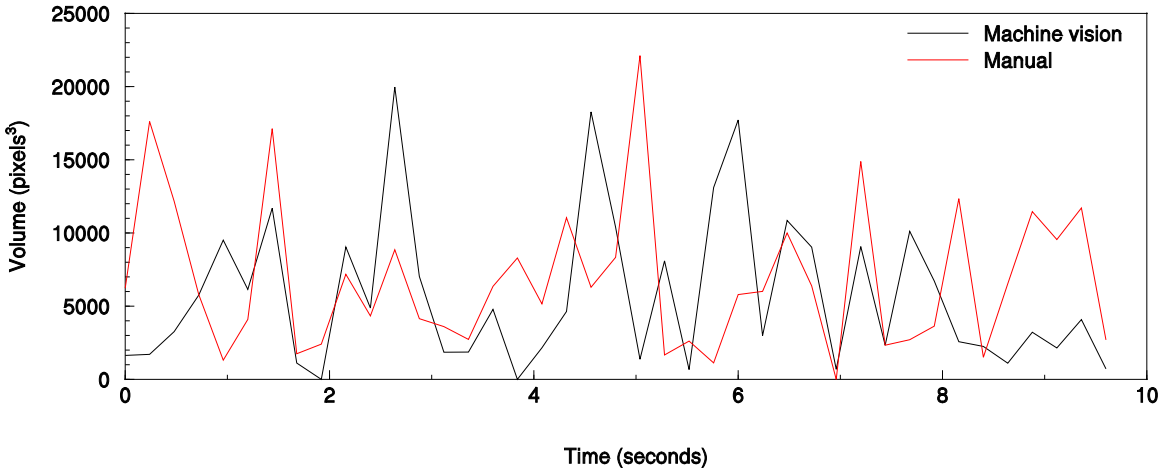

(a)

Figure 4.35.: A comparison between the automatic and manual measurement of air lost through the froth surface, where the measurement bias has been corrected.

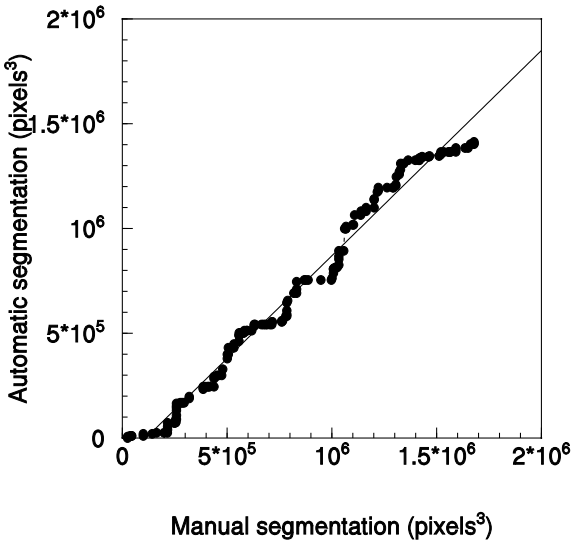

Figure 4.36.: Comparison of the cumulative sum of air lost as determined using the automatic versus manual measurement

on the top end of the bubble size distribution. The results from this regression analysis are presented in appendix B.2.

Figure 4.39 shows the comparison between the measured air lost through the froth surface and the modelled air loss through the froth surface using the burst rate measurement and a froth surface bubble size measurement. These results show excellent correlation between the

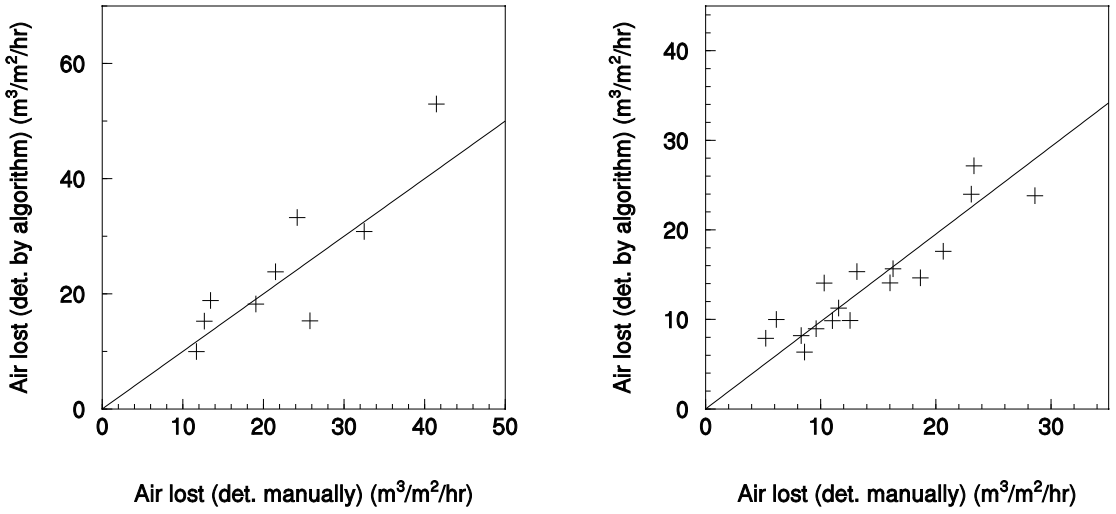

(a) Copper froth

(b) Platinum froth

Figure 4.37.: Comparison between the air loss measurements determined by the automatic algorithm and as determined by manually segmented images for (a) copper and (b) platinum froth data set, where the measurement bias has been corrected.

measured air loss and the linear regression in the case of the platinum results (b), while the results for the copper system (a) do show more noise. These findings do indicate that the burst rate measurement (count per time of burst events) and a bubble size distribution measurement (80th percentile) are key factors that drive air loss on the froth surface.

These results show that the burst rate is a strong indicator of froth stability and decouple the effect of bubble size on froth stability. However, the burst rate is related to the bubble size, as it increases with an increasing rate with bubble size, indicating that larger bubbles are much less stable on the froth surface than smaller bubbles.

4.2.5. Investigation of the effect of solids loading

The proposed algorithm described in section 4.1.2 measures the solids loading on each bubble within each image frame analysed. Thus, as the algorithm described in section 4.2.2 identifies individual bubbles that have burst, it is possible to obtain the solids loading information for these bubbles.

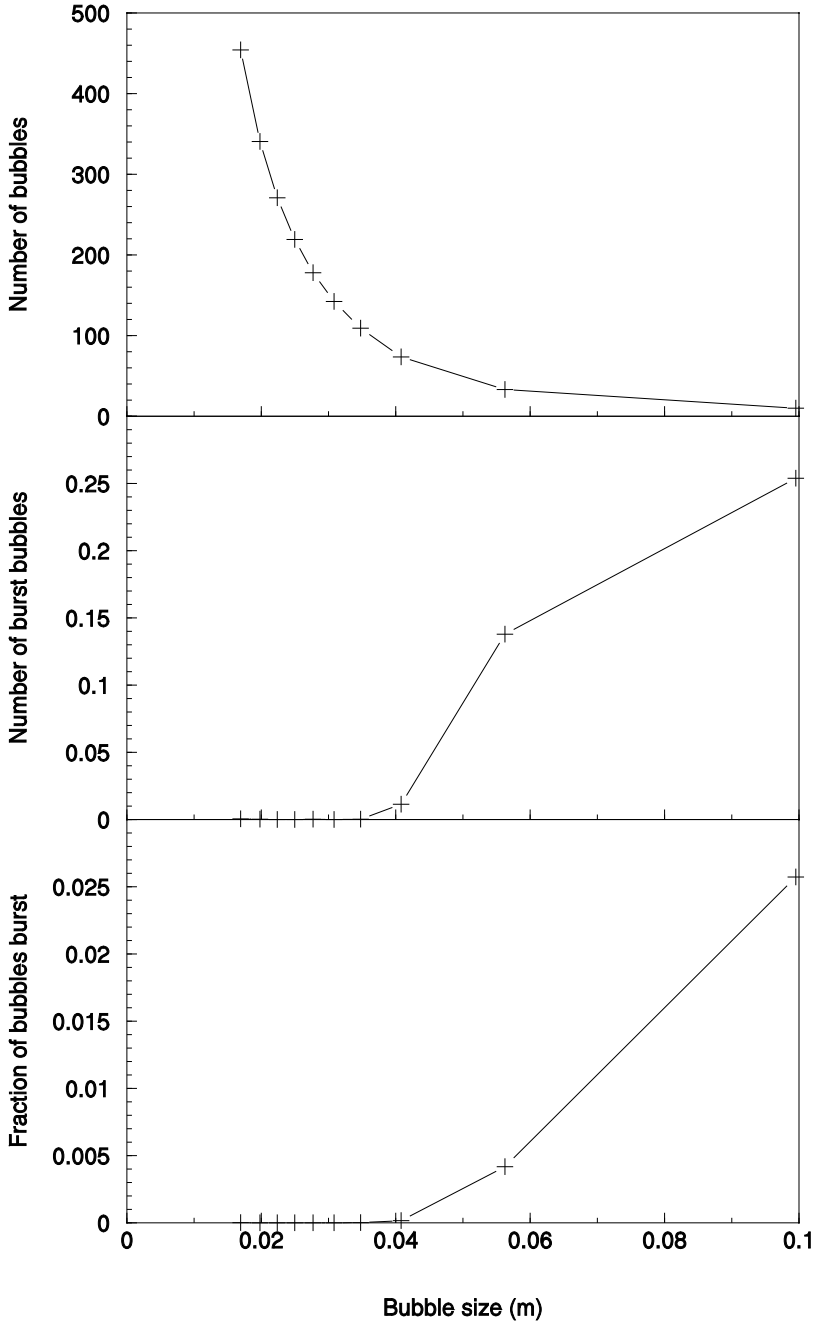

Figure 4.38.: The fraction of burst bubbles versus bubble size.

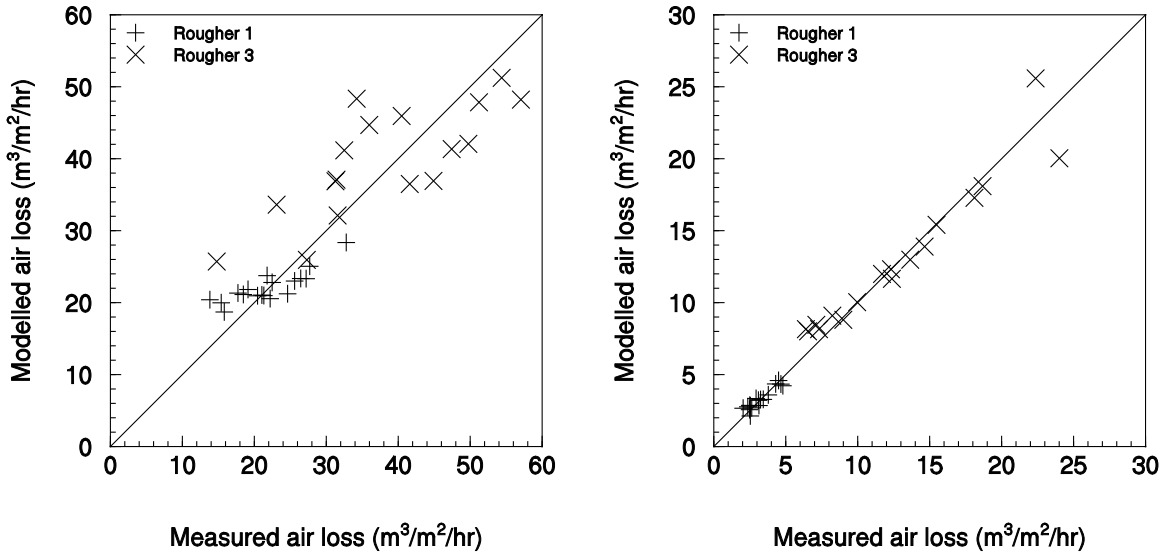

(a) Copper system

(b) Platinum system

Figure 4.39.: The measured air loss versus modelled air loss using a linear regression from the burst rate and the bubble size measurement on the froth surface.

An example of this measurement is shown in figure 4.40. The solids loading on the unburst bubbles shown are for comparison. These results show that, as expected, the solids loading of the burst bubbles is significantly different and less than that of the unburst bubbles.

The effect of solids loading on froth stability is well known. These results illustrate the effect where bubbles with a lower than average solids loading burst, which supports hypothesis 4.5. Thus, these results show that a primary mechanism responsible for busting bubbles on the froth surface relates to the solids loading on the bubble.

4.2.6. Measurement limitations

A limitation of the proposed burst rate measurement is that it only identifies bubbles that have burst in the area of the froth visible to the camera and analysed by the software. Thus, should the burst rate vary across different locations on the froth surface, it would be inappropriate to extrapolate this measure to areas dissimilar to the measured area. For example, a comparison between the edge of the launder and the middle of the cell. This limitation will affect the relationship between the burst rate measurement and any measurement of air recovery.

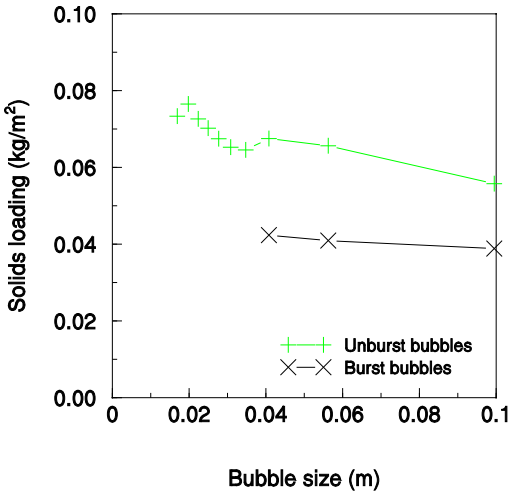

Figure 4.40.: The average solids loading on burst and unburst bubbles versus bubble size on the froth surface.

The measurement of air loss on the froth surface is strongly dependent on the quality of segmentation. Should bubbles be either under or over segmented, the accuracy of the estimated volume of burst bubbles decreases. Furthermore, variation in the segmentation quality between consecutive frames, due to image artifacts, such as motion blur, or poor focus, will cause an increase in the identification of false burst events. Therefore, better segmentation methods are required for problematic froths, such as froths with transparent and semi-transparent bubbles.

Air loss due to both 'boiling' and froth collapse, as described in section 4.2.1 cannot be measured using this method, as the amount of air lost is not apparent visually. Thus, the air lost through froth surface when these conditions occur will result in a large underestimation of air loss. However, these conditions are considered undesirable and are not prevalent under 'normal' operating conditions.

4.2.7. Burst rate as a stability measure

The burst rate on the froth surface provides a direct indication of froth stability. The measurements performed in sections 4.2.4 and 4.2.5 show that the burst rate is a function of both bubble size and solids loading.

Higher burst rates on the froth surface occur in the presence of larger bubbles formed on or below the froth surface. This effect accounts for the increased coalescence rate within the froth

phase. Froths where only limited coalescence occurs internally, have a surface composed of smaller bubbles with a lower burst rate. Conversely, high internal coalescence gives rise to large surface bubbles with a high burst rate. In addition, bubbles that have a lower solids loading tend to burst more rapidly than bubbles with higher solids loadings.

Therefore, the burst rate is a measurement that has the potential to reflect the stability state of the froth. However, the use of burst rate as a stability measurement has advantages and disadvantages over other stability measures. These relative advantages and disadvantages are discussed further.

Machine vision stability measures

Machine vision based froth stability measurements have been proposed by Hatfield (2006), Hyotyniemi *et al.* (2000) and de Jager *et al.* (2005). These studies all used methods which involve the comparison of consecutive video frames. Their methods measure the correlation and disparity between consecutive frames.

The disadvantages of this approach is that the machine vision algorithms output measurements which do not relate directly to a physical aspect of the froth. Thus, these measurements are difficult to interpret and perform non-linearly with respect to differences in froth structure.

The burst rate measurement solves these problems by simply detecting and counting bubble burst events. The burst events represent a physical process occurring to the froth structure. The signal of each event is not skewed by bubble size or any other froth structural effects.

The advantages of the previous machine vision measurements are that they are independent of froth segmentation processes and are thus computationally easier measurements to make. However, the burst rate measurement requires the output of a coarse image segmentation which does not necessarily need to be accurate (segmentation accuracy is a requirement for a measure of air flux lost from bursting bubbles).

Column based measures

Barbian *et al.* (2005) and Zanin *et al.* (2009) developed froth stability measurement devices using a column inserted into a flotation cell. Their devices measure the rise rate of the froth surface, with the device developed by Zanin *et al.* also measuring the froth half-life. Hadler

and Cilliers (2009) subsequently developed a device that can be permanently installed for on-line measurement.

The advantage of these methods is that they measure a differential froth stability as a function of froth height. This information may be more easily used to determine the stability effect of changing the froth height, which would be useful in on-line froth phase modelling. However, this relationship to froth height is, to a large degree, dependent on the geometry of the froth column, which may not linearly scale up to the entire flotation cell.

In order to determine similar data using the machine vision method, the operating conditions would be required to be stepped, by taking measurements at different froth depths, disrupting the process.

The disadvantage of any column based measurements are that they are intrusive to the process. They disrupt the flow of the froth and decrease the flotation cell's efficiency. In addition, the column system takes up more physical area relative to the machine vision approach and thus is not practical for use on smaller flotation cells. Finally, a flotation cell is a hostile environment to any equipment with moving parts. The maintenance requirements of a column based instrument are likely to be frequent and awkward.

Both measurements are localised which means that if the froth stability varies across the froth surface, neither measurement will be able to detect or measure this variation.

Air recovery

Ventura-Medina *et al.* (2003) developed a measure related to froth stability based upon the recovery of air to the concentrate launder relative to the amount of air added into the flotation cell. This measurement also relates to froth transport factors.

The air recovery measure depends on the measurement of two key parameters. The first parameter required is either the measurement of the amount of air flowing into the cell (Q_a) discounting the air lost to the tails, or the superficial gas velocity (J_g) through the flotation cell. The air flowing into the cell is usually measured for air input into forced aerated mechanical flotation cells. The superficial gas velocity is usually measured using a probe inserted through the froth into the pulp.

The second parameter that needs to determined is the volumetric flow rate of the froth recovered to the launder. This can be determined by measuring the height of the froth flowing over the weir ($h_{froth,weir}$), which can either be measured manually, or using a range meter located

above the start of the launder, the length of the weir (l_{weir}) and the velocity of the top surface of the froth (v_f). Typically, machine vision methods are used to determine froth velocity, as described in more detail in appendix C.2.4.

Thus, the air recovery, as defined by Ventura-Medina *et al.* (2003) can be determined using equation 4.2.

$$\alpha = \frac{V_{froth,rec}}{Q_a} = \frac{v_f \cdot h_{froth,weir} \cdot l_{weir}}{Q_a} \tag{4.2}$$

This measure utilises the volume of the froth recovered, without accounting for the volume occupied by the water and solids within the froth. While air takes up the majority of the volume, the proportion of the air making up the froth varies with the state of the froth. Generally, froths with smaller bubbles are comprised of more water than froths with large bubbles.

The air recovery was measured using this method within the copper system, referred to in section 3.4. By the consideration of the measured air recovery and the amount of air entering the cell, the results of this measurement can be compared to the measurement of the air loss through the froth surface.

The amount of air entering the froth was calibrated using a measurement of the superficial gas velocity. The height of the froth overflowing the launder was measured manually with a measuring tape. The froth velocity was measured using the velocity measurement output from the SmartFroth machine vision system.

Figure 4.41 shows a comparison between the air lost through the froth surface measured using the machine vision method, from which the burst rate is determined and the air lost through the froth surface calculated by using the measured alpha value and the average superficial gas velocity through the flotation cell.

These results show that the average air loss measured using the machine vision method most often underestimates the average air loss across the entire surface when compared to the air loss determined using the alpha value. This occurs owing to volume of air lost determined using the alpha value considering the air loss across the entire froth surface. The air loss estimated using the machine vision method is only able to estimate the air loss in the vicinity of the camera.

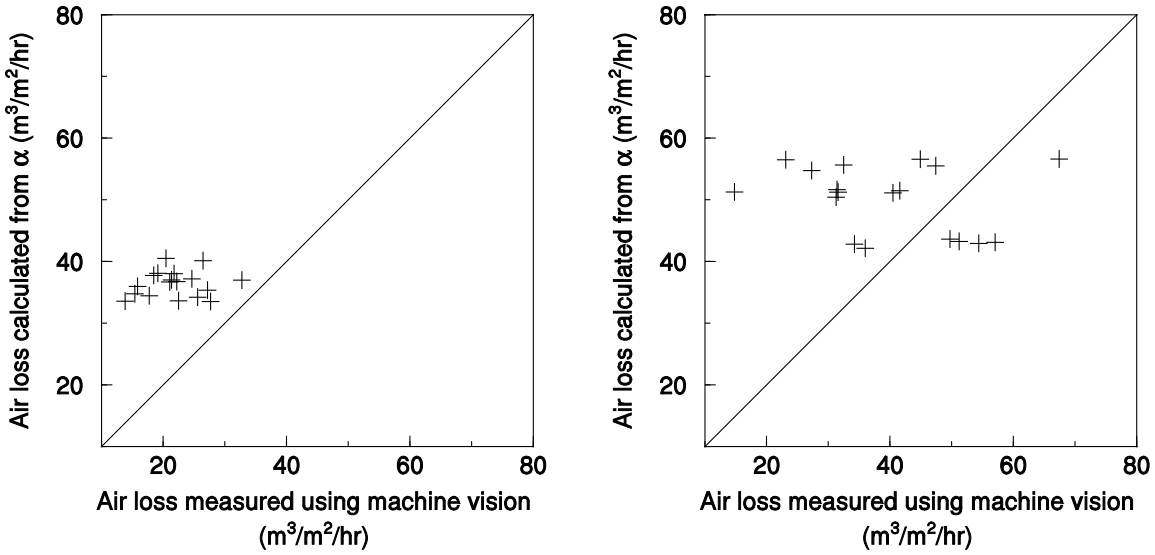

(a) Rougher 1 (b) Rougher 3

Figure 4.41.: Comparison between the air loss measurement by the developed algorithm and the air loss measurement calculated using the measurement of air recovery and the superficial gas velocity for the copper data set.

Other potential factors that may explain the variation between these two measurements are that the velocity measured may not be representative of the velocity of the froth overflowing the launder. Lower layers of the froth may be travelling over the launder slower than the froth surface, resulting in an under-estimation of velocity and thus alpha value. In addition, the froth accelerates as it moves to the launder, which means that the average velocity of the froth in view of the camera is less than the velocity of the froth at the launder, resulting in an over-estimation of velocity and thus alpha value.

The machine vision measurement of air lost through the froth surface is more sensitive to changes near the launder, while the air recovery method is sensitive to the average air loss across the entire froth surface. However, the difference between these two regions appears to decrease further down the bank, where the machine vision measurement underestimated the average air loss fewer times.

The broader range of air loss measurements obtained from the machine vision measurement as compared to the air recovery measurement implies that the air loss near the launder is more sensitive to the cell operating conditions than the overall air loss across the entire cell surface.

The advantage of the air recovery method is that the effect of variation in stability across the froth surface is averaged across the entire cell. Thus, the air recovery method is a more applicable measurement relating to the overall transport rate of the froth.

This finding implies that different zones exist on the froth surface where bubbles burst at different rates, supporting the transport models proposed by Moys (1984) and Woodburn *et al.* (1994). To obtain the equivalent information to the air recovery method only using the burst rate measure, multiple cameras would be required. However, the simpler approach would be to measure the volumetric flow-rate of the froth using the excess froth height, froth velocity and launder length. The variation in excess froth height needs to be taken into account in the estimation of air recovery, and the assumption that the velocity profile through the froth overflowing the weir is constant, and equal to the froth surface velocity needs further investigation.

Thus, as the burst rate measurement measures the stability of the froth close to the launder, it is more sensitive and relates more closely to the stability influenced by the material in the froth in the recovery zone. The burst rate measurement relates poorly to the transport characteristics of the froth.

4.3. Summary

Two machine vision measurements have been developed; one which relates to the solids loading on bubbles on the froth surface and one that measures the burst rate on the froth surface. In addition, these machine vision measurements have been evaluated for effectiveness and sensitivity.

4.3.1. Solids loading measurement

Images of bubbles on the froth surface exhibit textural variation dependent on the solids concentration, or loading observed on the froth surface. A proposed machine vision based method exploits this textural variation to measure solids loading on the froth surface. This method isolates high frequency variation on the froth surface by removing the low frequency variation and the effect of the highlights. The resultant measure, termed the bubble surface noise amplitude, represents the surface roughness of the bubbles. This measure, when combined with bubble segmentation outputs determines the surface roughness for each bubble observed.

A visual assessment of the bubble surface noise amplitude measurement performed showed that the lower values determined for the froth surface appeared to have high solid loadings. The converse was true for high bubble surface noise amplitude values and low solids loadings.

Generally, solids loading increases with bubble size. However, when bubbles on the froth surface coalesce with bubbles below the froth surface, the solids loading on the surface lamella decreases. This process results in high levels of variance associated with the solids loading of larger bubbles on the froth surface. The bubble surface noise amplitude was sensitive to both of the identified coalescence mechanisms that govern the solids loading on the froth surface. In addition, it showed a variation as a function of bubble size. These results support hypothesis 4.2.

The bubble surface noise amplitude measurement has been correlated to a gravimetric solids loading measurement referred to in the literature. However, the gravimetric measurement may result in biased measurements, as larger bubbles are easier to sample than smaller bubbles and the solids loading varies with bubble size. Despite this limitation, it was still possible to calibrate the bubble surface noise amplitude to the gravimetric solids loading measurements.

The measurement of solids loading has been shown to, under certain conditions, improve the determination of the solids recovery to the concentrate. However, this improvement was

only marginal, where the use of velocity in combination with bubble size provides the best solids loading estimation. However, this relationship to solids loading was not shown to be a significant one under all of the conditions tested, disproving hypothesis 4.3.

The verification of this measurement was difficult owing to the variation in solids on the froth surface and may require further validation. However, the evidence shown in this work does indicate that this measure relates to solids loading. Thus, this non-intrusive, on-line measurement that relates to solids loading shows promise. These findings support hypothesis 4.1.

4.3.2. Burst rate measurement

The rate at which bubbles burst on the froth surface is a strong indicator of froth stability. In addition, air loss on the froth surface is a primary driver of the rate of froth transport to the launder.

A proposed machine vision measurement that identifies bursting bubbles on the froth surface counts the rate at which bubbles burst by comparing the segmentation outputs of consecutive images. In addition, an estimation of the volume of the burst bubbles measures the volumetric rate of air loss on the froth surface.

The comparison of the machine vision method with manually segmented images validated the method, supporting hypothesis 4.4. However, a consistent bias was observed due to the underestimation of bubble size by the watershed algorithm, over-segmentation of large bubbles and not detecting occasional burst events. Within systems where this bias is consistent across a number of conditions, this measurement is suitable as a relative measure of air loss. The confidence interval of the measurement of air loss was proportional to the air loss rate. Thus, as the rate of air loss increases, the number of samples required for an acceptable confidence interval will increase.

The burst rate measurement decouples the effect of bubble size from the volumetric rate of air loss on the froth surface. Thus, the burst rate is a more direct measure of froth stability than the rate of air loss and is not subject to the bias resulting from inaccuracies in bubble segmentation. The factors shown to affect the burst rate are the bubble size and the solids loading on the bubbles, supporting hypotheses 4.5 and 4.6. Increased bubble size occurs as a result of increased coalescence within the froth and the solids loading is a strong factor affecting froth stability.

This method has the following advantages over current froth stability measurement methods; it is a non-intrusive measurement; it is a more intuitive measurement than current machine vision stability measurements as it relates to physical and dynamic properties of the froth. However, this measurement is a localised measure and only relates to the stability of the froth in view of the camera (usually next to the launder). A comparison between the average air loss across the froth surface shows that this measure relates poorly to froth transport. Despite this limitation, it is more sensitive to changes in operating conditions than the measurement of the average air loss across the froth surface.

Chapter 5.

Assessment of froth phase stability

In many flotation feeds, the hydrophobicity and concentration of the hydrophobic material change owing to the heterogeneity of ores and variability in upstream processes. In addition, the concentration of hydrophobic solids present usually decreases through a flotation bank. Thus, one of the biggest challenges in managing flotation banks and circuits is dealing with ore variability.

Froth stability is a key factor that relates to flotation performance, and it has been suggested that the effective management of flotation performance is possible through the effective management of froth stability.

Thus, this chapter investigates the relationships between operating variables, machine vision measurements, froth phase stability and flotation performance to address the second, third and fourth objectives of this thesis.

5.1. Introduction

Findings from the literature review show that froth stability is a key factor that affects flotation selectivity and recovery. Thus, previous authors, such as Subrahmanyam and Forssberg (1988) propose that the management of flotation performance is possible through the effective management of froth stability. However, froth stability behaviour is only subjectively described and factors that affect it are often not clear.

Individual factors that affect froth stability behaviour are well known. These include solid particle and dissolved surfactant molecule effects at the air/water interface. Aspects of froth stability that are less well known are interactions between mechanisms occurring within the

froth phase that can cause counter intuitive responses. In addition, currently no adequate froth stability measures are available for on-line measurement.

Within laboratory systems, froth stability measurement techniques are often derived from measurements based upon two-phase foam stability measurements (Bikerman, 1973, Sun, 1952). These methods often use column based measurements which relate factors such as froth rise rate, froth breakdown rate or the equilibrium froth height to an aspect of froth stability behaviour. Some laboratory techniques described measure stability in three-phase froths by measuring the volume and persistence of a froth in an agitated glass cylinder containing solids and aqueous frother solution (Dippenaar, 1982b, Livshits and Dudenkov, 1965).

Barbian *et al.* (2005) adapted a method proposed by Bikerman (1973) for use in industrial systems. Their method fits the rise rate of the froth to a function to determine a fit parameter, used as a froth stability measure. The basis of this measurement is that specific conditions cause a certain rate of air loss from the froth surface owing to the bursting bubbles. This changes as the froth depth grows with height and until it reaches an equilibrium height where the rate of air entering the froth is equal to the rate of air leaving the froth surface via bubble bursting. This measurement incorporates the effect of froth depth and thus accounts for factors relating to froth depth that influence the froth stability behaviour. In addition, the froth height grows during this measurement due to the addition of bubbles at the pulp-froth interface. Attached solid particles accumulate in the froth, as the attached solid particles enter the froth and none flow out of the froth, despite the air and water leaving the froth due to bubble bursting and slurry drainage respectively. This results in the measurement deviating from the relative steady state conditions that occur in flowing froth conditions.

The column based measurements in industrial systems are inadequate. Despite their convenience for specific manual measurements, they are impractical as long term on-line measurements used as inputs into a control system. This is due to factors such as the highly abrasive environment within a flotation cell and the intrusive nature of the column, which disrupts the froth flow within a flotation cell, impinging upon the performance of the froth.

Ventura-Medina *et al.* (2003) proposed a stability measurement based upon the measurement of the recovery of air to the concentrate. Results in section 4.2.7 imply that the air rate is less sensitive to changes in stability near the froth launder due to the non-uniform air loss across the froth surface.

The image processing based measurements developed by Cipriano *et al.* (1997) and Hatfield (2006) measure either the disparity or correlation of consecutive froth images. If no bubbles burst across two frames, the images are well correlated and have little difference, inferring a

stable froth. However, when bubbles burst, coalesce or move relative to each other across two frames, the correlation between the images decreases and the disparity increases, inferring a less stable froth. These measurements work well across similar appearing froths and are sensitive to small changes in stability. However, these measurements are inadequate across large changes in froth structure. This is due to a number of mechanisms affecting them disproportionately, such as bubble coalescence, bursting and mobility. Thus, these measurements do not directly account for specific physical froth behaviour and are difficult to interpret.

Hatfield (2006) proposed a froth stability index, defined as *the inverse rate of lamella rupture per second per number of lamella within a given volume*. This definition resolves into the determination of an average bubble lifetime for the froth. When applied across the entire froth phase, this definition compares the froth surface bubble size and an estimated pulp bubble size while considering the froth residence time (air rate and froth height). Froth stability as determined by this definition is a function of solids loading and particle hydrophobicity. While the particle hydrophobicity may remain consistent within a system, the solids loading changes as a function of bubble size and operating conditions. In addition, lamella size affects this measure where equivalently loaded but larger lamellae may rupture more readily than smaller lamellae. Thus, as the solids loading and size of bubbles within a froth varies to a large extent across the froth phase, the measurement of this stability factor would be subject to a wide range of variability. Thus, it would ideally be better suited to be measured as a function of bubble size, loading and possibly position within the froth, within a modelling context.

Froth stability encompasses a number of interacting mechanisms that occur through the froth, such as bubble coalescence, surface area loss, particle detachment, slurry drainage and particle re-attachment. These mechanisms interact with different operating parameters with different magnitudes, as outlined in section 5.3. Thus, any single froth stability measurement, as defined by the previously mentioned authors, result in stability measurements that may not reflect the relevant proportional effect on a dominant mechanism.

The above-mentioned stability measurements measure specific aspects of froth stability behaviour, while ignoring other factors. The column based measurements depend upon the air rate and volumetric loss of air on the froth surface. The volumetric loss of air on the froth surface comprises of factors such as the burst rate, bubble size and amount of solids present stabilising the froth surface. The air recovery rate to the concentrate depends upon froth transport factors and the excess froth height above the weir, which are also related to the volumetric loss of air on the froth surface factors. However, the air recovery rate is less sensitive to changes near the launder, as it aggregates the stability effect across the entire froth surface.

Apart from the excess froth height, all of the stability factors that these stability measurements rely upon are apparent on the froth surface and measurable as froth surface descriptors using machine vision. Changes in operating conditions will change the froth surface descriptors in a specific manner in the presence of specific system conditions.

Thus, from the objectives described in section 1.1, the following are addressed in this chapter:

2. To test the sensitivity of machine vision measurements in measuring expected changes on the froth surface from changes in operating variables within a flotation system when the solids environment changes.
3. To determine the extent to which the operating variable effect on the froth surface behaviour and froth stability is consistent across a range of operating conditions within a single flotation cell when the solids environment changes.
4. To investigate the relationship between the froth stability and flotation performance across a range of operating conditions within a single flotation cell when the solids environment changes.

5.2. Experimental details

Four data sets from two flotation systems with specific characteristics investigate the effect of operating variables on froth stability. The characteristics considered were the concentration of hydrophobic solids present within the pulp and the relative hydrophobicity of these solids.

A data set from a copper flotation system (from Northparkes mine, chalcopyrite/bornite copper ore) contains highly hydrophobic solids. Whereas a platinum system (from a pilot plant, Merensky reef platinum ore from the Bushveld complex) contains solids with a low hydrophobicity, or floatability.

Within these data sets, the first rougher has a high concentration of floatable material, while the third rougher has a lower concentration of floatable material. Figure 5.1 shows the feed rate of the valuable element into the first and third rougher in both flotation systems, as determined from a mass balance performed around each rougher circuit. Given that the mass flow rate of the valuable material decreased to less than half of the feed into the first rougher, the amount of floatable material assumed to be present in the third rougher is less than half that present in the first rougher.

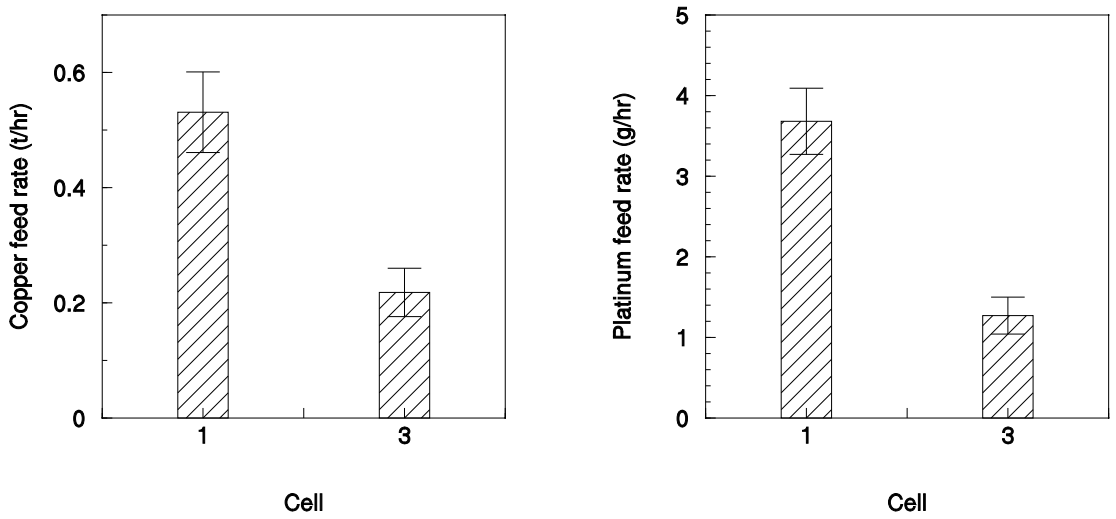

(a) Copper system

(b) Platinum system

Figure 5.1.: The feed rate of the copper and platinum elemental species into the first and third rougher cells, determined from a mass balance, for the (a) copper and (b) platinum systems respectively. The error bars denote one standard deviation of these values across all of the conditions tested.

The operating condition variation made to the copper and platinum systems were changes to the air flow rate, froth height and frother concentration, with additional variations in the platinum system to the frother type and use of activator.

Within both systems, measurements obtained include the burst rate of bubbles, solids loading, bubble size and velocity of the froth on the froth surface for each of the operating conditions.

Chapter 3 details the experimental procedure and measurements taken for each of the above-mentioned data sets. Appendix A contains the raw results from these measurements, that are subsequently analysed and discussed in this chapter.

5.3. Expected observations

5.3.1. Flotation mechanistic behaviour

Froth flotation is a complex system, in which operating variables interact with mechanisms internal to the process (Section 2.2). This section outlines some of these interactions and determines the key drivers within the process under each of the different operating conditions.

The behaviour of *air rate*, *froth height* and *frother concentration* on the *froth stability*, *solids loading* and *froth velocity* is of interest. The optimization of the flotation process across varying ore conditions, such as particle *hydrophobicity* and *floatable solids concentration* requires the understanding of the relationships between these operating variables and system parameters.

Previous authors in the literature, described in more detail in section 2.2, have determined the following behaviour:

- The bubble size entering the froth is proportional to the *air rate* entering the flotation cell (Cappuccitti and Nesset, 2009, Dai *et al.*, 2000).
- The frequency of bubble-particle collision events is inversely proportional to bubble size (Dai *et al.*, 2000, Schuhmann, 1942, Sutherland, 1948, Yoon and Luttrell, 1989).
- The attachment rate is proportional to particle *hydrophobicity* (Laskowski, 1986, Laskowski *et al.*, 1991).
- The bubble-particle aggregate stability is proportional to *hydrophobicity* and inversely proportional to *particle size* (Dai *et al.*, 2000, Nguyen *et al.*, 1998, Schuhmann, 1942, Sutherland, 1948).
- The solids flux into the froth is proportional to the particle-bubble collision frequency, attachment rate and bubble-particle aggregate stability factors, bubble surface area flux and *floatable solids concentration* (Dai *et al.*, 2000, Gorain *et al.*, 1997, Schuhmann, 1942, Sutherland, 1948).
- The transport of solids into the froth is a selective process (Seaman *et al.*, 2006).
- The amount of *coalescence* that occurs through the froth is dependent upon:
  - The bubble size, as larger lamellae or thin films rupture more easily (Kitchener and Cooper, 1959).
  - The solids loading on the bubble lamellae (Aveyard *et al.*, 1994, Dippenaar, 1982a,b).
  - The solids hydrophobicity (Aveyard *et al.*, 1994, Dippenaar, 1982a,b).
  - The frother or surfactant concentration (Comley *et al.*, 2002, Sweet *et al.*, 1997).
  - Froth residence time. The froth height plays a role where deeper froths tend to facilitate more coalescence to occur in cases where the froth lamellae are not stabilised, such as under low solids coverage or loading.

5.3.2. Operating variables

Operating variables are commonly modified to enhance flotation performance. A hypothesis, based upon the mechanisms and interactions described from the literature, states that the effect of operating variables on flotation performance will change under different *hydrophobicity* and *floatable solids concentration* conditions.

- **Air rate**
  An increase in air rate requires the bubble generation region in the flotation cell to break up an increased volume of air. Bubble breakup mechanisms within this region are not well understood, however, increased air rate generally results in an increase in the generated bubble size. Despite this increase in bubble size (faster rise rate through the froth), the gas holdup within the pulp phase increases due to the additional volume of air present.

  A combination of larger individual bubbles that rise faster, and a greater surface area with the same amount of floatable solids present contribute to lower rates of collision between particles and bubbles. Thus, the solids loading on individual bubbles entering the froth phase will decrease, causing a decrease in the amount of solids to liquid ratio entering the froth. This has implications with regards to lamella stability through the froth, which will influence the froth surface solids loading and burst rate. In addition, an increase in air rate will increase the amount of water entering the froth, resulting in higher levels of detached solids dropping out of the froth.

  Despite a lower average solids loading on bubbles entering the froth, owing to the higher gas holdup within the system, the overall solid flux entering the froth may increase.

- **Froth height**
  The decrease of the pulp-froth interface level within the flotation cell results in an increase in froth height. This facilitates the development of a froth structure under which further liquid drainage has occurred. The top layers of the froth will have a lower liquid content than the top layers of a shallower froth.

  Under conditions where high concentrations of highly hydrophobic solids enter the froth, the froth height will have a reduced effect on coalescence owing to lamella coverage saturation and stabilisation due to armouring. Armouring is a mechanism by which the increase in the packing density of solids attached at the air / water interface further stabilises the bubble. However, under conditions where lower concentrations of solids enter the froth or at lower lamella coverage, an increase in froth depth will result in

higher amounts of coalescence, causing a decrease in available surface area and an increase in solids loading.

- **Frother concentration**
  Frothers are surfactants that typically have a molecular structure that consists of a hydrophobic non-polar component and hydrophilic polar component.

  The frother concentration present in the solution affects the concentration of the frother adsorbed onto the air/water interface. As the concentration in the solution increases, higher adsorption densities, or loading of frother occurs at the air/water interface.

  Typically, increases in frother concentration result in a decrease in generated bubble size. However, despite the higher frother adsorption densities, bubbles generated within the pulp do not decrease in size above a critical frother concentration, termed the critical coalescence concentration (CCC). The frother concentration in typical flotation operation is usually above the CCC and thus frother concentration is not considered as a factor that modifies pulp bubble size in this work.

  Frother molecules at the air/water interface form weak hydrogen bonds between polar groups and water molecules. Higher adsorption densities result in the association of more polar groups with the air/water interface, thus dragging more water into the froth phase. This additional water forms the basis of the solution stabilisation effect. However, this effect is less significant in the presence of hydrophobic particles attached at the air/water interface.

  The change in the amount of coalescence within the froth that occurs when frother concentration changes is small while other stronger stabilising factors such as solids loading are present, especially in the presence of highly hydrophobic material. However, in the presence of low solids loadings and particles of low hydrophobicity, frother concentration will have a large effect on decreasing the coalescence rate and hence on flotation performance.

- **Frother type**
  Frother type varies across a wide range of different organic molecule families. In this work, the characteristics of a stronger frother chosen was a longer polyglycol chain length. This polymeric frother consists of monomers with a hydrophobic non-polar organic component and a polar group that is able to form hydrogen bonds with surrounding

water molecules. The strong frother consists of more monomers, resulting in a higher number of hydrophobic and polar groups per molecule.

The two frothers used in the low hydrophobicity system are the weaker, shorter chained polyglycol frother and the stronger, longer chained polyglycol frother. The increased frother strength should have a small stabilising effect owing to the increased number of polar groups present per molecule. However, high concentrations of hydrophobic material result in a dampening of this effect due to the strong influence that hydrophobic particles have on froth stability.

- **Activator presence**
  Activators may typically perform a number of functions to enhance the floatability of particles, ranging from cleaning mineral surfaces by dissolving precipitates to aiding ion and collector adsorption.

  The presence of an activator tends to increase the amount of hydrophobic solids entering the froth. Therefore, the froth should remain more stable due to the presence of higher concentrations of hydrophobic solids in the froth, owing to the activation of more hydrophobic material. However, in the presence low concentrations of floatable solids, activator will have little stabilising effect, and instead, as poorly liberated particles are present, the activator will activate these particles, resulting in particles that may also destabilise the froth.

5.3.3. Froth surface descriptors

Froth phase stability behaviour is only observable on the froth surface. Thus, the factors which effect mechanisms within the froth are not directly measurable. However, these factors may have an effect on the froth surface, which may affect easily measurable properties.

It is possible to measure a number of physical properties on the froth surface using machine vision (and gravimetrically in the case of solids loading). Based upon the mechanisms and interactions described, the following froth properties may behave differently, due to effect on internal mechanisms, as *hydrophobicity* and *floatable solids concentration* changes.

- **Solids loading**
  The solids loading on the froth surface depends upon the bubble size and solids loading on the bubbles entering the froth, the amount of coalescence through the froth that decreases available surface area, the amount of solid detachment occurring due to coa-

lescence and the amount of re-attachment that occurs from the draining material. Thus, the solids loading that reaches the froth surface is dependent on a large number of operating parameters. The bubble size and solids loading on bubbles entering the froth depends upon the air rate and amount of floatable solids available within the pulp. The amount of coalescence through the froth also depends upon solids loading and other factors relating to the properties of the attached solid particles and solution factors such as frother type and concentration. The amount of solids that detach during coalescence depends upon solid particle properties, such as hydrophobicity and the re-attachment rate would depend upon factors such as the concentration of floatable solids available in the draining slurry, and the availability of space on bubble lamellae for re-attachment.

Under all of the test conditions (high and low particle hydrophobicity and floatable solids concentration), the solids loading is expected to decrease with an increase in *air rate*, as an increase in air rate decreases the solids to water ratio entering the froth. This effect may be dampened owing to a decrease in solids loading resulting in an increased burst rate on the froth surface, releasing attached material that may be re-attached near the froth surface and stabilise the remaining bubbles.

In the presence of *highly hydrophobic solids*, an increase in *froth height* is expected to result in the decrease of the solids loaded on the froth surface, as increased froth depth results in higher amounts of coalescence within the froth, releasing more water, draining more detached solids out of the froth. This effect is expected to be dampened by the effect of the loss of surface area due to coalescence. In the presence of *low hydrophobicity solids*, froth stabilisation is more dependent on solids loading than particle hydrophobicity. Thus, an increase in froth height is expected to result in more coalescence than occurs in the high hydrophobicity case. This results in an increase in solids loading due to the loss of froth surface area to ensure that the froth remains stabilised near the froth surface.

Frother concentration will have negligible effect on the solids loading in the presence of *highly hydrophobic particles*, due to the stabilisation effect of the highly hydrophobic particles. However, in the presence of *low hydrophobic particles*, an increase in frother concentration will result in less coalescence occurring to increase the solids loading and stabilise the froth. Thus, an increase in frother concentration will result in a lower solids loading on the froth surface.

The use of a stronger *frother type* in the presence of *low hydrophobic particles* will have a similar effect on the solids loading as an increase in frother concentration, where, due to increased stability, the solids loading will decrease.

The presence of *activator* will only affect the solids loading under *high floatable solids concentration* conditions, which is likely to increase the solids loading, due to an increased amount of solids entering the froth phase.

- **Burst rate**
  The burst rate on the froth surface depends upon the bubble size on the froth surface, the solids loading on the bubble lamellae, the hydrophobicity of the attached solids and the frother concentration.

  Due to the lower amounts of floatable solids entering the froth per volume of air when the *air rate* is increased, the stability of the froth will decrease. Thus, it is expected that an increase in air rate will result in an increase in the rate at which bubbles burst on the froth surface.

  When *froth height* is increased, the water content at the froth surface decreases. This will result in a decrease in froth stability and thus, an increase in burst rate. The increase in burst rate will be more significant in *low floatable solid concentration* conditions, due to a lower froth stability owing to the presence of fewer hydrophobic particles.

  In the presence of *high floatable particle concentrations*, an increase in *frother concentration* will have very little to zero effect on the burst rate, owing to the dominating affect that the hydrophobic particles have on stability. However, under *low hydrophobic particle concentrations*, an increase in frother concentration will further stabilise the froth and decrease the rate at which bubbles burst on the froth surface, but increase the water and entrained material recovery.

  A stronger *frother type* is expected to decrease the burst rate owing to the effect that a higher adsorption density results in more water weakly associated with the interface. This effect will be greatly dampened in the presence of a *high concentration of floatable particles*.

  In the presence of a *high concentration of floatable particles*, the use of an *activator* will decrease the burst rate, due to an increase in the concentration of hydrophobic particles entering the froth.

- **Bubble size**
  The bubble size on the froth surface depends upon the coalescence rate through the froth, which is influenced by the factors that directly affect froth stability. However, bubble size interacts with the solids loading which tends to increase with bubble size and retard further coalescence.

  An increase in *air rate* is expected to increase the bubble size on the froth surface, due to the destabilising effect owing to the increased air rate. This effect is expected to be more pronounced under conditions where *high concentrations of floatable solids* are present and dampened under *low concentrations of floatable solids*.

  The bubble size is expected to increase with *froth height* due to the decreased water content and thus stabilisation in the top layers of the froth. However, this effect is expected to be dampened under conditions where *high concentrations of floatable solids* are present owing to the stabilising effect of the floatable solids present.

  Under *high floatable solids concentration* conditions, the *frother concentration* will have little to zero effect on bubble size owing to the stabilising effect of the floatable solids overriding the solution stability effect. However, at *low floatable solids concentration* conditions, an increase in frother concentration is expected to result in a decrease in bubble size owing to the increased water content from the increased frother loading at the air/water interface. However, this effect will be dampened in the presence of *highly hydrophobic particles*.

  A stronger *frother type*, in the presence of *high concentrations of floatable particles* will result in a decrease in bubble size due to a lower solids loading threshold required to stabilise the froth surface. However, in the presence of *low concentrations of floatable particles*, a stronger frother tends to result in an increased bubble size due to the additional stabilisation from the frother.

  Under *high concentrations of low hydrophobicity particles*, the presence of an *activator* will result in an increase in bubble size due to greater solids loadings being reached at larger bubble sizes from increased amounts of floatable particles in the froth. The activator will have little to zero effect under *low floatable solid concentration* conditions.

- **Velocity**
  The froth velocity depends upon the air rate entering the flotation cell, the burst rate on the froth surface and the distribution of air loss on the froth surface.

An increase in *air rate* is expected to result in an increase in froth velocity due to the air added into the froth phase. However, this effect will be dampened as the concentration of floatable solids present decreases, due to froth destabilisation.

An increase in *froth height* is expected to result in a decrease in froth velocity, as a higher rate of bubble bursting occurs in deeper froths due to the lower water content in the top layers of the froth.

Increased *frother concentration* is expected to result in an increase in velocity due to the increased stability owing to the increased water content from a higher concentration of polar groups attached at the air/water interface. Thus, this effect will be most prominent under a *low concentration of floatable solids*. Under *high concentrations of floatable solids*, this effect will be dampened, owing to the hydrophobic solid particles controlling the stability of the froth.

A stronger *frother type* is expected to result in a similar effect to an increased frother concentration, where froth velocity increases. This is due to the increased number of polar groups available per frother molecule attached to the air/water interface.

Under a *high concentration of floatable solids*, the presence of *activator* will result in increased velocity, due to increased stability owing to the increase in hydrophobic solids within the froth.

The behaviour of the froth surface across the operating conditions changed have been described above, and is complex. However, within normal operating conditions, changes occur on the froth surface due to uncontrolled disturbances brought upon the system by factors such as changes in the concentration and hydrophobicity of the floatable solids. This work tests whether the physical froth surface descriptor measurements are sensitive to the expected changes to the specific physical froth surface descriptors across changes in operating conditions.

5.4. Results

5.4.1. Effect of operating conditions on solids loading and froth stability

This section presents the results of an investigation into the relationships between the operating conditions on the physical froth surface descriptors within each system. This analysis was performed using the raw data presented in appendix A.

The data within each system and in different flotation cells are not directly comparable as the operating conditions were different and the changes made differed in magnitude. Thus, the analysis method required should be able to determine the coarse relationships between factors by measuring the significance and direction of the relationship.

Flotation is a non-linear system. Many researchers have shown that the froth phase exhibits non-linear behaviour. Despite this, within this work, linear regression was chosen as a tool to determine whether the direction that a factor is changed affects a system consistently, as it was judged robust enough over the range of operating variables tested. Thus, only two levels of change, usually high and low, were made when investigating the effects of the factors in the system.

Therefore, linear regression was used to analyse the data and determine the significance and the direction of the relationship between the operating conditions and the measured froth surface descriptors.

When performing the regression analysis for solids loading on the froth surface, the y-axis intercept was determined, as a naturally high abundance of hydrophobic material will influence the level of solids loading on the froth surface. Thus, the intercept value relates to the abundance of hydrophobic material within the system. However, for all the other factors, the intercept was forced through zero. This analysis shows potential relationships between the factors and the response variables. The use of an intercept within the regression can mask those relationships. In addition, within normal operation, the manipulated or measured factors are unlikely to be zero, and hence an intercept value has little intrinsic value.

The importance of the factors were determined and ranked based upon the level of significance of the factor and the direction of the correlation. Highly significant relationships ($++$ or $--$) require a p-value of less than 0.05 (95 % confidence), while significant relationships ($+$ or $-$) require a p-value less than 0.15 (85 % confidence).

5.4.2. Regression analysis

Multiple regression analyses were performed relating operating variables to the froth surface descriptors and flotation performance factors. By way of an example, the regression analysis relating the operating variables to the machine vision solids loading measurement is shown in table 5.1. All of the regression analyses performed for this thesis are presented in appendix B.

Table 5.1.: Regression results relating the *machine vision solids loading* to the *air rate*, *froth height* and *frother concentration* in the first copper rougher.

Multiple R	0.322
R^2	0.103
Standard Error	0.003
Adjusted R^2	0.241
Observations	19

	df	SS	MS	F	Significance of F
Regression	5	0.0000140	0.00000281	0.50	0.771
Residual	13	0.000122	0 00000937		
Total	18	0.000136			

	Coefficients	Standard Error	t-Statistics	p-Value	Significance
Intercept	0.0284	0.0153	+ 1.851	0.09	++
Air rate	1.16	1.30	+ 0.892	0.39	
Froth depth	− 0.0125	0.0403	− 0.311	0.76	
Frother concentration	− 0.0000302	0.0000485	− 0.622	0.54	

The regression analysis shows that in this case, the variation in the operating conditions are not significant in describing the variation observed in the solids loading measured on the froth due to the obtained R^2 and ANOVA results. However, the direction (positive or negative) of the determined coefficients give an indication as to the type of behaviour that the factor has on the solids loading and the p-Value gives a level of confidence. Thus, this information is useful to determine the type of influence that a factor may have on a measured quantity. In this case, the results show that the intercept is a highly significant positive factor on the machine vision solids loading measurement.

The results from the remainder of the regression analyses performed are reported in appendix B. The direction and significance of factors on the measured quantity are presented in summary tables in section 5.4.3.

5.4.3. Summary of regression results

The results from the regression analyses performed have been summarised and are shown in tables 5.2, 5.3, 5.4 and 5.5.

Table 5.2 and 5.3 shows the effect of the operating conditions on the froth surface solids loading, bubble size, burst rate and velocity in addition to the recovery rate and grade of the solids recovered to the concentrate. Given that the operating conditions can and are explicitly modified within a flotation system, the correlation between parameters shown in these results have been assumed to imply causation.

Table 5.5 shows the relationship between key factors relating the froths stability behaviour to the velocity of the froth and the recovery rate and grade of the solids recovered to the concentrate. Given that the froth stability factors are not inputs into the system, correlation between them (with the exception of frother concentration) and flotation performance factors does not imply causation.

Based upon the results shown in these tables, different operating conditions had different levels of effect on various aspects of the flotation system under each different condition. For example, within both systems, in rougher one, an increase in the air rate resulted in an increase in the burst rate on the froth surface, indicating a decrease in froth stability. This may be explained, in the case of the copper system, by the measured decrease in the solids loading due to the increased air rate. However, within the platinum system, an increase in air rate did not show a highly significant effect on the solids loading. Instead the increase in air rate resulted in a physically measured increase in the bubble size on the froth surface. In addition, further down the bank, in both systems, the air rate had a much less significant effect on the froth stability.

From the point of view of relating operating conditions to flotation performance, the results show that more significant relationships existed between the flotation performance characteristics and aspects that relate to the froth stability as opposed to the operating variables that can be manipulated to control a flotation cell. Thus, these results illustrate that the understanding of the relationship between operating conditions and froth stability behaviour and the relationship between froth stability and flotation performance is essential to develop an effective on-line control and optimisation system.

These results, are discussed in more detail in section 5.5.

Table 5.2.: The expected and measured influence and confidence (measured in percent) between operating conditions and *solids loading*, *froth surface bubble size (p^{80})*, *burst rate*, *velocity*, *solids recovery* and *valuable grade* under conditions where differing concentrations and hydrophobicity of the floatable solids were available.

System	Operating variables	Expected and measured influence and confidence of measure															
		Solids loading						p^{80} bubble size		Burst rate		Velocity		Solids recovery		Valuable grade	
		E^a	MV^b	MV^b_{p80}	MV^b_b	$MV^b_{b,p80}$	G^c	E^a	M^d	E^a	M^d	E^a	M^d	E^a	M^d	E^a	M^d
High hydrophobicity High solids concentration (Copper rougher 1)	Intercept	++	+ 91	+ 85	+ 94	+ 98	+ 100										
	Air rate	−−	+ 61	+ 53	− 70	− 14	− 100	++	+ 92	++	+ 100	++	+ 90	++	+ 49	−−	+ 92
	Froth height	−	− 24	− 74	− 76	− 100	− 85	+	+ 90	+	− 97	−−	+ 57	−	+ 86	+	+ 56
	Frother concentration	0	− 46	− 45	+ 16	− 42	+ 1	0	− 74	0	+ 30	0	− 60	+	− 81	−	+ 62
High hydrophobicity Low solids concentration (Copper rougher 3)	Intercept	++	+ 100	+ 100	+ 100	+ 100	+ 100										
	Air rate	−−	− 95	− 99	− 97	− 89	− 100	0	+ 1	+	+ 98	+	+ 96	+	+ 96	−	− 77
	Froth height	−	− 87	− 45	− 100	− 100	− 87	++	+ 93	++	+ 62	−	− 86	−−	− 85	++	+ 100
	Frother concentration	0	+ 64	+ 24	+ 66	+ 50	+ 1	−	+ 43	−	− 83	++	+ 92	++	+ 80	−−	− 14
Low hydrophobicity High solids concentration (Platinum rougher 1)	Intercept	+	+ 100	+ 100	+ 100	+ 100	+ 90										
	Air rate	−−	− 91	− 82	− 59	− 86	+ 52	++	+ 97	++	+ 100	++	+ 76	++	+ 100	−−	+ 99
	Froth height	++	+ 99	+ 96	+ 20	+ 96	− 92	+	+ 58	+	− 100	−−	− 75	−	− 100	+	− 76
	Frother concentration	−	− 99	− 91	+ 97	− 25	+ 15	0	− 19	0	+ 84	+	+ 86	+	+ 35	−	+ 51
	Frother type	−	− 100	− 95	+ 96	− 39	− 5	−	− 74	−	+ 58	+	+ 89	+	+ 100	−	− 51
	Activator presence	++	+ 98	+ 99	− 89	+ 96	+ 54	++	+ 99	−−	− 90	++	− 41	++	− 89	−−	− 70
Low hydrophobicity Low solids concentration (Platinum rougher 3)	Intercept	0	+ 63	+ 80	+ 100	+ 100	− 17										
	Air rate	−	+ 64	+ 64	+ 47	+ 51	− 61	+	+ 44	+	+ 62	+	+ 41	+	+ 63	−	+ 38
	Froth height	++	+ 88	− 3	+ 20	+ 12	+ 94	++	+ 96	++	+ 94	−	+ 7	−−	− 13	++	+ 74
	Frother concentration	−	− 93	− 95	+ 100	+ 100	− 65	−−	− 92	−−	− 99	++	+ 88	++	− 38	−−	− 63
	Frother type	−	− 73	− 88	− 24	− 19	− 61	++	+ 94	−−	+ 90	+	+ 67	+	+ 83	−	− 77
	Activator presence	0	+ 10	+ 58	− 67	− 64	+ 89	0	+ 36	0	+ 37	0	− 37	0	+ 40	0	+ 43

a. Expected based upon hypothesised behaviour

b. Machine vision solids loading measurement for different bubble classes ($_{p80}$: bubbles larger than the p80, $_b$: bursting bubbles)

c. Gravimetric solids loading measurement

d. Measured

Table 5.3.: Summary of relationships between operating conditions and the expected and measured *solids loading*, *froth surface bubble size (p^{80})*, *burst rate*, *velocity*, *solids recovery* and *valuable grade* under conditions where differing concentrations and hydrophobicity of the floatable solids were available.

System	Operating variables	Significance															
		Solids loading						p^{80} bubble size		Burst rate		Velocity		Solids recovery		Valuable grade	
		E^a	MV^b	MV^b_{p80}	MV^b_b	$MV^b_{b,p80}$	G^c	E^a	M^d	E^a	M^d	E^a	M^d	E^a	M^d	E^a	M^d
High hydrophobicity High solids concentration (Copper rougher 1)	Intercept	++	+	+	+	++	++										
	Air rate	−−					−−	++	+	++	++	++	+	++		−−	+
	Froth height	−				−−	−	+	+	+	−−	−−		−	+	+	
	Frother concentration	0						0		0		0		+	−	−	
High hydrophobicity Low solids concentration (Copper rougher 3)	Intercept	++	++	++	++	++	++										
	Air rate	−−	−−	−−	−−	−	−−	0		+	++	+	++	+	++	−	
	Froth height	−	−		−−	−	−	++	+	++		−	−	−−	−	++	++
	Frother concentration	0						−		−	−	++	+	++		−−	
Low hydrophobicity High solids concentration (Platinum rougher 1)	Intercept	+	++	++	++	++	+										
	Air rate	−−	−	−		−		++	++	++	++	++		++	++	−−	++
	Froth height	++	++	++		++	−	+		+	−−	−−		−	−−	+	
	Frother concentration	−	−−	−	++			0		0	+	+	+	+		−	
	Frother type	−	−−	−−	++			−		−		+	+	+	++	−	
	Activator presence	++	++	++	−	++		++	++	−−	−	++		++	−	−−	
Low hydrophobicity Low solids concentration (Platinum rougher 3)	Intercept	0		+	++	++											
	Air rate	−						+		+		+		+		−	
	Froth height	++	+				+	++	++	++	+	−		−−		++	
	Frother concentration	−	−	−−	++	++		−−	−	−−	−−	++	+	++		−−	
	Frother type	−		−				++	+	−−	+	+		+	+	−	
	Activator presence	0					+	0		0		0		0		0	

a. Expected based upon hypothesised behaviour

b. Machine vision solids loading measurement for different bubble classes ($_{p80}$: bubbles larger than the p80, $_b$: bursting bubbles)

c. Gravimetric solids loading measurement

d. Measured

Table 5.4.: The measured influence and confidence (measured in percent) between stability factors and the measured *froth velocity*, *solids recovery*, *water recovery* and *valuable grade* under conditions where differing concentrations and hydrophobicity of the floatable solids were available.

System	Stability factor	Significance							
		Froth velocity		Solids recovery		Water recovery		Valuable grade	
		MV[a]	G[b]	MV[a]	G[b]	MV[a]	G[b]	MV[a]	G[b]
High hydrophobicity High solids concentration (Copper rougher 1)	Intercept								
	Burst rate	− 32	+ 48	− 41	+ 41	+ 77	+ 91	+ 28	+ 71
	Solids loading (MV / GV)	+ 62	+ 37	+ 23	− 99	− 74	− 99	+ 41	+ 98
	p^{80} bubble size	+ 38	+ 97	+ 92	+100	+ 98	+100	+ 37	+ 88
	Frother concentration	− 8	+ 8	− 57	− 17	− 72	− 76	+ 95	+ 97
High hydrophobicity Low solids concentration (Copper rougher 3)	Intercept								
	Burst rate	− 49	+ 56	+ 43	+ 85	+ 62	+ 90	+ 81	+ 28
	Solids loading (MV / GV)	+100	+ 98	+ 98	+ 91	+ 99	+ 84	− 98	− 68
	p^{80} bubble size	− 94	− 40	− 94	− 70	− 98	− 81	+100	+ 99
	Frother concentration	− 21	+ 75	+ 8	+ 72	− 30	+ 49	+ 88	+ 42
Low hydrophobicity High solids concentration (Platinum rougher 1)	Intercept								
	Burst rate	+ 55	+ 87	− 96	+ 94	− 80	+ 90	+ 98	+100
	Solids loading (MV / GV)	+ 33	+ 45	+100	+ 81	+ 97	− 37	− 71	− 62
	p^{80} bubble size	− 35	− 25	−100	− 59	− 98	− 42	+ 88	+ 92
	Frother concentration	+ 36	+ 66	−100	− 39	− 77	+ 39	+ 60	+ 20
Low hydrophobicity Low solids concentration (Platinum rougher 3)	Intercept								
	Burst rate	− 99	−100	− 95	− 97	− 94	− 99	+ 92	+100
	Solids loading (MV / GV)	− 65	− 65	+ 30	− 80	− 46	− 96	+ 96	+ 93
	p^{80} bubble size	+100	+100	+ 99	+ 99	+ 99	+100	− 96	− 99
	Frother concentration	+ 32	+ 8	− 95	− 95	− 16	− 13	+ 78	+ 97

a. Machine vision solids loading measurement used in regression

b. Gravimetric solids loading measurement used in regression

Table 5.5.: Summary of relationships between stability factors and the measured *froth velocity*, *solids recovery*, *water recovery* and *valuable grade* under conditions where differing concentrations and hydrophobicity of the floatable solids were available.

System	Stability factor	Significance							
		Froth velocity		Solids recovery		Water recovery		Valuable grade	
		MV[a]	G[b]	MV[a]	G[b]	MV[a]	G[b]	MV[a]	G[b]
High hydrophobicity High solids concentration (Copper rougher 1)	Intercept								
	Burst rate						+		
	Solids loading (MV / GV)				−−		−−		++
	p^{80} bubble size		++	+	++	++	++		+
	Frother concentration							++	++
High hydrophobicity Low solids concentration (Copper rougher 3)	Intercept								
	Burst rate				+		+	+	
	Solids loading (MV / GV)	++	++	++	+	++	+	−−	
	p^{80} bubble size	−		−		−−	−	++	++
	Frother concentration							+	
Low hydrophobicity High solids concentration (Platinum rougher 1)	Intercept								
	Burst rate		+	−−	+		+	++	++
	Solids loading (MV / GV)			++	+	++			
	p^{80} bubble size			−−		−−		+	+
	Frother concentration			−−					
Low hydrophobicity Low solids concentration (Platinum rougher 3)	Intercept								
	Burst rate	−−	−−	−−	−−	−	−−	+	++
	Solids loading (MV / GV)				−		−−	++	+
	p^{80} bubble size	++	++	++	++	++	++	−−	−−
	Frother concentration			−−	−				++

a. Machine vision solids loading measurement used in regression

b. Gravimetric solids loading measurement used in regression

5.5. Discussion

New machine vision measurements have been proposed within this thesis, described in chapter 4, to measure the bubble burst rate and solids loading on the froth surface.

These measurements, along with other machine vision based physical froth surface descriptors have been used to analyse images of the froth surface obtained from two experimental campaigns performed on different flotation systems. The two flotation systems chosen have different mineral hydrophobicities. The floatable minerals within the copper system were chalcopyrite and bornite, which tend to be highly hydrophobic. The floatable minerals within the platinum system were mostly pentlandite and pyrrhotite with some chalcopyrite, and tend to be of much lower hydrophobicity.

Furthermore, this analysis was performed at two locations within the rougher bank (roughers 1 and 3) to account for a decrease in concentration of floatable solids present within the flotation cell.

Both of the proposed measurements, in addition to other available machine vision measurements, have been used to investigate the driving factors in the relationship between the operating conditions and froth stability, froth transport and flotation performance measurements. The results from this analysis are shown in section 5.4.3.

The expected froth behaviour with respect to the machine vision measurements has been hypothesised under each condition in section 5.3. The correspondence between the machine vision measurements and the expected behaviour is investigated to determine the validity and usefulness of the machine vision measurements.

Under specific conditions, the measured froth behaviour may not correspond with the expected, or hypothesised behaviour. This may occur due to two possibilities; experimental error in either the measurements or experimental setup, or a poor understanding of the froth behaviour under certain conditions.

Within this section, the performance of the machine vision measurements are evaluated by correlating the measured performance with the expected froth behaviour. In addition, for the conditions where the measured behaviour does not correspond with the expected behaviour, experimental error is considered, along with potential alternative mechanisms that may explain the measured behaviour. The froth phase mechanisms that are attributed to affect key processes occurring within the froth phase that result in the observed effects, are considered across changes in the floatable solid concentration and hydrophobicity regimes.

The role that froth stability, as interpreted using the physical froth surface descriptor measurements, have on flotation performance under each of the solids regimes is also discussed. This work investigates the potential for the use of stability measurements to interpret (or potentially control) performance in a flotation cell.

5.5.1. Evaluation of machine vision measurements

Tables 5.2 and 5.3 show the measurement of physical froth factors in a response to changes made in operating conditions. In addition the expected response, determined from the hypothesised behaviour is noted.

Solids loading

The machine vision measurement of solids loading can be determined as a function of bubble size and on specific bubbles, such as bubbles that burst in a subsequent video frame. Thus, a number of different solids loading measures that are related to bubble size and bubbles that are less stable are obtained. Within this work, the average solids loading was determined for either across the top 20 % of bubbles in the bubble size distribution, or across the entire bubble size distribution. These two measurements were also applied to determine the solids loading on bubbles that subsequently burst in the next video frame. Gravimetric solid loading measurements were also taken using the method described in section 3.3. Thus, both of these methods can be compared to the expected solids loading behaviour within the froth, hypothesised in section 5.3.

The results show that in the presence of highly hydrophobic solids, the gravimetric measurements correspond well with the hypothesised behaviour, indicating that the gravimetric method is sensitive to the expected behaviour. However, all of the machine vision measurements are only sensitive to these variations at low solid concentration conditions.

At the high solids concentration condition, machine vision solid loading measurements across all bubbles (including bursting bubbles) show a weak increase in solids loading when air rate is increased and a weak decrease in solids loading when froth height is increased. However, the solids loading on the bursting bubbles have been measured to decrease more strongly, both as the air rate and froth depth increases. Thus, the bursting bubbles show similar solids loading behaviour to the gravimetric measurements and the hypothesised behaviour which indicates that the bubbles that are bursting may have a decreased solids loading under these conditions.

In the case of the increased air rate condition, where the average solids loading increases with air rate, detached solids, potentially, from the larger (bursting) bubbles may become re-attached to the smaller bubbles, resulting in increased solids loading, further stabilising the smaller bubbles near the froth surface.

In the presence of low hydrophobicity solids, little correspondence exists between the gravimetric measurement and the hypothesised measurements. However, the machine vision measurements show high levels of correspondence with the hypothesised behaviour, especially at high floatable solids conditions.

In the presence of high concentrations of floatable solids, the solids loading on the bursting bubbles increases when froth height increases. However, a stronger relationship is observed with the larger bursting bubbles than across all of the bubbles that burst. This behaviour may be consistent with an armouring mechanism responsible for increasing the froth stability by stabilising the larger bubbles, reducing their burst rate.

Under both low and high floatable solids concentrations where the frother concentration increased or a stronger frother is used, the bursting bubbles have also been measured to reflect an increase in solids loading across all bursting bubble sizes, while the average loading was measured to reflect a decrease in loading across all bubbles. This measurement may reflect the stabilisation of poorly loaded bubbles due to the frother and be more sensitive to the more highly loaded bubbles that are loaded with solids which may destabilise the bubbles, such as composite particles, triggering more burst events.

These findings show that the gravimetric solids loading measurement may be more sensitive to changes in solids loading behaviour in systems that have high hydrophobicity particles and may not be sensitive enough to changes in systems with low hydrophobicity particles. However, the machine vision results correspond to the hypothesised behaviour in the presence of low hydrophobicity solids and at low floatable solid concentrations. In addition, under certain conditions, the machine vision solids loading measurements are able to measure differences in the solids loading behaviour on both bursting and larger bubbles.

Machine vision solids loading measurements, in conjunction with bubble segmentation methods have the potential to measure the solids loading distribution between different classes of bubbles. Each class of bubbles contribute to an aggregated behaviour on the froth surface. Thus it is now possible to decouple solids loading effects on bursting bubbles from the stabilised bubbles and decouple the solids loading effects on the larger bubbles from the smaller bubbles. These findings have shown to be consistent with the expected results in each of the scenarios investigated.

Burst rate

The burst rate is expected to increase as the froth becomes less stable. This decrease in stability occurs at higher air rates and froth depths, and at lower frother concentrations, in the presence of weaker frothers, or lower concentrations of activator.

The burst rate measurement results show that the burst rate increases with increased air rate under all conditions. These results correspond with the hypothesis that an increase in air rate destabilises the froth.

The burst rate measurement results show that the burst rate increases when froth height increases in the presence of a low concentration of floatable solids. These results are consistent with the expected decrease in water content near the froth surface at higher froth depth conditions. However, in the presence of high concentrations of floatable solids, the burst rate was measured to decrease when the froth height was increased. This result contradicts the expected behaviour under these conditions which, is a dampened increase in burst rate.

Typically, when froth height increases, the bubble size on the froth surface increases, as is observed from the bubble size measurements. As the bubble size increases, the available surface area in the froth decreases, which results in an increase in the solids loading at the air/water interface. The increased loading may stabilise the air/water interface. This increase in loading has been measured in the low hydrophobicity case, which would account for the decreased burst rate in the form of an armouring mechanism. Armouring refers to an increase in the packing density of particles on the lamella surface. However, the solids loading measurement decreased in the high hydrophobicity case, with a significant decrease occurring on the larger, bursting bubbles.

When the bubble size increases, the number of bubbles on the froth surface decreases, which may explain the observed decrease in burst rate under these conditions. In the presence of high concentrations of highly hydrophobic solids, the average p^{80} bubble diameter has increased by 26 % from 37.2 to 46.7 mm when the froth height was increased at the low frother concentration conditions. This increase in bubble size translates to an increase in the cross-sectional surface area of the bubbles by 57 %.

Assuming that the bottom 60 % of bubbles in the cumulative bubble size distribution are of similar size, and that the bubble size distributions differ across the top 40 % of bubble sizes, based upon the cross-sectional area of the p^{80} bubbles, 368 and 234 bubbles are present per square meter of froth in the top 40 % of the bubble size distribution in the low and high froth depth conditions respectively. Based upon this difference and that on average 69.9 and 52.8

bubbles per second burst per square meter of froth in the low and high froth depth conditions respectively, 19.0 % and 22.6 % of the larger bubbles present ($>p^{60}$) burst. Thus, a higher proportion of bubbles burst at the high froth depth condition.

The average increase in bubble diameter observed across the low and high froth depth conditions result in an average increase in bubble volume by 97 % across these conditions. Thus, the p^{80} bubble volume at the high froth depth condition is twice that of the low froth depth condition. However, in terms of air loss estimates, only 0.0019 and 0.0028 $m^3/m^2/s$ is lost to bubble bursting near the launder in the low and high froth depth conditions respectively. Despite the volume of the large bubbles being twice the size at the high froth depth condition, only 33 % more air is lost at the high froth depth condition.

These results illustrate that a difference in stability exists between the low and high froth depth conditions. Either the low froth depth condition is less stable than expected, or the high froth depth condition is more stable than expected. Due to an expected and observed decrease in solids loading on the froth surface as froth depth is increased, the role of highly hydrophobic solids may be destabilising the froth. This is consistent with findings from previous authors that highly hydrophobic particles tend to destabilise the froth after a critical hydrophobicity (Ata *et al.*, 2003). However, in this case, this appears to occur as a function of solids loading.

The burst rate is not expected to be affected significantly by increases in frother concentration in the presence of high concentrations of hydrophobic solid particles. Under these conditions, an increase in frother concentration has been measured to increase the burst rate, however, these measurements are not highly significant and may relate to the solids loading measured on the bursting bubbles.

In the presence of low concentrations of hydrophobic solid particles, an increase in frother concentration is expected to increase the froth stability and thus decrease the burst rate. The results show that the burst rate does decrease under these conditions, however, most significantly in the presence of low hydrophobicity solids.

In the presence of low hydrophobicity solids, a stronger frother is expected to stabilise the froth and decrease the burst rate on the froth surface. However, the results show that the burst rate increases in the presence of both low and high concentrations of floatable solids. While the increase observed in the presence of high concentrations of solids is of low confidence, the increase in burst rate observed at low concentrations of solids may be due to the significant increase in bubble size under this condition, as larger bubbles tend to burst more easily than smaller bubbles.

In the presence of low hydrophobicity solids, the presence of an activator is expected to result in higher attachment rates of solids within the pulp, thus larger concentrations of floatable solids would enter and stabilise the froth. Under these conditions, the presence of activator is expected to result in a decrease in the burst rate. Due to the effect of the activator being dependent on floatable solids, the effect is only expected to be apparent under high concentrations of floatable solids. The results confirm this hypothesised behaviour, as in the presence of high concentrations of floatable solids the burst rate decreases with a high level of confidence, while in the presence of low concentrations of floatable solids a burst rate increase is measured, however with low confidence.

These findings show that the burst rate measurement corresponds with its hypothesised behaviour under most operating condition changes. However, of notable exception is the effect that an increase in froth height has on the burst rate in the presence of high concentration of floatable solids. Under these conditions, the measured behaviour can be accounted for by considering the solids loading and its effect on froth stabilisation.

Bubble size

The bubble size distribution on the froth surface is affected by and reflects the amount of coalescence that has occurred within the froth. The bubble size measurement chosen to represent bubble size changes was the bubble diameter of the 80^{th} percentile bubble in the bubble size distribution (p^{80}). This measurement was chosen based upon work performed by Forbes (2007), who showed that the 80^{th} percentile bubble size is the size that differs most, and more so than other mean values. This finding promotes a better signal to noise ratio than using the mean, median or Sauter mean bubble diameter to differentiate between separate bubble size distributions. However, for other purposes, the Sauter mean bubble diameter may be a more appropriate measurement.

In the presence of high concentrations of floatable solids, an increase in the air rate is expected to result in an increase in bubble size. The increased air rate results in a decrease in the concentration of solids entering the froth, resulting in more coalescence being required to increase the solids loading to sufficient levels to stabilise bubbles on the froth surface. However, in the presence of low concentrations of floatable solids, air rate is expected to have little effect, due to the lower relative effect on the solids entering the froth. The results show that the measured bubble size does increase under these conditions. In addition, in the presence of low concentrations of floatable solids, the bubble size does not change significantly.

The bubble size is expected to increase with froth height owing to the destabilisation caused by the extra slurry drainage that occurs near the froth surface in deeper froths. However, this increase in bubble size will be dampened in the presence of high concentrations of floatable solids, owing to their stabilising effect overriding the solution stabilising effect. The results show that an increase in bubble size is measured when the froth depth is increased under all of the conditions. The change is observed with greater confidence in the low floatable solids concentration conditions. These results correspond with the hypothesised behaviour.

The bubble size is expected to decrease with an increase in frother concentration. This effect is expected to be dampened in the presence of high concentrations of floatable solids. The results from the low hydrophobicity system correspond with this hypothesised behaviour. However, the results from the high hydrophobicity system may be coupled closely with the solids loading behaviour on the froth surface and correspond with the solids loading measurements. In the high concentration of floatable solids case, a decrease in solids loading is measured, with low significance, which corresponds with a low significance measure of a decreased bubble size and increased burst rate. These measurements indicate that, due to lower solids loading, smaller bubbles persist on the froth surface, with higher burst rates in larger bubble sizes. The converse is apparent in the presence of a low concentration of highly hydrophobic solids. These results indicate that more hydrophobic solids tend to override the effect of the frother to an extent where the solids loading influences bubble size behaviour more than the frother concentration.

The bubble size is expected to decrease in the presence of high concentrations of floatable solids when a stronger frother type is used. However, in the presence of low concentrations of floatable solids, the bubble size increases. The difference between these two conditions occur due to the added effect of the solids. When high concentrations of floatable solids are present, the stronger frother retards coalescence within the froth, resulting in smaller bubbles on the froth surface. However, when low concentrations of floatable solids are present, high rates of coalescence exist within the froth. Despite the lower stability within the froth, the frother exerts a more significant effect, stabilising larger bubbles on the froth surface, enabling them to exist for longer periods of time. The results from the low hydrophobicity conditions confirm these hypotheses.

The bubble size is expected to increase in the presence of high concentrations of floatable solids when activator is used owing to increased levels of hydrophobic solids stabilising larger bubbles on the froth surface. However, no significant effect on bubble size is expected in the presence of low concentrations of floatable solids, due to a proportionally smaller level of

activation under these conditions. The results show that the bubble size measurements confirm this hypothesis.

The machine vision bubble size measurements show a large degree of correspondence between the measured and expected bubble size changes across each condition tested. However, in the presence of highly hydrophobic solids, frother concentration effects are over-ridden by solids loading effects, possibly owing to the higher stabilising factors present from the high hydrophobic solids. In addition, the frother type was shown to result in differing effects on the froth surface as a function of the available floatable solids concentration. Under the changes observed, the dominant effect of frother type on bubble size changed from acting within the froth phase (high floatable solids concentration) to acting on the froth surface (low floatable solids concentration).

Velocity

The froth velocity reflects the transport rate of the froth moving towards the launder. However, additional information is required to determine factors such as surface area, solids or water recovery rate to the concentrate. Froth velocity is however strongly related to froth stability, and in particular the surface bubble size and burst rate. In conditions where a large amount of air is lost on the froth surface, the transport of the froth towards the launder will be low, while in conditions where small amounts of air is lost on the froth surface, the froth transport rate towards the launder will be high.

The froth velocity is expected to increase with an increase in air rate, reach a maximum and then decrease (Hadler and Cilliers, 2009). The increase in velocity will occur under conditions where the increase in air loss due to an increased burst rate owing to froth destabilisation is less than the increase in air rate to the flotation cell. Once the increase in air lost from bursting is greater than the additional air fed into the cell, the froth velocity will start to decrease with air rate.

The results from the high hydrophobicity conditions show a strong increase in velocity, while an increase in velocity is measured, with a low confidence in the low hydrophobicity conditions. These results show that the conditions investigated were performed prior to the attainment of the peak air rate.

An increase in froth height is hypothesised to result in a decrease in froth velocity. This is due to a decreased water content near the froth surface resulting in a less stable froth, with more bursting occurring, decreasing the froth transport rate. The results show that a

decrease in froth velocity is measured under the low concentration of high hydrophobicity solids and high concentration of low hydrophobicity solids conditions. An increase in velocity was measured, with low confidence in the high concentration of high hydrophobicity solids and low concentration of low hydrophobicity solids conditions, owing to a high variation in the measurement data.

An increase in frother concentration is expected to result in an increase in froth velocity. This is due to the increased water associated with the air/water interface from the extra polar groups attached to the interface and the stabilising effect that this has on the froth. However, this effect is expected to be dampened in the presence of high concentrations of hydrophobic solids due to the stronger effect that the solids have on froth stability and effect of higher solid loadings decreasing the amount of water present at the air/water interface. The results show more significant relationships where an increase in frother concentration results in an increase in velocity measured at low concentrations of hydrophobic solid conditions. In the presence of a high concentration of highly hydrophobic solids, a decrease in velocity was measured. However, the confidence of this measurement is low, due to variations in the results. The results of the effect of frother concentration on velocity correspond well to the changes in the measured burst rate under these conditions.

A stronger frother is expected to result in a similar effect as the increased frother concentration, where the froth stability is enhanced, resulting in a higher froth velocity. The results show that an increase in velocity is measured in the presence of a stronger frother.

The presence of an activator will result in a greater concentration of floatable solids entering the froth. The presence of increased amounts of hydrophobic solids is hypothesised to stabilise the froth under conditions where high concentrations of floatable solids are available, while having an insignificant effect under low concentrations of floatable solids. However, the results show that a decrease in velocity is measured, with low confidence. This may be due to increased variation in the velocity under these conditions. More samples would be required to obtain a measurement with a higher confidence.

Expected froth velocity behaviour was observed under most conditions. However, anomalous behaviour was observed in the high concentration of highly hydrophobic conditions when the froth height is increased. This is due to a high variation in froth velocity under these conditions, where small changes in the amount of solids reaching the froth surface may interact strongly with froth stability factors.

5.5.2. Relating operating conditions to froth stability

This analysis investigates the effect of operating conditions on both the solids loading, bubble size and bubble burst rate on the froth surface, which relate to aspects that describe or determine the froth's stability. This section evaluates dominant mechanisms controlling the froth stability behaviour across the different floatable solid regimes tested.

Air rate

As determined by Jachimska *et al.* (1995), the behaviour of foam retention time within a *two-phase system* shows that additional air does not affect the foam's stability, as at higher air rates, the retention time remains constant, resulting in a constant residence time of the air moving through the foam. Thus, within an equilibrium foam, the foam merely expands at a rate that is proportional to the air addition rate.

However, within a *three-phase system* Hadler and Cilliers (2009) showed that the equilibrium froth height would increase, reach a peak and then decrease. This results in an air residence time that increases, reaches a peak and ultimately decreases at higher air rates.

Assuming that, in the absence of hydrophobic solids, the froth behaviour would mirror that of the two-phase system, it follows that the hydrophobic solids serve to act as a surface active component that affects the froth stability. If the hydrophobicity and the concentrate of the solids through the froth remain constant, it would be expected that the froth would exhibit similar stability behaviour to two-phase foams. However, while particle hydrophobicity remains constant, it is expected that the distribution of floatable solids through the froth changes, which would account for the observed three-phase froth stability behaviour within the literature.

The results summarised in table 5.3 show that under high solids concentration conditions, the effect of solids loading tends to override the effect of the solution stabilising factors, such as the frother concentration. These results show that where high concentrations of available floatable solids or highly hydrophobic solids are present the increased air rate destabilised the froth, resulting in an increased burst rate on the froth surface.

In the presence of the highly hydrophobic particles, the air rate decreased the solids loading on the froth surface. This decrease in solids loading may be related to the concentration of available floatable solids present. However, in the presence of the low hydrophobic particles, no significant difference was observed in the solids loading at the froth surface. Instead, in

the presence of these particles, larger bubbles were formed and remained stable on the froth surface.

The role that the air rate played within the mechanisms that influence the froth stability behaviour is not immediately apparent as it manifests more significantly in different mechanisms when the floatable particle hydrophobicity is changed. In the presence of high concentrations of high hydrophobicity solids, froth destabilisation, owing to an increased air rate, is observed due to a significant decrease in the solids loading on the bursting bubbles. However, the solids loading on bubbles that did not burst was observed to increase. In the presence of low hydrophobicity floatable solids, or low concentrations of floatable solids, froth destabilisation occurs in the form of both a lower solids loading and larger bubbles present on the froth surface.

When the air rate increases, two main effects may have an influence on the behaviour of the froth. Firstly the number of bubbles generated increases and secondly, the average bubble size tends to increase due to an increased number of larger bubbles. However, despite the increase in bubble size, the net result of an air increase is an increase in gas holdup within the pulp phase.

These two effects result in an increase in the bubble surface area flux (S_b) entering the froth which generally, results in a higher flux of both solution and solids entering the froth (Gorain *et al.*, 1997).

An increase in bubble surface area flux under conditions where the average pulp bubble size increases results in a *decrease in the solids loading* per unit surface area of bubble entering the froth. This also implies that an *increase in the absolute amount of water* entering the froth will occur in addition to an *increase in the ratio of water to solids* entering the froth.

The consequence of these factors on the froth surface loading is such that the *decrease in solids loading* on bubbles entering the froth may have a direct effect and higher amounts of coalescence would be required to reach a saturated loading and stabilise the bubbles at the froth surface, resulting in either a lower solids loading or larger bubbles on the froth surface.

The consequence of an *increase in the absolute amount of water* and *an increase in the water to solids ratio* is that an increase in the air rate will increase the slurry drainage rate within the froth. The *increase in the absolute amount of water* entering the froth will result in an increase in the size and number of Plateau borders, or slurry drainage channels within the froth, and the *increase in the water to solids ratio* will decrease the viscous effects within these drainage channels, causing smoother and faster slurry flow. This faster slurry flow will

result in an increased shearing rate at the air/water interface, potentially destabilising attached solids, resulting in increased levels of detachment.

Thus, higher concentrations of detached hydrophobic material will drain from the froth and this class of material will have less opportunity to re-attach within the froth. Hence, the effect of air rate on the water entering the froth results in a secondary, indirect cause for a decrease in the solids loading on the froth surface, which leads to froth destabilisation.

The extent to which the direct effect influences the solids loading and froth stability can be evaluated by observing the effect of the increased air rate (J_g) on the increase in bubble size (d_{32}), and thus, increase in bubble surface area flux (S_b).

$$S_b = 6 \cdot \frac{J_g}{d_{32}} \tag{5.1}$$

In the copper tests, only the superficial gas velocity was measured. Cappuccitti and Nesset (2009) performed studies on the characterisation of the effect of air rate on the pulp Sauter mean bubble size in industrial cells. Based upon their data from a number of plants, the increase in the Sauter mean bubble size can vary from 0.3–1.0 mm for every cm/s increase in superficial gas velocity. These values illustrate that the change in the Sauter mean bubble size is small in industrial cells. Within the copper system it is expected that the bubble size will increase by at most, 0.14 mm in the first cell and 0.35 mm in the third cell between the low and high air rate conditions. In the platinum system, both the superficial gas velocity and pulp Sauter mean bubble size were measured.

Within the literature, it is widely established that the bubble surface area flux is proportional to a flotation rate constant (Gorain *et al.*, 1997), which means that it is proportional to the concentration of solids entering the froth. Under conditions where the bubble surface area flux increases it is expected that the overall solids flux entering the froth increases and that the converse would be true as the bubble surface area flux decreases.

Thus, by determining the behaviour of the bubble surface area flux as the air rate increases, one can interpret the effect of air rate on the overall solids flux entering the froth.

Figure 5.2 shows the behaviour of the bubble surface area flux within the pulp as the air rate to the flotation cell is increased. The bubble size data for the copper system was estimated from typical values presented in the literature, while in the platinum system, the bubble surface

area flux in the pulp is determined from the measured values of the pulp Sauter mean bubble diameter and superficial gas velocity.

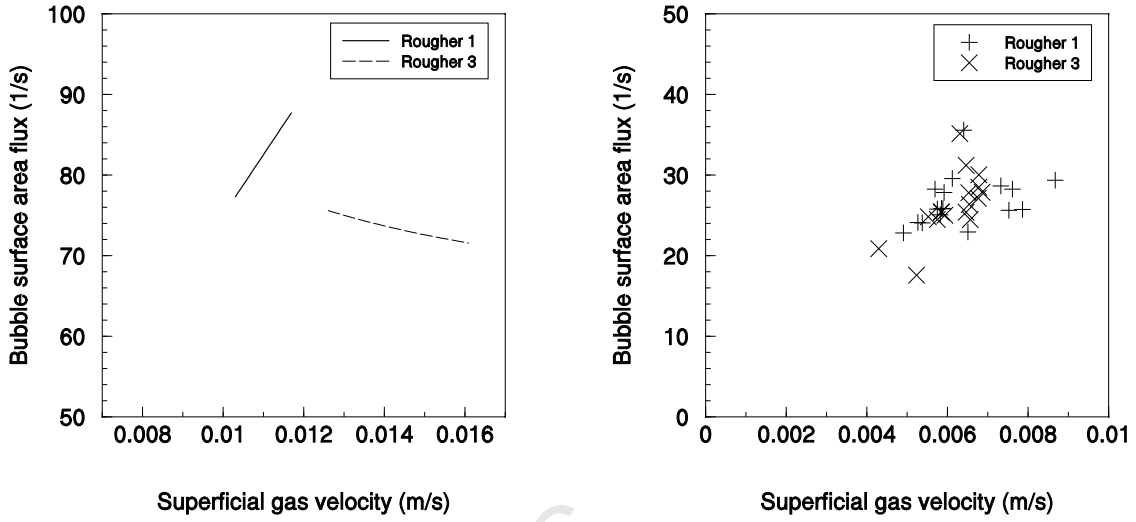

(a) Copper system

(b) Platinum system

Figure 5.2.: The relationship between the superficial gas velocity and the bubble surface area flux. The bubble surface area flux within the copper system was calculated using an estimated Sauter mean bubble diameter, based upon the relationship between the Sauter mean bubble diameter and air rate shown measured in a number of industrial plants measured by Cappuccitti and Nesset (2009).

The results shown in figure 5.2 show that as the air rate increases in rougher one of both the copper and platinum experimental systems, the bubble surface area flux increases. In the case of the third rougher of the copper system, the bubble surface area flux may decrease, due to a higher increase in bubble size as the air rate increases. Thus, the total solids flux entering the froth increases in the cases where air rate results in a higher bubble surface area flux.

Within each system, an increase in the air rate has been shown to result in a decrease in froth stability by an increase in the burst rate measured on the froth surface. Two mechanisms were hypothesised to explain this observation. The first mechanism, referred to as the direct effect, can only be explained by a decrease in the solids loading on bubbles that enter the froth.

Despite an increased solids flux entering the froth, the solids loading per bubble may decrease due a combination of the presence of a higher of number of bubbles, lowering the concentration of floatable solids within the pulp and an increase in bubble size. An increase in bubble size decreases the bubble residence time within the pulp, and thus, bubble-particle collision

rate (Yoon and Luttrell, 1989). In-pulp solids loading measurements (Seaman *et al.*, 2004, Yianatos *et al.*, 2008) are required to test this hypothesis.

The research performed by Cappuccitti and Nesset (2009) and Yoon and Luttrell (1989) supports this hypothesis. Thus, assuming that this hypothesis is true, an increase in air flow rate will result in an increase in solids flux until it reaches a maximum, as the influencing effects of the increased number of bubbles and increased bubble size cancel each other out and reverse. This effect is only expected under conditions of low floatable solid concentrations.

The second mechanism which may explain the effects of an increased air rate resulting in the destabilisation of the froth phase relates to that of the slurry drainage rate through and out of the froth. This hypothesis states that should the slurry drainage rate increase, both the shearing rate within the froth increases, detaching more solids and owing to the increased water in the Plateau borders, less detached solids have an opportunity to re-attach to the air/water interface, and provide further stability to the froth.

To test the effect that air rate has on the slurry drainage rate, an assumption of the dynamic water carrying capacity of bubbles in the presence of frother is required. Finch *et al.* (2006) determined the extent that water is dynamically bound at the air/water interface of bubbles in the presence of various frothers using infrared (structure) and ultra-violet + visible spectrum interferometry (film thickness). They determined that two alcohol based frothers, MIBC and *n*-Pentanol resulted in a dynamically bound water layer around a bubble of $<$160 nm while the polyglycol frother, DowFroth 250 resulted in a dynamically bound water layer of 600 nm. Based upon these measurements, a bubble's water carrying capacity of 0.16 and 0.60 kg/m^2 can be assumed in the presence of alcohol and polyglycol based frothers respectively.

In the two experimental systems used within this thesis, the frother used in the copper system was Interfroth 68, which is a proprietary alcohol based frother blend, while within the platinum system, Senmin XP 200 and XP 250 were used, which are polyglycol based frothers similar to that of DowFroth 200 and 250 respectively.

An analysis to determine the water carrying capacity can be performed by considering the surface area recovery rate and the water recovery rate to the concentrate. However, this analysis includes the effects of the water in the Plateau borders and the solids loading on the froth surface.

The surface area recovery rate can be estimated by determining the volumetric recovery rate of the froth through the measurement of the froth velocity, height of the froth over the launder, the launder length and the Sauter mean bubble diameter on the froth surface. A water loading

estimate which includes the entrained water within the Plateau borders can be determined by dividing the volumetric water recovery by this surface area recovery. The values used in this analysis are shown in table 5.6.

Table 5.6.: Estimating the range in water loading for the first rougher in the copper and platinum systems, using cell dimensions, velocity, height of the froth flowing over the lip (H_{lip}), Sauter mean bubble diameter (d_{32}) and the measured water recovery rate.

System	Froth velocity m/s	Launder length m	H_{lip} m	Froth volume recovery m^3/s	d_{32} m	Surface area recovery m^2/s	Water recovery kg/s	Water loading kg/m^2
Copper	0.0096	9.34	0.0358	0.00323	0.0201	0.97	0.077	0.079
	0.0132	9.34	0.0458	0.00566	0.0299	1.14	0.584	0.513
Platinum	0.0176	1.2	0.01	0.000212	0.0102	0.125	0.0102	0.082
	0.0039	1.2	0.01	0.000047	0.0171	0.017	0.0139	0.824

This analysis resulted in water loading estimates ranging from 0.08 to 0.51 and from 0.08 to 0.82 kg/m^2 in the case of the first rougher in the copper and platinum systems respectively. A large amount of variation exists within these results due to the effects of the Plateau borders and solids loading on the froth surface. Cases where the water estimate is low may be due to a high surface area coverage of attached solids on the recovered bubbles. A high water loading estimate may occur due to an abundance of finer bubbles on the froth surface, which result in an increase Plateau border density and thus, more water. However, these results illustrate that the dynamically bound water measurements obtained by Finch *et al.* (2006) are realistic, and are within the correct order of magnitude for each of the systems considered.

Thus, the amount of water bound to bubbles that enter the froth can be estimated using the attached water loading and the bubble surface area flux. By performing a water balance across the froth phase, the bound water is considered as entering the froth and the measured water recovery rate to the concentrate, an estimate of the amount of water that drains out of the froth can be determined. However, this estimate excludes any trapped or entrained water that enters the froth, which is required to determine the actual water drainage rate out of the froth.

Figure 5.3 shows the behaviour of the estimated amount of water draining from the froth, based upon the above-mentioned assumptions, as the air rate to the flotation cell is increased. In this analysis, the amount of water bound to the bubbles entering the froth has been estimated based upon measurements made within the literature and in the case of the copper system, an estimated bubble size.

The results in figure 5.3 show that as the air rate increases, the amount of water that drains from the froth increases. While it is unclear whether the increase in water drainage rate results

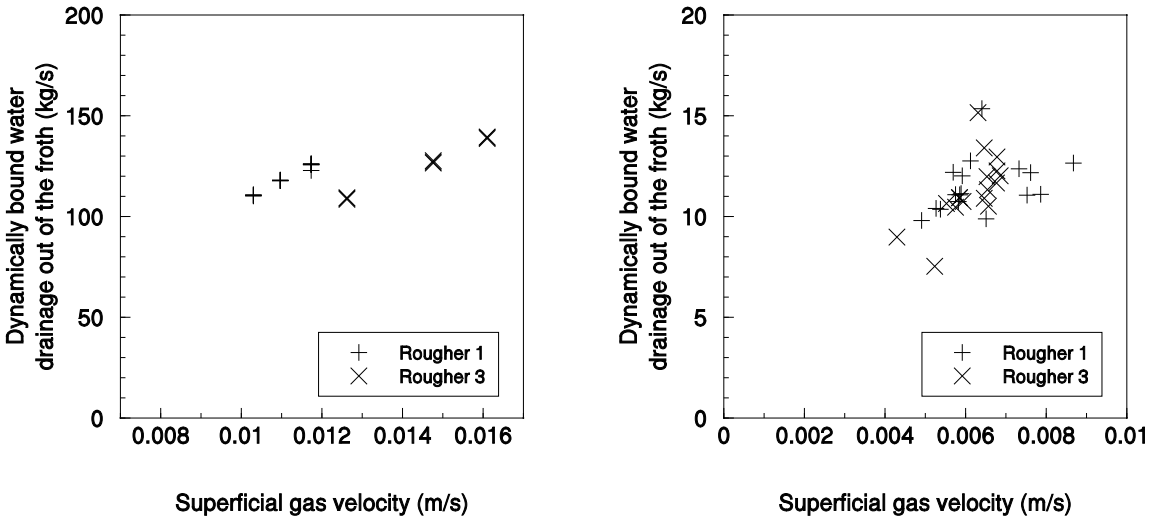

(a) Copper system

(b) Platinum system

Figure 5.3.: The relationship between the superficial gas velocity and the amount of water drained from the froth. The bound water shell thickness on bubbles entering the froth was assumed to be 0.16 and 0.60 nm in the copper and platinum systems respectively. In the copper system, the pulp Sauter mean bubble diameter was assumed to be 0.8 and 1.0 mm in rougher 1 and 3 respectively.

in higher water velocities within the Plateau borders, or larger Plateau borders, the water added is likely to affect the concentration of detached particles within the froth. The potential that this effect has to lower the concentration of detached solids may result in higher outflows of detached solids, which would have served to stabilise the froth had the particles been given an opportunity to re-attach.

The summary of results shown in table 5.3 shows that the air rate effect on froth stability is highly significant under high floatable solids concentration conditions, however, this effect is diminished under low solids concentration conditions. The detached particle drainage effect described above is consistent with the decreasing effect of the hydrophobic solids on froth stability. The concentration of floatable solids present decreases down the bank resulting in a decrease in the concentration of detached particles present, which facilitates the solution stabilising factors to start dominating the froth phase stability.

Based upon the above analysis, the destabilising effect that was observed when air rate was increased was most likely due to an increase in the drainage of detached solids out of the froth, facilitating lower re-attachment rates of these particles. This was directly manifested by a decrease in the solids loading on the froth surface. However, in the presence of high

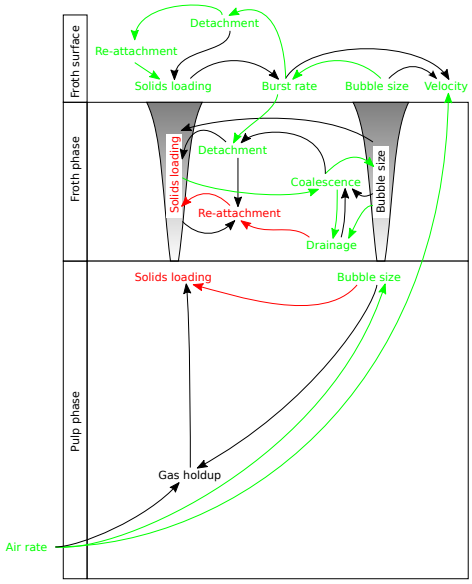

(a) High hydrophobicity, high solids concentration

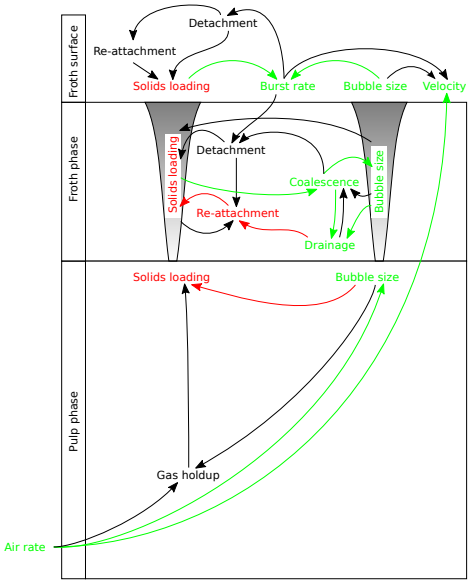

(b) High hydrophobicity, low solids concentration

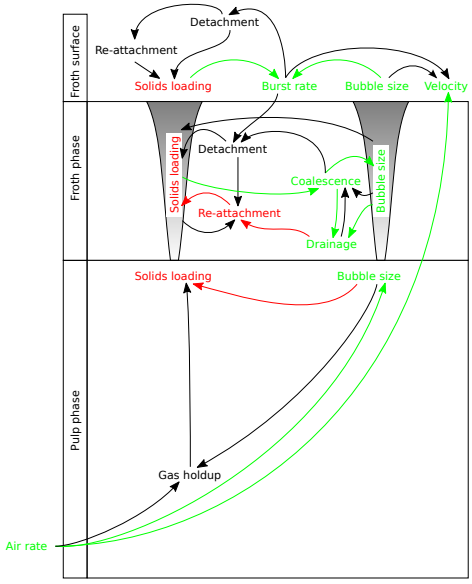

(c) Low hydrophobicity, high solids concentration

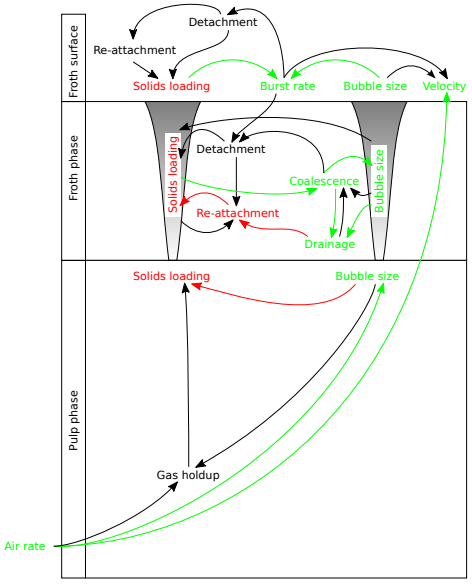

(d) Low hydrophobicity, low solids concentration

Figure 5.4.: Dominant mechanisms affecting froth phase behaviour when the air rate is increased under different conditions of particle hydrophobicity and floatable solids concentration (green represents an increase and red represents a decrease).

concentrations of highly hydrophobic particles, particles that detached from bursting bubbles re-attached near the froth surface, due to the fast floating nature of the solid particles. The dominant mechanisms that have been proposed to explain this behaviour are highlighted in figure 5.4.

Based upon the above analysis, it can be surmised that an increase in air rate generally tends to destabilise the froth under certain conditions. In addition, under the conditions tested, the behaviour of air rate within the flotation system was not consistent across systems with differing particle hydrophobicity and floatable solids concentration.

Froth height

As the froth height increases, upper levels of the froth contain less water, as more drainage has occurred near the froth surface than in shallower froth depths. The increased drainage may be a dominating effect due to the froth depth increase on froth stability. However, based upon the concentration of floatable solids present and behaviour of other parameters such as froth surface solids loading, bubble size must interact with other mechanisms within the froth to produce the difference in behaviour shown in the results. The potential interactions between the mechanisms are described below.

The results shown in table 5.3 show that froth height had a significant influence on froth stability, which was reflected by the burst rate. Despite the increased slurry drainage rate, due to the increased froth height, the froth stability in the presence of high concentrations of floatable solids increased. In the high hydrophobicity case, this occurred despite a measured decrease in solids loading and increase in the bubble size.

The measurement of solids loading showed a decrease in the presence of highly hydrophobic particles when the froth height increased. Assuming that the flotation kinetics did not change significantly within the pulp phase, this can only have occurred due to changes brought upon within the froth phase. An increase in froth height results in an increased drainage rate. The increased drainage rate increases the coalescence rate. However, for the solids loading to decrease within the froth, the amount of solids detached per coalescence event needs to increase. Alternatively, due to the increased drainage rate more water is present within the Plateau borders which may facilitate an increased amount of detached solids leaving the froth, thus lowering the re-attachment rate.

However, in the presence of low hydrophobicity particles, the solids loading measurement increased when the froth height increased. Under these conditions, the detachment rate would

need to be low enough for the solids loading to increase with each coalescence event. In addition, the lower re-attachment mechanism is less significant due to the comparatively low re-attachment rates from the low hydrophobicity particles and the smaller effect that increased froth height has on the drainage rate when compared to air rate.

The bubble size increased under all conditions, due to increased coalescence within the froth owing to increased lamella thinning from drainage.

Apart from the high concentration of highly hydrophobic condition, the burst rate behaviour can be explained by the solids loading and bubble size behaviour. These factors also relate consistently to the measured velocity behaviour.

Based upon these interactions, it can be surmised that the behaviour of the froth depth was strongly influenced by the lamella process within the froth. This either resulted in lower rates of re-attachment, or increased solids loading due to the loss in surface area, dependent on the properties of the floatable solids. The dominant mechanisms that have been proposed to explain this behaviour are highlighted in figure 5.5.

Frother concentration

An increase in frother concentration results in a higher adsorption density of frother at the air/water interface. This tends to increase the amount of water that is dynamically associated with the interface owing to the additional polar species attached at the interface. These polar species increase the viscous effects near the interface, retarding drainage.

The results in table 5.3 show that the bubble size decreased in the presence of high concentrations of floatable solids. This may have occurred due to a retardation of coalescence lower down in the froth, where the solids loading is lower. The solids loading was observed to decrease, most likely due to smaller bubbles reaching the froth surface. However, this decrease in solids loading may have resulted in an observed increase in the burst rate. The solids loading decrease in the presence of highly hydrophobic solids was marginal, however, this decrease may have resulted in the increased burst rate. In the case of the high hydrophobicity solids, the burst rate controls the velocity, while in the presence of low hydrophobicity solids, lower air loss occurred owing to the smaller bubble size.

A decreased burst rate on froth surface was measured under low concentrations of floatable solids, which facilitated larger bubbles to persist for longer. This resulted in an increase in froth velocity as the air loss rate decreased. The low solids loading within the froth facilitated

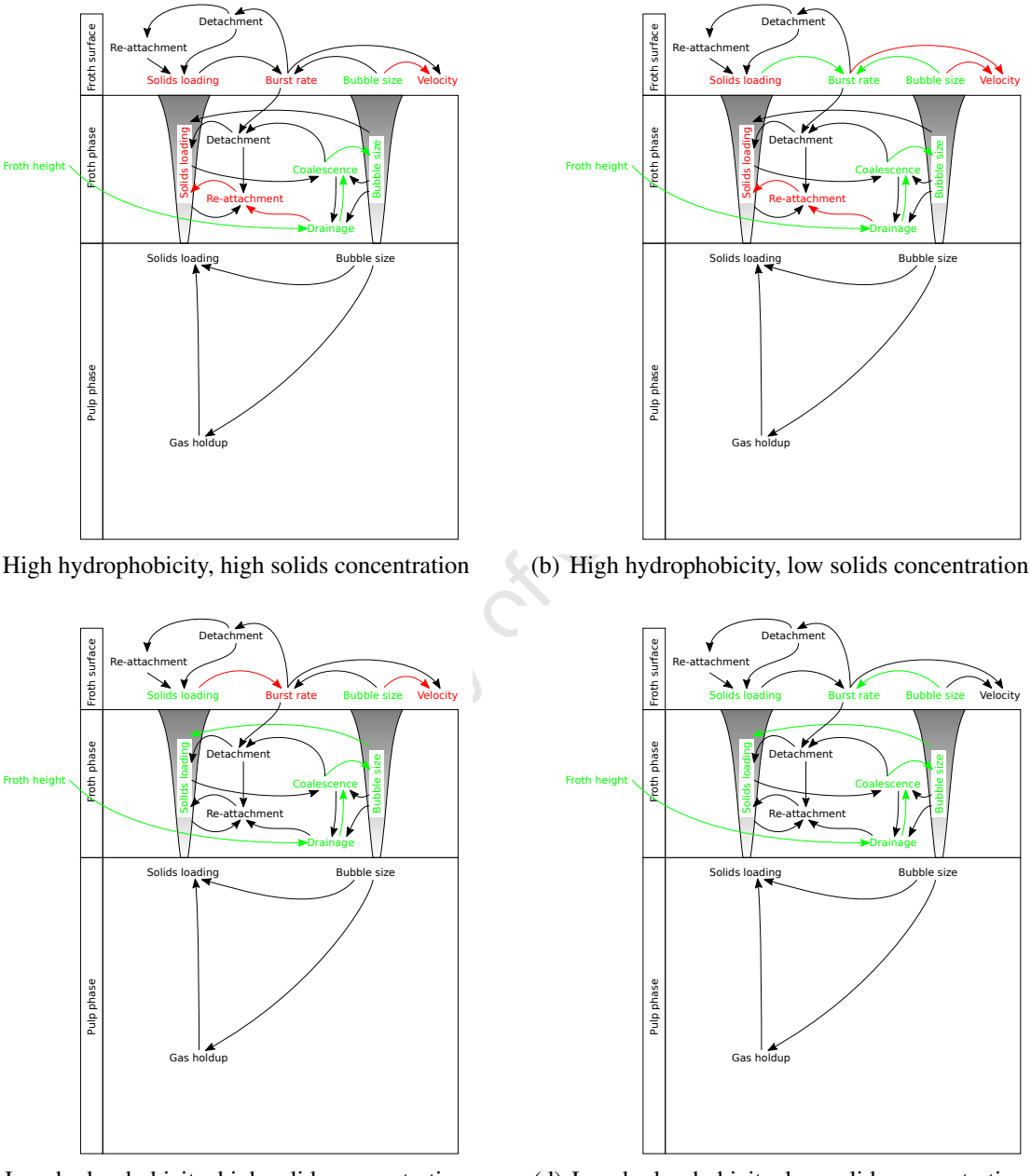

(a) High hydrophobicity, high solids concentration

(b) High hydrophobicity, low solids concentration

(c) Low hydrophobicity, high solids concentration

(d) Low hydrophobicity, low solids concentration

Figure 5.5.: Dominant mechanisms affecting froth phase behaviour when the froth height is increased under different conditions of particle hydrophobicity and floatable solids concentration (green represents an increase and red represents a decrease).

the frother effect reaching the froth surface, as opposed to being confined to the lower regions of the froth phase, which was the case in the high solids concentration condition.

The effect of frother concentration was controlled by the solids coverage at the air/water interface and was most significant under conditions of a low availability of hydrophobic solids. This is due to the highly hydrophobic particles overriding the stabilising effect of the frother and having a much stronger stabilising effect on the froth. The dominant mechanisms that have been proposed to explain this behaviour are highlighted in figure 5.6.

Frother type and activator

Within the platinum system, the frother type and use of a copper sulphate activator was investigated. The results shown in table 5.3 show that from a froth stability point of view, both the frother type and activator had little impact on the burst rate.

The frother type was also modified, where a weaker polyglycol frother (XP 200) was replaced by a longer chained (stronger) polyglycol frother (XP 250). The stronger frother used in this case caused an increase in bubble size in regions where a low abundance of floatable material occurred. The increase in bubble size may have occurred due to an ability for slightly larger bubbles to remain stable or persist longer in the presence of the stronger frother than the weaker frother. However, these bubbles burst at a higher rate (they were larger), resulting in the observed higher burst rate.

A stronger frother is similar to a higher frother concentration in that it only significantly affects the froth in regions in a bank where the hydrophobic solids are at a lower concentration and unable to dominate.

An activator was added to enhance the floatability of sulphide minerals. The results show that the presence of the activator resulted in an increase in bubble size in regions where a high abundance of floatable material occurred. This may be due to the inadvertent activation of lower hydrophobic, or gangue, particles that destabilize the froth at low loadings, or cleaning particle surfaces such that their hydrophobicity is enhanced above a the critical hydrophobicity beyond which the hydrophobic particles start to destabilise the froth.

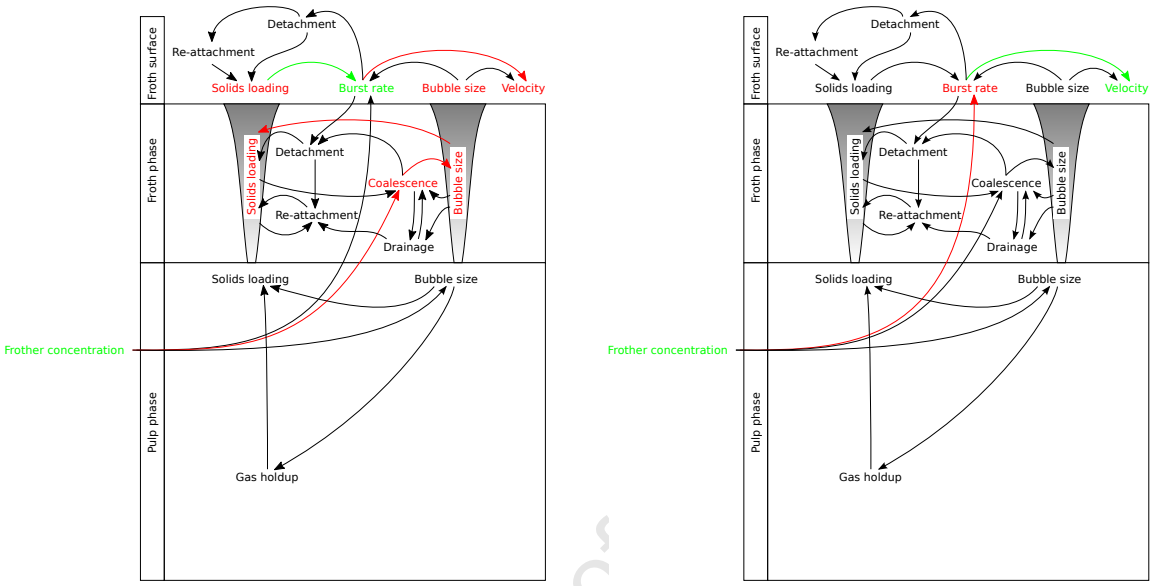

(a) High hydrophobicity, high solids concentration

(b) High hydrophobicity, low solids concentration

(c) Low hydrophobicity, high solids concentration

(d) Low hydrophobicity, low solids concentration

Figure 5.6.: Dominant mechanisms affecting froth phase behaviour when the frother concentration is increased under different conditions of particle hydrophobicity and floatable solids concentration (green represents an increase and red represents a decrease).

5.5.3. Froth phase effect on flotation performance

The froth phase plays a significant role in determining the flotation performance within a flotation cell. The analysis performed in this chapter investigates the effect of operating variables on froth stability and flotation performance factors and the relationship between froth stability factors to flotation performance factors. Using this information, the extent to which the operating variables affect froth stability has been assessed. This section investigates the relationships linking the operating variables and froth stability to flotation performance.

Operating variables

The results from an analysis investigating the relationship between the operating variables and the flotation performance factors; solids recovery and valuable grade are shown in tables 5.2 and 5.3.

The operating variables that were modified across both experimental systems are the air rate, froth depth and frother concentration. The effect that these operating variables have on flotation performance is described below.

Air rate

When the air rate to a flotation cell is increased, it is expected that the transport rate of the froth moving towards the launder will increase, resulting in an increase in the solids recovery and a decrease in concentrate grade.

The results show that in the presence of low concentrations of highly hydrophobic particles and high concentrations of low hydrophobic particles, changes in air rate resulted in the expected increase in solids recovery. However, the expected decrease in grade only occurred in the presence of low concentrations of highly hydrophobic solid particles. In the case of the high concentrations of floatable solids conditions the concentrate grade increased with an increase in air rate. This increase in grade may have occurred due to increased drainage of entrained as opposed to the detached material out of the lower levels of the froth.

An increase in air rate results in the competition between two mechanisms. These two competing mechanistic effects are the decrease in the solids loading on bubbles reaching the froth surface, resulting in a decreased froth stability and increased surface area flux to the concentrate. Under the conditions where the expected behavior occurred, an increase in air rate resulted in an increase in the surface area flux recovered to the concentrate. However, in the

conditions where the concentrate grade increased with an increase in air rate, a mechanism by which the extra air added resulted in a greater amount of air lost, explains this behaviour. Thus, the transport rate decreased and the destabilisation resulted in higher drainage, removing more entrained material.

Froth height

When the froth height within a flotation cell is increased, the solids recovery is expected to decrease, with an increase in the concentrate grade. An increase in froth height increases the froth retention time, resulting in more drainage out of lamellae having occurred at the froth surface. Thus, the bubble lamellae are thinner and more brittle, resulting in greater instability. Therefore, as more air is lost from bursting on the froth surface, the transport rate decreases resulting in the decreased solids recovery. In addition, the extra bursting and coalescence results in more water being released, draining more entrained material, resulting in higher grades.

The results show the expected solids recovery behaviour in the presence of low concentrations of high hydrophobic solids and the high concentration of low hydrophobic solids conditions. In addition, the expected grade behaviour was observed in the presence of a low concentration of floatable material. In the case of the high concentration of highly hydrophobic solids and low concentration of low hydrophobicity solids, an increase in froth height resulted in the solids recovery increasing, and in the presence of a high concentration of low hydrophobicity solids, the grade decreased.

In the case of the high concentration of highly hydrophobic solids, an increase in the froth height resulted in a decrease in the burst rate, indicating a more stable froth with larger bubbles. This behaviour is anomalous and suggests that the increased stability may have occurred due to an armouring effect caused by the solids packing more tightly on the bubble lamellae. However, this hypothesis contradicts with the observed decrease in solids loading.

Frother concentration

The frother concentration was used as a factor within the regression analysis, both when considering the operating conditions (Tables 5.2 and 5.3) and the stability factors (Tables 5.4 and 5.5).

When the frother concentration is increased, it is expected that solids recovery will increase and concentrate grade will decrease. The increase in solids recovery would occur due to an increased water content within the froth, resulting in increased froth stability and a higher

transport rate to the concentrate. The decrease in concentrate grade would occur due to an increased amount of entrained material being recovered with the added water to the concentrate.

The results show that the expected behaviour due to changes in frother concentration was only observed in the case of solids recovery for the low concentration of highly hydrophobic solid and high concentration of low hydrophobicity solid conditions. In the case of grade performance only the low floatable solids concentration conditions resulted in the expected performance.

The anomalous behaviour where the solids recovery was observed to decrease may have occurred owing to a combination of effects due to the decreasing solids loading and bubble size and increased froth stability. Under these conditions, the water content within the froth remained high, lowering the viscous dissipation forces within the froth which would facilitate a greater rate of drop back of entrained and detached material out of the froth.

Stability factors

The results from an analysis investigating the relationship between factors affecting the froth stability and the flotation performance measurements; solids recovery, water recovery and valuable grade are shown in tables 5.4 and 5.5.

The froth stability factors that were used to investigate relationships to the flotation performance factors are the burst rate, solids loading, bubble size and frother concentration. The relationship between these parameters and flotation performance is described below.

Burst rate

The burst rate is expected to be related to the flotation performance primarily through its effect on froth transport, where an increase in the burst rate results in a decrease in froth transport. A secondary effect is the effect that the burst rate has on the proportion and amount of floatable solids present on the froth surface. Owing to these effects, an increase in burst rate will result in an increased amount of water and attached particles being released, resulting in an increased rate of drainage. The net effect of these mechanisms would be a decrease in solids recovery and an increase in grade.

The results show that the expected concentrate grade behaviour was observed under all conditions. The expected solids recovery behaviour occurred in all of the conditions, with the exception of the low concentration of high hydrophobicity solids when the machine vision based solids loading was used in the regression. However, the regression between operat-

ing variables and stability factors showed that the burst rate and solids recovery behaviour were consistent with expectation. Thus, in this case, relationships between the factors may be obscuring the results.

A comparison between the use of the two solids loading measurements in the regression show that the gravimetric solids loading measurement resulted in negative coefficients in the high solids concentration conditions too.

These results show that while the burst rate shows a relationship to flotation performance, other factors need to be considered within the regression model to determine performance changes. However, under certain conditions, this model can fail, as was observed in the low concentration of high hydrophobicity solids conditions.

Solids loading

The solids loading on the froth surface is expected to be a key factor relating to flotation performance. Concentrate grade is expected to relate directly to solids loading, where an increase in solids loading will correspond to in an increase in grade, due to the increased proportion of floatable solids present near the froth surface. However, the relationship between solids loading to solids recovery depends upon other key froth parameters. These key parameters relate to the froth structure (bubble size) and froth transport rate (velocity). Assuming that the froth transport rate and bubble size remain the same, an increase in the solids loading will correspond to an increase in solids recovery. However, under conditions where either the bubble size increases, or the velocity decreases, an increase in solids loading may correspond with a decrease in solids recovery under conditions where the bubble size increase or velocity decrease is more significant than the solids loading increase.

The results show that this expected behaviour was observed with respect to concentrate grade in the high concentration of high hydrophobicity material and low concentration of low hydrophobicity material conditions. The solids loading was observed to increase and decrease in the high and low concentrations of the highly hydrophobic material conditions respectively.

The solids recovery behaviour observed under the high concentrations of highly hydrophobic material conditions may have occurred due to the solids loading increase with bubble size, leading to increased stabilisation due to bubble armouring.

These results show that the use of solids loading to interpret froth performance behaviour requires the use of other parameters. The determination of the solids recovery rate depends strongly on factors such as froth velocity and bubble size, as discussed in section 4.1.6.

Bubble size

The bubble size on the froth surface reflects the structure of the froth near the surface. Froths composed of large bubbles have a lower surface area to volume ratio than a froth with smaller bubbles. Thus, as the average bubble size increases within a froth, its water content and solids carrying capacity decreases. Therefore, it is expected that bubble size will have a significant effect on water recovery and solids recovery, as when the bubble size increases, the amount of water and solids carried by the froth per unit volume of froth decreases. However, an increase in bubble size tends to result in an increase in solids loading due to the loss of inter-facial surface area. As the surface area decreases, more of the entrained material in the Plateau borders decreases resulting in an increase in grade due to the increased proportion of floatable material present.

The results show the expected solids recovery behaviour was observed under conditions where low concentrations of highly hydrophobic solids and high concentrations of low hydrophobicity solids are present. The expected concentrate grade behaviour was observed under all conditions, except in the presence of low concentrations of low hydrophobicity solids.

The conditions where high concentrations of highly hydrophobic solids and low concentrations of low hydrophobicity solids are present show anomalous behavior. In the presence of the high concentrations of the highly hydrophobic solids, the burst rate decreased with bubble size, resulting in a more stable froth. This observation indicates that bubble armouring was occurring, which may explain the observed increase in solids recovery with bubble size under this condition. Under the low concentration of low hydrophobicity solids condition, the froth velocity showed a strong positive relationship with the bubble size. Thus, as the bubble size increased, the transport rate increased. The concentrate grade decreased for this condition owing to only low concentrations of floatable solids being present.

Summary

Table 5.7 shows a summary of the key mechanisms that influence operating variable effects on froth stability.

Table 5.7 shows that the operating variables have a primary effect which is related to the solution behaviour with respect to that operating variable. The interaction between the solution behaviour and concentration and type of solids present then result in a particular froth stability change.

Table 5.7.: Summary of mechanistic behaviour due to an increase in operating variable.

Operating variable	Primary effect	Secondary effect	Effect on stability
Air rate	Increased drainage through the froth	Increased loss of floatable solids from the froth	Decrease in stability
Froth height	Lower water content at froth surface	**High solids concentration:** Solids more tightly loaded on lamella (armouring)	Increase in stability
		Low solids concentration: Film thinning	Decrease in stability
Frother concentration	Associates more water with bubbles	**High solids concentration:** Decreased solids loading	Decrease in stability
		Low solids concentration: Increased lamella thickness	Increase in stability

With respect to the use of froth height and frother concentration as operating variables that can be manipulated within a control strategy, where managing froth stability is a control objective, it is clear that the concentration of floatable solids present within the system is a key parameter in managing the stability behaviour.

Typically, the concentration of floatable solids entering a flotation bank is not known and is likely to vary due to natural variation within the ore and operational variation within the plant grinding and classification sections. However, the concentration of floatable solids present will decrease down the bank.

Table 5.8 shows a summary of the relationships showing the direction that froth stability parameters and operating variables are required to change to effect a consistent increase in the solids recovery within the flotation cell under different solid regimes, across a wide range of operating conditions.

Table 5.8 shows that in the presence of a low concentration of high hydrophobicity solids and a high concentration of low hydrophobicity solids, an increase in the burst rate and solids loading both resulted in higher solids recoveries. However, under these conditions an increase in air rate resulted in an increased burst rate, and an opposite decrease in the air rate resulted in an increased solids loading. This may occur due to competing mechanisms occurring where one mechanism dominates the system and the other is a secondary effect. Given that an increase in air rate has a direct effect on solids recovery, it is plausible that the air rate effect on burst rate was the dominant effect while the air rate effect on solids loading was a second order effect.

In the presence of a low concentration of low hydrophobicity solids, a decrease in burst rate and increase in bubble size both effected an increase in solids recovery. However, in this

Table 5.8.: Determining the operating variable changes required to effect a consistent *increase* in the *solids recovery* in a flotation cell.

Solids conditions	Stability factor	Operating variable
High hydrophobicity *High concentration of solids*	↑ Bubble size ↓ Solids loading –	↑ Air rate, ↑ Froth height ↑ Froth height ↑ Froth height, ↓ Frother concentration
High hydrophobicity *Low concentration of solids*	↑ Burst rate ↑ Solids loading ↓ Bubble size –	↑ Air rate, ↓ Frother concentration ↓ Air rate, ↓ Froth height ↓ Froth height ↑ Air rate, ↓ Froth height, ↑ Frother concentration
Low hydrophobicity *High concentration of solids*	↑ Burst rate ↑ Solids loading –	↑ Air rate, ↓ Froth height, ↑ Frother concentration ↓ Air rate, ↑ Froth height, ↓ Frother concentration, ↑ Activator ↑ Air rate, ↓ Froth height, ↑ Frother concentration, ↓ Activator
Low hydrophobicity *Low concentration of solids*	↓ Burst rate ↑ Bubble size –	↓ Froth height, ↑ Frother concentration ↑ Froth height, ↓ Frother concentration ↑ Froth height, ↓ Frother concentration

case, the operating variables required to determine these stability changes oppose each other, indicating that an alternate, stronger driver must be present which causes this behaviour.

Table 5.9 shows a summary of the relationships showing the direction that froth stability parameters and operating variables are required to change to effect a consistent increase in the concentrate grade within the flotation cell under different solid regimes across a wide range of operating conditions.

Table 5.9.: Determining the operating variable changes required to effect a consistent *increase* in the *concentrate grade* in a flotation cell.

Solids conditions	Stability factor	Operating variable
High hydrophobicity *High concentration of solids*	↑ Solids loading ↑ Bubble size –	↓ Air rate, ↓ Froth height ↑ Air rate, ↑ Froth height ↑ Air rate, ↑ Frother concentration
High hydrophobicity *Low concentration of solids*	↑ Burst rate ↓ Solids loading ↑ Bubble size –	↑ Air rate, ↓ Frother concentration ↑ Air rate, ↑ Froth height ↑ Froth height ↑ Froth height, ↑ Frother concentration
Low hydrophobicity *High concentration of solids*	↑ Burst rate ↑ Bubble size –	↑ Air rate, ↓ Froth height, ↑ Frother concentration ↑ Air rate, ↑ Activator ↑ Air rate
Low hydrophobicity *Low concentration of solids*	↑ Burst rate ↑ Solids loading ↓ Bubble size –	↑ Froth height, ↓ Frother concentration ↑ Froth height, ↓ Frother concentration, ↑ Activator ↓ Froth height, ↑ Frother concentration ↑ Frother concentration

These results in table 5.9 show that the type and concentration of the floatable solids present within the flotation system profoundly affects the froth phase performance. Within different

floatable solids regimes, operating variables have been shown to switch their effect. This may be due to the flotation system being non-linear, however, the interaction between mechanisms within the froth affecting the distribution of the solids can explain much of this behaviour.

The results show that similar and typically expected behaviour was observed in the moderate conditions (high hydrophobicity, low solids concentration and low hydrophobicity, high solids concentration). Under the extreme conditions (high hydrophobicity, high solids concentration and low hydrophobicity, low solids concentration), the froth behaviour deviated from the expected behaviour.

5.5.4. Control and optimisation of froth flotation

Predictable behaviour is a requirement in order for a system to be controllable. However, the findings from sections 5.5.2 and 5.5.3 show that the froth stability behaviour changes depending on the solids environment. Within flotation, the main process disturbance is the variation in quality and quantity of the solids in the feed.

Thus, the control and optimisation of a flotation cell to achieve specific flotation performance characteristics (recovery and grade) is a non-trivial problem.

Current use of froth velocity

Currently, within common practice, flotation froths are typically controlled to maintain a velocity within certain acceptable limits by varying either the air rate or froth depth.

The experimental results shown in chapter 5, show that under the range of operating conditions tested, froth velocity only correlated strongly with the air rate in the high concentration of high hydrophobicity solids case, illustrating that with the exception of this case, the froth velocity is not linearly related to either froth height or air rate across a wide range of operating conditions in the presence of differing solids regimes.

The results from a froth stability perspective show that the froth velocity relates to solids recovery and sometimes grade under certain conditions. However, under conditions where factors other than froth velocity affect the solids recovery, no relationship between the velocity and solids recovery was observed.

Thus, it can be surmised that the relationship between froth velocity and flotation performance is not robust and only works under a narrow range of conditions. The findings from this thesis

illustrate that froth velocity cannot be used to control to either a specific solids recovery rate, or a specific grade target under conditions where ore quality varies. Therefore, the only benefit obtained from the use of this measurement is the assurance that flotation cells do not operate in specific undesirable regimes.

Considering mechanistic behaviour

No single operating variable relates to either concentrate grade or solids recovery rate consistently across differing operating conditions, such as variation in solids concentration and hydrophobicity.

A flotation control solution that maintains a target solids recovery or concentrate grade objective will need to require the use of an integrated model which combines individual measurements to infer an extent to which each internal froth mechanism is occurring. In addition, this model will need to determine which of these mechanisms are dominating froth behaviour to determine which operating variable to manipulate to adjust the system to obtain the desired output.

Within the discussion in this chapter a framework that considers the significant mechanisms occurring within the froth has been proposed. From this framework, the following mechanisms need to be identified and characterised in future work.

- **Solids detachment**
  Changes in the distribution of solids through the froth phase has been proposed as a hypothesis that provides a plausible explanation for the observed destabilising effect that an increase in air rate has on the froth. Under conditions where less detachment occurs, an increase in air rate will result in a lower amount of destabilisation, which is related to the concentration of floatable solids lost due to drainage.

- **Slurry drainage rate**
  The slurry drainage rate through the froth is important, as it relates to all three easily manipulable operating conditions; air rate, froth depth and frother concentration.

  The effect of air rate on drainage rate is such that conditions with increased drainage rates will result in a destabilised froth, due to the increased expulsion of detached solids back into the pulp.

  The effect of froth depth or frother concentration on drainage rate is such that conditions where the drainage rate does not change significantly, or decreases with an increase

in froth depth or frother concentration will result in a more stable froth, while where drainage rate increases, the froth stability decreases.

- **Froth coalescence**
  The coalescence rate through the froth is important, as this defines the froth structure near the froth surface. This also affects the drainage and detachment rates, as coalescence drives these factors.

  Froth structural aspects that are important near the froth surface relate to the size of the bubbles. In froths where large bubble sizes exist, a higher ratio of floatable to entrained solids is present, resulting in higher concentrate grades.

  In addition, higher levels of coalescence result in higher levels of both detached solids and higher solids loadings. In addition, the amount of water released within the froth increases, resulting in higher rates of drainage in the lower levels of the froth.

Chapter 6.

Conclusions & Recommendations

The overall objective of this work was to determine the mechanisms that change froth stability behaviour and develop more appropriate, non-intrusive machine vision measures that relate to froth behaviour, including stability.

More specifically:

1. To develop machine vision measurements that obtain more appropriate froth surface descriptors which relate to specific physical froth characteristics, such as:
    a) Solids loading
    b) Froth stability
2. To test the sensitivity of machine vision measurements in measuring expected changes on the froth surface from changes in operating variables within a flotation system when the solids environment changes.
3. To determine the extent to which the operating variable effect on the froth surface behaviour and froth stability is consistent across a range of operating conditions within a single flotation cell when the solids environment changes.
4. To investigate the relationship between the froth stability and flotation performance across a range of operating conditions within a single flotation cell when the solids environment changes.

6.1. Machine vision measurement of the solids loading on the froth surface (Objective 1a)

Solids loading is known to be a factor that affects froth stability. However, no robust methods are currently available to measure the solids loading in a manner suitable for on-line operation. Thus, a machine vision measure for the solids loading on the froth surface was developed.

The solids loading measure is based upon the measurement of the roughness or texture on images of individual bubbles on the froth surface. Poorly loaded bubbles are more transparent and have a 'rough' texture owing to interference from the froth structure below the froth surface, while highly loaded bubbles tend to have a smooth surface.

A manual, gravimetric solids loading method (Sadr-Kazemi and Cilliers, 2000) was used as a basis of comparison for the machine vision measurement. It was found that the correlation between these methods was somewhat variable. The difference was ascribed to the occurrence on the froth surface of two different coalescence events:

a. coalescence of adjoining bubbles, which results in a new bubble with a higher solids loading.

b. coalescence of a bubble on the surface with bubbles below the froth surface, which results in bubbles with a lower solids loading.

It was found that the gravimetric measurements were biased towards the measurement of solids loading on bubbles affected by the coalescence mechanism that decreased solids loading. The machine vision measure includes all the bubbles above a threshold detection size (typically all bubbles greater than a few millimeters), so it is not affected by this behaviour.

It was expected that the use of solids loading in conjunction with froth velocity and bubble size would be significantly better in estimating the solids recovery rate relative to current measurements which use froth velocity or bubble size and froth velocity. However, the solids loading measurements do not take into account entrained material and thus was not shown to improve estimation of solids recovery. This was attributed to the changing ratios of attached and entrained material within the concentrate across different operating conditions. Thus, for this solids loading measurement to be useful in increasing the accuracy of a solids recovery rate measurement, a model is required to incorporate the proportion of attached and entrained components in the concentrate.

6.2. Machine vision measurement of the burst rate on the froth surface (Objective 1b)

Within the literature, no robust methods are available to measure the froth stability in a manner suitable for on-line operation. Thus, a measure for the burst rate on the froth surface was developed to provide a robust and non-intrusive froth stability measurement.

The bubble size distribution was measured by segmenting froth surface images. The burst rate measurement determines the burst rate of bubbles by comparing the segmentation outputs of consecutive video frames to identify the bursting bubbles.

The burst rate measurement was expected to relate to the solids loading and bubble size on the froth surface. Results have shown that the bubbles that burst have lower than average solids loading. In addition, the burst rate was shown to increase exponentially with bubble size. Thus, by accounting for the effect of bubble size and solids loading on bursting bubbles, this measure may be useful to quantify the quality of attached solids reaching the froth surface.

The combination of the burst rate and bubble size measurements can be used to measure the rate of air loss on the froth surface. This measurement was expected to correlate with the air loss on the froth surface determined from a measurement of the air recovery (Ventura-Medina *et al.*, 2003), as both measures relate to the amount of air released from bursting on the froth surface.

Comparing the burst rate and bubble size measurement with manually segmented bubbles showed that the rate of air loss was under-estimated owing to the over-segmentation of bubbles, which was independent from the burst rate measurement. A corrected air loss measurement, when compared to the air loss determined from the air recovery measurement showed a lower rate of air loss measured near the launder than across the entire froth surface. Thus stability factors such as burst rate, bubble size or solids loading must change across the froth surface. Furthermore, the machine vision burst rate measurement is a localised stability measurement and is more sensitive than the air recovery measurement to the material recovered and froth structure near the launder.

The burst rate measurement is dependent upon the determination of a coarse segmentation, optimised to segment large and medium sized bubbles well. Thus, better techniques are required as current segmentation techniques are problematic with large bubbles, which are often over-segmented. In addition better segmentation techniques of poorly loaded froths that appear transparent are required.

6.3. Evaluating machine vision measurement performance (Objective 2)

In conjunction with the bubble size and velocity measurements, the new machine vision measures were evaluated under different operating conditions. Different froth behaviour is expected in the presence of different solids environments, differentiated by floatable solids concentration and hydrophobicity.

The two flotation systems chosen had different mineral hydrophobicities. The floatable minerals within the copper system were chalcopyrite and bornite, which tend to be highly hydrophobic. The floatable minerals within the platinum system were mostly pentlandite and pyrrhotite with some chalcopyrite, and tend to be of much lower hydrophobicity. Within each of these systems, two flotation rougher cells were chosen to study the change in the concentration of floatable solids within the pulp phase. The operating variables changed in the copper system were air rate, froth height and frother concentration, and in addition to these in the platinum system, frother type and use of activator.

- The machine vision **solids loading** measurement correlated well to the expected behaviour in all cases except in the presence of high concentrations of highly hydrophobic solids and low concentrations of low hydrophobicity solids when the air rate is increased. This was attributed to an armouring process at the high condition and poor sensitivity at the low condition.
- The **burst rate** measurement correlated to expected behaviour under most conditions. However, this correspondence was closely related to the solids loading behaviour in the presence of high concentrations of floatable solids and bubble size in the presence of low concentrations of floatable solids. Thus, intuitive behaviour relating to this parameter should derive from that of the solids loading and the bubble size, and the relative importance that these factors have on the burst rated depends upon the solids environment within the flotation cell.
- The **bubble size** measurement performed as expected across all of the conditions tested and the **velocity** measurement performed as expected under the majority of conditions.

Thus, the evaluation of the sensitivity of the physical froth surface descriptors showed that they measure expected changes under the majority of cases.

6.4. Relating operating variables to froth stability and froth mechanistic behaviour (Objective 3)

The stability of the froth affects flotation performance. Thus, it is expected that effective management of froth stability is required to manage a flotation cell. However, for this to be possible, the relationships between the operating conditions, froth stability behaviour and flotation performance attributes need to be understood and managed.

Regression analysis was used to determine the effect of changing operating variables on the physical and dynamic froth stability factors, froth transport and flotation performance in the presence of the different solids environments mentioned above.

- Increased **air flow rate** was determined to be an important factor that destabilised the froth. This destabilisation was more significant in the first rougher, where higher concentrations of floatable solids were present and was reflected by a decrease in solids loading. This decrease in solids loading was attributed to either a decrease in solids loading on bubbles entering the froth, or an increase in the slurry drainage rate from the froth. The increased slurry drainage rate from the froth may have increased the rate of particle detachment and decreased the rate that detached particles re-attach in the lower levels of the froth. Either of these effects resulted in a reduction in the stability of the froth. The effect that air rate had on froth stability was diminished by a decrease in the concentration of floatable solids.
- The effect of **froth height** on the froth stability depended on the concentration of floatable solids available. At high solids concentrations, increased coalescence occurred when the froth height increased. As the interfacial surface area in the froth decreased from coalescence, the solids loading increased resulting in the armoured bubbles and the stabilisation of the froth closer to the surface, and larger bubble sizes were measured. Conversely, in the presence of a low concentration of floatable solids within the pulp, an increase in froth depth destabilised the froth due to no armouring occurring and increased bursting. As a result, only smaller bubbles were able to remain stable on the froth surface and the maximum height that the froth could attain was reduced. Thus, the two opposing effects observed were dependent on the concentration of floatable solids.
- The stabilising effect of **frother concentration** had only been shown to be significant in the presence of a low concentration of floatable solids within the pulp. However, counter-intuitively, increased frother concentration in the presence of high concentra-

tion of floatable solids destabilised the froth. This was attributed to an increase in water content in the lower regions of the froth facilitating more of the unattached floatable solids to drop back into the pulp. This decreased the re-attachment rate of these solids, resulting in froth destabilisation. Thus, the two opposing effects observed were dependent on the concentration of floatable solids.

- The role of a stronger **frother type** was shown to mirror that of increased frother concentrations and the presence of an **activator** served to increase the solids entering and stabilising the froth in the presence of high concentrations of floatable solids.

These findings showed that the nature and concentration of floatable solids dictated the effects that operating variables have on the froth stability.

Despite the air rate and froth depth having significant relationships to concentrate grade in the presence of high and low floatable solids conditions respectively, the relationships were not consistent across the changes in operating variables made. No changes to operating variables were able to consistently affect the solids recovery rate across systems with different floatable solids hydrophobicity and concentration conditions.

Currently the critical solids concentration that causes this behaviour to switch is unknown. Further work to determine this concentration will enable the use of froth height to accurately modify froth stability across intermediate ranges of floatable solids concentrations in the froth. The same is also true for the destabilising effect of an increase in frother concentration in the presence of high concentrations of floatable solids.

In addition, the relationship between solids recovery rate was not consistent with the froth transport rate, as measured by the froth velocity. This finding implies that the machine vision froth surface measurements alone cannot be individually used to relate to flotation performance attributes within an ore system with varying hydrophobicity and floatable solids concentrations.

Changes in froth height have shown to either stabilise or destabilise the froth phase based upon the concentration of floatable solids within the froth.

6.5. Relating flotation performance to froth stability and froth mechanistic behaviour (Objective 4)

For the effective management of a flotation cell to be possible, the relationships between froth stability behaviour and flotation performance attributes need to be understood.

Regression analysis was used to test the relationship between the measured stability factors and the froth transport rate and flotation performance measurements in the presence of the different solids environments mentioned above.

In contrast to the relationship between the operating variables and flotation performance, the stability factors related more consistently to the solids recovery behaviour. Within the highly hydrophobic system, the bubble size and solids loading strongly influenced the solids recovery, while in the low hydrophobicity system, the burst rate consistently influenced the solids recovery. However, under both these conditions, the effect of floatable solids concentration caused a reverse in the expected trend. In addition, bubble size strongly influenced solids recovery under all conditions, with a positive influence occurring at the extreme conditions and a negative influence occurring at the moderate conditions.

An analysis performed to determine the operating variable effect on a measured stability factor with the purpose to affect a specific change in solids recovery or grade shows that often an operating variable change in either direction will affect appropriate changes in different stability factors. Thus, a level of significance is required, which can only be determined from a quantitative mechanistic analysis.

Thus, these results demonstrate that the use of raw machine vision based froth surface descriptors and/or other measurements to control and optimise a flotation cell, or bank is not possible without the incorporation of an interpretation of froth structure, froth stability and internal froth mechanisms, and their relationships between each other.

Therefore, further work is required to develop an interpretive model that is able to determine dominating mechanisms within the froth from analysis of froth surface descriptors. Only once methods that accomplish this are developed, can it be expected that these tools can be used within a robust flotation control and optimisation system.

6.6. Concluding remarks

This work has shown that the froth stability is the aggregate of the stability of individual lamellae across the entire froth phase. The factors that affect the stability of individual lamellae addressed in this thesis include the lamella size, concentration, hydrophobicity of solids attached to the interface and the concentration and type of surfactant adsorbed at the interface.

This work has developed methods to measure froth stability and the factors that affect it at the individual lamella level on the froth surface. The individual lamella level measurements determine the burst rate and solids loading as a function of bubble size and the measurement of solids loading on specific classes of bubbles, such as bursting bubbles.

This work also shows that the measurement of stability factors at this level and the observation of the behaviour of these factors facilitates the determination of dominant mechanistic behaviour that affects the overall froth stability behaviour. This is not possible to determine from other stability measures, as factors such as solids loading variation with bubble size and burst rate are not known.

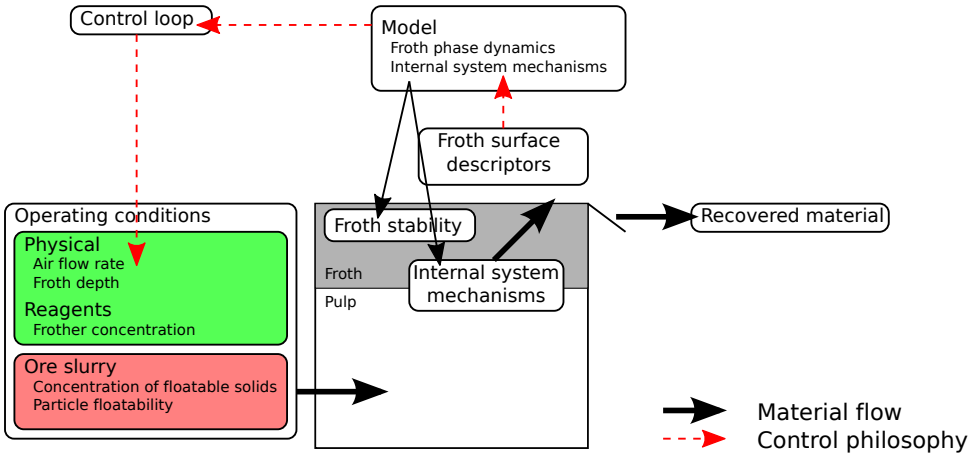

Figure 6.1.: Schematic illustrating the components required for a comprehensive control strategy to maintain consistent flotation performance across feed variation. (cf. Figure 1.1)

Figure 6.1 shows the components required for a control system to control the flotation performance in a system with varying feed conditions. While the development of a quantitative interpretive model that measures mechanistic interactions is the next step towards the development of a control system, the dynamics of these mechanisms also need to be accounted for, as each mechanism will have a different propagation rate through the froth phase.

Bibliography

Aktas, Z., Cilliers, J., Banford, A., 2008. Dynamic froth stability: Particle size, airflow rate and conditioning time effects. International Journal of Mineral Processing 87, 65–71.

Alexander, D., Franzidis, J., Manlapig, E., 2003. Froth recovery measurement in plant scale flotation cells. Minerals Engineering 16, 1197–1203.

Ata, S., 2009. The detachment of particles from coalescing bubble pairs. Journal of Colloid and Interface Science 338, 558–565.

Ata, S., Ahmed, N., Jameson, G., 2003. A study of bubble coalescence in flotation froths. International Journal of Mineral Processing 72, 255–266.

Aveyard, R., Blinks, B., Fletcher, P., Peck, T., Rutherford, C., 1994. Aspects of aqueous foam stability in the presence of hydrocarbon oils and solid particles. Advances in Colloid and Interface Science 48, 93–120.

Barbian, N., Cilliers, J., Morar, S., Bradshaw, D., 2007. Froth imaging, air recovery and bubble loading to describe flotation bank performance. International Journal of Mineral Processing 84, 81–88.

Barbian, N., Hadler, K., Ventura-Medina, E., Cilliers, J., 2005. The froth stability column: linking froth stability and flotation performance. Minerals Engineering 18, 317–324.

Bikerman, J., 1953. Foams: Theory and Industrial Applications. Reinhold Publishing, New York.

Bikerman, J., 1973. Foams. Springer-Verlag, New York.

Bonifazi, G., Giancontieri, V., Meloni, A., Serranti, S., Volpe, F., Zuco, R., Kovio, H., Hatonen, J., Hyotyniemi, H., Niemi, A., Sipari, P., Kuopanporrti, H., Ylinen, R., Keikkila, I., Lahteenmaki, S., Miettunen, J., Stephasson, O., Wang, W., Carlsson, L., 2000a. Characterisation of the flotation froth structure and color by machine vision (ChaCo). Developments in Mineral Processing 13, C8a39–C8a49.

Bonifazi, G., Massacci, P., Meloni, A., 2000b. Prediction of complex sulfide flotation performances by a combined 3d fractal and colour analysis of the froths. Minerals Engineering 13, 737–746.

Bonifazi, G., Massacci, P., Meloni, A., 2002. A 3d froth surface rendering and analysis technique to characterize flotation processes. International Journal of Mineral Processing 64, 153–161.

Bradshaw, D., O'Connor, C., 1996. Measurement of the sub-process of bubble leading in flotation. Minerals Engineering 9, 443–448.

Cappuccitti, F., Nesset, J., August 2009. Frother and collector effects on flotation cell hydrodynamics and their implication on circuit performance. In: Gomez, C., Nesset, J., Rao, S. (Eds.), Advances in Mineral Processing Science and Technology, Proceedings of the 7th UBC-McGill-UA International Symposium of Minerals Processing. Metallurgical Society of CIM, Sudbury, Canada.

Chen, F., Gomez, C., Finch, J., 2002. Bubble size measurement in flotation machines. Minerals Engineering 14, 427–432.

Cipriano, A., Guarini, M., Soto, A., Briceno, H., Mery, D., 1997. Expert supervision of flotation cells using digital image processing. In: Proceedings of the XX International Mineral Processing Congress. Aachen, Germany, pp. 281–292.

Comley, B., 2001. Dynamic surface tension as a means of characterising flotation frother performance. MSc thesis, University of Cape Town.

Comley, B., Harris, P., Bradshaw, D., Harris, M., 2002. Frother characterisation using dynamic surface tension measurements. International Journal of Mineral Processing, 81–100.

Dai, Z., Fornasiero, D., Ralston, J., 2000. Particle-bubble collision models - a review. Advances in Colloid and Interface Science 85, 231–256.

Day, A. (Ed.), 2002. Mining Chemicals Handbook, Revised Edition. Cytec Industries Inc.

de Jager, G., Francis, J., Hatfield, D., Oostendorp, B., Bradshaw, D., Morar, S., Nicolls, F., Forbes, G., Heinrich, G., Markham, H., 2004. A method and a control system for extracting valuable minerals from mined ore, "SmartFroth". Adams & Adams Patent Attorneys Pretoria A&A REF: 2004/16402.

de Jager, G., Hatfield, D., Bradshaw, D., Francis, J., Morar, S., 2005. A method and a control system for extracting valuable minerals from mined ore, "SmartFroth". South African

Patent 2005/04232.

Dippenaar, A., 1982a. The destabilisation of froth by solids: II The rate determining step. International Journal of Mineral Processing 9, 15–27.

Dippenaar, A., 1982b. The destabilisation of froths by solids: I The mechanism of film rupture. International Journal of Mineral Processing 9, 1–14.

Falutsu, M., Dobby, G., 1989. Direct measurement of froth drop back and collection zone recovery in a laboratory flotation column. Minerals Engineering 2, 377–386.

Fan, L.-S., 1989. Gas-Solid-Liquid fluidization engineering. Butterworths, pp. 47–52.

Feteris, S., Frew, J., Jowett, A., 1987. Modelling the effect of froth depth in flotation. International Journal of Mineral Processing 20, 121–135.

Finch, J., Dobby, G., 1990. Column flotation. Pergamon Press, New York.

Finch, J., Gelinas, S., Moyo, P., 2006. Frother-related research at McGill University. Minerals Engineering 19, 726–733.

Forbes, G., 2007. Texture and bubble size measurements for modelling concentrate grade in flotation froth systems. PhD thesis, University of Cape Town.

Forbes, G., de Jager, G., 2004. Texture measures for improved watershed segmentation of froth images. In: Proceedings of the Twelfth Annual Symposium of the Pattern of South Africa.

Forbes, G., de Jager, G., 2006. A method of determining the size distribution of bubbles in the froth and a froth flotation process, "SmartFroth 5". Adams & Adams Patent Attorneys Pretoria A&A REF: 2006/01520.

Fowkes, F., 1964. Attractive forces at interfaces. Industrial and Engineering Chemistry 56, 40–52.

Francis, J., 2001. Machine vision for froth flotation. PhD thesis, University of Cape Town.

Francis, J., de Jager, G., 1998. An investigation into the suitability of various motion estimation algorithms for froth imaging. In: Proceedings of COMSIG 1998. pp. 139–143.

Fuerstenau, D., Wayman, C., June 1958. Effect of chemical reagents on the motion of single air bubbles in water. Transactions of the AIME, 694–699.

Gaudin, A., 1957. Flotation, 2nd Edition. McGraw-Hill, New York, NY, USA.

Gelinas, S., Finch, J., Gouet-Kaplan, M., 2005. Comparative real-time characterisation of frother bubble thin-films. Journal of Colloid and Interface Science 291, 187–191.

Gomez, C., Cortes-Lopez, F., Finch, J., 2003. Industrial testing of a gas holdup sensor for flotation systems. Minerals Engineering 16, 493–501.

Gorain, B., 2005. Optimisation of floation circuits with large flotation cells. In: Proceedings of Centenary of Flotation Symposium. AUSIMM, Brisbane, Australia, pp. 843–851.

Gorain, B., Franzidis, J., Manlapig, E., 1996. Studies on impeller type, impeller speed and air flow rate in an industrial cell. Part 3: Effect on superficial gas velocity. Minerals Engineering 9, 639–654.

Gorain, B., Franzidis, J., Manlapig, E., 1997. Studies on impeller type, impeller speed and air flow rate in an industrial scale flotation cell. part 4: Effect of bubble surface area flux on flotation performance. Minerals Engineering 10, 367–379.

Gotlieb, C., Kreysig, H., 1990. Texture based descriptors based on co-occurrence matrices. Computer Vision, Graphics and Image Processing, 70–86.

Grau, R., Heiskanen, K., 2002. Visual technique for measuring bubble size in flotation machines. Minerals Engineering 15, 507–513.

Grau, R., Laskowski, J., 2006. Effect of frothers on bubble generation and coalescence in a mechanical flotation cell. The Canadian Journal of Chemical Engineering 84, 170–182.

Guarini, M., Cipriano, A., Soto, A., Guesalaga, A., 1995. Using image processing techniques to evaluate the quality of mineral flotation process. In: Proceedings of the international conference on Signal Processing, Applications of Technology. Boston, USA, pp. 1227–1231.

Hadler, K., Aktas, Z., Cilliers, J., 2005. The effects of frother and collector distribution on flotation performance. Minerals Engineering 18, 171–177.

Hadler, K., Cilliers, J., 2009. The relationship between the peak in air recovery and flotation performance. Minerals Engineering 22, 451–455.

Haralick, R., 1979. Statistical and structural approaches to texture. Proceedings of the IEEE 67, 786–804.

Hargrave, J., Hall, S., 1997. Diagnosis of concentrate grade and mass flowrate in tin flotation from colour and surface texture analysis. Minerals Engineering 10, 613–621.

Harris, P., 1982. Principles of flotation (editor: R. P. King). SAIMM, Chapter: 13: Frothing phenomena and frothers, pp. 237–250.

Hatfield, D., 2006. The implications of froth structure and surface appearance for flotation performance. PhD thesis, University of Cape Town.

Hatfield, D., Bradshaw, D., 2003. The relationship between concentrate yield and descriptors from a machine vision system in a platinum flotation application. In: Proceedings of XXII International Mineral Processing Congress. Cape Town, South Africa, pp. 929–936.

Hatonen, J., Hyotyniemi, H., Miettunen, J., Carlsson, L., 1999. Using image information and PLS for predicting mineral concentrations in the flotation froth. In: Proceedings of the second International Conference on Intelligent Processing and Manufacturing of Materials (IPMM'99). Hawaii, USA.

Heinrich, G., 2003. An investigation into the use of froth colour as a sensor for metallurgical grade in a copper system. MSc thesis, University of Cape Town.

Hernandez-Aguilar, J., Finch, J., 2005. Validation of bubble sizes obtained with incoherent imaging on a sloped viewing window. Chemical Engineering Science 60, 3323–3336.

Holtham, P., Nguyen, K., 2002. On-line analysis of froth surface in coal and mineral flotation using JKFrothCam. International Journal of Mineral Processing 64, 163–180.

Honaker, R., Ozsever, A., 2003. Evaluation of the selective detachment process in flotation froth. Minerals Engineering 16, 975–982.

Honaker, R., Ozsever, A., Parekh, B., 2006. Selective detachment process in column flotation froth. Minerals Engineering 19, 687–695.

Hu, S., Ofori, P., Firth, B., 2009. Monitoring of froth stability using electrical impedeance spectroscopy. International Journal of Mineral Processing 92, 15–21.

Hyotyniemi, H., Ylinen, R., Miettunen, J., 2000. AI in practise: Case study on a flotation plant. STeP 2000 - Millennium of Artificial Intelligence, Vol. 2: AI of Today 2, 281–292.

Jachimska, B., Lunkenheimer, K., Malysa, K., 1995. Effect of position of the functional group on the equilibrium and dynamic surface properties of butyl alcohols. Journal of Colloid and Interface Science 176, 31–38.

Johansson, G., Pugh, R., 1992. The influence of particle size and hydrophobicity on the stability of mineralised froths. International Journal of Mineral Processing 34, 1–21.

Johnson, N. W., McKee, D., Lynch, A. J., 1974. Flotation rates of nonsulfide minerals in chalcopyrite flotation processes. Transactions of the American Institute of Mineral Engineers 256, 204–209.

Kitchener, J., Cooper, C., 1959. Current concepts in the theory of foaming. Quarterly Reviews, Chemical Society 13, 71–97.

Klassen, V., Makroussov, V., 1963. Introduction to the theory of flotation. Butterworth, London, Chapter: Frothers and Flotation froths, pp. 353–385.

Koh, P., Hao, F., Smith, L., Chau, T., Bruckard, W., 2009. The effect of particle shape and hydrophobicity in flotation. International Journal of Mineral Processing 93, 128–134.

Laskowski, J., October 1974. Particle-bubble attachment in flotation. Minerals Science and Engineering 6, 223–235.

Laskowski, J., 1986. Advances in Mineral Processing (Ed: Somasundaran, P.). AIME, Chapter: The relationship between floatability and hydrophobicity, pp. 189–208.

Laskowski, J., 1998. Frothing in Flotation II (Eds: J. S. Laskowski and E. T. Woodburn). Gordon and Breach Science Publishers, Amsterdam, Chapter: 1, Frothers and Frothing, pp. 1–49.

Laskowski, J., Tlhone, T., Williams, P., Ding, K., 2003. Fundamental properties of the polyoxypropylene alkyl ether flotation frothers. International Journal of Mineral Processing.

Laskowski, J., Xu, Z., Yoon, R., 1991. Energy barrier in particle-to-bubble attachment and its effect on flotation kinetics. In: 17th International Mineral Processing Congress. Dresden, pp. 237–249.

Leja, J., Schulman, J., February 1954. Flotation theory: Molecular interactions between frothers and collectiors at solid-liquid-air interfaces. Mining Engineering, 221–228.

Levich, V., 1962. Physicochemical Hydrodynamics. Prentice-Hall International, Inc.

Livshits, A., Dudenkov, S., 1965. Some factors in flotation froth stability. In: Proceedings of the VIIth International Mineral Processing Congress. Gordon and Breach, New York, pp. 367–371.

Louw, M., 2009. A Population Monte Carlo approach to estimating parametric Bidirectional Reflectance Distribution Functions through Markov Random Field Parameter estimation. PhD thesis, University of Cape Town.

Malysa, K., Lunkenheimer, K., Miller, R., Hartenstein, C., 1981. Surface elasticity and frothability of n-octanol and n-octanoic acid solutions. Colloids and Surfaces 3, 329–338.

Malysa, K., Pawlikowska-Czubak, J., Pomianowski, A., 1978. Proceedings of the VIIth International Congress of Surface Active Substances (Moscow 1976). Vol. 3. Moscow, Chapter: 4. Frothing properties of solutions and their influence on the floatability, pp. 513–520.

Melo, F., Laskowski, J., 2005. Fundamental properties of flotation frothers and their effect on flotation. In: Proceedings of Centenary of Flotation Symposium. AUSIMM, pp. 348–353.

Moolman, D., Aldrich, C., van Deventer, J., Stange, W., 1994. Digital image processing as a tool for on-line monitoring of froth in flotation plants. Minerals Engineering 7, 1149–1164.

Morar, S., Forbes, G., Heinrich, G., Bradshaw, D., King, D., Adair, B., Esdaile, L., June 2005. The use of a colour parameter in a machine vision system, SmartFroth, to evaluate copper flotation performance at Rio Tinto's Kennecott Utah copper concentrator. In: Proceedings of Centenary of Flotation Symposium. AUSIMM, Brisbane, Australia, pp. 147–152.

Morar, S., Hatfield, D., Barbian, N., Bradshaw, D., Cilliers, J., Triffett, B., 2006. A comparison of flotation froth stability measurements and their use in the prediction of concentrate grade. In: Proceedings of XXIII International Minerals Processing Congress. Istanbul, Turkey, pp. 937–945.

Moys, M., 1984. Residence time distribution and mass transport in the froth phase of the flotation process. International Journal of Mineral Processing 13, 117–142.

Murphy, D., Zimmerman, W., Woodburn, E., 1996. Kinematic model of bubble motion in a flotation froth. Powder Technology 87, 3–12.

Navarra, A., Acuna, C., Finch, J., 2009. Impact of frother on the terminal velocity of small bubbles. International Journal of Mineral Processing 91, 68–73.

Neethling, S., Cilliers, J., 2002. Solids motion in flowing froths. Chemical Engineering Science 57, 607–615.

Neethling, S., Cilliers, J., 2003. Modelling flotation froths. International Journal of Mineral Processing 72, 267–287.

Neethling, S., Lee, H., Cilliers, J., 2003. Simple relationships for predicting the recovery of liquid from flowing foams and froths. Minerals Engineering 16, 1123–1130.

Nesset, J., Hernandez-Aguilar, J., Acuna, C., Gomez, C., Finch, J., 2005. Some gas dispersion characteristics of mechanical flotation machines. In: Proceedings of Centenary of Flotation Symposium. AUSIMM, Brisbane, Australia, pp. 243–249.

Nguyen, A., Ralston, J., Schulze, H., 1998. On modelling of bubble-particle attachment probability in flotation. International Journal of Mineral Processing 53, 225–249.

Nguyen, K., 1998. The application of texture based image analysis techniques in froth flotation. PhD thesis, University of Queensland.

Nguyen, K., Thornton, A., 1995. The application of texture based image analysis techniques in froth flotation. In: Proceedings of DICTA-95, the 3rd Conference on Digital Image Computing Techniques and Applications. Australian Pattern Recognition Society, Brisbane, Australia, pp. 371–376.

Phan, C., Nguyen, A., Miller, J., Evans, G., Jameson, G., 2003. Investigations of bubble-particle interactions. International Journal of Mineral Processing 72, 239–254.

Pugh, R., 1996. Foaming, foam films, antifoaming and defoaming. Advances in Colloid and Interface Science 64, 67–142.

Randall, E., Goodall, C., Fairlamb, P., Dold, P., O'Connor, C., 1989. A method for measuring the sizes of bubbles in two and three phase systems. Journal of Physics E: Scientific Instruments 22, 827–833.

Reddick, J., Hesketh, A., Morar, S., Bradshaw, D., 2009. An evaluation of factors affecting the robustness of colour measurement and its potential to predict the grade of flotation concentrate. Minerals Engineering 22, 64–69.

Ritter, G., Wilson, J., 2001. Handbook of Computer Vision Algorithms in Image Algebra, 2nd Edition. CRC Press Inc., Boca Raton, FL, USA.

Ross, V., 1997. Particle-bubble attachment in flotation froths. Minerals Engineering 10, 695–706.

Runge, K., McMaster, J., Wortley, M., La Rosa, D., Guyot, O., March 2007. A correlation between Visiofroth measurements and the performance of a flotation cell. In: Proceedings of Ninth Mill Operator's Conference. Freemantle, Australia, pp. 79–86.

Sadr-Kazemi, N., Cilliers, J., 2000. Technical note: A technique for measuring flotation bubble shell thickness and concentration. Minerals Engineering 13, 773–776.

Sam, A., Gomez, C., Finch, J., 1996. Axial velocity profiles of single bubbles in water/frother solutions. International Journal of Mineral Processing 47, 177–196.

Savassi, O., Alexander, D., Franzidis, J., Manlapig, E., 1998. An empirical model for entrainment in industrial flotation plants. Minerals Engineering 11, 243–256.

Savassi, O., Alexander, D., Johnson, N., Franzidis, J., Manlapig, E., 1997. Measurement of froth recovery of attached particles in industrial flotation cells. In: Sixth Mill operators conference. Australian Institute of Mining and Metallurgy, Mandag, Papua New Guinea, pp. 149–156.

Schuhmann, R., 1942. Flotation kinetics. I. Methods for steady-state study of flotation problems. Journal of Physical Chemistry 46, 891.

Schulze, H., 1977. New theoretical and experimental investigations on stability of bubble/particle aggregates in flotation: A theory on the upper particle size of floatability. International Journal of Mineral Processing 4, 241–259.

Schwarz, S., March 2004. The relationship between froth recovery and froth structure. PhD thesis, Ian Wark Research Institute, University of South Australia.

Schwarz, S., Grano, S., 2005. Effect of particle hydrophobicity on particle and water transport across a flotation froth. Colloids and Surfaces A: Physicochemical and Engineering Aspects 256, 157–164.

Seaman, D., Franzidis, J., Manlapig, E., 2004. Bubble load measurement in the pulp zone of industrial flotation machines - a new device for determining the froth recovery of attached particles. International Journal of Mineral Processing 74, 1–13.

Seaman, D., Manlapig, E., Franzidis, J., 2005. Selective transport of attached particles across the pulp-froth interface. In: Proceedings of the Centenary of Flotation Symposium. AUSIMM, Brisbane, Australia, pp. 601–609.

Seaman, D., Manlapig, E., Franzidis, J., 2006. Selective transport of attached particles across the pulp-froth interface. Minerals Engineering 19, 841–851.

Stevenson, P., 2007. Hydrodynamic theory of rising foam. Minerals Engineering 20, 282–289.

Subrahmanyam, T., Forssberg, E., 1988. Froth stability, particle entrainment and drainage in flotation - a review. International Journal of Mineral Processing 23, 33–53.

Sun, S., 1952. Frothing characteristics of pine oils in flotation. Transactions of the AIME 193, 65–71.

Supomo, A., Yap, E., Zheng, X., Banini, G., Mosher, J., Partanen, A., 2008. PT Freeport Indonesia's mass-pull control strategy for rougher flotation. Minerals Engineering 21, 808–816.

Sutherland, K., 1948. Physical chemistry of flotation. XI. Kinetics of the flotation process. Journal of Physical and Colloid Chemistry 52, 394–425.

Sweet, C., 2000. The application of a machine vision system to relate froth surface characteristics to the metallurgical performance of a PGM flotation process. MSc thesis, University of Cape Town.

Sweet, C., Bradshaw, D., Cilliers, J., Wright, B., de Jager, G., Francis, J., 2000. The extraction of valuable minerals from mined ore."SmartFroth". South African Patent 2000/7079.

Sweet, C., van Hoogstraten, J., Harris, M., Laskowski, J., 1997. The effects of frothers on bubble size and frothability of aqueous solutions. In: Finch, J., Rao, S., Holubec, I. (Eds.), Processing of Complex Ores - Proc. 2nd UBC-McGill Int. Symposium. pp. 235–245.

Taute, J., Mc Clelland, A., 2006. Introduction to the Anglo Platinum bubble sizer. Presented at the SAIMM Conference, Cape Town.

Torrealba-Vargas, J., Gomez, C., Finch, J., 2004. Continuous air rate measurement in flotation cells: a step towards gas distribution management. Minerals Engineering 17, 761–765.

van Deventer, J., Feng, D., Burger, A., 2004. Transport phenomena at the pulp-froth interface in a flotation column: II. Detachment. International Journal of Mineral Processing 74, 217–231.

Ventura-Medina, E., Barbian, N., Cilliers, J., 2003. Froth stability and flotation performance. In: Proceedings of XXII International Mineral Processing Congress. Cape Town, South Africa, pp. 937–945.

Ventura-Medina, E., Cilliers, J., 1999. Calculation of the specific surface area in flotation. Minerals Engineering 13, 265–275.

Vera, M., Franzidis, J., Manlapig, E., 1999. Simultaneous determination of collection zone rate constant and froth recovery in a mechanical flotation environment. Minerals Engineering 12, 1163–1176.

Vincent, L., 1992. Morphological grayscale reconstruction: Definition, efficient algorithm, and applications in image analysis. In: Proceedings of IEEE Conference on Computer Vision and Pattern Recognition. Champagne, IL, USA, pp. 633–635.

Vincent, L., 1993. Morphological grayscale reconstruction in image analysis: Applicatons and efficient algorithms. IEEE Transactions on Image Processing 2, 176–201.

Vincent, L., Soille, P., June 1991. Watershed in digital spaces: An efficient algorithm based on immersion simulations. IEEE Transactions on pattern analysis and machine intelligence 13, 583–598.

Wang, Y., Neethling, S., 2007. The structure of flotation froth surfaces: The relationship between surface film and bubble sizes. Minerals Engineering, Cape Town, Flotation 2007.

Weaire, D., Phelan, R., 1994. A counter-example to Kelvin's conjecture on minimal surfaces. Philosophical Magazine Letters 69, 107–110.

Wilson, S., Stratton-Crawley, R., 1991. Design of production scale flotation columns using a first order kinetic model. In: Agar, G. E., Huls, B. J., Hyma, D. B. (Eds.), Column '91, Proceedings of an International Conference on Column Flotation. Sudbury, Ontario, Canada, pp. 165–179.

Woodburn, E., Austin, L., Stockton, J., March 1994. A froth based flotation kinetic model. Transactions of the IChemE 72, 211–226.

Wright, B., 1997. An investigation into the use of the watershed transform for the real-time segmentation of flotation froth images. MSc thesis, University of Cape Town.

Yianatos, J., Moys, M., Contreras, F., Villanueva, A., 2008. Froth recovery of industrial flotation cells. Minerals Engineering 21, 817–825.

Yoon, R., 2000. The role of hydrodynamic and surface forces in bubble-particle interaction. International Journal of Mineral Processing 58, 129–143.

Yoon, R., Luttrell, G., 1989. The effect of bubble size on fine particle flotation. Mineral Processing and Extractive Metallurgy Review 5, 101–122.

Zanin, M., Wightman, E., Grano, S., Franzidis, J.-P., 2009. Quantifying contributions to froth stability in porphyry copper plants. International Journal of Mineral Processing 91, 19–27.

Zhang, J., Fan, L., 2003. On the rise velocity of an interactive bubble in liquids. Chemical Engineering Journal 92, 169–176.

Zheng, X., Franzidis, J., Manlapig, E., 2004. Modelling of froth transportation in industrial flotation cells: Part I. Development of froth transportation models for attached particles. Minerals Engineering 17, 981–988.

Zheng, X., Knopjes, L., 2004. Modelling of froth transportation in industrial flotation cells: Part II. Modelling of froth transportation in an Outokumpu tank flotation cell at the Anglo Platinum Bafokeng-Rasimone platinum mine (BRPM) concentrator. Minerals Engineering 17, 989–1000.

Appendix A.

Raw Data and Regression Analysis Outputs

This section contains the raw data measured from the systems described in chapter 3. Within this thesis, the data from the first and third roughers in these systems were used.

This data contains the chosen operating conditions and measured machine vision and metallurgical parameters. Other additional measurements, such as solids loading, as determined from the gravimetric measurement technique and superficial gas velocity and pulp bubble size measurements are included.

A.1. Copper rougher data

Table A.1.: Copper rougher 1 machine vision and metallurgical measurements.

Air flow		Frother conc		Froth depth		Jg	Velocity	Solids loading					Burst rate		Air lost	Bubble size	Solids	Water	% solids	Cu	Notes
								MV	MV_{burst}	MV_{p80}	$MV_{burst,\ p80}$	Gravimetric	Large	Small		d_{80}					
	m^3/hr		ppm		m	m/s	m/s	kg/m^2	kg/m^2	kg/m^2	kg/m^2	kg/m^2	$1/m^2/s$	$1/m^2/s$	$m^3/m^2/hr$	m	t/hr	t/hr	%	%	
L	321	L	102	L	0.155	0.0103	0.0161	0.035	0.0124	0.031	0.0064	0.038	32.5	19.3	15.41	0.037	0.26	0.58	30.79	41.2	
L	321	L	100	H	0.200	0.0103	0.0167	0.042	0.0093	0.037	0.0058	0.030	21.2	23.0	22.49	0.047	0.41	0.97	29.77	38.3	
L	321	H	138	H	0.200	0.0103	0.0208	0.036	0.0198	0.032	0.0051	0.035	20.6	19.2	13.83	0.042	0.48	1.02	32.02	39.0	
M	351	L	102	L	0.155	0.0110	0.0126	0.049	0.0198	0.040	0.0158	0.038	49.3	31.3	24.64	0.035	0.27	0.72	27.17	31.6	
M	351	L	100	H	0.200	0.0110	0.0192	0.043	0.0091	0.037	0.0024	0.024	29.7	27.1	27.21	0.046	0.49	1.27	27.62	35.2	
M	351	H	130	H	0.200	0.0110	0.0139	0.033	0.0091	0.030	0.0049	0.031	29.8	21.4	15.84	0.035	0.11	0.28	29.31	37.2	
H	381	L	100	L	0.155	0.0117	0.0136	0.039	0.0110	0.034	0.0091	0.024	34.0	28.9	26.45	0.045	0.38	2.92	11.50	36.6	
H	381	L	98	H	0.200	0.0117	0.0202	0.044	0.0086	0.038	0.0072	0.023	31.3	30.1	21.78	0.046	0.62	1.92	24.27	27.9	
H	381	H	138	H	0.200	0.0117	0.0204	0.043	0.0043	0.037	0.0036	0.028	31.5	26.8	19.14	0.042	0.43	0.98	30.26	38.3	
L	321	L	102	L	0.155	0.0103	0.0154	0.043	0.0111	0.036	0.0131	0.044	28.1	24.6	25.60	0.045	0.25	0.60	29.53	37.0	
L	321	L	100	H	0.200	0.0103	0.0131	0.041	0.0175	0.036	0.0074	0.043	30.3	22.0	17.74	0.041	0.34	0.76	31.29	40.9	
L	321	H	138	H	0.200	0.0103	0.0135	0.036	0.0087	0.033	0.0035	0.030	16.4	21.7	27.70	0.054	0.47	1.20	28.21	32.7	
M	351	L	102	L	0.155	0.0110	0.0197	0.047	0.0194	0.039	0.0135	0.030	44.4	28.5	21.35	0.036	0.36	0.89	28.55	33.5	
M	351	L	100	H	0.200	0.0110	0.0170	0.040	0.0152	0.034	0.0087	0.035	34.2	27.1	21.07	0.039	0.27	0.59	31.09	41.1	
M	351	H	130	H	0.200	0.0110	0.0089	0.044	0.0087	0.038	0.0041	0.026	34.8	27.3	18.48	0.039	0.37	0.81	31.53	40.5	
H	381	L	100	L	0.155	0.0117	0.0162	0.047	0.0217	0.039	0.0039	0.027	81.6	23.9	22.21	0.025	3.56	13.89	20.41	6.5	1.
H	381	L	98	H	0.200	0.0117	0.0178	0.036	0.0065	0.033	0.0021	0.023	17.4	23.9	32.78	0.061	0.78	2.11	27.13	32.9	
H	381	H	138	H	0.200	0.0117	0.0109	0.044	0.0165	0.037	0.0065	0.026	40.2	28.4	20.46	0.037	0.41	0.98	29.36	37.3	

1. Condition excluded from some regressions as an outlier due to high solids and water recovery.

Table A.2.: Copper rougher 3 machine vision and metallurgical measurements.

Air flow		Frother conc		Froth depth	Jg	Velocity	Solids loading				Burst rate		Air lost	Bubble size	Solids	Water	% solids	Cu	Notes
							MV	MV_{burst}	MV_{p80}	$MV_{burst\ p80}$	Gravimetric	Large	Small		d_{SO}				
	m^3/hr		ppm		m	m/s	m/s	kg/m^2	kg/m^2	kg/m^2	kg/m^2	kg/m^2	$1/m^2/s$	$1/m^2/s$	$m^3/m^2/hr$	m	t/hr	t/hr	%	%	
L	321	L	102	L	0.155	0.0126	0.0429	0.022	0.0126	0.0281	0.0150	0.025	18.1	19.5	34.25	0.035	0.24	0.60	28.44	28.0	
L	321	L	100	H	0.200	0.0126	0.0321	0.019	0.0087	0.0238	0.0076	0.017	35.4	37.8	49.75	0.030	0.17	0.43	28.57	31.6	
L	321	H	138	H	0.200	0.0126	0.0370	0.022	0.0112	0.0277	0.0105	0.017	20.9	26.1	54.40	0.037	0.17	0.37	31.44	36.3	
M	351	L	102	L	0.155	0.0148	0.0488	0.021	0.0076	0.0238	0.0120	0.020	28.6	22.8	31.28	0.026	0.28	1.03	21.29	15.9	
M	351	L	100	H	0.200	0.0148	0.0303	0.016	0.0025	0.0188	0.0046	0.018	43.6	36.8	41.61	0.026	0.18	0.50	26.91	33.8	
M	351	H	130	H	0.200	0.0148	0.0145	0.022	0.0057	0.0166	0.0000	0.022	45.9	18.4	14.80	0.018	0.60	2.23	21.12	13.1	
H	381	L	100	L	0.155	0.0161	0.0432	0.019	0.0136	0.0233	0.0143	0.016	31.7	21.1	47.43	0.030	0.15	0.37	28.15	30.9	
H	381	L	98	H	0.200	0.0161	0.0256	0.018	0.0044	0.0203	0.0063	0.015	43.0	37.2	44.92	0.026	0.18	0.49	26.42	30.0	
H	381	H	138	H	0.200	0.0161	0.0377	0.020	0.0069	0.0238	0.0082	0.015	26.5	28.0	32.50	0.030	0.27	0.71	28.02	31.6	
L	321	L	102	L	0.155	0.0126	0.0493	0.021	0.0124	0.0277	0.0141	0.031	22.2	25.0	35.99	0.032	0.26	0.64	28.45	30.6	
L	321	L	100	H	0.200	0.0126	0.0381	0.022	0.0098	0.0265	0.0099	0.025	24.8	28.4	51.24	0.034	0.19	0.41	31.19	34.1	
L	321	H	138	H	0.200	0.0126	0.0309	0.019	0.0082	0.0245	0.0117	0.026	25.4	31.0	57.07	0.035	0.21	0.55	27.76	32.2	
M	351	L	102	L	0.155	0.0148	0.0443	0.021	0.0116	0.0204	0.0090	0.018	41.2	17.4	31.58	0.023	0.43	1.85	18.66	11.3	
M	351	L	100	H	0.200	0.0148	0.0320	0.021	0.0087	0.0261	0.0106	0.019	22.1	25.4	40.48	0.033	0.18	0.41	31.11	35.1	
M	351	H	130	H	0.200	0.0148	0.0319	0.021	0.0069	0.0238	0.0074	0.015	32.9	26.4	31.42	0.026	0.15	0.35	30.41	30.8	
H	381	L	100	L	0.155	0.0161	0.0560	0.018	0.0071	0.0136	0.0068	0.013	42.7	7.1	27.32	0.018	1.21	5.99	16.85	6.0	1.
H	381	L	98	H	0.200	0.0161	0.0213	0.019	0.0046	0.0243	0.0093	0.015	30.1	36.6	67.45	0.036	0.21	0.59	26.29	31.3	
H	381	H	138	H	0.200	0.0161	0.0362	0.018	0.0058	0.0198	0.0069	0.016	33.0	23.5	23.11	0.024	0.26	0.78	24.74	28.2	

1. Condition excluded from some regressions as an outlier due to high solids and water recovery.

A.2. Platinum rougher data

Table A.3.: Platinum rougher 1 machine vision and metallurgical measurements.

Frother Type	Conc		Froth depth		Activator	Jg	Velocity	Solids loading					Burst rate		Air lost	Bubble size		Solids	Water	Pt	Ni	Notes
								MV	MV_{burst}	MV_{p80}	$MV_{burst,\ p80}$	Gravimetric	Large	Small		Pulp d_{32}	FS d_{80}					
		ppm		m		m/s	m/s	kg/m^2	kg/m^2	kg/m^2	kg/m^2	kg/m^2	$1/m^2/s$	$1/m^2/s$	$m^3/m^2/s$	m	m	kg/hr	kg/hr	ppm	%	
XP200	H	60	H	0.098	L	0.00592	0.0177	0.0771	0.0156	0.0734	0.0140	0.0363	467	121	14.65	0.00128	0.016	9.84	36.69	137.0	4.84	
XP200	H	60	L	0.064	H	0.00569	0.0194	0.0744	0.0156	0.0749	0.0144	0.0751	390	229	18.12	0.00121	0.020	12.33	54.88	75.6	2.64	
XP200	H	60	L	0.054	L	0.00491	0.0105	0.0712	0.0158	0.0667	0.0143	0.0665	373	7	6.56	0.00129	0.010	25.49	187.60	49.0	1.59	
XP200	M	40	M	0.076	M	0.00612	0.0066	0.0707	0.0156	0.0680	0.0139	0.0776	474	84	11.69	0.00124	0.014	18.49	58.70	93.2	3.14	
XP200	M	40	M	0.085	M	0.00753	0.0088	0.0700	0.0156	0.0655	0.0137	0.0689	503	87	12.32	0.00176	0.015	19.34	50.84	112.0	3.07	
XP200	M	40	M	0.075	M	0.00761	0.0116	0.0730	0.0156	0.0701	0.0136	0.0691	554	81	12.38	0.00162	0.014	15.07	85.77	130.0	2.55	
XP200	L	20	L	0.057	H	0.00640	0.0099	0.0807	0.0155	0.0825	0.0147	0.0829	337	264	24.02	0.00108	0.022	22.03	49.55	91.8	2.88	
XP200	L	20	L	0.053	L	0.00585	0.0065	0.0686	0.0157	0.0649	0.0141	0.0476	407	13	7.14	0.00136	0.010	60.23	334.50	87.8	1.49	1.
XP200	L	20	L	0.056	L	0.00589	0.0116	0.0751	0.0156	0.0718	0.0138	0.0719	508	125	13.65	0.00137	0.015	22.33	59.73	88.8	3.11	
XP250	H	60	H	0.161	H	0.00787	0.0040	0.0825	0.0156	0.0865	0.0153	0.0278	182	273	22.37	0.00184	0.028	5.21	49.91	74.5	3.14	2.
XP250	H	60	H	0.114	L	0.00733	0.0110	0.0686	0.0157	0.0641	0.0141	0.0665	396	12	7.32	0.00154	0.010	20.32	37.04	74.2	2.58	
XP250	H	60	L	0.066	H	0.00538	0.0153	0.0660	0.0157	0.0675	0.0139	0.0701	447	26	8.24	0.00134	0.011	26.84	126.34	52.6	2.03	
XP250	H	60	L	0.066	L	0.00575	0.0153	0.0658	0.0157	0.0669	0.0142	0.0637	377	10	6.40	0.00134	0.010	26.66	187.86	88.4	1.87	
XP250	L	20	H	0.111	H	0.00868	0.0092	0.0752	0.0155	0.0761	0.0144	0.0543	387	243	18.68	0.00177	0.020	21.04	108.56	54.6	1.89	
XP250	L	20	H	0.091	L	0.00651	0.0224	0.0716	0.0156	0.0667	0.0138	0.0739	483	46	9.97	0.00170	0.012	31.22	103.53	101.0	2.91	
XP250	L	20	L	0.053	H	0.00527	0.0118	0.0734	0.0156	0.0720	0.0143	0.0742	404	170	15.48	0.00131	0.018	21.69	56.36	94.8	2.86	
XP250	L	20	L	0.049	L	0.00582	0.0113	0.0690	0.0156	0.0667	0.0147	0.0414	510	22	9.01	0.00140	0.011	35.17	283.13	79.7	1.88	

1. Condition excluded from some regressions as an outlier due to high solids and water recovery.
2. Condition excluded from some regressions as an outlier due to low solids recovery.

Table A.4.: Platinum rougher 3 machine vision and metallurgical measurements.

Frother Type	Conc		Froth depth		Activator	Jg	Velocity	Solids loading					Burst rate		Air lost	Bubble size		Solids	Water	Pt	Ni	Notes
								MV	MV_{burst}	MV_{p80}	$MV_{burst,\ p80}$	Gravimetric	Large	Small		Pulp d_{32}	FS d_{80}					
		ppm		m		m/s	m/s	kg/m^2	kg/m^2	kg/m^2	kg/m^2	kg/m^2	$1/m^2/s$	$1/m^2/s$	$m^3/m^2/s$	m	m	kg/hr	kg/hr	ppm	%	
XP200	H	60	H	0.0808	L	0.0065	0.0149	0.0287	0.0200	0.0160	0.0160	0.0132	988	37	2.64	0.00124	0.0113	11.4	241.1	12.8	0.23	
XP200	H	60	L	0.0808	H	0.0059	0.0158	0.0279	0.0199	0.0198	0.0158	0.0294	1058	58	3.14	0.00143	0.0122	12.6	219.9	12.3	0.23	
XP200	H	60	L	0.0794	L	0.0068	0.0101	0.0330	0.0201	0.0206	0.0166	0.0143	902	17	2.05	0.00143	0.0096	10.3	158.1	18.4	0.35	
XP200	M	40	M	0.0805	M	0.0068	0.0114	0.0321	0.0200	0.0207	0.0162	0.0200	976	27	2.54	0.00150	0.0105	10.3	193.0	11.1	0.20	
XP200	M	40	M	0.0804	M	0.0058	0.0123	0.0315	0.0199	0.0189	0.0155	0.0248	1103	50	3.25	0.00138	0.0117	15.5	136.0	18.0	0.42	
XP200	M	40	M	0.0720	M	0.0052	0.0135	0.0257	0.0198	0.0160	0.0155	0.0143	1103	57	3.11	0.00179	0.0119	13.4	229.9	11.1	0.19	
XP200	L	20	L	0.0811	H	0.0068	0.0060	0.0360	0.0196	0.0272	0.0147	0.0207	1334	152	4.80	0.00136	0.0131	12.9	67.2	18.6	0.41	
XP200	L	20	L	0.0706	L	0.0058	0.0124	0.0299	0.0199	0.0197	0.0157	0.0132	1105	51	2.94	0.00141	0.0114	40.4	413.9	23.3	0.45	1.
XP200	L	20	L	0.0820	L	0.0069	0.0078	0.0336	0.0196	0.0221	0.0146	0.0226	1333	99	4.30	0.00148	0.0126	8.3	53.4	17.4	0.41	
XP250	H	60	H	0.0884	H	0.0063	0.0095	0.0307	0.0200	0.0156	0.0160	0.0203	981	27	2.51	0.00108	0.0105	8.8	105.7	16.9	0.36	
XP250	H	60	H	0.0804	L	0.0055	0.0174	0.0264	0.0200	0.0142	0.0164	0.0139	903	35	2.55	0.00134	0.0116	17.2	275.3	2.4	0.30	
XP250	H	60	L	0.0732	H	0.0065	0.0137	0.0233	0.0200	0.0111	0.0160	0.0182	966	38	2.49	0.00153	0.0113	12.4	216.1	10.7	0.24	
XP250	H	60	L	0.0728	L	0.0043	0.0112	0.0259	0.0199	0.0125	0.0160	0.0152	992	51	2.36	0.00124	0.0111	7.2	136.4	12.0	0.21	
XP250	L	20	H	0.0804	H	0.0059	0.0122	0.0316	0.0198	0.0210	0.0152	0.0292	1191	83	3.79	0.00138	0.0124	45.5	201.0	24.8	0.63	2.
XP250	L	20	H	0.0724	L	0.0065	0.0137	0.0268	0.0198	0.0156	0.0153	0.0152	1138	76	3.44	0.00149	0.0124	21.2	213.0	12.1	0.28	
XP250	L	20	L	0.0623	H	0.0066	0.0114	0.0304	0.0196	0.0240	0.0146	0.0099	1358	131	4.66	0.00161	0.0132	23.2	231.8	12.2	0.31	
XP250	L	20	L	0.0684	L	0.0065	0.0098	0.0295	0.0195	0.0227	0.0144	0.0149	1394	148	4.51	0.00141	0.0131	10.4	120.0	12.4	0.25	

1. Condition excluded from some regressions as an outlier due to high solids and water recoveries.
2. Condition excluded from some regressions as an outlier due to high solids recovery and a high solids content.

Appendix B.

Regression analysis

B.1. Modelling solids recovery

This section contains the results from the regression analysis performed in section 4.1.6.

These regressions were used to determined the measured versus modelled relationship shown in figure 4.26, and correlations summarised in table 4.1.

Appendix B: Regression analysis

Table B.1.: Regression results relating the solids recovery rate to froth velocity in the copper rougher 1.

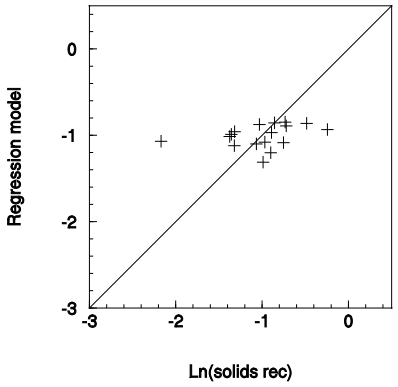

Ln(Solids recovery rate)	Ln(Velocity)
-1.36	-4.13
-0.891	-4.09
-0.734	-3.87
-1.32	-4.37
-0.72	-3.95
-2.17	-4.28
-0.968	-4.3
-0.483	-3.9
-0.855	-3.89
-1.38	-4.18
-1.07	-4.33
-0.752	-4.31
-1.03	-3.92
-1.32	-4.07
-0.988	-4.72
-0.244	-4.03
-0.899	-4.52

Multiple R	0.307
R^2	0.094
Standard Error	0.421
Adjusted R^2	0.0336
Observations	17

	df	SS	MS	F	Significance of F
Regression	1	0.276	0.276	1.56	0.231
Residual	15	2.66	0.177		
Total	16	2.94			

	Coefficients	Standard Error	t-Statistics	p-Value	
Intercept	1.28	1.83	0.695	0.501	49.9
Ln(velocity)	0.548	0.439	1.25	0.238	76.2

Table B.2.: Regression results relating the solids recovery rate to froth velocity and bubble size (p^{80}) in the copper rougher 1.

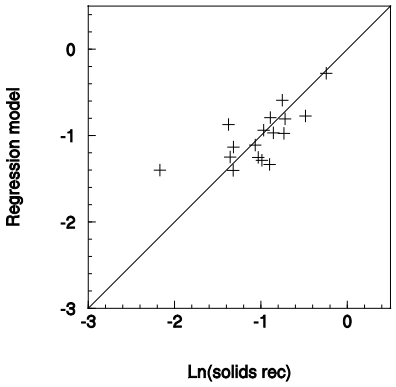

Ln(Solids recovery rate)	Ln(Velocity)	Ln(FS bubble size)
-1.36	-4.13	-3.29
-0.891	-4.09	-3.06
-0.734	-3.87	-3.18
-1.32	-4.37	-3.34
-0.72	-3.95	-3.08
-2.17	-4.28	-3.35
-0.968	-4.3	-3.11
-0.483	-3.9	-3.07
-0.855	-3.89	-3.18
-1.38	-4.18	-3.09
-1.07	-4.33	-3.2
-0.752	-4.31	-2.93
-1.03	-3.92	-3.32
-1.32	-4.07	-3.24
-0.988	-4.72	-3.24
-0.244	-4.03	-2.8
-0.899	-4.52	-3.29

Multiple R	0.717
R^2	0.515
Standard Error	0.319
Adjusted R^2	0.445
Observations	17

	df	SS	MS	F	Significance of F	
Regression	2	1.51	0.756	7.42	0.00634	++
Residual	14	1.43	0.102			
Total	16	2.94				

	Coefficients	Standard Error	t-Statistics	p-Value		
Intercept	6.04	1.95	3.1	0.0102	99.0	++
Ln(velocity)	0.237	0.345	0.688	0.506	49.4	
Ln(bubb size)	1.92	0.55	3.48	0.00512	99.5	++

Appendix B: Regression analysis

Table B.3.: Regression results relating the solids recovery rate to froth velocity, bubble size (p^{80}) and solids loading in the copper rougher 1.

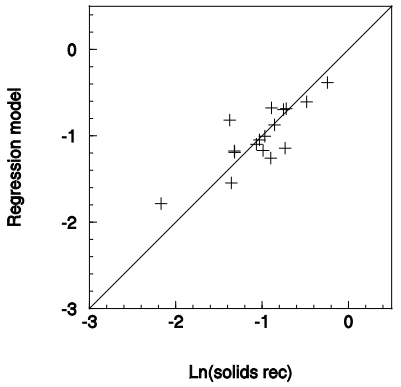

Ln(Solids recovery rate)	Ln(Velocity)	Ln(FS bubble size)	Ln(Solids loading (MV))
-1.36	-4.13	-3.29	-3.48
-0.891	-4.09	-3.06	-3.3
-0.734	-3.87	-3.18	-3.43
-1.32	-4.37	-3.34	-3.22
-0.72	-3.95	-3.08	-3.3
-2.17	-4.28	-3.35	-3.52
-0.968	-4.3	-3.11	-3.38
-0.483	-3.9	-3.07	-3.27
-0.855	-3.89	-3.18	-3.3
-1.38	-4.18	-3.09	-3.32
-1.07	-4.33	-3.2	-3.33
-0.752	-4.31	-2.93	-3.41
-1.03	-3.92	-3.32	-3.24
-1.32	-4.07	-3.24	-3.37
-0.988	-4.72	-3.24	-3.28
-0.244	-4.03	-2.8	-3.42
-0.899	-4.52	-3.29	-3.3

Multiple R	0.823
R^2	0.677
Standard Error	0.27
Adjusted R^2	0.602
Observations	17

	df	SS	MS	F	Significance of F	
Regression	3	1.99	0.663	9.08	0.00167	++
Residual	13	0.949	0.073			
Total	16	2.94				

	Coefficients	Standard Error	t-Statistics	p-Value		
Intercept	13.5	3.34	4.03	0.00199	99.8	++
Ln(velocity)	0.27	0.292	0.924	0.375	62.5	
Ln(bubb size)	2.03	0.468	4.35	0.00116	99.9	++
Ln(loading MV)	2.06	0.808	2.55	0.0268	97.3	++

Table B.4.: Regression results relating the solids recovery rate to froth velocity, bubble size (p^{80}) and solids loading in the copper rougher 1. (gravimetric solids loading used)

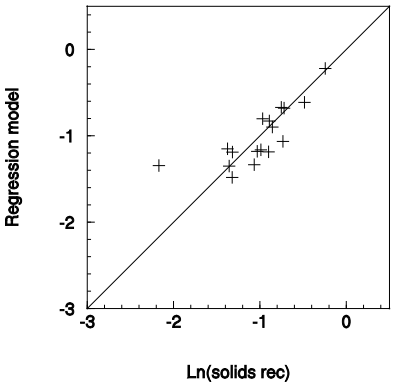

Ln(Solids recovery rate)	Ln(Velocity)	Ln(FS bubble size)	Ln(Solids loading (GV))
-1.36	-4.13	-3.29	-3.27
-0.891	-4.09	-3.06	-3.5
-0.734	-3.87	-3.18	-3.34
-1.32	-4.37	-3.34	-3.28
-0.72	-3.95	-3.08	-3.72
-2.17	-4.28	-3.35	-3.47
-0.968	-4.3	-3.11	-3.73
-0.483	-3.9	-3.07	-3.77
-0.855	-3.89	-3.18	-3.58
-1.38	-4.18	-3.09	-3.13
-1.07	-4.33	-3.2	-3.15
-0.752	-4.31	-2.93	-3.52
-1.03	-3.92	-3.32	-3.5
-1.32	-4.07	-3.24	-3.36
-0.988	-4.72	-3.24	-3.65
-0.244	-4.03	-2.8	-3.79
-0.899	-4.52	-3.29	-3.65

Multiple R	0.78
R^2	0.609
Standard Error	0.297
Adjusted R^2	0.519
Observations	17

	df	SS	MS	F	Significance of F	
Regression	3	1.79	0.596	6.75	0.00553	++
Residual	13	1.15	0.0884			
Total	16	2.94				

	Coefficients	Standard Error	t-Statistics	p-Value		
Intercept	2.49	2.7	0.922	0.376	62.4	
Ln(velocity)	0.262	0.321	0.815	0.432	56.8	
Ln(bubb size)	1.51	0.56	2.7	0.0207	97.9	++
Ln(loading GV)	-0.68	0.384	-1.77	0.104	89.6	-

Appendix B: Regression analysis

Table B.5.: Regression results relating the solids recovery rate to froth velocity in the copper rougher 3.

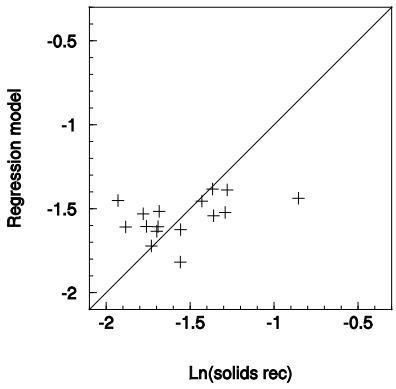

Ln(Solids recovery rate)	Ln(Velocity)
-1.43	-3.15
-1.76	-3.44
-1.78	-3.3
-1.28	-3.02
-1.7	-3.5
-1.93	-3.14
-1.73	-3.66
-1.29	-3.28
-1.37	-3.01
-1.68	-3.27
-1.56	-3.48
-0.855	-3.12
-1.69	-3.44
-1.88	-3.45
-1.56	-3.85
-1.36	-3.32

Multiple R	0.429
R^2	0.184
Standard Error	0.259
Adjusted R^2	0.125
Observations	16

	df	SS	MS	F	Significance of F	
Regression	1	0.212	0.212	3.15	0.0976	+
Residual	14	0.941	0.0672			
Total	15	1.15				

	Coefficients	Standard Error	t-Statistics	p-Value		
Intercept	0.178	0.977	0.182	0.859	14.1	
Ln(velocity)	0.519	0.292	1.78	0.104	89.6	+

Table B.6.: Regression results relating the solids recovery rate to froth velocity and bubble size (p^{80}) in the copper rougher 3.

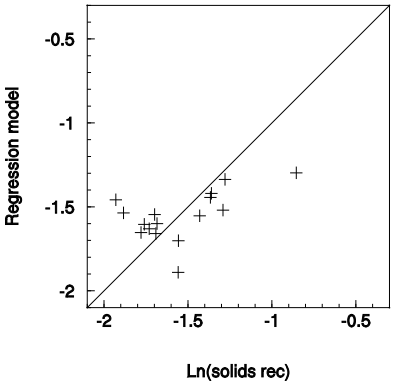

Ln(Solids recovery rate)	Ln(Velocity)	Ln(FS bubble size)
-1.43	-3.15	-3.36
-1.76	-3.44	-3.5
-1.78	-3.3	-3.3
-1.28	-3.02	-3.64
-1.7	-3.5	-3.65
-1.93	-3.14	-3.52
-1.73	-3.66	-3.64
-1.29	-3.28	-3.52
-1.37	-3.01	-3.44
-1.68	-3.27	-3.37
-1.56	-3.48	-3.36
-0.855	-3.12	-3.78
-1.69	-3.44	-3.41
-1.88	-3.45	-3.63
-1.56	-3.85	-3.33
-1.36	-3.32	-3.73

Multiple R	0.527
R^2	0.278
Standard Error	0.253
Adjusted R^2	0.166
Observations	16

	df	SS	MS	F	Significance of F	
Regression	2	0.32	0.16	2.5	0.121	+
Residual	13	0.833	0.0641			
Total	15	1.15				

	Coefficients	Standard Error	t-Statistics	p-Value		
Intercept	-2.0	1.93	-1.04	0.322	67.8	
Ln(velocity)	0.462	0.289	1.6	0.138	86.2	+
Ln(bubb size)	-0.565	0.435	-1.3	0.22	78.0	

Appendix B: Regression analysis

Table B.7.: Regression results relating the solids recovery rate to froth velocity, bubble size (p^{80}) and solids loading in the copper rougher 3.

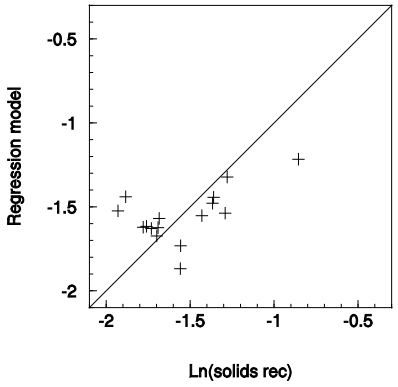

Ln(Solids recovery rate)	Ln(Velocity)	Ln(FS bubble size)	Ln(Solids loading (MV))
-1.43	-3.15	-3.36	-3.83
-1.76	-3.44	-3.5	-3.96
-1.78	-3.3	-3.3	-3.81
-1.28	-3.02	-3.64	-3.87
-1.7	-3.5	-3.65	-4.17
-1.93	-3.14	-3.52	-3.96
-1.73	-3.66	-3.64	-4.04
-1.29	-3.28	-3.52	-3.94
-1.37	-3.01	-3.44	-3.86
-1.68	-3.27	-3.37	-3.82
-1.56	-3.48	-3.36	-3.95
-0.855	-3.12	-3.78	-3.86
-1.69	-3.44	-3.41	-3.87
-1.88	-3.45	-3.63	-3.87
-1.56	-3.85	-3.33	-3.96
-1.36	-3.32	-3.73	-4.02

Multiple R	0.562
R^2	0.315
Standard Error	0.256
Adjusted R^2	0.144
Observations	16

	df	SS	MS	F	Significance of F	
Regression	3	0.363	0.121	1.84	0.193	+
Residual	12	0.789	0.0658			
Total	15	1.15				

	Coefficients	Standard Error	t-Statistics	p-Value		
Intercept	-0.383	2.78	-0.138	0.893	10.7	
Ln(velocity)	0.265	0.379	0.7	0.499	50.1	
Ln(bubb size)	-0.835	0.552	-1.51	0.158	84.2	-
Ln(loading MV)	0.82	1.01	0.813	0.433	56.7	

Table B.8.: Regression results relating the solids recovery rate to froth velocity, bubble size (p^{80}) and solids loading in the copper rougher 3. (gravimetric solids loading used)

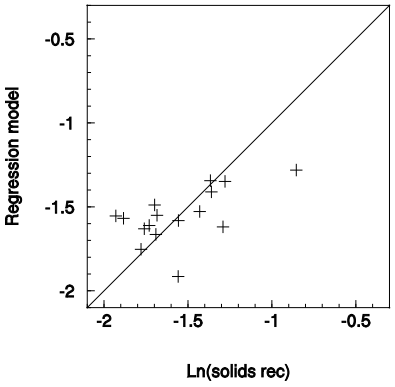

Ln(Solids recovery rate)	Ln(Velocity)	Ln(FS bubble size)	Ln(Solids loading (GV))
-1.43	-3.15	-3.36	-3.7
-1.76	-3.44	-3.5	-4.1
-1.78	-3.3	-3.3	-4.06
-1.28	-3.02	-3.64	-3.93
-1.7	-3.5	-3.65	-4.02
-1.93	-3.14	-3.52	-4.13
-1.73	-3.66	-3.64	-4.2
-1.29	-3.28	-3.52	-4.22
-1.37	-3.01	-3.44	-3.49
-1.68	-3.27	-3.37	-3.7
-1.56	-3.48	-3.36	-3.63
-0.855	-3.12	-3.78	-4.02
-1.69	-3.44	-3.41	-3.97
-1.88	-3.45	-3.63	-4.21
-1.56	-3.85	-3.33	-4.19
-1.36	-3.32	-3.73	-4.11

Multiple R	0.577
R^2	0.332
Standard Error	0.253
Adjusted R^2	0.165
Observations	16

	df	SS	MS	F	Significance of F	
Regression	3	0.383	0.128	1.99	0.169	+
Residual	12	0.769	0.0641			
Total	15	1.15				

	Coefficients	Standard Error	t-Statistics	p-Value		
Intercept	-2.17	1.93	-1.12	0.286	71.4	
Ln(velocity)	0.254	0.356	0.713	0.491	50.9	
Ln(bubb size)	-0.852	0.522	-1.63	0.131	86.9	-
Ln(loading GV)	0.383	0.386	0.993	0.342	65.8	

Appendix B: Regression analysis

Table B.9.: Regression results relating the solids recovery rate to froth velocity in the platinum rougher 1.

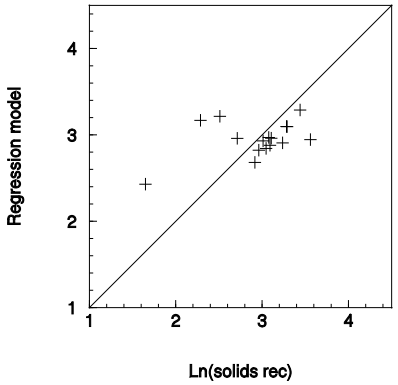

Ln(Solids recovery rate)	Ln(Velocity)
2.29	-4.04
2.51	-3.94
3.24	-4.56
2.92	-5.02
2.96	-4.73
2.71	-4.45
3.09	-4.62
3.11	-4.45
1.65	-5.53
3.01	-4.51
3.29	-4.18
3.28	-4.18
3.05	-4.69
3.44	-3.8
3.08	-4.44
3.56	-4.49

Multiple R	0.44
R^2	0.194
Standard Error	0.441
Adjusted R^2	0.136
Observations	16

	df	SS	MS	F	Significance of F	
Regression	1	0.654	0.654	3.36	0.0881	+
Residual	14	2.72	0.195			
Total	15	3.38				

	Coefficients	Standard Error	t-Statistics	p-Value		
Intercept	5.17	1.22	4.25	0.00137	99.9	++
Ln(velocity)	0.497	0.271	1.83	0.0939	90.6	+

Table B.10.: Regression results relating the solids recovery rate to froth velocity and bubble size (p^{80}) in the platinum rougher 1.

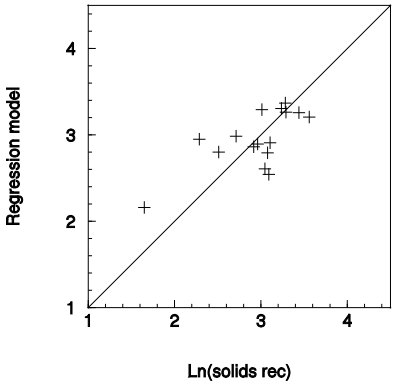

Ln(Solids recovery rate)	Ln(Velocity)	Ln(FS bubble size)
2.29	-4.04	-4.12
2.51	-3.94	-3.94
3.24	-4.56	-4.64
2.92	-5.02	-4.25
2.96	-4.73	-4.22
2.71	-4.45	-4.26
3.09	-4.62	-3.81
3.11	-4.45	-4.18
1.65	-5.53	-3.59
3.01	-4.51	-4.61
3.29	-4.18	-4.5
3.28	-4.18	-4.62
3.05	-4.69	-3.9
3.44	-3.8	-4.41
3.08	-4.44	-4.04
3.56	-4.49	-4.51

Multiple R	0.698
R^2	0.488
Standard Error	0.365
Adjusted R^2	0.409
Observations	16

	df	SS	MS	F	Significance of F	
Regression	2	1.65	0.823	6.18	0.013	++
Residual	13	1.73	0.133			
Total	15	3.38				

	Coefficients	Standard Error	t-Statistics	p-Value		
Intercept	0.072	2.12	0.0339	0.974	2.65	
Ln(velocity)	0.209	0.248	0.844	0.417	58.3	
Ln(bubb size)	-0.902	0.33	-2.73	0.0195	98.0	- -

Appendix B: Regression analysis

Table B.11.: Regression results relating the solids recovery rate to froth velocity, bubble size (p^{80}) and solids loading in the platinum rougher 1.

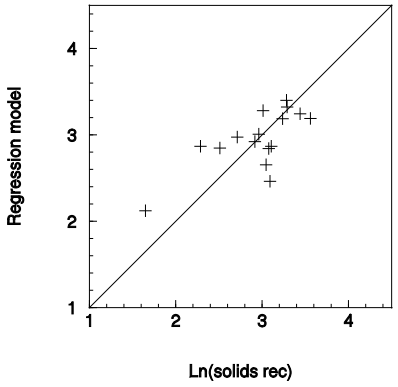

Ln(Solids recovery rate)	Ln(Velocity)	Ln(FS bubble size)	Ln(Solids loading (MV))
2.29	-4.04	-4.12	-2.58
2.51	-3.94	-3.94	-2.59
3.24	-4.56	-4.64	-2.64
2.92	-5.02	-4.25	-2.63
2.96	-4.73	-4.22	-2.64
2.71	-4.45	-4.26	-2.62
3.09	-4.62	-3.81	-2.53
3.11	-4.45	-4.18	-2.6
1.65	-5.53	-3.59	-2.51
3.01	-4.51	-4.61	-2.66
3.29	-4.18	-4.5	-2.67
3.28	-4.18	-4.62	-2.68
3.05	-4.69	-3.9	-2.58
3.44	-3.8	-4.41	-2.64
3.08	-4.44	-4.04	-2.6
3.56	-4.49	-4.51	-2.65

Multiple R	0.711
R^2	0.505
Standard Error	0.373
Adjusted R^2	0.381
Observations	16

	df	SS	MS	F	Significance of F	
Regression	3	1.71	0.568	4.08	0.0327	++
Residual	12	1.67	0.139			
Total	15	3.38				

	Coefficients	Standard Error	t-Statistics	p-Value	
Intercept	-7.24	11.5	-0.63	0.542	45.8
Ln(velocity)	0.192	0.255	0.753	0.468	53.2
Ln(bubb size)	-0.418	0.821	-0.509	0.621	37.9
Ln(loading MV)	-3.55	5.48	-0.648	0.531	46.9

Table B.12.: Regression results relating the solids recovery rate to froth velocity, bubble size (p^{80}) and solids loading in the platinum rougher 1. (gravimetric solids loading used)

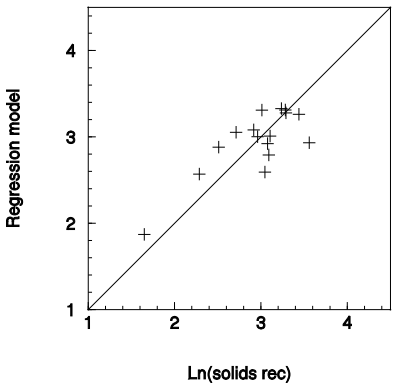

Ln(Solids recovery rate)	Ln(Velocity)	Ln(FS bubble size)	Ln(Solids loading (GV))
2.29	-4.04	-4.12	-3.32
2.51	-3.94	-3.94	-2.59
3.24	-4.56	-4.64	-2.71
2.92	-5.02	-4.25	-2.56
2.96	-4.73	-4.22	-2.67
2.71	-4.45	-4.26	-2.67
3.09	-4.62	-3.81	-2.49
3.11	-4.45	-4.18	-2.63
1.65	-5.53	-3.59	-3.58
3.01	-4.51	-4.61	-2.71
3.29	-4.18	-4.5	-2.66
3.28	-4.18	-4.62	-2.75
3.05	-4.69	-3.9	-2.91
3.44	-3.8	-4.41	-2.6
3.08	-4.44	-4.04	-2.6
3.56	-4.49	-4.51	-3.19

Multiple R	0.791
R^2	0.625
Standard Error	0.325
Adjusted R^2	0.532
Observations	16

	df	SS	MS	F	Significance of F	
Regression	3	2.11	0.704	6.68	0.00667	++
Residual	12	1.27	0.105			
Total	15	3.38				

	Coefficients	Standard Error	t-Statistics	p-Value		
Intercept	1.6	2.02	0.791	0.446	55.4	
Ln(velocity)	0.0701	0.23	0.304	0.767	23.3	
Ln(bubb size)	-0.806	0.298	-2.71	0.0203	98.0	- -
Ln(loading GV)	0.625	0.298	2.1	0.0594	94.1	+

Table B.13.: Regression results relating the solids recovery rate to froth velocity in the platinum rougher 3.

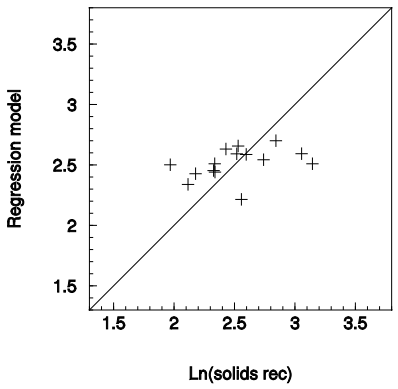

Ln(Solids recovery rate)	Ln(Velocity)
2.43	-4.2
2.53	-4.15
2.33	-4.6
2.34	-4.47
2.74	-4.4
2.6	-4.3
2.56	-5.12
2.12	-4.85
2.18	-4.65
2.84	-4.05
2.52	-4.29
1.97	-4.49
3.06	-4.29
3.15	-4.47
2.34	-4.62

Multiple R	0.382
R^2	0.146
Standard Error	0.317
Adjusted R^2	0.0806
Observations	15

	df	SS	MS	F	Significance of F	
Regression	1	0.224	0.224	2.23	0.159	+
Residual	13	1.31	0.101			
Total	14	1.53				

	Coefficients	Standard Error	t-Statistics	p-Value		
Intercept	4.54	1.36	3.33	0.00669	99.3	++
Ln(velocity)	0.455	0.305	1.49	0.164	83.6	+

Table B.14.: Regression results relating the solids recovery rate to froth velocity and bubble size (p^{80}) in the platinum rougher 3.

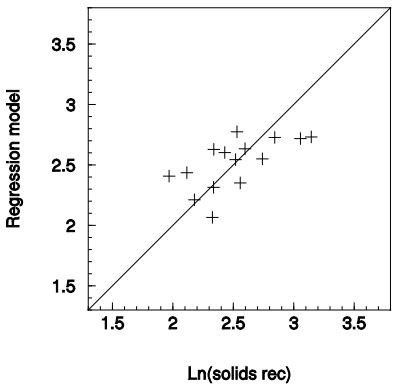

Ln(Solids recovery rate)	Ln(Velocity)	Ln(FS bubble size)
2.43	-4.2	-4.48
2.53	-4.15	-4.4
2.33	-4.6	-4.65
2.34	-4.47	-4.55
2.74	-4.4	-4.45
2.6	-4.3	-4.43
2.56	-5.12	-4.33
2.12	-4.85	-4.37
2.18	-4.65	-4.55
2.84	-4.05	-4.46
2.52	-4.29	-4.48
1.97	-4.49	-4.5
3.06	-4.29	-4.39
3.15	-4.47	-4.33
2.34	-4.62	-4.34

Multiple R	0.634
R^2	0.402
Standard Error	0.276
Adjusted R^2	0.302
Observations	15

	df	SS	MS	F	Significance of F	
Regression	2	0.616	0.308	4.03	0.0459	++
Residual	12	0.917	0.0764			
Total	14	1.53				

	Coefficients	Standard Error	t-Statistics	p-Value		
Intercept	13.3	4.03	3.29	0.00721	99.3	++
Ln(velocity)	0.571	0.271	2.11	0.0585	94.2	+
Ln(bubb size)	1.84	0.815	2.26	0.0448	95.5	++

Appendix B: Regression analysis

Table B.15.: Regression results relating the solids recovery rate to froth velocity, bubble size (p^{80}) and solids loading in the platinum rougher 3.

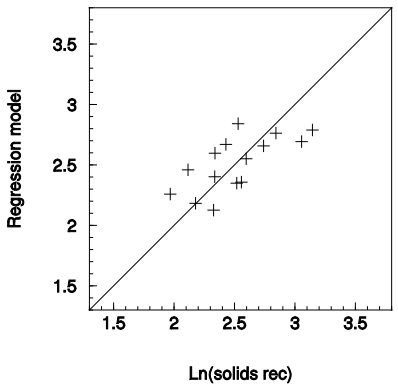

Ln(Solids recovery rate)	Ln(Velocity)	Ln(FS bubble size)	Ln(Solids loading (MV))
2.43	-4.2	-4.48	-3.55
2.53	-4.15	-4.4	-3.58
2.33	-4.6	-4.65	-3.41
2.34	-4.47	-4.55	-3.44
2.74	-4.4	-4.45	-3.46
2.6	-4.3	-4.43	-3.66
2.56	-5.12	-4.33	-3.32
2.12	-4.85	-4.37	-3.39
2.18	-4.65	-4.55	-3.48
2.84	-4.05	-4.46	-3.63
2.52	-4.29	-4.48	-3.76
1.97	-4.49	-4.5	-3.65
3.06	-4.29	-4.39	-3.62
3.15	-4.47	-4.33	-3.49
2.34	-4.62	-4.34	-3.52

Multiple R	0.686
R^2	0.471
Standard Error	0.271
Adjusted R^2	0.327
Observations	15

	df	SS	MS	F	Significance of F	
Regression	3	0.722	0.241	3.27	0.063	+
Residual	11	0.811	0.0737			
Total	14	1.53				

	Coefficients	Standard Error	t-Statistics	p-Value		
Intercept	19.4	6.47	3.0	0.012	98.8	++
Ln(velocity)	0.935	0.403	2.32	0.0405	96.0	++
Ln(bubb size)	1.98	0.808	2.45	0.0324	96.8	++
Ln(loading MV)	1.11	0.924	1.2	0.255	74.5	

Table B.16.: Regression results relating the solids recovery rate to froth velocity, bubble size (p^{80}) and solids loading in the platinum rougher 3. (gravimetric solids loading used)

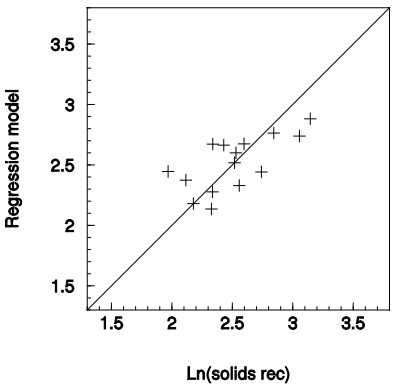

Ln(Solids recovery rate)	Ln(Velocity)	Ln(FS bubble size)	Ln(Solids loading (GV))
2.43	-4.2	-4.48	-4.33
2.53	-4.15	-4.4	-3.53
2.33	-4.6	-4.65	-4.25
2.34	-4.47	-4.55	-3.91
2.74	-4.4	-4.45	-3.7
2.6	-4.3	-4.43	-4.25
2.56	-5.12	-4.33	-3.88
2.12	-4.85	-4.37	-3.79
2.18	-4.65	-4.55	-3.9
2.84	-4.05	-4.46	-4.28
2.52	-4.29	-4.48	-4.0
1.97	-4.49	-4.5	-4.19
3.06	-4.29	-4.39	-4.18
3.15	-4.47	-4.33	-4.61
2.34	-4.62	-4.34	-4.21

Multiple R	0.677
R^2	0.459
Standard Error	0.275
Adjusted R^2	0.311
Observations	15

	df	SS	MS	F	Significance of F	
Regression	3	0.703	0.234	3.11	0.0709	+
Residual	11	0.83	0.0754			
Total	14	1.53				

	Coefficients	Standard Error	t-Statistics	p-Value		
Intercept	11.6	4.29	2.71	0.0203	98.0	++
Ln(velocity)	0.513	0.274	1.87	0.0881	91.2	+
Ln(bubb size)	1.79	0.811	2.21	0.0492	95.1	++
Ln(loading GV)	-0.285	0.265	-1.08	0.305	69.5	

B.2. Modelling air loss on the froth surface

This section contains the results from the regression analysis performed in section 4.2.4.

These regressions were used to determine the measured versus modelled relationship shown in figure 4.39.

Table B.17.: Regression results relating the measured air loss on the froth surface to the burst rate and bubble size (p^{80}) on the froth surface in the copper rougher 1.

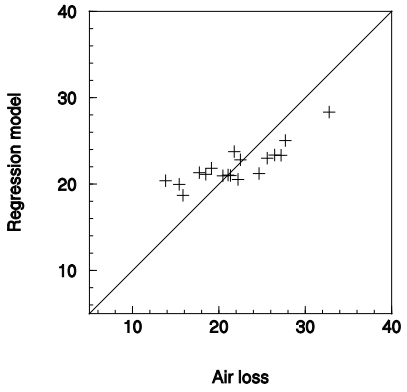

Air loss $m^3/m^2/s$	Burst rate $1/m^2/s$	FS bubble size (p^{80}) m
15.4	32.5	0.0372
22.5	21.2	0.047
13.8	20.6	0.0415
24.6	49.3	0.0353
27.2	29.7	0.0458
15.8	29.8	0.035
26.5	34.0	0.0446
21.8	31.3	0.0463
19.1	31.5	0.0418
25.6	28.1	0.0455
17.7	30.3	0.041
27.7	16.4	0.0535
21.3	44.4	0.0362
21.1	34.2	0.0392
18.5	34.8	0.0392
22.2	81.6	0.0246
32.8	17.4	0.0609
20.5	40.2	0.0373

Multiple R^2	0.825
Adjusted multiple R^2	0.802
R^2	0.981
Adjusted R^2	0.979
Standard Error	3.32
Observations	18

	df	SS	MS	F	Significance of F	
Regression	2	8860.0	4430.0	403.0	2.07e-14	++
Residual	16	176.0	11.0			
Total	18	9040.0				

	Coefficients	Standard Error	t-Statistics	p-Value		
Intercept	0					
Burst rate large	0.122	0.0403	3.03	0.0115	98.9	++
FS Bubble size p80	430.0	34.8	12.4	8.44e-08	100.0	++

Table B.18.: Regression results relating the measured air loss on the froth surface to the burst rate and bubble size (p^{80}) on the froth surface in the copper rougher 3.

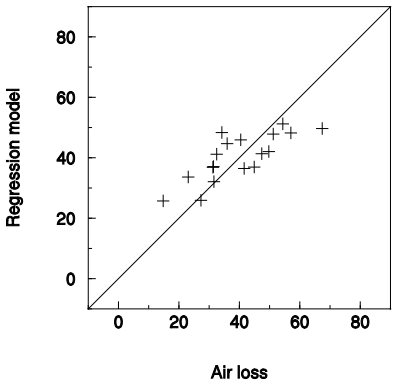

Air loss $m^3/m^2/s$	Burst rate $1/m^2/s$	FS bubble size (p^{80}) m
34.2	18.1	0.0348
49.8	35.4	0.0301
54.4	20.9	0.0369
31.3	28.6	0.0264
41.6	43.6	0.0259
14.8	45.9	0.0181
47.4	31.7	0.0296
44.9	43.0	0.0262
32.5	26.5	0.0295
36.0	22.2	0.0321
51.2	24.8	0.0344
57.1	25.4	0.0347
31.6	41.2	0.0228
40.5	22.1	0.033
31.4	32.9	0.0265
27.3	42.7	0.0183
67.4	30.1	0.0357
23.1	33.0	0.024

Multiple R^2	0.884
Adjusted multiple R^2	0.868
R^2	0.959
Adjusted R^2	0.957
Standard Error	8.93
Observations	18

	df	SS	MS	F	Significance of F	
Regression	2	30200.0	15100.0	189.0	7.28e-12	++
Residual	16	1280.0	79.8			
Total	18	31500.0				

	Coefficients	Standard Error	t-Statistics	p-Value		
Intercept	0					
Burst rate large	0.0177	0.152	0.116	0.91	9.03	
FS Bubble size p80	1380.0	170.0	8.12	5.69e-06	100.0	++

Appendix B: Regression analysis

Table B.19.: Regression results relating the measured air loss on the froth surface to the burst rate and bubble size (p^{80}) on the froth surface in the platinum rougher 1.

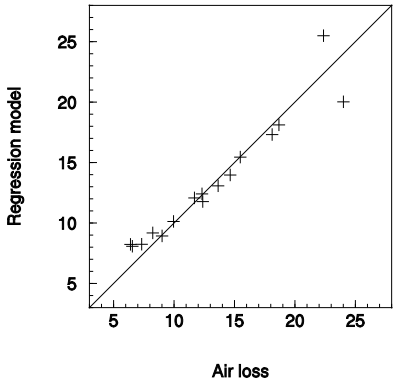

Air loss $m^3/m^2/s$	Burst rate $1/m^2/s$	FS bubble size (p^{80}) m
14.7	467.0	0.0162
18.1	390.0	0.0195
6.56	373.0	0.00966
11.7	474.0	0.0142
12.3	503.0	0.0146
12.4	554.0	0.0141
24.0	337.0	0.0222
13.6	508.0	0.0154
22.4	182.0	0.0275
7.32	396.0	0.00991
8.24	447.0	0.0111
6.4	377.0	0.00985
18.7	387.0	0.0203
9.97	483.0	0.0122
15.5	404.0	0.0176
9.01	510.0	0.011

Multiple R^2	0.948
Adjusted multiple R^2	0.94
R^2	0.989
Adjusted R^2	0.988
Standard Error	1.59
Observations	16

	df	SS	MS	F	Significance of F	
Regression	2	3190.0	1590.0	630.0	1.93e-14	++
Residual	14	35.4	2.53			
Total	16	3220.0				

	Coefficients	Standard Error	t-Statistics	p-Value		
Intercept	0					
Burst rate large	-0.00283	0.00207	-1.37	0.198	80.2	-
FS Bubble size p80	944.0	55.6	17.0	3.08e-09	100.0	++

Table B.20.: Regression results relating the measured air loss on the froth surface to the burst rate and bubble size (p^{80}) on the froth surface in the platinum rougher 3.

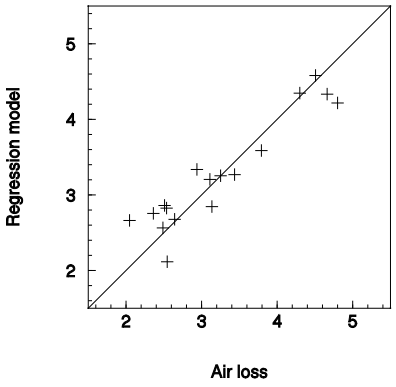

Air loss $m^3/m^2/s$	Burst rate $l/m^2/s$	FS bubble size (p^{80}) m
2.64	988.0	0.0113
3.14	1060.0	0.0122
2.05	902.0	0.00956
2.54	976.0	0.0105
3.25	1100.0	0.0117
3.11	1100.0	0.0119
4.8	1330.0	0.0131
2.94	1100.0	0.0114
4.3	1330.0	0.0126
2.51	981.0	0.0105
2.55	903.0	0.0116
2.49	966.0	0.0113
2.36	992.0	0.0111
3.79	1190.0	0.0124
3.44	1140.0	0.0124
4.66	1360.0	0.0132
4.51	1390.0	0.0131

Multiple R^2	0.969
Adjusted multiple R^2	0.965
R^2	0.991
Adjusted R^2	0.99
Standard Error	0.337
Observations	17

	df	SS	MS	F	Significance of F	
Regression	2	189.0	94.5	832.0	4.31e-16	++
Residual	15	1.7	0.114			
Total	17	191.0				

	Coefficients	Standard Error	t-Statistics	p-Value		
Intercept	0					
Burst rate large	0.00587	0.000919	6.39	5.17e-05	100.0	++
FS Bubble size p80	-275.0	87.1	-3.16	0.00903	99.1	- -

B.3. Operating variable effect on froth stability and flotation performance factors

This section contains the results from the regression analysis performed in section 5.4.2.

These regressions were used to determine the direction and significance of the relationship between operating variables and measured froth stability and flotation performance factors. These results have been summarised in tables 5.2 and 5.3.

Table B.21.: Regression results relating the machine vision solids loading measurement to the operating variables in the copper rougher 1.

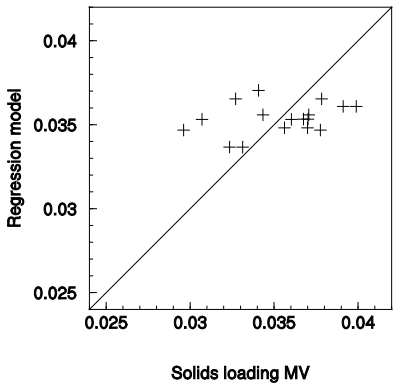

Solids loading (MV) kg/m^2	Air rate m^3/m^2/s	Froth height m	Frother concentration ppm
0.0307	0.0103	0.155	102
0.037	0.0103	0.2	100
0.0324	0.0103	0.2	138
0.0399	0.011	0.155	102
0.0371	0.011	0.2	100
0.0296	0.011	0.2	130
0.0341	0.0117	0.155	100
0.0378	0.0117	0.2	98
0.0368	0.0117	0.2	138
0.036	0.0103	0.155	102
0.0356	0.0103	0.2	100
0.0331	0.0103	0.2	138
0.0391	0.011	0.155	102
0.0343	0.011	0.2	100
0.0378	0.011	0.2	130
0.0327	0.0117	0.2	98
0.037	0.0117	0.2	138

Multiple R	0.322
R^2	0.103
Standard Error	0.00306
Adjusted R^2	-0.104
Observations	17

	df	SS	MS	F	Significance of F
Regression	3	1.4e-05	4.68e-06	0.5	0.689
Residual	13	0.000122	9.37e-06		
Total	16	0.000136			

	Coefficients	Standard Error	t-Statistics	p-Value		
Intercept	0.0284	0.0153	1.85	0.0912	90.9	+
Air rate	1.16	1.3	0.892	0.391	60.9	
Froth height	-0.0125	0.0403	-0.311	0.762	23.8	
Frother concentration	-3.02e-05	4.85e-05	-0.622	0.547	45.3	

Table B.22.: Regression results relating the machine vision solids loading measurement to the operating variables in the copper rougher 3.

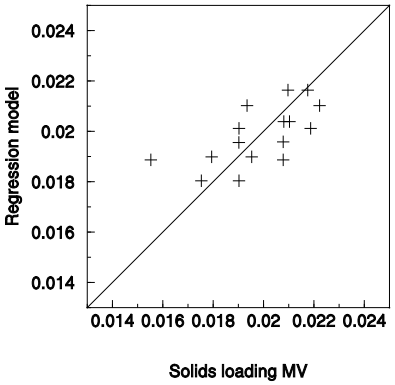

Solids loading (MV) kg/m^2	Air rate m^3/m^2/s	Froth height m	Frother concentration ppm
0.0218	0.0126	0.155	102
0.019	0.0126	0.2	100
0.0222	0.0126	0.2	138
0.0208	0.0148	0.155	102
0.0155	0.0148	0.2	100
0.019	0.0161	0.155	100
0.0175	0.0161	0.2	98
0.0195	0.0161	0.2	138
0.021	0.0126	0.155	102
0.0219	0.0126	0.2	100
0.0193	0.0126	0.2	138
0.021	0.0148	0.155	102
0.0208	0.0148	0.2	100
0.0208	0.0148	0.2	130
0.019	0.0161	0.2	98
0.0179	0.0161	0.2	138

Multiple R	0.641
R^2	0.41
Standard Error	0.00155
Adjusted R^2	0.263
Observations	16

	df	SS	MS	F	Significance of F	
Regression	3	2e-05	6.67e-06	2.79	0.0864	+
Residual	12	2.87e-05	2.4e-06			
Total	15	4.88e-05				

	Coefficients	Standard Error	t-Statistics	p-Value		
Intercept	0.0317	0.00515	6.15	7.16e-05	100.0	++
Air rate	-0.585	0.267	-2.19	0.0507	94.9	-
Froth height	-0.0327	0.0204	-1.61	0.136	86.4	-
Frother concentration	2.38e-05	2.51e-05	0.946	0.364	63.6	

Table B.23.: Regression results relating the machine vision solids loading measurement to the operating variables in the platinum rougher 1.

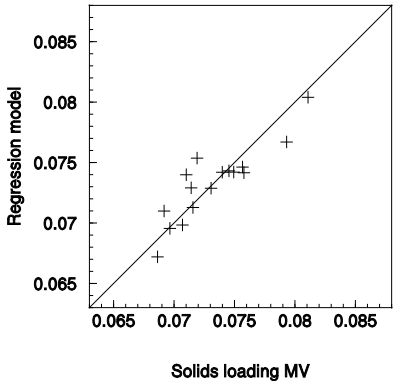

Solids loading (MV) kg/m^2	Air rate m^3/m^2/s	Froth height m	Frother concentration ppm	Frother type	Activator presence
0.0758	0.00592	0.0984	60	1	0
0.0749	0.00569	0.0643	60	1	2
0.0716	0.00491	0.0537	60	1	0
0.0719	0.00612	0.0763	40	1	1
0.071	0.00753	0.085	40	1	1
0.0731	0.00761	0.0753	40	1	1
0.0793	0.0064	0.0567	20	1	2
0.0745	0.00589	0.0558	20	1	0
0.0811	0.00787	0.161	60	1	2
0.0697	0.00733	0.114	60	2	0
0.0692	0.00538	0.0662	60	2	2
0.0686	0.00575	0.0656	60	2	0
0.0757	0.00868	0.111	20	2	2
0.0714	0.00651	0.0908	20	2	0
0.074	0.00527	0.0527	20	2	2
0.0707	0.00582	0.0493	20	2	0

Multiple R	0.883
R^2	0.78
Standard Error	0.00202
Adjusted R^2	0.669
Observations	16

	df	SS	MS	F	Significance of F	
Regression	5	0.000145	2.9e-05	7.08	0.0045	++
Residual	10	4.09e-05	4.09e-06			
Total	15	0.000186				

	Coefficients	Standard Error	t-Statistics	p-Value		
Intercept	0.0843	0.00508	16.6	3.92e-09	100.0	++
Air rate	-1.61	0.87	-1.85	0.0916	90.8	-
Froth height	0.101	0.0323	3.12	0.00982	99.0	++
Frother concentration	-0.00011	3.67e-05	-2.99	0.0122	98.8	- -
Frother type	-0.00393	0.00105	-3.73	0.00334	99.7	- -
Activator presence	0.00156	0.000582	2.68	0.0213	97.9	++

Table B.24.: Regression results relating the machine vision solids loading measurement to the operating variables in the platinum rougher 3.

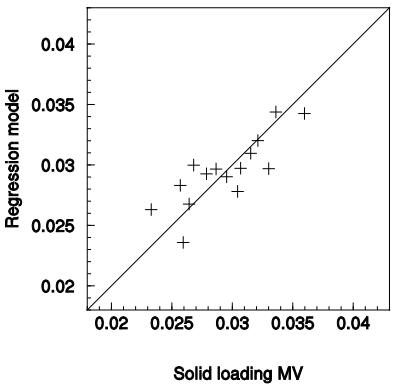

Solids loading (MV) kg/m^2	Air rate m^3/m^2/s	Froth height m	Frother concentration ppm	Frother type	Activator presence
0.0287	0.00646	0.0808	60	1	0
0.0279	0.00594	0.0808	60	1	2
0.033	0.00678	0.0794	60	1	0
0.0321	0.00677	0.0805	40	1	1
0.0315	0.00585	0.0804	40	1	1
0.0257	0.00523	0.072	40	1	1
0.036	0.00678	0.0811	20	1	2
0.0336	0.00686	0.082	20	1	0
0.0307	0.00631	0.0884	60	2	2
0.0264	0.00553	0.0804	60	2	0
0.0233	0.00646	0.0732	60	2	2
0.0259	0.0043	0.0728	60	2	0
0.0268	0.00654	0.0724	20	2	0
0.0304	0.00657	0.0623	20	2	2
0.0295	0.00653	0.0684	20	2	0

Multiple R	0.813
R^2	0.661
Standard Error	0.00253
Adjusted R^2	0.473
Observations	15

	df	SS	MS	F	Significance of F	
Regression	5	0.000112	2.25e-05	3.51	0.0489	++
Residual	9	5.76e-05	6.4e-06			
Total	14	0.00017				

	Coefficients	Standard Error	t-Statistics	p-Value		
Intercept	0.0111	0.0116	0.952	0.362	63.8	
Air rate	1.12	1.15	0.972	0.352	64.8	
Froth height	0.236	0.136	1.73	0.111	88.9	+
Frother concentration	-9.92e-05	4.92e-05	-2.02	0.0685	93.1	-
Frother type	-0.00177	0.0015	-1.18	0.264	73.6	
Activator presence	9.33e-05	0.000752	0.124	0.903	9.65	

Appendix B: Regression analysis

Table B.25.: Regression results relating the machine vision solids loading measurement on the large bubbles to the operating variables in the copper rougher 1.

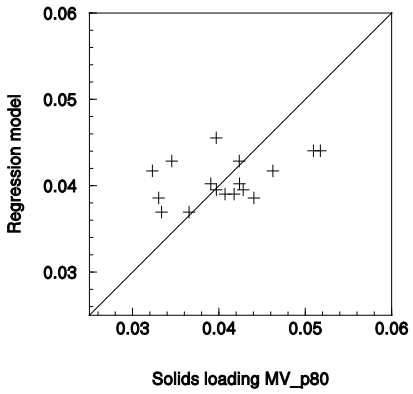

Solids loading MV_{p80} kg/m^2	Air rate m^3/m^2/s	Froth height m	Frother concentration ppm
0.0345	0.0103	0.155	102
0.0418	0.0103	0.2	100
0.0365	0.0103	0.2	138
0.051	0.011	0.155	102
0.0424	0.011	0.2	100
0.033	0.011	0.2	130
0.0397	0.0117	0.155	100
0.0463	0.0117	0.2	98
0.0397	0.0117	0.2	138
0.0424	0.0103	0.155	102
0.0407	0.0103	0.2	100
0.0334	0.0103	0.2	138
0.0518	0.011	0.155	102
0.0391	0.011	0.2	100
0.0441	0.011	0.2	130
0.0323	0.0117	0.2	98
0.0428	0.0117	0.2	138

Multiple R	0.443
R^2	0.197
Standard Error	0.00569
Adjusted R^2	0.0113
Observations	17

	df	SS	MS	F	Significance of F
Regression	3	0.000103	3.44e-05	1.06	0.399
Residual	13	0.000421	3.24e-05		
Total	16	0.000524			

	Coefficients	Standard Error	t-Statistics	p-Value		
Intercept	0.0434	0.0285	1.52	0.156	84.4	+
Air rate	1.8	2.42	0.743	0.473	52.7	
Froth height	-0.0873	0.0749	-1.17	0.268	73.2	
Frother concentration	-5.48e-05	9.02e-05	-0.608	0.556	44.4	

Table B.26.: Regression results relating the machine vision solids loading measurement on the large bubbles to the operating variables in the copper rougher 3.

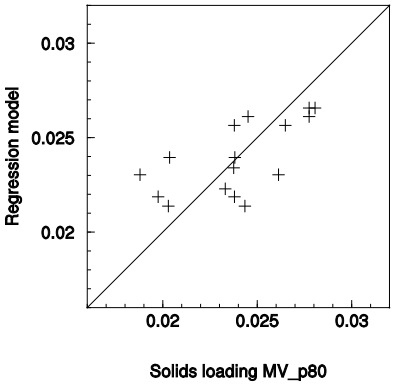

Solids loading MV_{p80} kg/m^2	Air rate $m^3/m^2/s$	Froth height m	Frother concentration ppm
0.0281	0.0126	0.155	102
0.0238	0.0126	0.2	100
0.0277	0.0126	0.2	138
0.0238	0.0148	0.155	102
0.0188	0.0148	0.2	100
0.0233	0.0161	0.155	100
0.0203	0.0161	0.2	98
0.0238	0.0161	0.2	138
0.0277	0.0126	0.155	102
0.0265	0.0126	0.2	100
0.0245	0.0126	0.2	138
0.0204	0.0148	0.155	102
0.0261	0.0148	0.2	100
0.0238	0.0148	0.2	130
0.0243	0.0161	0.2	98
0.0198	0.0161	0.2	138

Multiple R	0.658
R^2	0.433
Standard Error	0.00246
Adjusted R^2	0.291
Observations	16

	df	SS	MS	F	Significance of F	
Regression	3	5.55e-05	1.85e-05	3.05	0.0699	+
Residual	12	7.27e-05	6.06e-06			
Total	15	0.000128				

	Coefficients	Standard Error	t-Statistics	p-Value		
Intercept	0.0438	0.00819	5.35	0.000233	100.0	++
Air rate	-1.22	0.424	-2.88	0.015	98.5	- -
Froth height	-0.0198	0.0324	-0.611	0.553	44.7	
Frother concentration	1.23e-05	4e-05	0.307	0.764	23.6	

Appendix B: Regression analysis

Table B.27.: Regression results relating the machine vision solids loading measurement on the large bubbles to the operating variables in the platinum rougher 1.

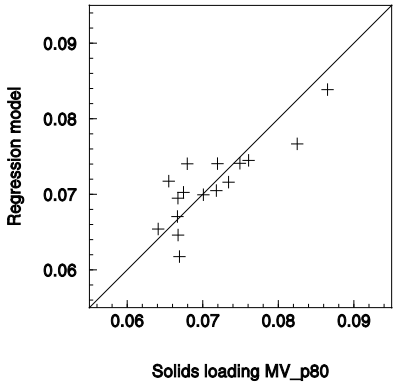

Solids loading MV_{p80} kg/m^2	Air rate m^3/m^2/s	Froth height m	Frother concentration ppm	Frother type	Activator presence
0.0734	0.00592	0.0984	60	1	0
0.0749	0.00569	0.0643	60	1	2
0.0667	0.00491	0.0537	60	1	0
0.068	0.00612	0.0763	40	1	1
0.0655	0.00753	0.085	40	1	1
0.0701	0.00761	0.0753	40	1	1
0.0825	0.0064	0.0567	20	1	2
0.0718	0.00589	0.0558	20	1	0
0.0865	0.00787	0.161	60	1	2
0.0641	0.00733	0.114	60	2	0
0.0675	0.00538	0.0662	60	2	2
0.0669	0.00575	0.0656	60	2	0
0.0761	0.00868	0.111	20	2	2
0.0667	0.00651	0.0908	20	2	0
0.072	0.00527	0.0527	20	2	2
0.0667	0.00582	0.0493	20	2	0

Multiple R	0.837
R^2	0.7
Standard Error	0.00422
Adjusted R^2	0.55
Observations	16

	df	SS	MS	F	Significance of F	
Regression	5	0.000415	8.31e-05	4.66	0.0186	++
Residual	10	0.000178	1.78e-05			
Total	15	0.000594				

	Coefficients	Standard Error	t-Statistics	p-Value		
Intercept	0.0849	0.0106	8.01	6.44e-06	100.0	++
Air rate	-2.64	1.81	-1.46	0.173	82.7	-
Froth height	0.161	0.0673	2.39	0.0358	96.4	++
Frother concentration	-0.000142	7.66e-05	-1.85	0.0909	90.9	-
Frother type	-0.005	0.0022	-2.27	0.044	95.6	- -
Activator presence	0.0037	0.00121	3.05	0.011	98.9	++

Table B.28.: Regression results relating the machine vision solids loading measurement on the large bubbles to the operating variables in the platinum rougher 3.

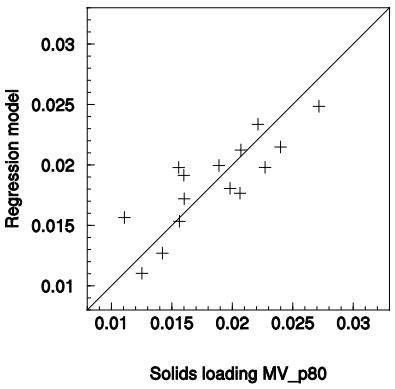

Solids loading MV_{p80} kg/m^2	Air rate m^3/m^2/s	Froth height m	Frother concentration ppm	Frother type	Activator presence
0.016	0.00646	0.0808	60	1	0
0.0198	0.00594	0.0808	60	1	2
0.0206	0.00678	0.0794	60	1	0
0.0207	0.00677	0.0805	40	1	1
0.0189	0.00585	0.0804	40	1	1
0.016	0.00523	0.072	40	1	1
0.0272	0.00678	0.0811	20	1	2
0.0221	0.00686	0.082	20	1	0
0.0156	0.00631	0.0884	60	2	2
0.0142	0.00553	0.0804	60	2	0
0.0111	0.00646	0.0732	60	2	2
0.0125	0.0043	0.0728	60	2	0
0.0156	0.00654	0.0724	20	2	0
0.024	0.00657	0.0623	20	2	2
0.0227	0.00653	0.0684	20	2	0

Multiple R	0.828
R^2	0.686
Standard Error	0.00316
Adjusted R^2	0.512
Observations	15

	df	SS	MS	F	Significance of F	
Regression	5	0.000196	3.92e-05	3.93	0.0361	++
Residual	9	8.97e-05	9.97e-06			
Total	14	0.000286				

	Coefficients	Standard Error	t-Statistics	p-Value		
Intercept	0.0203	0.0145	1.4	0.189	81.1	+
Air rate	1.4	1.44	0.973	0.351	64.9	
Froth height	-0.00693	0.17	-0.0407	0.968	3.18	
Frother concentration	-0.00014	6.13e-05	-2.28	0.0432	95.7	- -
Frother type	-0.0032	0.00188	-1.7	0.117	88.3	-
Activator presence	0.000796	0.000939	0.847	0.415	58.5	

Appendix B: Regression analysis

Table B.29.: Regression results relating the machine vision solids loading measurement on the bursting bubbles to the operating variables in the copper rougher 1.

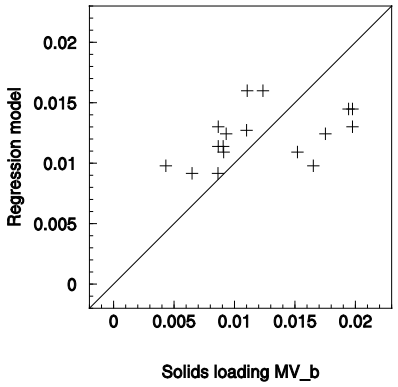

Solids loading MV_b kg/m^2	Air rate m^3/m^2/s	Froth height m	Frother concentration ppm
0.0124	0.0103	0.155	102
0.00932	0.0103	0.2	100
0.0198	0.0103	0.2	138
0.0198	0.011	0.155	102
0.00911	0.011	0.2	100
0.00906	0.011	0.2	130
0.011	0.0117	0.155	100
0.00864	0.0117	0.2	98
0.00433	0.0117	0.2	138
0.0111	0.0103	0.155	102
0.0175	0.0103	0.2	100
0.00866	0.0103	0.2	138
0.0194	0.011	0.155	102
0.0152	0.011	0.2	100
0.00866	0.011	0.2	130
0.00649	0.0117	0.2	98
0.0165	0.0117	0.2	138

Multiple R	0.442
R^2	0.196
Standard Error	0.00489
Adjusted R^2	0.0102
Observations	17

	df	SS	MS	F	Significance of F
Regression	3	7.55e-05	2.52e-05	1.05	0.402
Residual	13	0.00031	2.39e-05		
Total	16	0.000386			

	Coefficients	Standard Error	t-Statistics	p-Value		
Intercept	0.0498	0.0245	2.04	0.0667	93.3	+
Air rate	-2.25	2.08	-1.08	0.301	69.9	
Froth height	-0.0784	0.0643	-1.22	0.248	75.2	
Frother concentration	1.55e-05	7.74e-05	0.2	0.845	15.5	

Table B.30.: Regression results relating the machine vision solids loading measurement on the bursting bubbles to the operating variables in the copper rougher 3.

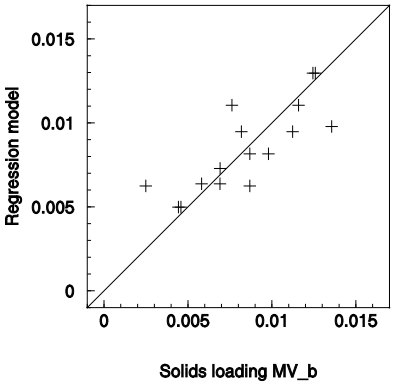

Solids loading MV_b kg/m^2	Air rate m^3/m^2/s	Froth height m	Frother concentration ppm
0.0126	0.0126	0.155	102
0.00868	0.0126	0.2	100
0.0112	0.0126	0.2	138
0.00762	0.0148	0.155	102
0.00249	0.0148	0.2	100
0.0136	0.0161	0.155	100
0.00443	0.0161	0.2	98
0.00691	0.0161	0.2	138
0.0124	0.0126	0.155	102
0.00979	0.0126	0.2	100
0.00818	0.0126	0.2	138
0.0116	0.0148	0.155	102
0.00869	0.0148	0.2	100
0.00691	0.0148	0.2	130
0.00459	0.0161	0.2	98
0.00581	0.0161	0.2	138

Multiple R	0.804
R^2	0.647
Standard Error	0.00215
Adjusted R^2	0.559
Observations	16

	df	SS	MS	F	Significance of F	
Regression	3	0.000102	3.4e-05	7.33	0.00475	++
Residual	12	5.57e-05	4.64e-06			
Total	15	0.000158				

	Coefficients	Standard Error	t-Statistics	p-Value		
Intercept	0.037	0.00716	5.16	0.000312	100.0	++
Air rate	-0.892	0.371	-2.4	0.035	96.5	- -
Froth height	-0.105	0.0284	-3.71	0.00343	99.7	- -
Frother concentration	3.48e-05	3.5e-05	0.996	0.341	65.9	

Appendix B: Regression analysis

Table B.31.: Regression results relating the machine vision solids loading measurement on the bursting bubbles to the operating variables in the platinum rougher 1.

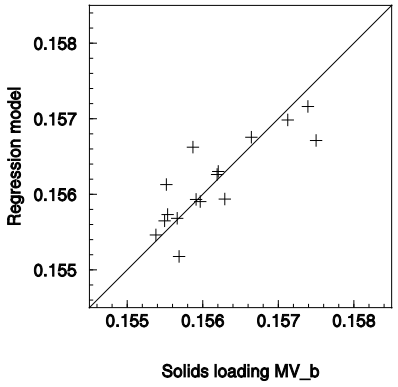

Solids loading MV_b kg/m^2	Air rate m^3/m^2/s	Froth height m	Frother concentration ppm	Frother type	Activator presence
0.156	0.00592	0.0984	60	1	0
0.156	0.00569	0.0643	60	1	2
0.158	0.00491	0.0537	60	1	0
0.156	0.00612	0.0763	40	1	1
0.156	0.00753	0.085	40	1	1
0.155	0.00761	0.0753	40	1	1
0.156	0.0064	0.0567	20	1	2
0.156	0.00589	0.0558	20	1	0
0.156	0.00787	0.161	60	1	2
0.157	0.00733	0.114	60	2	0
0.157	0.00538	0.0662	60	2	2
0.157	0.00575	0.0656	60	2	0
0.155	0.00868	0.111	20	2	2
0.156	0.00651	0.0908	20	2	0
0.156	0.00527	0.0527	20	2	2
0.156	0.00582	0.0493	20	2	0

Multiple R	0.835
R^2	0.697
Standard Error	0.000461
Adjusted R^2	0.545
Observations	16

	df	SS	MS	F	Significance of F	
Regression	5	4.88e-06	9.76e-07	4.6	0.0194	++
Residual	10	2.12e-06	2.12e-07			
Total	15	7e-06				

	Coefficients	Standard Error	t-Statistics	p-Value		
Intercept	0.156	0.00116	135.0	4.77e-19	100	++
Air rate	-0.17	0.198	-0.86	0.408	59.2	
Froth height	0.00186	0.00735	0.254	0.804	19.6	
Frother concentration	2.04e-05	8.35e-06	2.44	0.0326	96.7	++
Frother type	0.00057	0.00024	2.38	0.0368	96.3	++
Activator presence	-0.000235	0.000132	-1.77	0.104	89.6	-

Table B.32.: Regression results relating the machine vision solids loading measurement on the bursting bubbles to the operating variables in the platinum rougher 3.

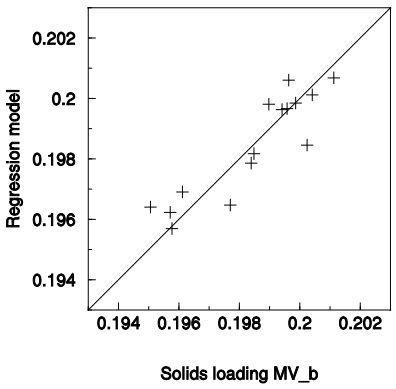

Solids loading MV_b kg/m^2	Air rate m^3/m^2/s	Froth height m	Frother concentration ppm	Frother type	Activator presence
0.2	0.00646	0.0808	60	1	0
0.199	0.00594	0.0808	60	1	2
0.201	0.00678	0.0794	60	1	0
0.2	0.00677	0.0805	40	1	1
0.198	0.00585	0.0804	40	1	1
0.198	0.00523	0.072	40	1	1
0.196	0.00678	0.0811	20	1	2
0.196	0.00686	0.082	20	1	0
0.2	0.00631	0.0884	60	2	2
0.2	0.00553	0.0804	60	2	0
0.2	0.00646	0.0732	60	2	2
0.199	0.0043	0.0728	60	2	0
0.198	0.00654	0.0724	20	2	0
0.196	0.00657	0.0623	20	2	2
0.195	0.00653	0.0684	20	2	0

Multiple R	0.902
R^2	0.813
Standard Error	0.00104
Adjusted R^2	0.709
Observations	15

	df	SS	MS	F	Significance of F	
Regression	5	4.25e-05	8.5e-06	7.83	0.00426	++
Residual	9	9.77e-06	1.09e-06			
Total	14	5.23e-05				

	Coefficients	Standard Error	t-Statistics	p-Value		
Intercept	0.192	0.00479	40.0	2.88e-13	100.0	++
Air rate	0.307	0.475	0.646	0.532	46.8	
Froth height	0.0149	0.0562	0.265	0.796	20.4	
Frother concentration	9.6e-05	2.02e-05	4.74	0.000606	99.9	++
Frother type	-0.000193	0.000619	-0.311	0.761	23.9	
Activator presence	-0.000317	0.00031	-1.02	0.328	67.2	

Appendix B: Regression analysis

Table B.33.: Regression results relating the machine vision solids loading measurement on the large bubbles that burst to the operating variables in the copper rougher 1.

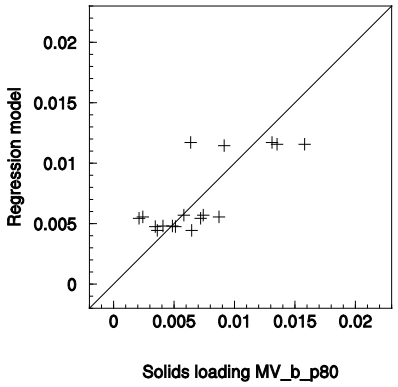

Solids loading $MV_{b,p80}$ kg/m^2	Air rate m^3/m^2/s	Froth height m	Frother concentration ppm
0.00638	0.0103	0.155	102
0.00582	0.0103	0.2	100
0.00511	0.0103	0.2	138
0.0158	0.011	0.155	102
0.00242	0.011	0.2	100
0.00487	0.011	0.2	130
0.00915	0.0117	0.155	100
0.00721	0.0117	0.2	98
0.00362	0.0117	0.2	138
0.0131	0.0103	0.155	102
0.00742	0.0103	0.2	100
0.00345	0.0103	0.2	138
0.0135	0.011	0.155	102
0.00872	0.011	0.2	100
0.00409	0.011	0.2	130
0.0021	0.0117	0.2	98
0.00647	0.0117	0.2	138

Multiple R	0.773
R^2	0.598
Standard Error	0.0028
Adjusted R^2	0.505
Observations	17

	df	SS	MS	F	Significance of F	
Regression	3	0.000151	5.04e-05	6.44	0.00659	++
Residual	13	0.000102	7.83e-06			
Total	16	0.000253				

	Coefficients	Standard Error	t-Statistics	p-Value		
Intercept	0.0374	0.014	2.67	0.0218	97.8	++
Air rate	-0.221	1.19	-0.185	0.856	14.4	
Froth height	-0.135	0.0368	-3.66	0.00376	99.6	- -
Frother concentration	-2.5e-05	4.44e-05	-0.565	0.584	41.6	

Table B.34.: Regression results relating the machine vision solids loading measurement on the large bubbles that burst to the operating variables in the copper rougher 3.

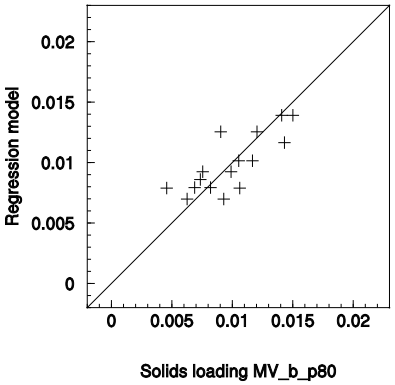

Solids loading $MV_{b,p80}$ kg/m^2	Air rate $m^3/m^2/s$	Froth height m	Frother concentration ppm
0.015	0.0126	0.155	102
0.00756	0.0126	0.2	100
0.0105	0.0126	0.2	138
0.012	0.0148	0.155	102
0.00458	0.0148	0.2	100
0.0143	0.0161	0.155	100
0.00627	0.0161	0.2	98
0.0082	0.0161	0.2	138
0.0141	0.0126	0.155	102
0.0099	0.0126	0.2	100
0.0117	0.0126	0.2	138
0.00905	0.0148	0.155	102
0.0106	0.0148	0.2	100
0.00736	0.0148	0.2	130
0.0093	0.0161	0.2	98
0.00689	0.0161	0.2	138

Multiple R	0.782
R^2	0.612
Standard Error	0.00211
Adjusted R^2	0.515
Observations	16

	df	SS	MS	F	Significance of F	
Regression	3	8.46e-05	2.82e-05	6.31	0.00814	++
Residual	12	5.36e-05	4.47e-06			
Total	15	0.000138				

	Coefficients	Standard Error	t-Statistics	p-Value		
Intercept	0.0354	0.00703	5.04	0.000378	100.0	++
Air rate	-0.637	0.364	-1.75	0.108	89.2	-
Froth height	-0.102	0.0278	-3.68	0.0036	99.6	- -
Frother concentration	2.36e-05	3.43e-05	0.688	0.506	49.4	

Appendix B: Regression analysis

Table B.35.: Regression results relating the machine vision solids loading measurement on the large bubbles that burst to the operating variables in the platinum rougher 1.

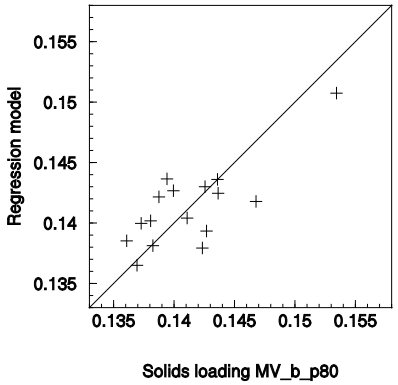

Solids loading $MV_{b,p80}$ kg/m^2	Air rate m^3/m^2/s	Froth height m	Frother concentration ppm	Frother type	Activator presence
0.14	0.00592	0.0984	60	1	0
0.144	0.00569	0.0643	60	1	2
0.143	0.00491	0.0537	60	1	0
0.139	0.00612	0.0763	40	1	1
0.137	0.00753	0.085	40	1	1
0.136	0.00761	0.0753	40	1	1
0.147	0.0064	0.0567	20	1	2
0.138	0.00589	0.0558	20	1	0
0.153	0.00787	0.161	60	1	2
0.141	0.00733	0.114	60	2	0
0.139	0.00538	0.0662	60	2	2
0.142	0.00575	0.0656	60	2	0
0.144	0.00868	0.111	20	2	2
0.138	0.00651	0.0908	20	2	0
0.143	0.00527	0.0527	20	2	2
0.137	0.00582	0.0493	20	2	0

Multiple R	0.763
R^2	0.582
Standard Error	0.00346
Adjusted R^2	0.373
Observations	16

	df	SS	MS	F	Significance of F	
Regression	5	0.000167	3.34e-05	2.79	0.0788	+
Residual	10	0.00012	1.2e-05			
Total	15	0.000287				

	Coefficients	Standard Error	t-Statistics	p-Value		
Intercept	0.146	0.00869	16.8	3.37e-09	100.0	++
Air rate	-2.35	1.49	-1.58	0.142	85.8	-
Froth height	0.127	0.0552	2.31	0.0416	95.8	++
Frother concentration	-2.05e-05	6.28e-05	-0.327	0.75	25.0	
Frother type	-0.000953	0.0018	-0.528	0.608	39.2	
Activator presence	0.00238	0.000995	2.39	0.036	96.4	++

Table B.36.: Regression results relating the machine vision solids loading measurement on the large bubbles that burst to the operating variables in the platinum rougher 3.

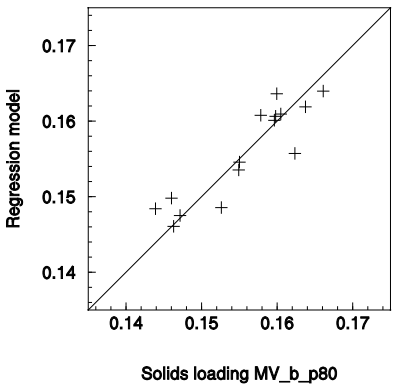

Solids loading $MV_{b,p80}$ kg/m^2	Air rate m^3/m^2/s	Froth height m	Frother concentration ppm	Frother type	Activator presence
0.16	0.00646	0.0808	60	1	0
0.158	0.00594	0.0808	60	1	2
0.166	0.00678	0.0794	60	1	0
0.162	0.00677	0.0805	40	1	1
0.155	0.00585	0.0804	40	1	1
0.155	0.00523	0.072	40	1	1
0.147	0.00678	0.0811	20	1	2
0.146	0.00686	0.082	20	1	0
0.16	0.00631	0.0884	60	2	2
0.164	0.00553	0.0804	60	2	0
0.16	0.00646	0.0732	60	2	2
0.16	0.0043	0.0728	60	2	0
0.153	0.00654	0.0724	20	2	0
0.146	0.00657	0.0623	20	2	2
0.144	0.00653	0.0684	20	2	0

Multiple R	0.903
R^2	0.816
Standard Error	0.00378
Adjusted R^2	0.714
Observations	15

	df	SS	MS	F	Significance of F	
Regression	5	0.000571	0.000114	7.99	0.00397	++
Residual	9	0.000129	1.43e-05			
Total	14	0.0007				

	Coefficients	Standard Error	t-Statistics	p-Value		
Intercept	0.132	0.0174	7.59	1.08e-05	100.0	++
Air rate	1.25	1.72	0.725	0.484	51.6	
Froth height	0.0326	0.204	0.16	0.876	12.4	
Frother concentration	0.000359	7.34e-05	4.88	0.000486	100.0	++
Frother type	-0.000545	0.00225	-0.243	0.813	18.7	
Activator presence	-0.00109	0.00112	-0.971	0.352	64.8	

Appendix B: Regression analysis

Table B.37.: Regression results relating the gravimetric solids loading measurement to the operating variables in the copper rougher 1.

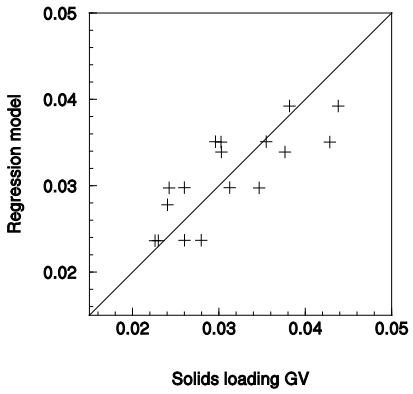

Solids loading (GV) kg/m^2	Air rate m^3/m^2/s	Froth height m	Frother concentration ppm
0.0382	0.0103	0.155	102
0.0302	0.0103	0.2	100
0.0355	0.0103	0.2	138
0.0377	0.011	0.155	102
0.0242	0.011	0.2	100
0.0313	0.011	0.2	130
0.0241	0.0117	0.155	100
0.023	0.0117	0.2	98
0.028	0.0117	0.2	138
0.0438	0.0103	0.155	102
0.0428	0.0103	0.2	100
0.0296	0.0103	0.2	138
0.0303	0.011	0.155	102
0.0347	0.011	0.2	100
0.026	0.011	0.2	130
0.0226	0.0117	0.2	98
0.026	0.0117	0.2	138

Multiple R	0.789
R^2	0.622
Standard Error	0.00459
Adjusted R^2	0.535
Observations	17

	df	SS	MS	F	Significance of F	
Regression	3	0.000451	0.00015	7.13	0.00447	++
Residual	13	0.000274	2.11e-05			
Total	16	0.000725				

	Coefficients	Standard Error	t-Statistics	p-Value		
Intercept	0.136	0.023	5.9	0.000104	100.0	++
Air rate	-7.97	1.95	-4.08	0.00182	99.8	- -
Froth height	-0.0924	0.0604	-1.53	0.154	84.6	-
Frother concentration	1.15e-06	7.28e-05	0.0157	0.988	1.23	

Table B.38.: Regression results relating the gravimetric solids loading measurement to the operating variables in the copper rougher 3.

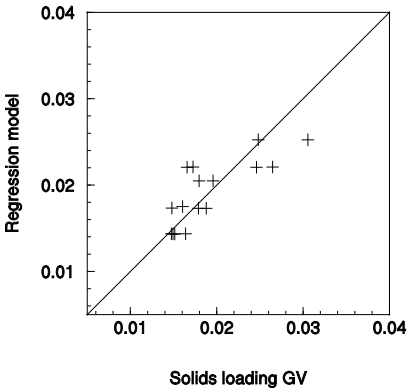

Solids loading (GV) kg/m^2	Air rate m^3/m^2/s	Froth height m	Frother concentration ppm
0.0248	0.0126	0.155	102
0.0166	0.0126	0.2	100
0.0173	0.0126	0.2	138
0.0196	0.0148	0.155	102
0.0179	0.0148	0.2	100
0.016	0.0161	0.155	100
0.0149	0.0161	0.2	98
0.0147	0.0161	0.2	138
0.0306	0.0126	0.155	102
0.0246	0.0126	0.2	100
0.0265	0.0126	0.2	138
0.018	0.0148	0.155	102
0.0188	0.0148	0.2	100
0.0148	0.0148	0.2	130
0.0151	0.0161	0.2	98
0.0164	0.0161	0.2	138

Multiple R	0.79
R^2	0.623
Standard Error	0.00331
Adjusted R^2	0.529
Observations	16

	df	SS	MS	F	Significance of F	
Regression	3	0.000217	7.24e-05	6.62	0.00687	++
Residual	12	0.000131	1.09e-05			
Total	15	0.000348				

	Coefficients	Standard Error	t-Statistics	p-Value		
Intercept	0.0642	0.011	5.84	0.000113	100.0	++
Air rate	-2.22	0.57	-3.9	0.00247	99.8	- -
Froth height	-0.0706	0.0435	-1.62	0.133	86.7	-
Frother concentration	6.71e-07	5.37e-05	0.0125	0.99	0.975	

Appendix B: Regression analysis

Table B.39.: Regression results relating the gravimetric solids loading measurement to the operating variables in the platinum rougher 1.

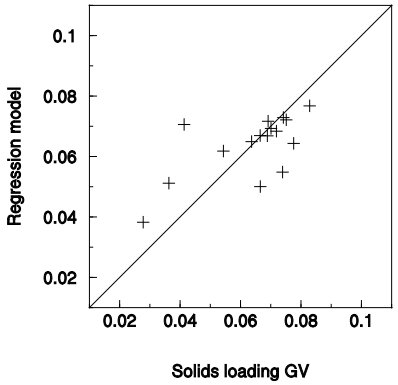

Solids loading (GV) kg/m^2	Air rate m^3/m^2/s	Froth height m	Frother concentration ppm	Frother type	Activator presence
0.0363	0.00592	0.0984	60	1	0
0.0751	0.00569	0.0643	60	1	2
0.0665	0.00491	0.0537	60	1	0
0.0776	0.00612	0.0763	40	1	1
0.0689	0.00753	0.085	40	1	1
0.0691	0.00761	0.0753	40	1	1
0.0829	0.0064	0.0567	20	1	2
0.0719	0.00589	0.0558	20	1	0
0.0278	0.00787	0.161	60	1	2
0.0665	0.00733	0.114	60	2	0
0.0701	0.00538	0.0662	60	2	2
0.0637	0.00575	0.0656	60	2	0
0.0543	0.00868	0.111	20	2	2
0.0739	0.00651	0.0908	20	2	0
0.0742	0.00527	0.0527	20	2	2
0.0414	0.00582	0.0493	20	2	0

Multiple R	0.653
R^2	0.427
Standard Error	0.0146
Adjusted R^2	0.14
Observations	16

	df	SS	MS	F	Significance of F
Regression	5	0.00158	0.000317	1.49	0.276
Residual	10	0.00213	0.000213		
Total	15	0.00371			

	Coefficients	Standard Error	t-Statistics	p-Value		
Intercept	0.0661	0.0366	1.81	0.0984	90.2	+
Air rate	4.59	6.27	0.732	0.479	52.1	
Froth height	-0.455	0.233	-1.96	0.0762	92.4	-
Frother concentration	5.2e-05	0.000265	0.196	0.848	15.2	
Frother type	-0.00045	0.0076	-0.0592	0.954	4.61	
Activator presence	0.0032	0.0042	0.764	0.461	53.9	

Table B.40.: Regression results relating the gravimetric solids loading measurement to the operating variables in the platinum rougher 3.

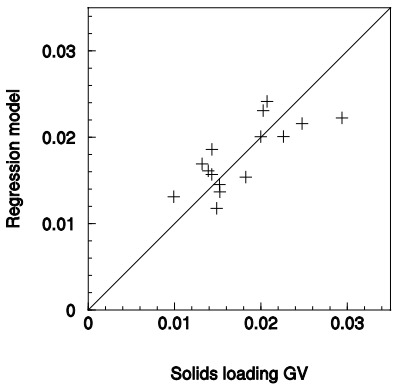

Solids loading (GV) kg/m^2	Air rate m^3/m^2/s	Froth height m	Frother concentration ppm	Frother type	Activator presence
0.0132	0.00646	0.0808	60	1	0
0.0294	0.00594	0.0808	60	1	2
0.0143	0.00678	0.0794	60	1	0
0.02	0.00677	0.0805	40	1	1
0.0248	0.00585	0.0804	40	1	1
0.0143	0.00523	0.072	40	1	1
0.0207	0.00678	0.0811	20	1	2
0.0226	0.00686	0.082	20	1	0
0.0203	0.00631	0.0884	60	2	2
0.0139	0.00553	0.0804	60	2	0
0.0182	0.00646	0.0732	60	2	2
0.0152	0.0043	0.0728	60	2	0
0.0152	0.00654	0.0724	20	2	0
0.00991	0.00657	0.0623	20	2	2
0.0149	0.00653	0.0684	20	2	0

Multiple R	0.759
R^2	0.576
Standard Error	0.00418
Adjusted R^2	0.34
Observations	15

	df	SS	MS	F	Significance of F	
Regression	5	0.000213	4.26e-05	2.44	0.116	+
Residual	9	0.000157	1.75e-05			
Total	14	0.00037				

	Coefficients	Standard Error	t-Statistics	p-Value		
Intercept	-0.00425	0.0192	-0.221	0.829	17.1	
Air rate	-1.73	1.9	-0.906	0.384	61.6	
Froth height	0.488	0.225	2.17	0.0531	94.7	+
Frother concentration	-8.07e-05	8.12e-05	-0.994	0.342	65.8	
Frother type	-0.00225	0.00248	-0.904	0.385	61.5	
Activator presence	0.0022	0.00124	1.77	0.105	89.5	+

Appendix B: Regression analysis

Table B.41.: Regression results relating the froth surface bubble size (p^{80}) to the operating variables in the copper rougher 1.

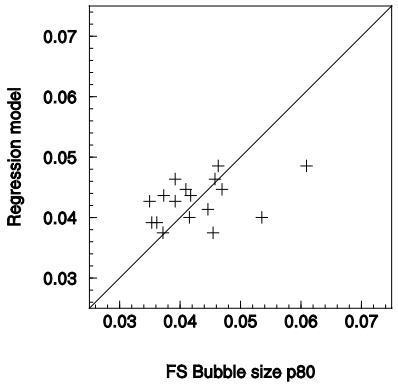

FS bubble size (p^{80}) m	Air rate $m^3/m^2/s$	Froth height m	Frother concentration ppm
0.0372	0.0103	0.155	102
0.047	0.0103	0.2	100
0.0415	0.0103	0.2	138
0.0353	0.011	0.155	102
0.0458	0.011	0.2	100
0.035	0.011	0.2	130
0.0446	0.0117	0.155	100
0.0463	0.0117	0.2	98
0.0418	0.0117	0.2	138
0.0455	0.0103	0.155	102
0.041	0.0103	0.2	100
0.0535	0.0103	0.2	138
0.0362	0.011	0.155	102
0.0392	0.011	0.2	100
0.0392	0.011	0.2	130
0.0609	0.0117	0.2	98
0.0373	0.0117	0.2	138

Multiple R^2	0.19
Adjusted multiple R^2	0.00295
R^2	0.98
Adjusted R^2	0.977
Standard Error	0.0067
Observations	17

	df	SS	MS	F	Significance of F	
Regression	3	0.0312	0.0104	232.0	3.6e-12	++
Residual	14	0.000628	4.48e-05			
Total	17	0.0319				

	Coefficients	Standard Error	t-Statistics	p-Value		
Intercept	0					
Air rate	2.53	1.33	1.9	0.0846	91.5	+
Froth height	0.154	0.0857	1.8	0.0995	90.0	+
Frother concentration	-0.000122	0.000105	-1.17	0.266	73.4	

Table B.42.: Regression results relating the froth surface bubble size (p^{80}) to the operating variables in the copper rougher 3.

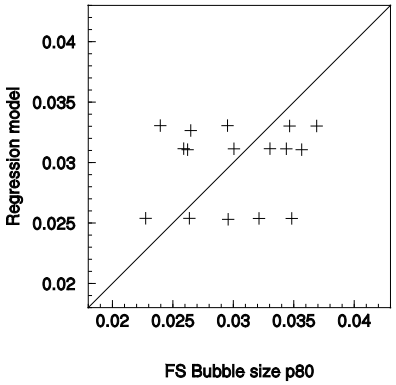

FS bubble size (p^{80}) m	Air rate $m^3/m^2/s$	Froth height m	Frother concentration ppm
0.0348	0.0126	0.155	102
0.0301	0.0126	0.2	100
0.0369	0.0126	0.2	138
0.0264	0.0148	0.155	102
0.0259	0.0148	0.2	100
0.0296	0.0161	0.155	100
0.0262	0.0161	0.2	98
0.0295	0.0161	0.2	138
0.0321	0.0126	0.155	102
0.0344	0.0126	0.2	100
0.0347	0.0126	0.2	138
0.0228	0.0148	0.155	102
0.033	0.0148	0.2	100
0.0265	0.0148	0.2	130
0.0357	0.0161	0.2	98
0.024	0.0161	0.2	138

Multiple R^2	0.34
Adjusted multiple R^2	0.174
R^2	0.973
Adjusted R^2	0.969
Standard Error	0.00554
Observations	16

	df	SS	MS	F	Significance of F	
Regression	3	0.0145	0.00482	157.0	1.87e-10	++
Residual	13	0.0004	3.07e-05			
Total	16	0.0149				

	Coefficients	Standard Error	t-Statistics	p-Value		
Intercept	0					
Air rate	0.00815	0.687	0.0119	0.991	0.925	
Froth height	0.13	0.0657	1.98	0.0729	92.7	+
Frother concentration	4.98e-05	8.62e-05	0.578	0.575	42.5	

Table B.43.: Regression results relating the froth surface bubble size (p^{80}) to the operating variables in the platinum rougher 1.

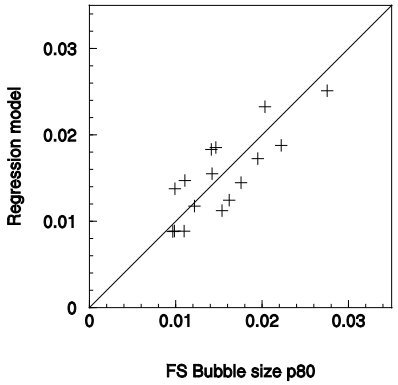

FS bubble size (p^{80}) m	Air rate $m^3/m^2/s$	Froth height m	Frother concentration ppm
0.0162	0.00592	0.0984	60
0.0195	0.00569	0.0643	60
0.00966	0.00491	0.0537	60
0.0142	0.00612	0.0763	40
0.0146	0.00753	0.085	40
0.0141	0.00761	0.0753	40
0.0222	0.0064	0.0567	20
0.0154	0.00589	0.0558	20
0.0275	0.00787	0.161	60
0.00991	0.00733	0.114	60
0.0111	0.00538	0.0662	60
0.00985	0.00575	0.0656	60
0.0203	0.00868	0.111	20
0.0122	0.00651	0.0908	20
0.0176	0.00527	0.0527	20
0.011	0.00582	0.0493	20

Multiple R^2	0.867
Adjusted multiple R^2	0.8
R^2	0.966
Adjusted R^2	0.954
Standard Error	0.00358
Observations	16

	df	SS	MS	F	Significance of F	
Regression	5	0.00401	0.000801	62.6	1.05e-07	++
Residual	11	0.000141	1.28e-05			
Total	16	0.00415				

	Coefficients	Standard Error	t-Statistics	p-Value		
Intercept	0					
Air rate	1.92	0.746	2.58	0.0258	97.4	++
Froth height	0.0383	0.0454	0.843	0.417	58.3	
Frother concentration	-1.17e-05	4.77e-05	-0.245	0.811	18.9	
Frother type	-0.002	0.00167	-1.2	0.256	74.4	
Activator presence	0.00327	0.00103	3.18	0.00882	99.1	++

Table B.44.: Regression results relating the froth surface bubble size (p^{80}) to the operating variables in the platinum rougher 3.

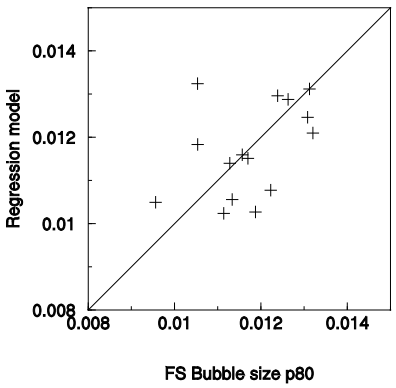

FS bubble size (p^{80}) m	Air rate $m^3/m^2/s$	Froth height m	Frother concentration ppm
0.0113	0.00646	0.0808	60
0.0122	0.00594	0.0808	60
0.00956	0.00678	0.0794	60
0.0105	0.00677	0.0805	40
0.0117	0.00585	0.0804	40
0.0119	0.00523	0.072	40
0.0131	0.00678	0.0811	20
0.0126	0.00686	0.082	20
0.0105	0.00631	0.0884	60
0.0116	0.00553	0.0804	60
0.0113	0.00646	0.0732	60
0.0111	0.0043	0.0728	60
0.0124	0.00654	0.0724	20
0.0132	0.00657	0.0623	20
0.0131	0.00653	0.0684	20

Multiple R^2	0.677
Adjusted multiple R^2	0.498
R^2	0.991
Adjusted R^2	0.988
Standard Error	0.00134
Observations	15

	df	SS	MS	F	Significance of F	
Regression	5	0.00207	0.000413	229.0	5.64e-10	++
Residual	10	1.8e-05	1.8e-06			
Total	15	0.00209				

	Coefficients	Standard Error	t-Statistics	p-Value		
Intercept	0					
Air rate	0.333	0.554	0.602	0.559	44.1	
Froth height	0.125	0.0519	2.4	0.0352	96.5	++
Frother concentration	-5.07e-05	2.61e-05	-1.94	0.0782	92.2	-
Frother type	0.00139	0.000641	2.17	0.0531	94.7	+
Activator presence	0.000193	0.000399	0.484	0.638	36.2	

Table B.45.: Regression results relating the burst rate to the operating variables in the copper rougher 1.

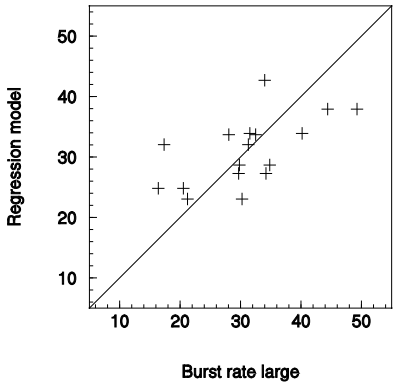

Burst rate $l/m^2/s$	Air rate $m^3/m^2/s$	Froth height m	Frother concentration ppm
32.5	0.0103	0.155	102
21.2	0.0103	0.2	100
20.6	0.0103	0.2	138
49.3	0.011	0.155	102
29.7	0.011	0.2	100
29.8	0.011	0.2	130
34.0	0.0117	0.155	100
31.3	0.0117	0.2	98
31.5	0.0117	0.2	138
28.1	0.0103	0.155	102
30.3	0.0103	0.2	100
16.4	0.0103	0.2	138
44.4	0.011	0.155	102
34.2	0.011	0.2	100
34.8	0.011	0.2	130
17.4	0.0117	0.2	98
40.2	0.0117	0.2	138

Multiple R^2	0.384
Adjusted multiple R^2	0.242
R^2	0.956
Adjusted R^2	0.949
Standard Error	7.46
Observations	17

	df	SS	MS	F	Significance of F	
Regression	3	16700.0	5580.0	100.0	1.06e-09	++
Residual	14	778.0	55.6			
Total	17	17500.0				

	Coefficients	Standard Error	t-Statistics	p-Value		
Intercept	0					
Air rate	6340.0	1490.0	4.27	0.00133	99.9	++
Froth height	-234.0	95.4	-2.46	0.0319	96.8	- -
Frother concentration	0.0463	0.116	0.398	0.698	30.2	

Table B.46.: Regression results relating the burst rate to the operating variables in the copper rougher 3.

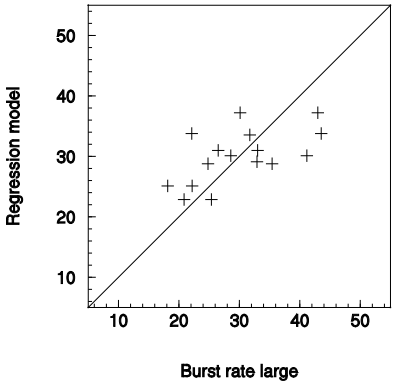

Burst rate $l/m^2/s$	Air rate $m^3/m^2/s$	Froth height m	Frother concentration ppm
18.1	0.0126	0.155	102
35.4	0.0126	0.2	100
20.9	0.0126	0.2	138
28.6	0.0148	0.155	102
43.6	0.0148	0.2	100
31.7	0.0161	0.155	100
43.0	0.0161	0.2	98
26.5	0.0161	0.2	138
22.2	0.0126	0.155	102
24.8	0.0126	0.2	100
25.4	0.0126	0.2	138
41.2	0.0148	0.155	102
22.1	0.0148	0.2	100
32.9	0.0148	0.2	130
30.1	0.0161	0.2	98
33.0	0.0161	0.2	138

Multiple R^2	0.353
Adjusted multiple R^2	0.191
R^2	0.96
Adjusted R^2	0.954
Standard Error	6.84
Observations	16

	df	SS	MS	F	Significance of F	
Regression	3	14700.0	4900.0	105.0	2.35e-09	++
Residual	13	609.0	46.8			
Total	16	15300.0				

	Coefficients	Standard Error	t-Statistics	p-Value		
Intercept	0					
Air rate	2330.0	849.0	2.75	0.0189	98.1	++
Froth height	74.5	81.0	0.919	0.378	62.2	
Frother concentration	-0.156	0.106	-1.46	0.171	82.9	-

Table B.47.: Regression results relating the burst rate to the operating variables in the platinum rougher 1.

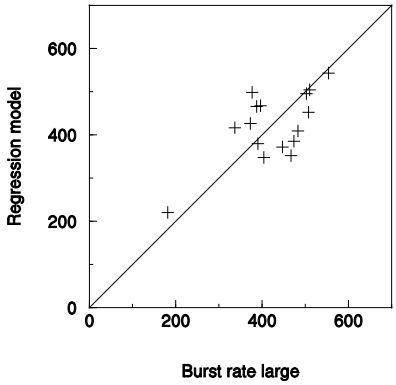

Burst rate $l/m^2/s$	Air rate $m^3/m^2/s$	Froth height m	Frother concentration ppm
467.0	0.00592	0.0984	60
390.0	0.00569	0.0643	60
373.0	0.00491	0.0537	60
474.0	0.00612	0.0763	40
503.0	0.00753	0.085	40
554.0	0.00761	0.0753	40
337.0	0.0064	0.0567	20
508.0	0.00589	0.0558	20
182.0	0.00787	0.161	60
396.0	0.00733	0.114	60
447.0	0.00538	0.0662	60
377.0	0.00575	0.0656	60
387.0	0.00868	0.111	20
483.0	0.00651	0.0908	20
404.0	0.00527	0.0527	20
510.0	0.00582	0.0493	20

Multiple R^2	0.553
Adjusted multiple R^2	0.329
R^2	0.975
Adjusted R^2	0.966
Standard Error	82.8
Observations	16

	df	SS	MS	F	Significance of F	
Regression	5	2930000.0	586000.0	85.4	2.02e-08	++
Residual	11	75500.0	6860.0			
Total	16	3000000.0				

	Coefficients	Standard Error	t-Statistics	p-Value		
Intercept	0					
Air rate	103000.0	17300.0	5.98	9.14e-05	100.0	++
Froth height	-3990.0	1050.0	-3.8	0.00296	99.7	- -
Frother concentration	1.67	1.1	1.51	0.159	84.1	+
Frother type	32.8	38.6	0.85	0.413	58.7	
Activator presence	-42.6	23.8	-1.79	0.101	89.9	-

Table B.48.: Regression results relating the burst rate to the operating variables in the platinum rougher 3.

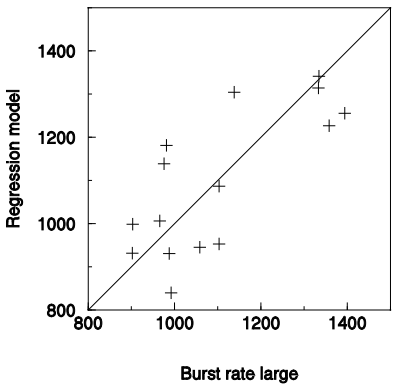

Burst rate $l/m^2/s$	Air rate $m^3/m^2/s$	Froth height m	Frother concentration ppm
988.0	0.00646	0.0808	60
1060.0	0.00594	0.0808	60
902.0	0.00678	0.0794	60
976.0	0.00677	0.0805	40
1100.0	0.00585	0.0804	40
1100.0	0.00523	0.072	40
1330.0	0.00678	0.0811	20
1330.0	0.00686	0.082	20
981.0	0.00631	0.0884	60
903.0	0.00553	0.0804	60
966.0	0.00646	0.0732	60
992.0	0.0043	0.0728	60
1140.0	0.00654	0.0724	20
1360.0	0.00657	0.0623	20
1390.0	0.00653	0.0684	20

Multiple R^2	0.823
Adjusted multiple R^2	0.725
R^2	0.989
Adjusted R^2	0.985
Standard Error	143.0
Observations	15

	df	SS	MS	F	Significance of F	
Regression	5	18400000.0	3690000.0	180.0	1.86e-09	++
Residual	10	205000.0	20500.0			
Total	15	18600000.0				

	Coefficients	Standard Error	t-Statistics	p-Value		
Intercept	0					
Air rate	54800.0	59000.0	0.929	0.373	62.7	
Froth height	12000.0	5530.0	2.18	0.0519	94.8	+
Frother concentration	-8.66	2.78	-3.12	0.00982	99.0	- -
Frother type	123.0	68.3	1.81	0.0981	90.2	+
Activator presence	21.4	42.5	0.504	0.624	37.6	

Table B.49.: Regression results relating the froth velocity to the operating variables in the copper rougher 1.

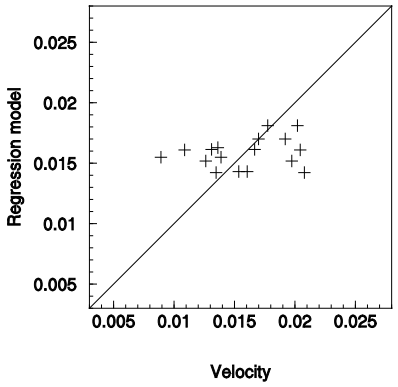

Velocity m/s	Air rate $m^3/m^2/s$	Froth height m	Frother concentration ppm
0.0161	0.0103	0.155	102
0.0167	0.0103	0.2	100
0.0208	0.0103	0.2	138
0.0126	0.011	0.155	102
0.0192	0.011	0.2	100
0.0139	0.011	0.2	130
0.0136	0.0117	0.155	100
0.0202	0.0117	0.2	98
0.0204	0.0117	0.2	138
0.0154	0.0103	0.155	102
0.0131	0.0103	0.2	100
0.0135	0.0103	0.2	138
0.0197	0.011	0.155	102
0.017	0.011	0.2	100
0.00892	0.011	0.2	130
0.0178	0.0117	0.2	98
0.0109	0.0117	0.2	138

Multiple R^2	0.0746
Adjusted multiple R^2	-0.139
R^2	0.957
Adjusted R^2	0.951
Standard Error	0.00371
Observations	17

	df	SS	MS	F	Significance of F	
Regression	3	0.00429	0.00143	104.0	8.41e-10	++
Residual	14	0.000193	1.38e-05			
Total	17	0.00448				

	Coefficients	Standard Error	t-Statistics	p-Value		
Intercept	0					
Air rate	1.31	0.74	1.77	0.105	89.5	+
Froth height	0.0384	0.0475	0.809	0.436	56.4	
Frother concentration	-5.04e-05	5.79e-05	-0.869	0.403	59.7	

Table B.50.: Regression results relating the froth velocity to the operating variables in the copper rougher 3.

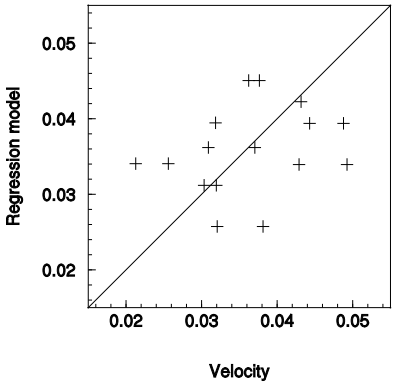

Velocity m/s	Air rate $m^3/m^2/s$	Froth height m	Frother concentration ppm
0.0429	0.0126	0.155	102
0.0321	0.0126	0.2	100
0.0371	0.0126	0.2	138
0.0488	0.0148	0.155	102
0.0303	0.0148	0.2	100
0.0432	0.0161	0.155	100
0.0256	0.0161	0.2	98
0.0377	0.0161	0.2	138
0.0493	0.0126	0.155	102
0.0381	0.0126	0.2	100
0.0309	0.0126	0.2	138
0.0443	0.0148	0.155	102
0.032	0.0148	0.2	100
0.0319	0.0148	0.2	130
0.0213	0.0161	0.2	98
0.0362	0.0161	0.2	138

Multiple R^2	0.788
Adjusted multiple R^2	0.735
R^2	0.951
Adjusted R^2	0.944
Standard Error	0.0091
Observations	16

	df	SS	MS	F	Significance of F	
Regression	3	0.021	0.007	84.5	8.83e-09	++
Residual	13	0.00108	8.28e-05			
Total	16	0.0221				

	Coefficients	Standard Error	t-Statistics	p-Value		
Intercept	0					
Air rate	2.55	1.13	2.26	0.0451	95.5	++
Froth height	-0.17	0.108	-1.58	0.143	85.7	-
Frother concentration	0.000275	0.000142	1.94	0.0779	92.2	+

Table B.51.: Regression results relating the froth velocity to the operating variables in the platinum rougher 1.

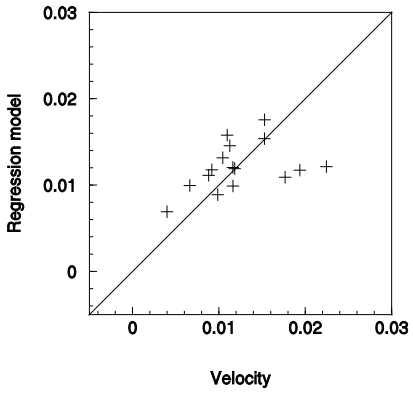

Velocity m/s	Air rate $m^3/m^2/s$	Froth height m	Frother concentration ppm
0.0177	0.00592	0.0984	60
0.0194	0.00569	0.0643	60
0.0105	0.00491	0.0537	60
0.00663	0.00612	0.0763	40
0.00882	0.00753	0.085	40
0.0116	0.00761	0.0753	40
0.00987	0.0064	0.0567	20
0.0116	0.00589	0.0558	20
0.00399	0.00787	0.161	60
0.011	0.00733	0.114	60
0.0153	0.00538	0.0662	60
0.0153	0.00575	0.0656	60
0.00919	0.00868	0.111	20
0.0224	0.00651	0.0908	20
0.0118	0.00527	0.0527	20
0.0113	0.00582	0.0493	20

Multiple R^2	0.272
Adjusted multiple R^2	-0.0918
R^2	0.893
Adjusted R^2	0.855
Standard Error	0.00516
Observations	16

	df	SS	MS	F	Significance of F	
Regression	5	0.00245	0.000491	18.4	5.15e-05	++
Residual	11	0.000293	2.66e-05			
Total	16	0.00275				

	Coefficients	Standard Error	t-Statistics	p-Value		
Intercept	0					
Air rate	1.35	1.08	1.25	0.236	76.4	
Froth height	-0.0804	0.0654	-1.23	0.245	75.5	
Frother concentration	0.00011	6.87e-05	1.61	0.136	86.4	+
Frother type	0.00423	0.0024	1.76	0.106	89.4	+
Activator presence	-0.000816	0.00148	-0.55	0.593	40.7	

Table B.52.: Regression results relating the froth velocity to the operating variables in the platinum rougher 3.

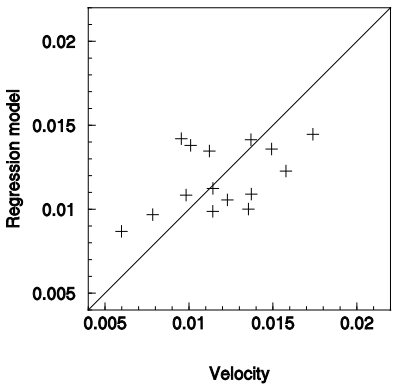

Velocity m/s	Air rate $m^3/m^2/s$	Froth height m	Frother concentration ppm
0.0149	0.00646	0.0808	60
0.0158	0.00594	0.0808	60
0.0101	0.00678	0.0794	60
0.0114	0.00677	0.0805	40
0.0123	0.00585	0.0804	40
0.0135	0.00523	0.072	40
0.00598	0.00678	0.0811	20
0.00785	0.00686	0.082	20
0.00954	0.00631	0.0884	60
0.0174	0.00553	0.0804	60
0.0137	0.00646	0.0732	60
0.0112	0.0043	0.0728	60
0.0137	0.00654	0.0724	20
0.0114	0.00657	0.0623	20
0.00983	0.00653	0.0684	20

Multiple R^2	0.4
Adjusted multiple R^2	0.0673
R^2	0.955
Adjusted R^2	0.937
Standard Error	0.00318
Observations	15

	df	SS	MS	F	Significance of F	
Regression	5	0.00216	0.000431	42.8	1.97e-06	++
Residual	10	0.000101	1.01e-05			
Total	15	0.00226				

	Coefficients	Standard Error	t-Statistics	p-Value		
Intercept	0					
Air rate	0.735	1.31	0.562	0.585	41.5	
Froth height	0.0117	0.123	0.0951	0.926	7.41	
Frother concentration	0.000105	6.17e-05	1.71	0.116	88.4	+
Frother type	0.00157	0.00151	1.03	0.323	67.7	
Activator presence	-0.000464	0.000943	-0.492	0.633	36.7	

Table B.53.: Regression results relating the solids recovery rate to the operating variables in the copper rougher 1.

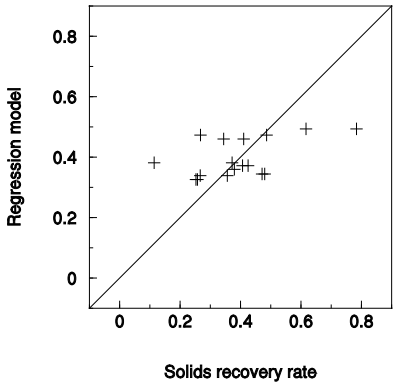

Solids recovery rate t/hr	Air rate $m^3/m^2/s$	Froth height m	Frother concentration ppm
0.258	0.0103	0.155	102
0.41	0.0103	0.2	100
0.48	0.0103	0.2	138
0.267	0.011	0.155	102
0.487	0.011	0.2	100
0.114	0.011	0.2	130
0.38	0.0117	0.155	100
0.617	0.0117	0.2	98
0.425	0.0117	0.2	138
0.253	0.0103	0.155	102
0.344	0.0103	0.2	100
0.471	0.0103	0.2	138
0.357	0.011	0.155	102
0.268	0.011	0.2	100
0.372	0.011	0.2	130
0.784	0.0117	0.2	98
0.407	0.0117	0.2	138

Multiple R^2	0.352
Adjusted multiple R^2	0.202
R^2	0.906
Adjusted R^2	0.892
Standard Error	0.142
Observations	17

	df	SS	MS	F	Significance of F	
Regression	3	2.73	0.91	44.9	1.98e-07	++
Residual	14	0.284	0.0203			
Total	17	3.01				

	Coefficients	Standard Error	t-Statistics	p-Value		
Intercept	0					
Air rate	19.0	28.4	0.67	0.516	48.4	
Froth height	2.84	1.82	1.56	0.147	85.3	+
Frother concentration	-0.00305	0.00222	-1.37	0.198	80.2	-

Table B.54.: Regression results relating the solids recovery rate to the operating variables in the copper rougher 3.

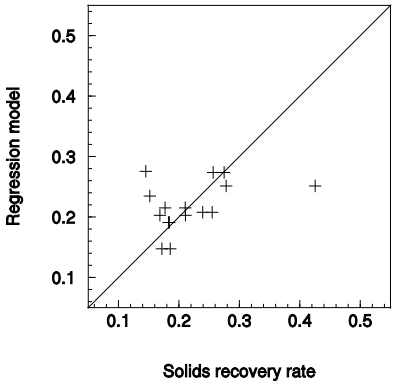

Solids recovery rate t/hr	Air rate $m^3/m^2/s$	Froth height m	Frother concentration ppm
0.239	0.0126	0.155	102
0.172	0.0126	0.2	100
0.169	0.0126	0.2	138
0.278	0.0148	0.155	102
0.183	0.0148	0.2	100
0.145	0.0161	0.155	100
0.177	0.0161	0.2	98
0.275	0.0161	0.2	138
0.255	0.0126	0.155	102
0.186	0.0126	0.2	100
0.211	0.0126	0.2	138
0.425	0.0148	0.155	102
0.184	0.0148	0.2	100
0.152	0.0148	0.2	130
0.21	0.0161	0.2	98
0.257	0.0161	0.2	138

Multiple R^2	0.303
Adjusted multiple R^2	0.128
R^2	0.925
Adjusted R^2	0.914
Standard Error	0.0698
Observations	16

	df	SS	MS	F	Significance of F	
Regression	3	0.783	0.261	53.6	1.4e-07	++
Residual	13	0.0633	0.00487			
Total	16	0.847				

	Coefficients	Standard Error	t-Statistics	p-Value		
Intercept	0					
Air rate	20.3	8.65	2.35	0.0386	96.1	++
Froth height	-1.28	0.826	-1.54	0.151	84.9	-
Frother concentration	0.00146	0.00109	1.35	0.206	79.4	

Appendix B: Regression analysis

Table B.55.: Regression results relating the solids recovery rate to the operating variables in the platinum rougher 1.

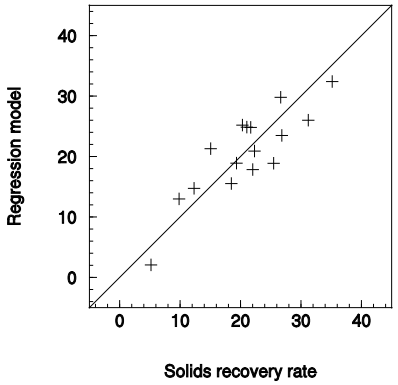

Solids recovery rate kg/hr	Air rate $m^3/m^2/s$	Froth height m	Frother concentration ppm
9.84	0.00592	0.0984	60
12.3	0.00569	0.0643	60
25.5	0.00491	0.0537	60
18.5	0.00612	0.0763	40
19.3	0.00753	0.085	40
15.1	0.00761	0.0753	40
22.0	0.0064	0.0567	20
22.3	0.00589	0.0558	20
5.21	0.00787	0.161	60
20.3	0.00733	0.114	60
26.8	0.00538	0.0662	60
26.7	0.00575	0.0656	60
21.0	0.00868	0.111	20
31.2	0.00651	0.0908	20
21.7	0.00527	0.0527	20
35.2	0.00582	0.0493	20

Multiple R^2	0.818
Adjusted multiple R^2	0.727
R^2	0.969
Adjusted R^2	0.958
Standard Error	4.68
Observations	16

	df	SS	MS	F	Significance of F	
Regression	5	7580.0	1520.0	69.3	6.14e-08	++
Residual	11	241.0	21.9			
Total	16	7820.0				

	Coefficients	Standard Error	t-Statistics	p-Value		
Intercept	0					
Air rate	3730.0	975.0	3.82	0.00282	99.7	++
Froth height	-216.0	59.3	-3.64	0.00391	99.6	- -
Frother concentration	0.0294	0.0623	0.472	0.646	35.4	
Frother type	10.4	2.18	4.75	0.000595	99.9	++
Activator presence	-2.39	1.35	-1.77	0.104	89.6	-

Table B.56.: Regression results relating the solids recovery rate to the operating variables in the platinum rougher 3.

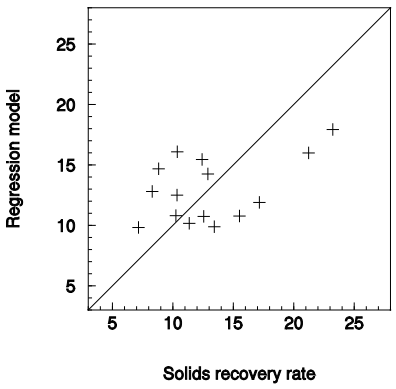

Solids recovery rate kg/hr	Air rate $m^3/m^2/s$	Froth height m	Frother concentration ppm
11.4	0.00646	0.0808	60
12.6	0.00594	0.0808	60
10.3	0.00678	0.0794	60
10.3	0.00677	0.0805	40
15.5	0.00585	0.0804	40
13.4	0.00523	0.072	40
12.9	0.00678	0.0811	20
8.3	0.00686	0.082	20
8.83	0.00631	0.0884	60
17.2	0.00553	0.0804	60
12.4	0.00646	0.0732	60
7.16	0.0043	0.0728	60
21.2	0.00654	0.0724	20
23.2	0.00657	0.0623	20
10.4	0.00653	0.0684	20

Multiple R^2	0.346
Adjusted multiple R^2	-0.0167
R^2	0.918
Adjusted R^2	0.885
Standard Error	4.83
Observations	15

	df	SS	MS	F	Significance of F	
Regression	5	2600.0	520.0	22.3	4e-05	++
Residual	10	233.0	23.3			
Total	15	2830.0				

	Coefficients	Standard Error	t-Statistics	p-Value		
Intercept	0					
Air rate	1880.0	1990.0	0.945	0.365	63.5	
Froth height	-31.8	186.0	-0.171	0.868	13.2	
Frother concentration	-0.0483	0.0938	-0.515	0.617	38.3	
Frother type	3.47	2.3	1.51	0.16	84.0	+
Activator presence	0.785	1.43	0.548	0.595	40.5	

Table B.57.: Regression results relating the copper grade to the operating variables in the copper rougher 1.

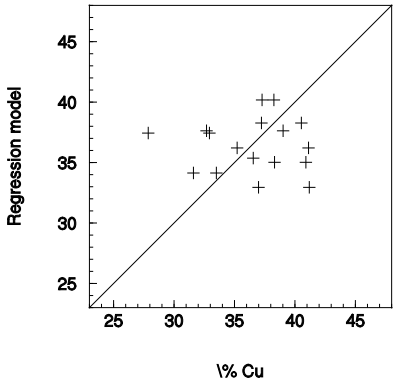

% Cu	Air rate	Froth height	Frother concentration
41.2	0.0103	0.155	102
38.3	0.0103	0.2	100
39.0	0.0103	0.2	138
31.6	0.011	0.155	102
35.2	0.011	0.2	100
37.2	0.011	0.2	130
36.6	0.0117	0.155	100
27.9	0.0117	0.2	98
38.3	0.0117	0.2	138
37.0	0.0103	0.155	102
40.9	0.0103	0.2	100
32.7	0.0103	0.2	138
33.5	0.011	0.155	102
41.1	0.011	0.2	100
40.5	0.011	0.2	130
32.9	0.0117	0.2	98
37.3	0.0117	0.2	138

Multiple R^2	0.199
Adjusted multiple R^2	0.0145
R^2	0.986
Adjusted R^2	0.984
Standard Error	4.78
Observations	17

	df	SS	MS	F	Significance of F	
Regression	3	22600.0	7540.0	330.0	3.2e-13	++
Residual	14	320.0	22.8			
Total	17	22900.0				

	Coefficients	Standard Error	t-Statistics	p-Value		
Intercept	0					
Air rate	1780.0	953.0	1.87	0.0886	91.1	+
Froth height	49.2	61.2	0.804	0.439	56.1	
Frother concentration	0.0685	0.0746	0.918	0.378	62.2	

Table B.58.: Regression results relating the copper grade to the operating variables in the copper rougher 3.

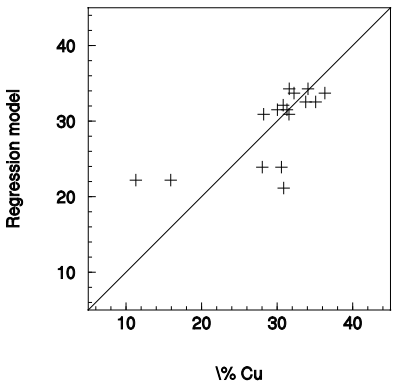

% Cu	Air rate	Froth height	Frother concentration
28.0	0.0126	0.155	102
31.6	0.0126	0.2	100
36.3	0.0126	0.2	138
15.9	0.0148	0.155	102
33.8	0.0148	0.2	100
30.9	0.0161	0.155	100
30.0	0.0161	0.2	98
31.6	0.0161	0.2	138
30.6	0.0126	0.155	102
34.1	0.0126	0.2	100
32.2	0.0126	0.2	138
11.3	0.0148	0.155	102
35.1	0.0148	0.2	100
30.8	0.0148	0.2	130
31.3	0.0161	0.2	98
28.2	0.0161	0.2	138

Multiple R^2	0.482
Adjusted multiple R^2	0.352
R^2	0.976
Adjusted R^2	0.972
Standard Error	5.18
Observations	16

	df	SS	MS	F	Significance of F	
Regression	3	14200.0	4740.0	177.0	8.79e-11	++
Residual	13	349.0	26.9			
Total	16	14600.0				

	Coefficients	Standard Error	t-Statistics	p-Value		
Intercept	0					
Air rate	-805.0	642.0	-1.25	0.236	76.4	
Froth height	229.0	61.4	3.74	0.00327	99.7	++
Frother concentration	-0.0149	0.0806	-0.185	0.857	14.3	

Table B.59.: Regression results relating the copper grade to the operating variables in the platinum rougher 1.

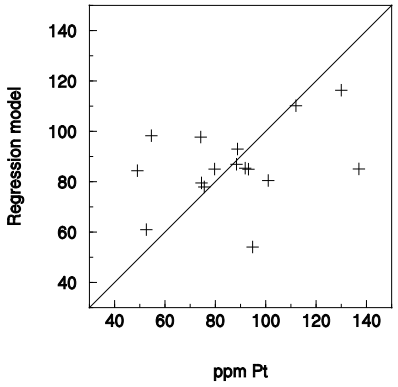

ppm Pt ppm	Air rate $m^3/m^2/s$	Froth height m	Frother concentration ppm
137	0.00592	0.0984	60
75.6	0.00569	0.0643	60
49.0	0.00491	0.0537	60
93.2	0.00612	0.0763	40
112	0.00753	0.085	40
130	0.00761	0.0753	40
91.8	0.0064	0.0567	20
88.8	0.00589	0.0558	20
74.5	0.00787	0.161	60
74.2	0.00733	0.114	60
52.6	0.00538	0.0662	60
88.4	0.00575	0.0656	60
54.6	0.00868	0.111	20
101	0.00651	0.0908	20
94.8	0.00527	0.0527	20
79.7	0.00582	0.0493	20

Multiple R^2	0.268
Adjusted multiple R^2	-0.0979
R^2	0.932
Adjusted R^2	0.907
Standard Error	28.5
Observations	16

	df	SS	MS	F	Significance of F	
Regression	5	123000.0	24500.0	30.2	4.55e-06	++
Residual	11	8940.0	812.0			
Total	16	131000.0				

	Coefficients	Standard Error	t-Statistics	p-Value		
Intercept	0					
Air rate	20800.0	5940.0	3.49	0.00503	99.5	++
Froth height	-451.0	361.0	-1.25	0.237	76.3	
Frother concentration	0.269	0.379	0.709	0.493	50.7	
Frother type	-9.49	13.3	-0.715	0.49	51.0	
Activator presence	-8.94	8.2	-1.09	0.299	70.1	

Table B.60.: Regression results relating the copper grade to the operating variables in the platinum rougher 3.

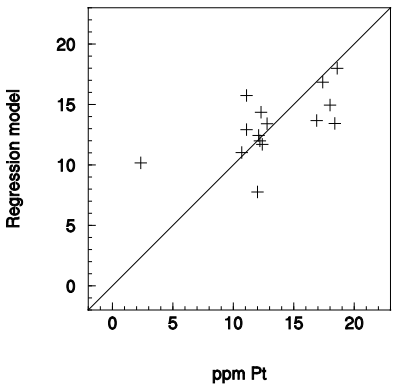

ppm Pt ppm	Air rate $m^3/m^2/s$	Froth height m	Frother concentration ppm
12.8	0.00646	0.0808	60
12.3	0.00594	0.0808	60
18.4	0.00678	0.0794	60
11.1	0.00677	0.0805	40
18	0.00585	0.0804	40
11.1	0.00523	0.072	40
18.6	0.00678	0.0811	20
17.4	0.00686	0.082	20
16.9	0.00631	0.0884	60
2.35	0.00553	0.0804	60
10.7	0.00646	0.0732	60
12	0.0043	0.0728	60
12.1	0.00654	0.0724	20
12.2	0.00657	0.0623	20
12.4	0.00653	0.0684	20

Multiple R^2	0.379
Adjusted multiple R^2	0.0333
R^2	0.946
Adjusted R^2	0.925
Standard Error	3.93
Observations	15

	df	SS	MS	F	Significance of F	
Regression	5	2720.0	543.0	35.2	4.95e-06	++
Residual	10	155.0	15.5			
Total	15	2870.0				

	Coefficients	Standard Error	t-Statistics	p-Value	
Intercept	0				
Air rate	835.0	1620.0	0.516	0.616	38.4
Froth height	182.0	152.0	1.2	0.255	74.5
Frother concentration	-0.0718	0.0763	-0.94	0.367	63.3
Frother type	-2.4	1.88	-1.28	0.227	77.3
Activator presence	0.69	1.17	0.591	0.566	43.4

B.4. Froth stability factor effect on froth transport and flotation performance factors

This section contains the results from the regression analysis performed in section 5.4.2.

These regressions were used to determine the direction and significance of the relationship between froth stability factors and measured froth transport and flotation performance factors. These results have been summarised in tables 5.4 and 5.5.

Table B.61.: Regression results relating the froth surface velocity to the stability factors in the copper rougher 1.

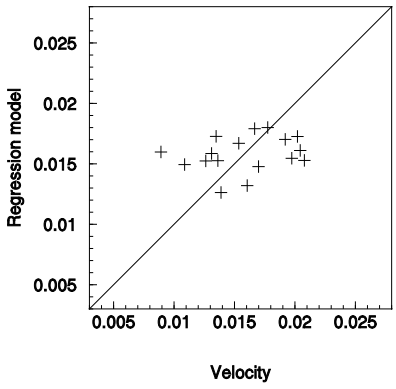

Velocity m/s	Burst rate $1/m^2/s$	Solids loading (MV) kg/m^2	FS bubble size (p^{80}) m	Frother concentration ppm
0.0161	32.5	0.0307	0.0372	102
0.0167	21.2	0.037	0.047	100
0.0208	20.6	0.0324	0.0415	138
0.0126	49.3	0.0399	0.0353	102
0.0192	29.7	0.0371	0.0458	100
0.0139	29.8	0.0296	0.035	130
0.0136	34.0	0.0341	0.0446	100
0.0202	31.3	0.0378	0.0463	98
0.0204	31.5	0.0368	0.0418	138
0.0154	28.1	0.036	0.0455	102
0.0131	30.3	0.0356	0.041	100
0.0135	16.4	0.0331	0.0535	138
0.0197	44.4	0.0391	0.0362	102
0.017	34.2	0.0343	0.0392	100
0.00892	34.8	0.0378	0.0392	130
0.0178	17.4	0.0327	0.0609	98
0.0109	40.2	0.037	0.0373	138

Multiple R^2	0.154
Adjusted multiple R^2	-0.129
R^2	0.956
Adjusted R^2	0.946
Standard Error	0.00389
Observations	17

	df	SS	MS	F	Significance of F	
Regression	4	0.00429	0.00107	70.8	1.08e-08	++
Residual	13	0.000197	1.51e-05			
Total	17	0.00448				

	Coefficients	Standard Error	t-Statistics	p-Value	
Intercept	0				
Burst rate large	-9.29e-05	0.000222	-0.418	0.684	31.6
Solids loading MV	0.414	0.453	0.914	0.38	62.0
FS Bubble size p80	0.107	0.208	0.515	0.617	38.3
Frother concentration	-4.73e-06	4.67e-05	-0.101	0.921	7.89

Table B.62.: Regression results relating the froth surface velocity to the stability factors in the copper rougher 3.

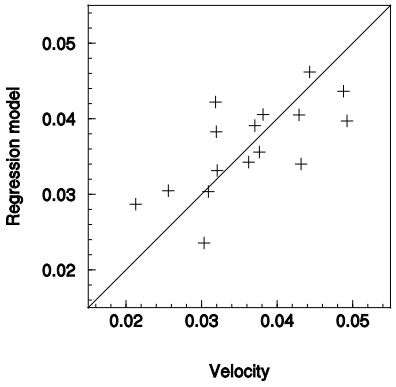

Velocity m/s	Burst rate $1/m^2/s$	Solids loading (MV) kg/m^2	FS bubble size (p^{80}) m	Frother concentration ppm
0.0429	18.1	0.0218	0.0348	102
0.0321	35.4	0.019	0.0301	100
0.0371	20.9	0.0222	0.0369	138
0.0488	28.6	0.0208	0.0264	102
0.0303	43.6	0.0155	0.0259	100
0.0432	31.7	0.019	0.0296	100
0.0256	43.0	0.0175	0.0262	98
0.0377	26.5	0.0195	0.0295	138
0.0493	22.2	0.021	0.0321	102
0.0381	24.8	0.0219	0.0344	100
0.0309	25.4	0.0193	0.0347	138
0.0443	41.2	0.021	0.0228	102
0.032	22.1	0.0208	0.033	100
0.0319	32.9	0.0208	0.0265	130
0.0213	30.1	0.019	0.0357	98
0.0362	33.0	0.0179	0.024	138

Multiple R^2	0.65
Adjusted multiple R^2	0.523
R^2	0.977
Adjusted R^2	0.972
Standard Error	0.00647
Observations	16

	df	SS	MS	F	Significance of F	
Regression	4	0.0216	0.0054	129.0	9.5e-10	++
Residual	12	0.000502	4.19e-05			
Total	16	0.0221				

	Coefficients	Standard Error	t-Statistics	p-Value		
Intercept	0					
Burst rate large	-0.000123	0.000179	-0.684	0.508	49.2	
Solids loading MV	3.55	0.825	4.3	0.00126	99.9	++
FS Bubble size p80	-0.917	0.431	-2.13	0.0568	94.3	-
Frother concentration	-2.44e-05	8.97e-05	-0.272	0.79	21.0	

Appendix B: Regression analysis

Table B.63.: Regression results relating the froth surface velocity to the stability factors in the platinum rougher 1.

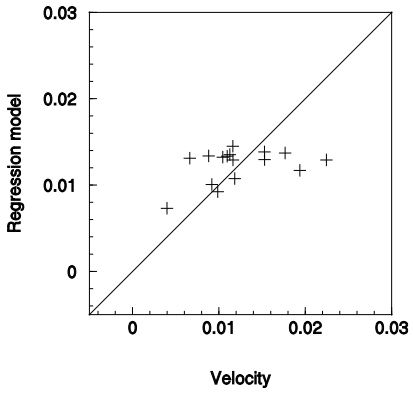

Velocity m/s	Burst rate $1/m^2/s$	Solids loading (MV) kg/m^2	FS bubble size (p^{80}) m	Frother concentration ppm
0.0177	467.0	0.0758	0.0162	60
0.0194	390.0	0.0749	0.0195	60
0.0105	373.0	0.0716	0.00966	60
0.00663	474.0	0.0719	0.0142	40
0.00882	503.0	0.071	0.0146	40
0.0116	554.0	0.0731	0.0141	40
0.00987	337.0	0.0793	0.0222	20
0.0116	508.0	0.0745	0.0154	20
0.00399	182.0	0.0811	0.0275	60
0.011	396.0	0.0697	0.00991	60
0.0153	447.0	0.0692	0.0111	60
0.0153	377.0	0.0686	0.00985	60
0.00919	387.0	0.0757	0.0203	20
0.0224	483.0	0.0714	0.0122	20
0.0118	404.0	0.074	0.0176	20
0.0113	510.0	0.0707	0.011	20

Multiple R^2	0.175
Adjusted multiple R^2	-0.126
R^2	0.899
Adjusted R^2	0.874
Standard Error	0.00481
Observations	16

	df	SS	MS	F	Significance of F	
Regression	4	0.00247	0.000617	26.7	6.83e-06	++
Residual	12	0.000278	2.31e-05			
Total	16	0.00275				

	Coefficients	Standard Error	t-Statistics	p-Value	
Intercept	0				
Burst rate large	1.57e-05	2e-05	0.782	0.451	54.9
Solids loading MV	0.101	0.231	0.439	0.669	33.1
FS Bubble size p80	-0.218	0.473	-0.46	0.654	34.6
Frother concentration	3.72e-05	7.82e-05	0.475	0.644	35.6

Table B.64.: Regression results relating the froth surface velocity to the stability factors in the platinum rougher 3.

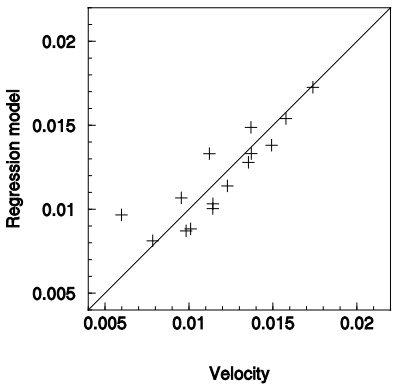

Velocity m/s	Burst rate $1/m^2/s$	Solids loading (MV) kg/m^2	FS bubble size (p^{80}) m	Frother concentration ppm
0.0149	988.0	0.0287	0.0113	60
0.0158	1060.0	0.0279	0.0122	60
0.0101	902.0	0.033	0.00956	60
0.0114	976.0	0.0321	0.0105	40
0.0123	1100.0	0.0315	0.0117	40
0.0135	1100.0	0.0257	0.0119	40
0.00598	1330.0	0.036	0.0131	20
0.00785	1330.0	0.0336	0.0126	20
0.00954	981.0	0.0307	0.0105	60
0.0174	903.0	0.0264	0.0116	60
0.0137	966.0	0.0233	0.0113	60
0.0112	992.0	0.0259	0.0111	60
0.0137	1140.0	0.0268	0.0124	20
0.0114	1360.0	0.0304	0.0132	20
0.00983	1390.0	0.0295	0.0131	20

Multiple R^2	0.794
Adjusted multiple R^2	0.712
R^2	0.987
Adjusted R^2	0.983
Standard Error	0.00164
Observations	15

	df	SS	MS	F	Significance of F	
Regression	4	0.00223	0.000557	206.0	2.89e-10	++
Residual	11	2.97e-05	2.7e-06			
Total	15	0.00226				

	Coefficients	Standard Error	t-Statistics	p-Value		
Intercept	0					
Burst rate large	-2.69e-05	8.87e-06	-3.04	0.0113	98.9	- -
Solid loading MV	-0.128	0.131	-0.974	0.351	64.9	
FS Bubble size p80	3.8	0.812	4.68	0.000677	99.9	++
Frother concentration	1.71e-05	4.06e-05	0.421	0.682	31.8	

Appendix B: Regression analysis

Table B.65.: Regression results relating the froth surface velocity to the stability factors in the copper rougher 1. (gravimetric solids loading used)

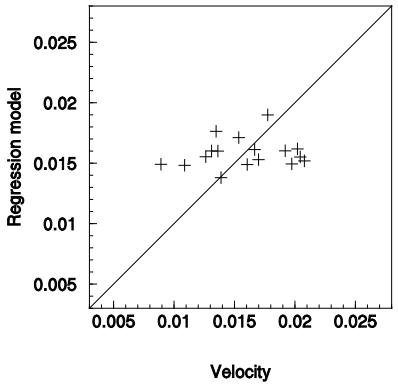

Velocity m/s	Burst rate $1/m^2/s$	Solids loading (GV) kg/m^2	FS bubble size (p^{80}) m	Frother concentration ppm
0.0161	32.5	0.0382	0.0372	102
0.0167	21.2	0.0302	0.047	100
0.0208	20.6	0.0355	0.0415	138
0.0126	49.3	0.0377	0.0353	102
0.0192	29.7	0.0242	0.0458	100
0.0139	29.8	0.0313	0.035	130
0.0136	34.0	0.0241	0.0446	100
0.0202	31.3	0.023	0.0463	98
0.0204	31.5	0.028	0.0418	138
0.0154	28.1	0.0438	0.0455	102
0.0131	30.3	0.0428	0.041	100
0.0135	16.4	0.0296	0.0535	138
0.0197	44.4	0.0303	0.0362	102
0.017	34.2	0.0347	0.0392	100
0.00892	34.8	0.026	0.0392	130
0.0178	17.4	0.0226	0.0609	98
0.0109	40.2	0.026	0.0373	138

Multiple R^2	0.168
Adjusted multiple R^2	-0.11
R^2	0.954
Adjusted R^2	0.944
Standard Error	0.00398
Observations	17

	df	SS	MS	F	Significance of F	
Regression	4	0.00428	0.00107	67.6	1.43e-08	++
Residual	13	0.000205	1.58e-05			
Total	17	0.00448				

	Coefficients	Standard Error	t-Statistics	p-Value		
Intercept	0					
Burst rate large	6.92e-05	0.000104	0.665	0.52	48.0	
Solids loading GV	0.0652	0.132	0.493	0.632	36.8	
FS Bubble size p80	0.26	0.103	2.53	0.0278	97.2	++
Frother concentration	4.56e-06	4.62e-05	0.0987	0.923	7.68	

Table B.66.: Regression results relating the froth surface velocity to the stability factors in the copper rougher 3. (gravimetric solids loading used)

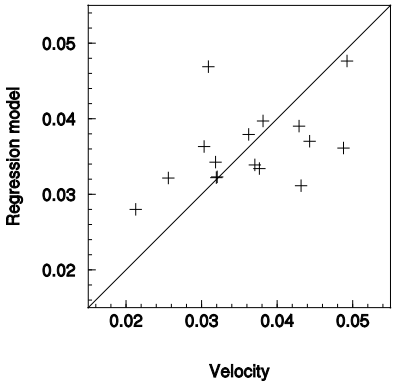

Velocity m/s	Burst rate $1/m^2/s$	Solids loading (GV) kg/m^2	FS bubble size (p^{80}) m	Frother concentration ppm
0.0429	18.1	0.0248	0.0348	102
0.0321	35.4	0.0166	0.0301	100
0.0371	20.9	0.0173	0.0369	138
0.0488	28.6	0.0196	0.0264	102
0.0303	43.6	0.0179	0.0259	100
0.0432	31.7	0.016	0.0296	100
0.0256	43.0	0.0149	0.0262	98
0.0377	26.5	0.0147	0.0295	138
0.0493	22.2	0.0306	0.0321	102
0.0381	24.8	0.0246	0.0344	100
0.0309	25.4	0.0265	0.0347	138
0.0443	41.2	0.018	0.0228	102
0.032	22.1	0.0188	0.033	100
0.0319	32.9	0.0148	0.0265	130
0.0213	30.1	0.0151	0.0357	98
0.0362	33.0	0.0164	0.024	138

Multiple R^2	0.677
Adjusted multiple R^2	0.559
R^2	0.964
Adjusted R^2	0.955
Standard Error	0.00814
Observations	16

	df	SS	MS	F	Significance of F	
Regression	4	0.0213	0.00532	80.4	1.47e-08	++
Residual	12	0.000795	6.62e-05			
Total	16	0.0221				

	Coefficients	Standard Error	t-Statistics	p-Value		
Intercept	0					
Burst rate large	0.000166	0.000209	0.794	0.444	55.6	
Solids loading GV	1.27	0.472	2.69	0.0209	97.9	++
FS Bubble size p80	-0.24	0.442	-0.542	0.599	40.1	
Frother concentration	0.000125	0.000103	1.21	0.25	75.0	

Appendix B: Regression analysis

Table B.67.: Regression results relating the froth surface velocity to the stability factors in the platinum rougher 1. (gravimetric solids loading used)

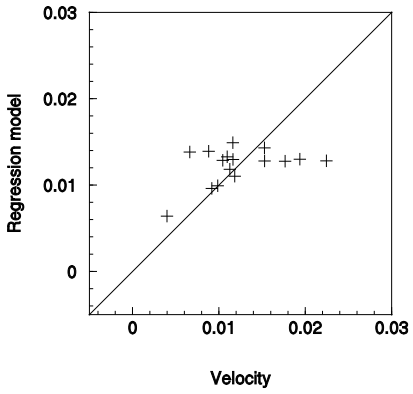

Velocity m/s	Burst rate $1/m^2/s$	Solids loading (GV) kg/m^2	FS bubble size (p^{80}) m	Frother concentration ppm
0.0177	467.0	0.0363	0.0162	60
0.0194	390.0	0.0751	0.0195	60
0.0105	373.0	0.0665	0.00966	60
0.00663	474.0	0.0776	0.0142	40
0.00882	503.0	0.0689	0.0146	40
0.0116	554.0	0.0691	0.0141	40
0.00987	337.0	0.0829	0.0222	20
0.0116	508.0	0.0719	0.0154	20
0.00399	182.0	0.0278	0.0275	60
0.011	396.0	0.0665	0.00991	60
0.0153	447.0	0.0701	0.0111	60
0.0153	377.0	0.0637	0.00985	60
0.00919	387.0	0.0543	0.0203	20
0.0224	483.0	0.0739	0.0122	20
0.0118	404.0	0.0742	0.0176	20
0.0113	510.0	0.0414	0.011	20

Multiple R^2	0.188
Adjusted multiple R^2	-0.107
R^2	0.9
Adjusted R^2	0.875
Standard Error	0.00477
Observations	16

	df	SS	MS	F	Significance of F	
Regression	4	0.00247	0.000618	27.1	6.26e-06	++
Residual	12	0.000273	2.28e-05			
Total	16	0.00275				

	Coefficients	Standard Error	t-Statistics	p-Value		
Intercept	0					
Burst rate large	1.84e-05	1.13e-05	1.63	0.132	86.8	+
Solids loading GV	0.0474	0.0775	0.612	0.553	44.7	
FS Bubble size p80	-0.0614	0.187	-0.328	0.749	25.1	
Frother concentration	5.7e-05	5.77e-05	0.989	0.344	65.6	

Table B.68.: Regression results relating the froth surface velocity to the stability factors in the platinum rougher 3. (gravimetric solids loading used)

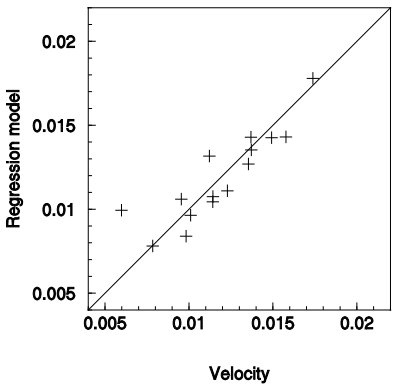

Velocity m/s	Burst rate $1/m^2/s$	Solids loading (GV) kg/m^2	FS bubble size (p^{80}) m	Frother concentration ppm
0.0149	988.0	0.0132	0.0113	60
0.0158	1060.0	0.0294	0.0122	60
0.0101	902.0	0.0143	0.00956	60
0.0114	976.0	0.02	0.0105	40
0.0123	1100.0	0.0248	0.0117	40
0.0135	1100.0	0.0143	0.0119	40
0.00598	1330.0	0.0207	0.0131	20
0.00785	1330.0	0.0226	0.0126	20
0.00954	981.0	0.0203	0.0105	60
0.0174	903.0	0.0139	0.0116	60
0.0137	966.0	0.0182	0.0113	60
0.0112	992.0	0.0152	0.0111	60
0.0137	1140.0	0.0152	0.0124	20
0.0114	1360.0	0.00991	0.0132	20
0.00983	1390.0	0.0149	0.0131	20

Multiple R^2	0.771
Adjusted multiple R^2	0.679
R^2	0.987
Adjusted R^2	0.983
Standard Error	0.00164
Observations	15

	df	SS	MS	F	Significance of F	
Regression	4	0.00223	0.000557	207.0	2.88e-10	++
Residual	11	2.96e-05	2.7e-06			
Total	15	0.00226				

	Coefficients	Standard Error	t-Statistics	p-Value		
Intercept	0					
Burst rate large	-3.12e-05	7.26e-06	-4.3	0.00126	99.9	- -
Solids loading GV	-0.0851	0.0868	-0.98	0.348	65.2	
FS Bubble size p80	4.06	0.776	5.23	0.000281	100.0	++
Frother concentration	3.34e-06	3.44e-05	0.0972	0.924	7.57	

Appendix B: Regression analysis

Table B.69.: Regression results relating the solids recovery rate to the stability factors in the copper rougher 1.

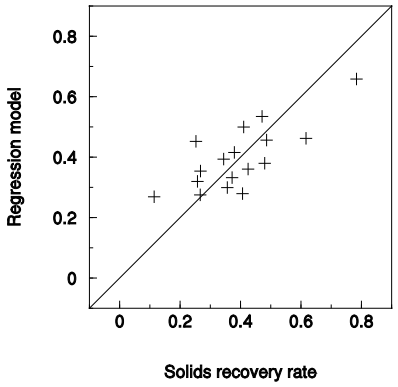

Solids recovery rate t/hr	Burst rate $1/m^2/s$	Solids loading (MV) kg/m^2	FS bubble size (p^{80}) m	Frother concentration ppm
0.258	32.5	0.0307	0.0372	102
0.41	21.2	0.037	0.047	100
0.48	20.6	0.0324	0.0415	138
0.267	49.3	0.0399	0.0353	102
0.487	29.7	0.0371	0.0458	100
0.114	29.8	0.0296	0.035	130
0.38	34.0	0.0341	0.0446	100
0.617	31.3	0.0378	0.0463	98
0.425	31.5	0.0368	0.0418	138
0.253	28.1	0.036	0.0455	102
0.344	30.3	0.0356	0.041	100
0.471	16.4	0.0331	0.0535	138
0.357	44.4	0.0391	0.0362	102
0.268	34.2	0.0343	0.0392	100
0.372	34.8	0.0378	0.0392	130
0.784	17.4	0.0327	0.0609	98
0.407	40.2	0.037	0.0373	138

Multiple R^2	0.698
Adjusted multiple R^2	0.598
R^2	0.945
Adjusted R^2	0.932
Standard Error	0.113
Observations	17

	df	SS	MS	F	Significance of F	
Regression	4	2.85	0.712	55.5	4.81e-08	++
Residual	13	0.167	0.0128			
Total	17	3.01				

	Coefficients	Standard Error	t-Statistics	p-Value		
Intercept	0					
Burst rate large	-0.00359	0.00646	-0.556	0.59	41.0	
Solids loading MV	4.02	13.2	0.305	0.766	23.4	
FS Bubble size p80	11.4	6.06	1.89	0.0855	91.4	+
Frother concentration	-0.0011	0.00136	-0.811	0.435	56.5	

Table B.70.: Regression results relating the solids recovery rate to the stability factors in the copper rougher 3.

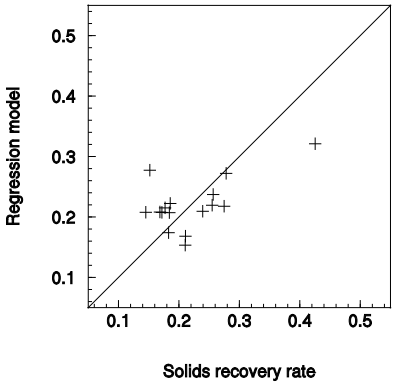

Solids recovery rate t/hr	Burst rate $1/m^2/s$	Solids loading (MV) kg/m^2	FS bubble size (p^{80}) m	Frother concentration ppm
0.239	18.1	0.0218	0.0348	102
0.172	35.4	0.019	0.0301	100
0.169	20.9	0.0222	0.0369	138
0.278	28.6	0.0208	0.0264	102
0.183	43.6	0.0155	0.0259	100
0.145	31.7	0.019	0.0296	100
0.177	43.0	0.0175	0.0262	98
0.275	26.5	0.0195	0.0295	138
0.255	22.2	0.021	0.0321	102
0.186	24.8	0.0219	0.0344	100
0.211	25.4	0.0193	0.0347	138
0.425	41.2	0.021	0.0228	102
0.184	22.1	0.0208	0.033	100
0.152	32.9	0.0208	0.0265	130
0.21	30.1	0.019	0.0357	98
0.257	33.0	0.0179	0.024	138

Multiple R^2	0.357
Adjusted multiple R^2	0.123
R^2	0.944
Adjusted R^2	0.93
Standard Error	0.063
Observations	16

	df	SS	MS	F	Significance of F	
Regression	4	0.799	0.2	50.3	2.12e-07	++
Residual	12	0.0477	0.00397			
Total	16	0.847				

	Coefficients	Standard Error	t-Statistics	p-Value		
Intercept	0					
Burst rate large	0.00101	0.00175	0.58	0.574	42.6	
Solids loading MV	22.2	8.04	2.76	0.0186	98.1	++
FS Bubble size p80	-8.64	4.2	-2.06	0.064	93.6	-
Frother concentration	9.06e-05	0.000874	0.104	0.919	8.07	

Appendix B: Regression analysis

Table B.71.: Regression results relating the solids recovery rate to the stability factors in the platinum rougher 1.

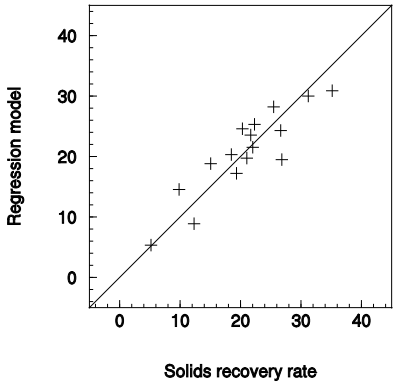

Solids recovery rate kg/hr	Burst rate $1/m^2/s$	Solids loading (MV) kg/m^2	FS bubble size (p^{80}) m	Frother concentration ppm
9.84	467.0	0.0758	0.0162	60
12.3	390.0	0.0749	0.0195	60
25.5	373.0	0.0716	0.00966	60
18.5	474.0	0.0719	0.0142	40
19.3	503.0	0.071	0.0146	40
15.1	554.0	0.0731	0.0141	40
22.0	337.0	0.0793	0.0222	20
22.3	508.0	0.0745	0.0154	20
5.21	182.0	0.0811	0.0275	60
20.3	396.0	0.0697	0.00991	60
26.8	447.0	0.0692	0.0111	60
26.7	377.0	0.0686	0.00985	60
21.0	387.0	0.0757	0.0203	20
31.2	483.0	0.0714	0.0122	20
21.7	404.0	0.074	0.0176	20
35.2	510.0	0.0707	0.011	20

Multiple R^2	0.878
Adjusted multiple R^2	0.833
R^2	0.978
Adjusted R^2	0.972
Standard Error	3.83
Observations	16

	df	SS	MS	F	Significance of F	
Regression	4	7640.0	1910.0	130.0	8.88e-10	++
Residual	12	176.0	14.7			
Total	16	7820.0				

	Coefficients	Standard Error	t-Statistics	p-Value		
Intercept	0					
Burst rate large	-0.0376	0.0159	-2.36	0.038	96.2	- -
Solids loading MV	1150.0	184.0	6.24	6.35e-05	100.0	++
FS Bubble size p80	-2290.0	376.0	-6.09	7.81e-05	100.0	- -
Frother concentration	-0.296	0.0622	-4.75	0.000598	99.9	- -

Table B.72.: Regression results relating the solids recovery rate to the stability factors in the platinum rougher 3.

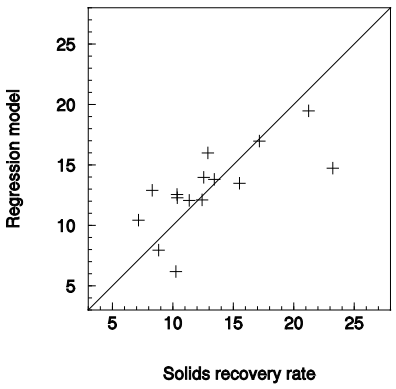

Solids recovery rate kg/hr	Burst rate $l/m^2/s$	Solids loading (MV) kg/m^2	FS bubble size (p^{80}) m	Frother concentration ppm
11.4	988.0	0.0287	0.0113	60
12.6	1060.0	0.0279	0.0122	60
10.3	902.0	0.033	0.00956	60
10.3	976.0	0.0321	0.0105	40
15.5	1100.0	0.0315	0.0117	40
13.4	1100.0	0.0257	0.0119	40
12.9	1330.0	0.036	0.0131	20
8.3	1330.0	0.0336	0.0126	20
8.83	981.0	0.0307	0.0105	60
17.2	903.0	0.0264	0.0116	60
12.4	966.0	0.0233	0.0113	60
7.16	992.0	0.0259	0.0111	60
21.2	1140.0	0.0268	0.0124	20
23.2	1360.0	0.0304	0.0132	20
10.4	1390.0	0.0295	0.0131	20

Multiple R^2	0.509
Adjusted multiple R^2	0.312
R^2	0.947
Adjusted R^2	0.933
Standard Error	3.69
Observations	15

	df	SS	MS	F	Significance of F	
Regression	4	2680.0	670.0	49.3	5.86e-07	++
Residual	11	150.0	13.6			
Total	15	2830.0				

	Coefficients	Standard Error	t-Statistics	p-Value		
Intercept	0					
Burst rate large	-0.0451	0.0199	-2.26	0.0448	95.5	- -
Solid loading MV	118.0	295.0	0.4	0.696	30.4	
FS Bubble size p80	5790.0	1820.0	3.18	0.00881	99.1	++
Frother concentration	-0.207	0.0912	-2.27	0.044	95.6	- -

Table B.73.: Regression results relating the solids recovery rate to the stability factors in the copper rougher 1. (gravimetric solids loading used)

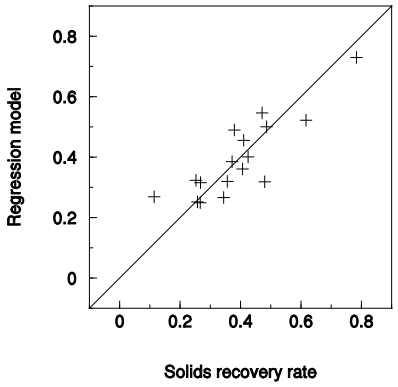

Solids recovery rate t/hr	Burst rate $1/m^2/s$	Solids loading (GV) kg/m^2	FS bubble size (p^{80}) m	Frother concentration ppm
0.258	32.5	0.0382	0.0372	102
0.41	21.2	0.0302	0.047	100
0.48	20.6	0.0355	0.0415	138
0.267	49.3	0.0377	0.0353	102
0.487	29.7	0.0242	0.0458	100
0.114	29.8	0.0313	0.035	130
0.38	34.0	0.0241	0.0446	100
0.617	31.3	0.023	0.0463	98
0.425	31.5	0.028	0.0418	138
0.253	28.1	0.0438	0.0455	102
0.344	30.3	0.0428	0.041	100
0.471	16.4	0.0296	0.0535	138
0.357	44.4	0.0303	0.0362	102
0.268	34.2	0.0347	0.0392	100
0.372	34.8	0.026	0.0392	130
0.784	17.4	0.0226	0.0609	98
0.407	40.2	0.026	0.0373	138

Multiple R^2	0.742
Adjusted multiple R^2	0.656
R^2	0.967
Adjusted R^2	0.959
Standard Error	0.0876
Observations	17

	df	SS	MS	F	Significance of F	
Regression	4	2.91	0.728	94.9	1.75e-09	++
Residual	13	0.0998	0.00768			
Total	17	3.01				

	Coefficients	Standard Error	t-Statistics	p-Value		
Intercept	0					
Burst rate large	0.00126	0.00229	0.548	0.594	40.6	
Solids loading GV	-8.68	2.92	-2.98	0.0126	98.7	- -
FS Bubble size p80	15.2	2.27	6.71	3.35e-05	100.0	++
Frother concentration	-0.000222	0.00102	-0.218	0.831	16.9	

Table B.74.: Regression results relating the solids recovery rate to the stability factors in the copper rougher 3. (gravimetric solids loading used)

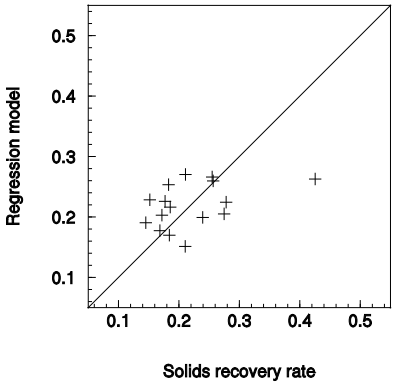

Solids recovery rate t/hr	Burst rate $1/m^2/s$	Solids loading (GV) kg/m^2	FS bubble size (p^{80}) m	Frother concentration ppm
0.239	18.1	0.0248	0.0348	102
0.172	35.4	0.0166	0.0301	100
0.169	20.9	0.0173	0.0369	138
0.278	28.6	0.0196	0.0264	102
0.183	43.6	0.0179	0.0259	100
0.145	31.7	0.016	0.0296	100
0.177	43.0	0.0149	0.0262	98
0.275	26.5	0.0147	0.0295	138
0.255	22.2	0.0306	0.0321	102
0.186	24.8	0.0246	0.0344	100
0.211	25.4	0.0265	0.0347	138
0.425	41.2	0.018	0.0228	102
0.184	22.1	0.0188	0.033	100
0.152	32.9	0.0148	0.0265	130
0.21	30.1	0.0151	0.0357	98
0.257	33.0	0.0164	0.024	138

Multiple R^2	0.324
Adjusted multiple R^2	0.0784
R^2	0.929
Adjusted R^2	0.911
Standard Error	0.0709
Observations	16

	df	SS	MS	F	Significance of F	
Regression	4	0.786	0.197	39.0	8.67e-07	++
Residual	12	0.0604	0.00503			
Total	16	0.847				

	Coefficients	Standard Error	t-Statistics	p-Value		
Intercept	0					
Burst rate large	0.00282	0.00182	1.55	0.15	85.0	+
Solids loading GV	7.67	4.11	1.87	0.089	91.1	+
FS Bubble size p80	-4.23	3.85	-1.1	0.296	70.4	
Frother concentration	0.00103	0.000901	1.14	0.278	72.2	

Appendix B: Regression analysis

Table B.75.: Regression results relating the solids recovery rate to the stability factors in the platinum rougher 1. (gravimetric solids loading used)

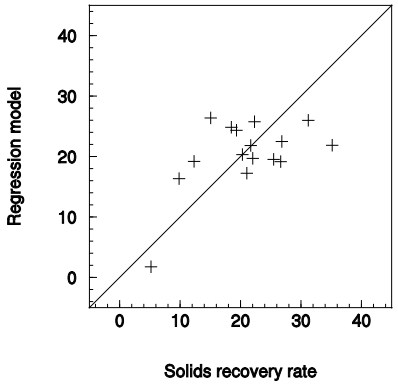

Solids recovery rate kg/hr	Burst rate $1/m^2/s$	Solids loading (GV) kg/m^2	FS bubble size (p^{80}) m	Frother concentration ppm
9.84	467.0	0.0363	0.0162	60
12.3	390.0	0.0751	0.0195	60
25.5	373.0	0.0665	0.00966	60
18.5	474.0	0.0776	0.0142	40
19.3	503.0	0.0689	0.0146	40
15.1	554.0	0.0691	0.0141	40
22.0	337.0	0.0829	0.0222	20
22.3	508.0	0.0719	0.0154	20
5.21	182.0	0.0278	0.0275	60
20.3	396.0	0.0665	0.00991	60
26.8	447.0	0.0701	0.0111	60
26.7	377.0	0.0637	0.00985	60
21.0	387.0	0.0543	0.0203	20
31.2	483.0	0.0739	0.0122	20
21.7	404.0	0.0742	0.0176	20
35.2	510.0	0.0414	0.011	20

Multiple R^2	0.869
Adjusted multiple R^2	0.822
R^2	0.918
Adjusted R^2	0.897
Standard Error	7.31
Observations	16

	df	SS	MS	F	Significance of F	
Regression	4	7180.0	1790.0	33.6	1.99e-06	++
Residual	12	642.0	53.5			
Total	16	7820.0				

	Coefficients	Standard Error	t-Statistics	p-Value		
Intercept	0					
Burst rate large	0.0364	0.0174	2.1	0.0597	94.0	+
Solids loading GV	166.0	119.0	1.4	0.189	81.1	+
FS Bubble size p80	-245.0	287.0	-0.855	0.411	58.9	
Frother concentration	-0.0458	0.0884	-0.518	0.615	38.5	

Table B.76.: Regression results relating the solids recovery rate to the stability factors in the platinum rougher 3. (gravimetric solids loading used)

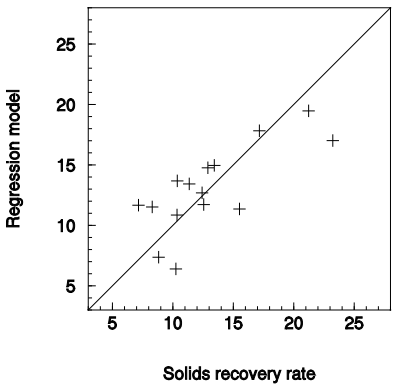

Solids recovery rate kg/hr	Burst rate $l/m^2/s$	Solids loading (GV) kg/m^2	FS bubble size (p^{80}) m	Frother concentration ppm
11.4	988.0	0.0132	0.0113	60
12.6	1060.0	0.0294	0.0122	60
10.3	902.0	0.0143	0.00956	60
10.3	976.0	0.02	0.0105	40
15.5	1100.0	0.0248	0.0117	40
13.4	1100.0	0.0143	0.0119	40
12.9	1330.0	0.0207	0.0131	20
8.3	1330.0	0.0226	0.0126	20
8.83	981.0	0.0203	0.0105	60
17.2	903.0	0.0139	0.0116	60
12.4	966.0	0.0182	0.0113	60
7.16	992.0	0.0152	0.0111	60
21.2	1140.0	0.0152	0.0124	20
23.2	1360.0	0.00991	0.0132	20
10.4	1390.0	0.0149	0.0131	20

Multiple R^2	0.584
Adjusted multiple R^2	0.417
R^2	0.954
Adjusted R^2	0.942
Standard Error	3.43
Observations	15

	df	SS	MS	F	Significance of F	
Regression	4	2700.0	676.0	57.5	2.65e-07	++
Residual	11	129.0	11.8			
Total	15	2830.0				

	Coefficients	Standard Error	t-Statistics	p-Value		
Intercept	0					
Burst rate large	-0.0384	0.0152	-2.53	0.028	97.2	- -
Solids loading GV	-251.0	181.0	-1.38	0.194	80.6	-
FS Bubble size p80	5660.0	1620.0	3.49	0.00503	99.5	++
Frother concentration	-0.159	0.0718	-2.21	0.0488	95.1	- -

Appendix B: Regression analysis

Table B.77.: Regression results relating the water recovery rate to the stability factors in the copper rougher 1.

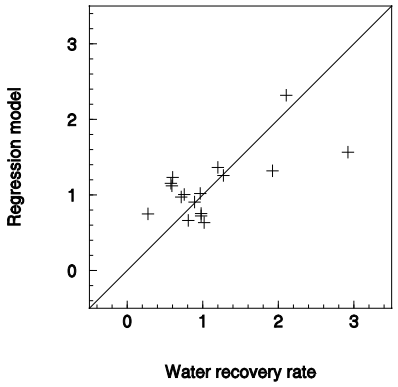

Water recovery rate t/hr	Burst rate $1/m^2/s$	Solids loading (MV) kg/m^2	FS bubble size (p^{80}) m	Frother concentration ppm
0.579	32.5	0.0307	0.0372	102
0.968	21.2	0.037	0.047	100
1.02	20.6	0.0324	0.0415	138
0.715	49.3	0.0399	0.0353	102
1.27	29.7	0.0371	0.0458	100
0.275	29.8	0.0296	0.035	130
2.92	34.0	0.0341	0.0446	100
1.92	31.3	0.0378	0.0463	98
0.98	31.5	0.0368	0.0418	138
0.603	28.1	0.036	0.0455	102
0.756	30.3	0.0356	0.041	100
1.2	16.4	0.0331	0.0535	138
0.893	44.4	0.0391	0.0362	102
0.593	34.2	0.0343	0.0392	100
0.809	34.8	0.0378	0.0392	130
2.11	17.4	0.0327	0.0609	98
0.979	40.2	0.037	0.0373	138

Multiple R^2	0.508
Adjusted multiple R^2	0.344
R^2	0.856
Adjusted R^2	0.823
Standard Error	0.55
Observations	17

	df	SS	MS	F	Significance of F	
Regression	4	23.4	5.84	19.3	2.21e-05	++
Residual	13	3.93	0.302			
Total	17	27.3				

	Coefficients	Standard Error	t-Statistics	p-Value		
Intercept	0					
Burst rate large	0.0398	0.0314	1.27	0.23	77.0	
Solids loading MV	-76.4	64.0	-1.19	0.258	74.2	
FS Bubble size p80	79.6	29.4	2.71	0.0204	98.0	++
Frother concentration	-0.0074	0.0066	-1.12	0.286	71.4	

Table B.78.: Regression results relating the water recovery rate to the stability factors in the copper rougher 3.

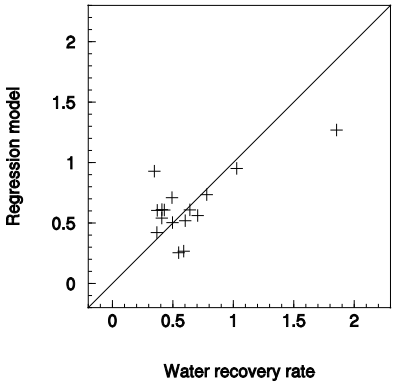

Water recovery rate t/hr	Burst rate $1/m^2/s$	Solids loading (MV) kg/m^2	FS bubble size (p^{80}) m	Frother concentration ppm
0.602	18.1	0.0218	0.0348	102
0.43	35.4	0.019	0.0301	100
0.368	20.9	0.0222	0.0369	138
1.03	28.6	0.0208	0.0264	102
0.497	43.6	0.0155	0.0259	100
0.371	31.7	0.019	0.0296	100
0.493	43.0	0.0175	0.0262	98
0.706	26.5	0.0195	0.0295	138
0.641	22.2	0.021	0.0321	102
0.41	24.8	0.0219	0.0344	100
0.549	25.4	0.0193	0.0347	138
1.85	41.2	0.021	0.0228	102
0.408	22.1	0.0208	0.033	100
0.348	32.9	0.0208	0.0265	130
0.59	30.1	0.019	0.0357	98
0.781	33.0	0.0179	0.024	138

Multiple R^2	0.472
Adjusted multiple R^2	0.28
R^2	0.869
Adjusted R^2	0.836
Standard Error	0.303
Observations	16

	df	SS	MS	F	Significance of F	
Regression	4	7.33	1.83	19.9	3.12e-05	++
Residual	12	1.1	0.0919			
Total	16	8.43				

	Coefficients	Standard Error	t-Statistics	p-Value		
Intercept	0					
Burst rate large	0.00764	0.0084	0.91	0.382	61.8	
Solids loading MV	112.0	38.7	2.9	0.0145	98.5	++
FS Bubble size p80	-54.2	20.2	-2.68	0.0213	97.9	- -
Frother concentration	-0.00166	0.0042	-0.395	0.7	30.0	

Appendix B: Regression analysis

Table B.79.: Regression results relating the water recovery rate to the stability factors in the platinum rougher 1.

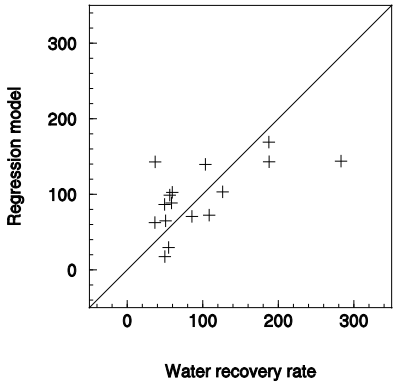

Water recovery rate kg/hr	Burst rate $1/m^2/s$	Solids loading (MV) kg/m^2	FS bubble size (p^{80}) m	Frother concentration ppm
36.7	467.0	0.0758	0.0162	60
54.9	390.0	0.0749	0.0195	60
188.0	373.0	0.0716	0.00966	60
58.7	474.0	0.0719	0.0142	40
50.8	503.0	0.071	0.0146	40
85.8	554.0	0.0731	0.0141	40
49.5	337.0	0.0793	0.0222	20
59.7	508.0	0.0745	0.0154	20
49.9	182.0	0.0811	0.0275	60
37.0	396.0	0.0697	0.00991	60
126.0	447.0	0.0692	0.0111	60
188.0	377.0	0.0686	0.00985	60
109.0	387.0	0.0757	0.0203	20
104.0	483.0	0.0714	0.0122	20
56.4	404.0	0.074	0.0176	20
283.0	510.0	0.0707	0.011	20

Multiple R^2	0.396
Adjusted multiple R^2	0.176
R^2	0.796
Adjusted R^2	0.746
Standard Error	61.1
Observations	16

	df	SS	MS	F	Significance of F	
Regression	4	175000.0	43800.0	11.7	0.000411	++
Residual	12	44800.0	3730.0			
Total	16	220000.0				

	Coefficients	Standard Error	t-Statistics	p-Value		
Intercept	0					
Burst rate large	-0.346	0.254	-1.36	0.201	79.9	
Solids loading MV	7380.0	2930.0	2.52	0.0286	97.1	++
FS Bubble size p80	-16100.0	6000.0	-2.68	0.0213	97.9	- -
Frother concentration	-1.25	0.993	-1.26	0.234	76.6	

Table B.80.: Regression results relating the water recovery rate to the stability factors in the platinum rougher 3.

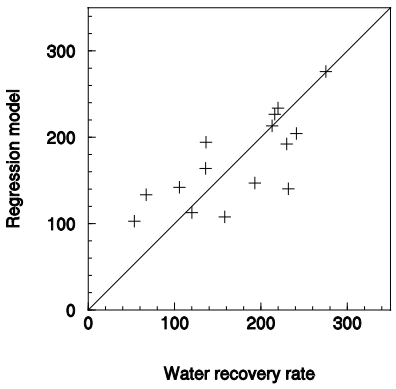

Water recovery rate kg/hr	Burst rate $l/m^2/s$	Solids loading (MV) kg/m^2	FS bubble size (p^{80}) m	Frother concentration ppm
241.0	988.0	0.0287	0.0113	60
220.0	1060.0	0.0279	0.0122	60
158.0	902.0	0.033	0.00956	60
193.0	976.0	0.0321	0.0105	40
136.0	1100.0	0.0315	0.0117	40
230.0	1100.0	0.0257	0.0119	40
67.2	1330.0	0.036	0.0131	20
53.4	1330.0	0.0336	0.0126	20
106.0	981.0	0.0307	0.0105	60
275.0	903.0	0.0264	0.0116	60
216.0	966.0	0.0233	0.0113	60
136.0	992.0	0.0259	0.0111	60
213.0	1140.0	0.0268	0.0124	20
232.0	1360.0	0.0304	0.0132	20
120.0	1390.0	0.0295	0.0131	20

Multiple R^2	0.605
Adjusted multiple R^2	0.447
R^2	0.945
Adjusted R^2	0.929
Standard Error	50.8
Observations	15

	df	SS	MS	F	Significance of F	
Regression	4	485000.0	121000.0	46.9	7.61e-07	++
Residual	11	28400.0	2580.0			
Total	15	513000.0				

	Coefficients	Standard Error	t-Statistics	p-Value		
Intercept	0					
Burst rate large	-0.571	0.275	-2.08	0.0619	93.8	-
Solid loading MV	-2600.0	4060.0	-0.64	0.535	46.5	
FS Bubble size p80	75700.0	25100.0	3.01	0.0119	98.8	++
Frother concentration	-0.255	1.26	-0.203	0.843	15.7	

Appendix B: Regression analysis

Table B.81.: Regression results relating the water recovery rate to the stability factors in the copper rougher 1. (gravimetric solids loading used)

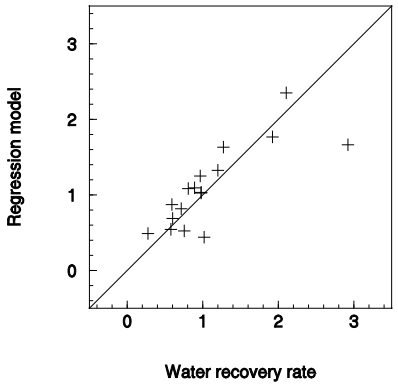

Water recovery rate t/hr	Burst rate $1/m^2/s$	Solids loading (GV) kg/m^2	FS bubble size (p^{80}) m	Frother concentration ppm
0.579	32.5	0.0382	0.0372	102
0.968	21.2	0.0302	0.047	100
1.02	20.6	0.0355	0.0415	138
0.715	49.3	0.0377	0.0353	102
1.27	29.7	0.0242	0.0458	100
0.275	29.8	0.0313	0.035	130
2.92	34.0	0.0241	0.0446	100
1.92	31.3	0.023	0.0463	98
0.98	31.5	0.028	0.0418	138
0.603	28.1	0.0438	0.0455	102
0.756	30.3	0.0428	0.041	100
1.2	16.4	0.0296	0.0535	138
0.893	44.4	0.0303	0.0362	102
0.593	34.2	0.0347	0.0392	100
0.809	34.8	0.026	0.0392	130
2.11	17.4	0.0226	0.0609	98
0.979	40.2	0.026	0.0373	138

Multiple R^2	0.636
Adjusted multiple R^2	0.514
R^2	0.907
Adjusted R^2	0.885
Standard Error	0.443
Observations	17

	df	SS	MS	F	Significance of F	
Regression	4	24.8	6.19	31.6	1.38e-06	++
Residual	13	2.55	0.196			
Total	17	27.3				

	Coefficients	Standard Error	t-Statistics	p-Value		
Intercept	0					
Burst rate large	0.0214	0.0116	1.85	0.0913	90.9	+
Solids loading GV	-44.8	14.7	-3.04	0.0112	98.9	- -
FS Bubble size p80	59.3	11.4	5.18	0.000304	100.0	++
Frother concentration	-0.00634	0.00514	-1.23	0.243	75.7	

Table B.82.: Regression results relating the water recovery rate to the stability factors in the copper rougher 3. (gravimetric solids loading used)

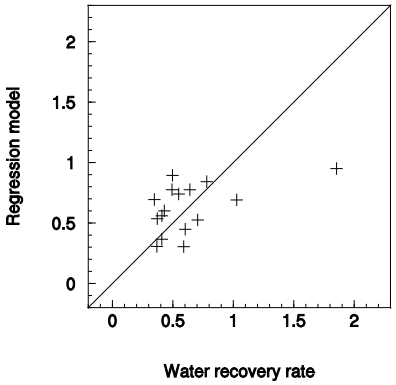

Water recovery rate t/hr	Burst rate $1/m^2/s$	Solids loading (GV) kg/m^2	FS bubble size (p^{80}) m	Frother concentration ppm
0.602	18.1	0.0248	0.0348	102
0.43	35.4	0.0166	0.0301	100
0.368	20.9	0.0173	0.0369	138
1.03	28.6	0.0196	0.0264	102
0.497	43.6	0.0179	0.0259	100
0.371	31.7	0.016	0.0296	100
0.493	43.0	0.0149	0.0262	98
0.706	26.5	0.0147	0.0295	138
0.641	22.2	0.0306	0.0321	102
0.41	24.8	0.0246	0.0344	100
0.549	25.4	0.0265	0.0347	138
1.85	41.2	0.018	0.0228	102
0.408	22.1	0.0188	0.033	100
0.348	32.9	0.0148	0.0265	130
0.59	30.1	0.0151	0.0357	98
0.781	33.0	0.0164	0.024	138

Multiple R^2	0.354
Adjusted multiple R^2	0.12
R^2	0.814
Adjusted R^2	0.767
Standard Error	0.362
Observations	16

	df	SS	MS	F	Significance of F	
Regression	4	6.86	1.72	13.1	0.000245	++
Residual	12	1.57	0.131			
Total	16	8.43				

	Coefficients	Standard Error	t-Statistics	p-Value		
Intercept	0					
Burst rate large	0.0168	0.00929	1.8	0.0989	90.1	+
Solids loading GV	32.0	21.0	1.53	0.155	84.5	+
FS Bubble size p80	-27.8	19.6	-1.41	0.185	81.5	-
Frother concentration	0.0031	0.00459	0.675	0.513	48.7	

Appendix B: Regression analysis

Table B.83.: Regression results relating the water recovery rate to the stability factors in the platinum rougher 1. (gravimetric solids loading used)

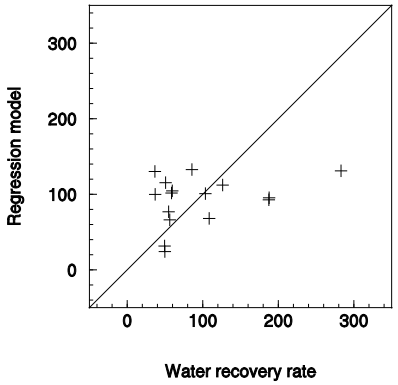

Water recovery rate kg/hr	Burst rate $1/m^2/s$	Solids loading (GV) kg/m^2	FS bubble size (p^{80}) m	Frother concentration ppm
36.7	467.0	0.0363	0.0162	60
54.9	390.0	0.0751	0.0195	60
188.0	373.0	0.0665	0.00966	60
58.7	474.0	0.0776	0.0142	40
50.8	503.0	0.0689	0.0146	40
85.8	554.0	0.0691	0.0141	40
49.5	337.0	0.0829	0.0222	20
59.7	508.0	0.0719	0.0154	20
49.9	182.0	0.0278	0.0275	60
37.0	396.0	0.0665	0.00991	60
126.0	447.0	0.0701	0.0111	60
188.0	377.0	0.0637	0.00985	60
109.0	387.0	0.0543	0.0203	20
104.0	483.0	0.0739	0.0122	20
56.4	404.0	0.0742	0.0176	20
283.0	510.0	0.0414	0.011	20

Multiple R^2	0.578
Adjusted multiple R^2	0.424
R^2	0.695
Adjusted R^2	0.619
Standard Error	74.7
Observations	16

	df	SS	MS	F	Significance of F	
Regression	4	153000.0	38200.0	6.84	0.00415	++
Residual	12	67000.0	5590.0			
Total	16	220000.0				

	Coefficients	Standard Error	t-Statistics	p-Value		
Intercept	0					
Burst rate large	0.322	0.177	1.82	0.0966	90.3	+
Solids loading GV	-595.0	1210.0	-0.49	0.634	36.6	
FS Bubble size p80	-1670.0	2930.0	-0.571	0.58	42.0	
Frother concentration	0.47	0.903	0.521	0.613	38.7	

Table B.84.: Regression results relating the water recovery rate to the stability factors in the platinum rougher 3. (gravimetric solids loading used)

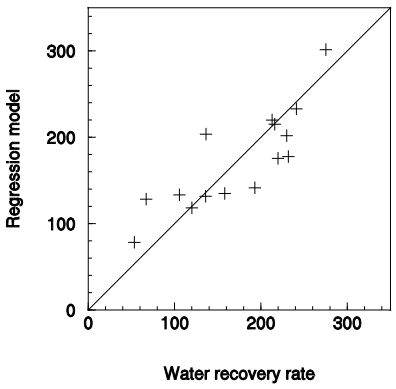

Water recovery rate kg/hr	Burst rate $l/m^2/s$	Solids loading (GV) kg/m^2	FS bubble size (p^{80}) m	Frother concentration ppm
241.0	988.0	0.0132	0.0113	60
220.0	1060.0	0.0294	0.0122	60
158.0	902.0	0.0143	0.00956	60
193.0	976.0	0.02	0.0105	40
136.0	1100.0	0.0248	0.0117	40
230.0	1100.0	0.0143	0.0119	40
67.2	1330.0	0.0207	0.0131	20
53.4	1330.0	0.0226	0.0126	20
106.0	981.0	0.0203	0.0105	60
275.0	903.0	0.0139	0.0116	60
216.0	966.0	0.0182	0.0113	60
136.0	992.0	0.0152	0.0111	60
213.0	1140.0	0.0152	0.0124	20
232.0	1360.0	0.00991	0.0132	20
120.0	1390.0	0.0149	0.0131	20

Multiple R^2	0.703
Adjusted multiple R^2	0.584
R^2	0.962
Adjusted R^2	0.952
Standard Error	41.9
Observations	15

	df	SS	MS	F	Significance of F	
Regression	4	494000.0	123000.0	70.3	9.21e-08	++
Residual	11	19300.0	1760.0			
Total	15	513000.0				

	Coefficients	Standard Error	t-Statistics	p-Value		
Intercept	0					
Burst rate large	-0.628	0.185	-3.39	0.00607	99.4	- -
Solids loading GV	-5340.0	2220.0	-2.41	0.0347	96.5	- -
FS Bubble size p80	82200.0	19800.0	4.15	0.00161	99.8	++
Frother concentration	-0.144	0.878	-0.164	0.873	12.7	

Table B.85.: Regression results relating the concentrate grade to the stability factors in the copper rougher 1.

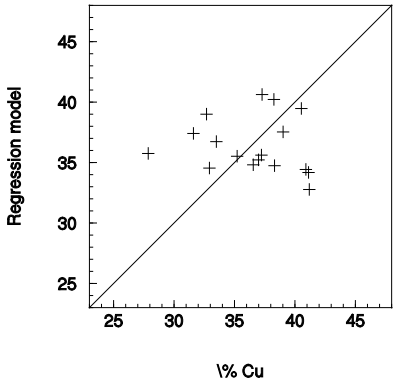

% Cu	Burst rate	Solids loading (MV)	FS bubble size (p^{80})	Frother concentration
41.2	32.5	0.0307	0.0372	102
38.3	21.2	0.037	0.047	100
39.0	20.6	0.0324	0.0415	138
31.6	49.3	0.0399	0.0353	102
35.2	29.7	0.0371	0.0458	100
37.2	29.8	0.0296	0.035	130
36.6	34.0	0.0341	0.0446	100
27.9	31.3	0.0378	0.0463	98
38.3	31.5	0.0368	0.0418	138
37.0	28.1	0.036	0.0455	102
40.9	30.3	0.0356	0.041	100
32.7	16.4	0.0331	0.0535	138
33.5	44.4	0.0391	0.0362	102
41.1	34.2	0.0343	0.0392	100
40.5	34.8	0.0378	0.0392	130
32.9	17.4	0.0327	0.0609	98
37.3	40.2	0.037	0.0373	138

Multiple R^2	0.432
Adjusted multiple R^2	0.243
R^2	0.985
Adjusted R^2	0.981
Standard Error	5.19
Observations	17

	df	SS	MS	F	Significance of F	
Regression	4	22600.0	5650.0	210.0	1.15e-11	++
Residual	13	350.0	26.9			
Total	17	22900.0				

	Coefficients	Standard Error	t-Statistics	p-Value		
Intercept	0					
Burst rate large	0.107	0.296	0.363	0.724	27.6	
Solids loading MV	336.0	604.0	0.556	0.59	41.0	
FS Bubble size p80	138.0	278.0	0.496	0.63	37.0	
Frother concentration	0.136	0.0623	2.18	0.0519	94.8	+

Table B.86.: Regression results relating the concentrate grade to the stability factors in the copper rougher 3.

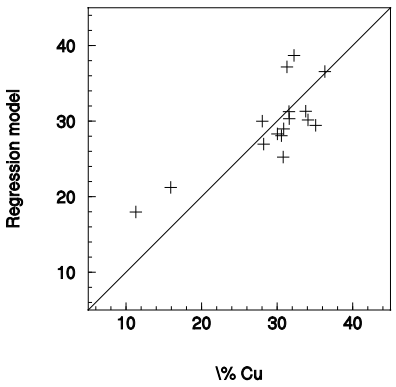

% Cu	Burst rate	Solids loading (MV)	FS bubble size (p^{80})	Frother concentration
28.0	18.1	0.0218	0.0348	102
31.6	35.4	0.019	0.0301	100
36.3	20.9	0.0222	0.0369	138
15.9	28.6	0.0208	0.0264	102
33.8	43.6	0.0155	0.0259	100
30.9	31.7	0.019	0.0296	100
30.0	43.0	0.0175	0.0262	98
31.6	26.5	0.0195	0.0295	138
30.6	22.2	0.021	0.0321	102
34.1	24.8	0.0219	0.0344	100
32.2	25.4	0.0193	0.0347	138
11.3	41.2	0.021	0.0228	102
35.1	22.1	0.0208	0.033	100
30.8	32.9	0.0208	0.0265	130
31.3	30.1	0.019	0.0357	98
28.2	33.0	0.0179	0.024	138

Multiple R^2	0.633
Adjusted multiple R^2	0.5
R^2	0.983
Adjusted R^2	0.978
Standard Error	4.59
Observations	16

	df	SS	MS	F	Significance of F	
Regression	4	14300.0	3580.0	170.0	1.9e-10	++
Residual	12	253.0	21.1			
Total	16	14600.0				

	Coefficients	Standard Error	t-Statistics	p-Value		
Intercept	0					
Burst rate large	0.179	0.127	1.41	0.186	81.4	+
Solids loading MV	-1570.0	586.0	-2.68	0.0215	97.8	- -
FS Bubble size p80	1430.0	306.0	4.68	0.000675	99.9	++
Frother concentration	0.108	0.0637	1.69	0.118	88.2	+

Appendix B: Regression analysis

Table B.87.: Regression results relating the concentrate grade to the stability factors in the platinum rougher 1.

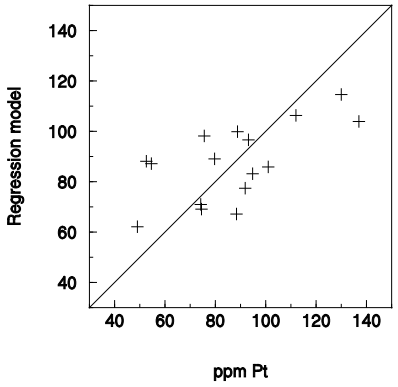

ppm Pt ppm	Burst rate $l/m^2/s$	Solids loading (MV) kg/m^2	FS bubble size (p^{80}) m	Frother concentration ppm
137	467.0	0.0758	0.0162	60
75.6	390.0	0.0749	0.0195	60
49.0	373.0	0.0716	0.00966	60
93.2	474.0	0.0719	0.0142	40
112	503.0	0.071	0.0146	40
130	554.0	0.0731	0.0141	40
91.8	337.0	0.0793	0.0222	20
88.8	508.0	0.0745	0.0154	20
74.5	182.0	0.0811	0.0275	60
74.2	396.0	0.0697	0.00991	60
52.6	447.0	0.0692	0.0111	60
88.4	377.0	0.0686	0.00985	60
54.6	387.0	0.0757	0.0203	20
101	483.0	0.0714	0.0122	20
94.8	404.0	0.074	0.0176	20
79.7	510.0	0.0707	0.011	20

Multiple R^2	0.476
Adjusted multiple R^2	0.285
R^2	0.957
Adjusted R^2	0.946
Standard Error	21.7
Observations	16

	df	SS	MS	F	Significance of F	
Regression	4	126000.0	31500.0	66.8	4.24e-08	++
Residual	12	5650.0	471.0			
Total	16	131000.0				

	Coefficients	Standard Error	t-Statistics	p-Value		
Intercept	0					
Burst rate large	0.244	0.0903	2.71	0.0204	98.0	++
Solids loading MV	-1160.0	1040.0	-1.11	0.291	70.9	
FS Bubble size p80	3620.0	2130.0	1.7	0.117	88.3	+
Frother concentration	0.311	0.353	0.88	0.398	60.2	

Table B.88.: Regression results relating the concentrate grade to the stability factors in the platinum rougher 3.

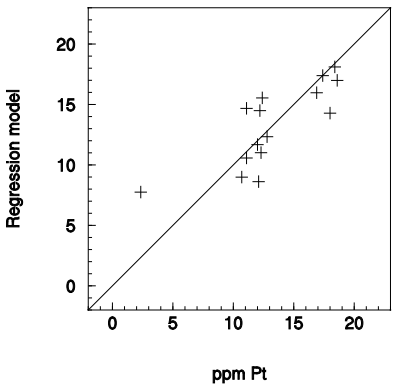

ppm Pt ppm	Burst rate l/m^2/s	Solids loading (MV) kg/m^2	FS bubble size (p^{80}) m	Frother concentration ppm
12.8	988.0	0.0287	0.0113	60
12.3	1060.0	0.0279	0.0122	60
18.4	902.0	0.033	0.00956	60
11.1	976.0	0.0321	0.0105	40
18	1100.0	0.0315	0.0117	40
11.1	1100.0	0.0257	0.0119	40
18.6	1330.0	0.036	0.0131	20
17.4	1330.0	0.0336	0.0126	20
16.9	981.0	0.0307	0.0105	60
2.35	903.0	0.0264	0.0116	60
10.7	966.0	0.0233	0.0113	60
12	992.0	0.0259	0.0111	60
12.1	1140.0	0.0268	0.0124	20
12.2	1360.0	0.0304	0.0132	20
12.4	1390.0	0.0295	0.0131	20

Multiple R^2	0.631
Adjusted multiple R^2	0.483
R^2	0.968
Adjusted R^2	0.959
Standard Error	2.89
Observations	15

	df	SS	MS	F	Significance of F	
Regression	4	2780.0	695.0	83.3	3.76e-08	++
Residual	11	91.7	8.34			
Total	15	2870.0				

	Coefficients	Standard Error	t-Statistics	p-Value		
Intercept	0					
Burst rate large	0.0307	0.0156	1.97	0.0751	92.5	+
Solid loading MV	534.0	231.0	2.31	0.0411	95.9	++
FS Bubble size p80	-3430.0	1430.0	-2.4	0.0353	96.5	- -
Frother concentration	0.0931	0.0715	1.3	0.219	78.1	

Table B.89.: Regression results relating the concentrate grade to the stability factors in the copper rougher 1. (gravimetric solids loading used)

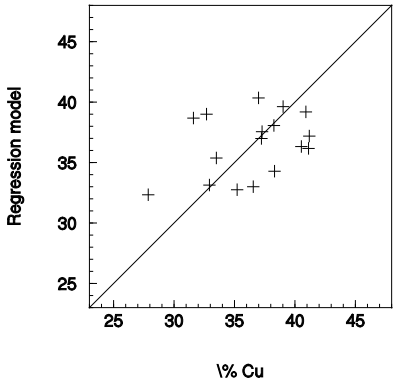

% Cu	Burst rate	Solids loading (GV)	FS bubble size (p^{80})	Frother concentration
41.2	32.5	0.0382	0.0372	102
38.3	21.2	0.0302	0.047	100
39.0	20.6	0.0355	0.0415	138
31.6	49.3	0.0377	0.0353	102
35.2	29.7	0.0242	0.0458	100
37.2	29.8	0.0313	0.035	130
36.6	34.0	0.0241	0.0446	100
27.9	31.3	0.023	0.0463	98
38.3	31.5	0.028	0.0418	138
37.0	28.1	0.0438	0.0455	102
40.9	30.3	0.0428	0.041	100
32.7	16.4	0.0296	0.0535	138
33.5	44.4	0.0303	0.0362	102
41.1	34.2	0.0347	0.0392	100
40.5	34.8	0.026	0.0392	130
32.9	17.4	0.0226	0.0609	98
37.3	40.2	0.026	0.0373	138

Multiple R^2	0.444
Adjusted multiple R^2	0.259
R^2	0.99
Adjusted R^2	0.988
Standard Error	4.13
Observations	17

	df	SS	MS	F	Significance of F	
Regression	4	22700.0	5680.0	333.0	5.95e-13	++
Residual	13	222.0	17.0			
Total	17	22900.0				

	Coefficients	Standard Error	t-Statistics	p-Value		
Intercept	0					
Burst rate large	0.121	0.108	1.12	0.288	71.2	
Solids loading GV	389.0	137.0	2.83	0.0164	98.4	++
FS Bubble size p80	180.0	107.0	1.69	0.119	88.1	+
Frother concentration	0.115	0.048	2.4	0.0355	96.4	++

Table B.90.: Regression results relating the concentrate grade to the stability factors in the copper rougher 3. (gravimetric solids loading used)

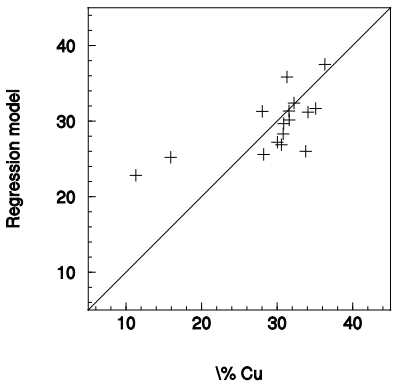

% Cu	Burst rate	Solids loading (GV)	FS bubble size (p^{80})	Frother concentration
28.0	18.1	0.0248	0.0348	102
31.6	35.4	0.0166	0.0301	100
36.3	20.9	0.0173	0.0369	138
15.9	28.6	0.0196	0.0264	102
33.8	43.6	0.0179	0.0259	100
30.9	31.7	0.016	0.0296	100
30.0	43.0	0.0149	0.0262	98
31.6	26.5	0.0147	0.0295	138
30.6	22.2	0.0306	0.0321	102
34.1	24.8	0.0246	0.0344	100
32.2	25.4	0.0265	0.0347	138
11.3	41.2	0.018	0.0228	102
35.1	22.1	0.0188	0.033	100
30.8	32.9	0.0148	0.0265	130
31.3	30.1	0.0151	0.0357	98
28.2	33.0	0.0164	0.024	138

Multiple R^2	0.49
Adjusted multiple R^2	0.304
R^2	0.975
Adjusted R^2	0.968
Standard Error	5.55
Observations	16

	df	SS	MS	F	Significance of F	
Regression	4	14200.0	3550.0	115.0	1.84e-09	++
Residual	12	370.0	30.9			
Total	16	14600.0				

	Coefficients	Standard Error	t-Statistics	p-Value		
Intercept	0					
Burst rate large	0.0518	0.143	0.363	0.723	27.7	
Solids loading GV	-339.0	322.0	-1.05	0.315	68.5	
FS Bubble size p80	993.0	302.0	3.29	0.0072	99.3	++
Frother concentration	0.0408	0.0706	0.578	0.575	42.5	

Appendix B: Regression analysis

Table B.91.: Regression results relating the concentrate grade to the stability factors in the platinum rougher 1. (gravimetric solids loading used)

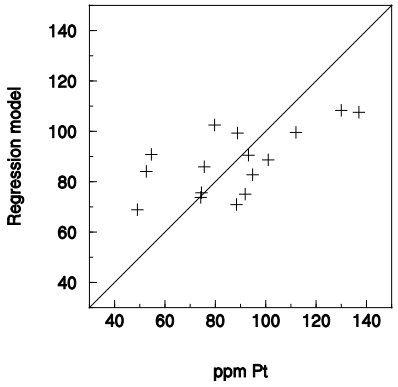

ppm Pt ppm	Burst rate 1/m^2/s	Solids loading (GV) kg/m^2	FS bubble size (p^{80}) m	Frother concentration ppm
137	467.0	0.0363	0.0162	60
75.6	390.0	0.0751	0.0195	60
49.0	373.0	0.0665	0.00966	60
93.2	474.0	0.0776	0.0142	40
112	503.0	0.0689	0.0146	40
130	554.0	0.0691	0.0141	40
91.8	337.0	0.0829	0.0222	20
88.8	508.0	0.0719	0.0154	20
74.5	182.0	0.0278	0.0275	60
74.2	396.0	0.0665	0.00991	60
52.6	447.0	0.0701	0.0111	60
88.4	377.0	0.0637	0.00985	60
54.6	387.0	0.0543	0.0203	20
101	483.0	0.0739	0.0122	20
94.8	404.0	0.0742	0.0176	20
79.7	510.0	0.0414	0.011	20

Multiple R^2	0.44
Adjusted multiple R^2	0.237
R^2	0.956
Adjusted R^2	0.945
Standard Error	22.0
Observations	16

	df	SS	MS	F	Significance of F	
Regression	4	126000.0	31400.0	64.8	5.05e-08	++
Residual	12	5820.0	485.0			
Total	16	131000.0				

	Coefficients	Standard Error	t-Statistics	p-Value		
Intercept	0					
Burst rate large	0.189	0.0522	3.61	0.0041	99.6	++
Solids loading GV	-329.0	357.0	-0.92	0.377	62.3	
FS Bubble size p80	1680.0	863.0	1.95	0.0772	92.3	+
Frother concentration	0.0695	0.266	0.261	0.799	20.1	

Table B.92.: Regression results relating the concentrate grade to the stability factors in the platinum rougher 3. (gravimetric solids loading used)

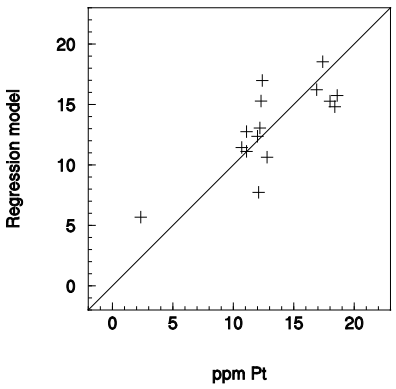

ppm Pt ppm	Burst rate l/m^2/s	Solids loading (GV) kg/m^2	FS bubble size (p^{80}) m	Frother concentration ppm
12.8	988.0	0.0132	0.0113	60
12.3	1060.0	0.0294	0.0122	60
18.4	902.0	0.0143	0.00956	60
11.1	976.0	0.02	0.0105	40
18	1100.0	0.0248	0.0117	40
11.1	1100.0	0.0143	0.0119	40
18.6	1330.0	0.0207	0.0131	20
17.4	1330.0	0.0226	0.0126	20
16.9	981.0	0.0203	0.0105	60
2.35	903.0	0.0139	0.0116	60
10.7	966.0	0.0182	0.0113	60
12	992.0	0.0152	0.0111	60
12.1	1140.0	0.0152	0.0124	20
12.2	1360.0	0.00991	0.0132	20
12.4	1390.0	0.0149	0.0131	20

Multiple R^2	0.687
Adjusted multiple R^2	0.561
R^2	0.965
Adjusted R^2	0.956
Standard Error	3.0
Observations	15

	df	SS	MS	F	Significance of F	
Regression	4	2770.0	693.0	76.9	5.76e-08	++
Residual	11	99.2	9.02			
Total	15	2870.0				

	Coefficients	Standard Error	t-Statistics	p-Value		
Intercept	0					
Burst rate large	0.0489	0.0133	3.68	0.00364	99.6	++
Solids loading GV	323.0	159.0	2.03	0.0671	93.3	+
FS Bubble size p80	-4510.0	1420.0	-3.18	0.0088	99.1	- -
Frother concentration	0.154	0.0629	2.45	0.0323	96.8	++

Appendix C.

SmartFroth machine vision analysis

The SmartFroth machine vision system was developed at the University of Cape Town. This section provides a detailed description of the video sampling procedures and image processing algorithms implemented in the system.

C.1. Capturing video for analysis

Of critical importance within the field of machine vision, is the capture of high quality video for analysis. Poorly selected equipment, conditions and improper setups can impact on the quality of video, and thus quality of data obtained from the image analysis.

This section outlines the equipment and procedures used to obtain the video footage used in this thesis.

C.1.1. Video cameras and recording of data

Two types of camera are typically used. The first type is a standard CCTV board camera with an appropriate lens (Figure C.1(a)), enclosed in an industrialised housing. These cameras have a PAL composite video output, and run off a 12V power supply. These cameras are best suited for long term installations.

The second type of camera used, especially for short data collection campaigns, are digital camcorders (Figure C.1(b)) that output PAL composite or IEEE 1394 firewire video signal.

(a) (b)

Figure C.1.: (a) A CCTV board camera with lens and (b) a typical camcorder used for capturing video sequences of flotation froths. (Source: Forbes (2007))

Under normal circumstances images are processed on-line. However, for the purposes of research and development, it may be necessary to store the video for off-line processing.

It is unfeasible to store uncompressed video to hard disk for a long duration, due to the data rates involved. A five minutes video segment of uncompressed footage utilises 2GB of storage at a resolution of 320×240, and at a frame rate of 25 fps.

Thus, the use of storage medium is necessary. The two storage mediums that are commonly used are Super VHS (S-VHS) and mini digital (miniDV) video tapes.

These formats have been chosen, as they maintain favourable a balance between data compression and data loss. Digital video from a camcorder is compressed using motion JPEG compression.

Newer video cameras which use mini DVD disks and hard disks for storage utilise MPEG-2 and MPEG-4 compression, which have a large impact on certain image processing algorithms, and thus, are avoided.

C.1.2. Camera and lighting setup

The camera needs to be mounted over an area that has no obstructions interfering with the field of view. Furthermore, it needs to be located away from cell corners, with the wider, horizontal, edge of the video frame parallel and close to the launder lip. The flow of the froth

needs to be perpendicular to the horizontal edge of the frame, and the flow of the froth in the field of view should be representative of that flowing into all of the launders around the cell. Figure C.2 shows examples of two such setups.

Figure C.2.: Two examples of digital video camera setups. (Source: Forbes (2007))

The froth surface needs to be illuminated, as illumination both improves the image quality and key algorithms within SmartFroth require a single highlight at the centre of each bubble. Typically, 200 or 500 Watt halogen lights are used, however light-emitting diode (LED) lighting solutions have also been used.

The key factors in evaluating the effectiveness of the lighting is whether the frame appears to have constant illumination, with no darker regions towards the image corners, and the presence of single highlights on each bubble. Figure C.3(a) shows an example of a poorly illuminated froth surface, where the lighting is uneven across the surface, and each bubble has more than one highlight. Figure C.3(b) shows an example of a froth surface where direct sunlight interferes with the lighting. This results in catastrophic image processing results, due to small dynamic range of the cameras, and the interference with the bubble highlights. Figure C.4 shows examples of good, well illuminated froths.

The camera zoom level is optimised to ensure that the largest bubbles in the frame occupy no more than 20% of the image area, while the smallest bubbles in the frame are still identifiable. Furthermore, occasionally, in the case of the digital video cameras, the focus level, which is controlled by the camera is too aggressive, resulting in video which oscillates in and out of focus. In these cases, manual focusing is preferred.

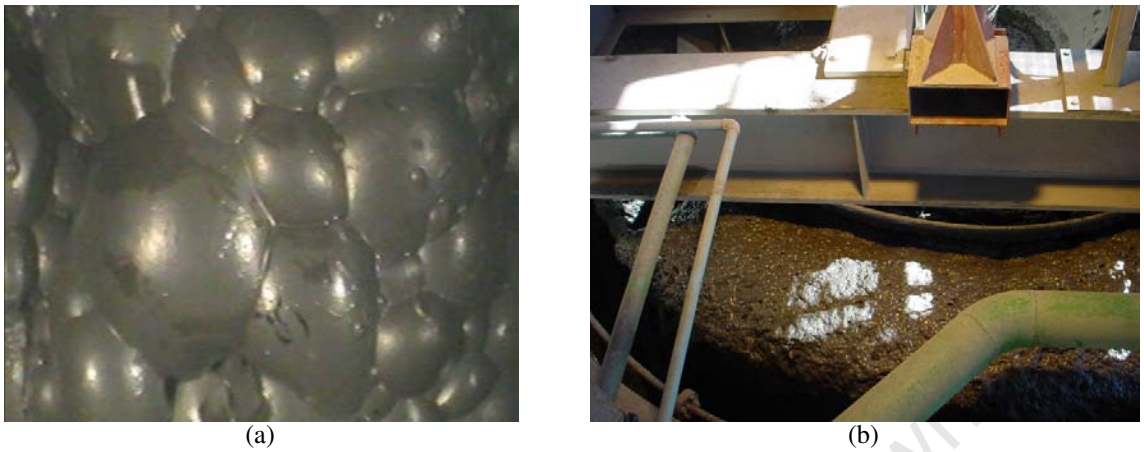

(a) (b)

Figure C.3.: Two examples of poorly illuminated froth surfaces, where (a) multiple highlights are visible on each bubble and (b) sunlight interference, which results in poor image quality and thus, poor image analysis results. (Source: Forbes (2007))

Figure C.4.: Two examples of well illuminated froth surfaces. Note the single highlights. (Source: Forbes (2007))

C.1.3. Calibration

Images are encoded into pixels. The size that the pixels represent depend upon the image resolution and the field of view. Thus, a calibration factor is required to convert output from image processing algorithms, such as velocity, which outputs results in pixel based units.

Typically, an object of known size, such as a tape measure or custom made checkerboard, as shown in figure C.5, is placed in front of a camera while video is being recorded or captured to some device. The resulting images are then analysed in an image processing package to determine the conversion factor between pixels and millimeters.

It is important to note that the horizontal and vertical resolution may not be constant, as some digital video cameras have a pixel aspect ratio of 1.067, requiring calibration in both the horizontal and vertical axes.

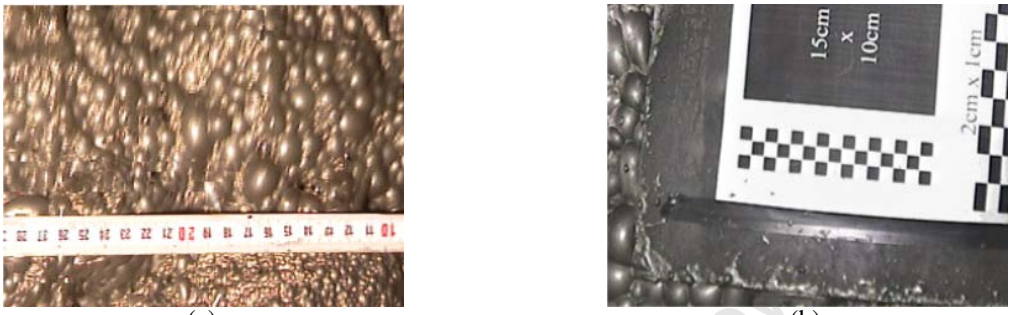

(a) (b)

Figure C.5.: Determining the calibration factor between pixels and millimeters using (a) a tape measure and (b) a checker board with known block sizes. (Source: Forbes (2007))

C.2. Machine vision analysis

SmartFroth, which has been developed at the University of Cape Town, has been developed primarily, as a research tool in machine vision for froth flotation. The image processing algorithms used within SmartFroth (de Jager *et al.*, 2004, 2005, Forbes and de Jager, 2006, Sweet *et al.*, 2000), are reviewed below.

The video samples used within this work were obtained using the methods and considerations outlined in appendix C.1.

C.2.1. Computing requirements

The SmartFroth software requires intensive processing capabilities. It runs under Microsoft Windows 2000, XP or Vista, and requires a 3GHz processor or better, with 1 GB RAM to run efficiently. In addition, a frame-grabber device to capture composite, or IEEE 1394 firewire video signal is required.

The SmartFroth software is designed with a batch processor system, where it samples a batch of images every so often. The number of images in the batch, and the sampling frequency is user configurable, and thus, the performance of SmartFroth can be tuned to the speed of

the computer hardware. Typically a set of measurements every two seconds is possible when processing an on-line stream of images. Alternatively, a data point can be obtained for every pair of frames when processing images off-line. However, in this case, the processing time can be 10-20 times the length of the video.

C.2.2. Watershed segmentation and measurement of bubble size

The froth surface is made up of curved lamella, which are assumed to represent the bubble size below the froth surface. One of the methods that the bubble size distribution of the froth surface can be determined is to measure the cross-sectional area that each bubble lamella takes up. This measurement can be performed using image segmentation, using watershed segmentation, as described by Wright (1997).

The performance of the watershed algorithm is good under conditions where the froth surface bubble size is relatively uniform, and of the same order of magnitude. It however, does not perform well over widely differing bubble size conditions, where large and small bubbles are present, resulting in either over-segmentation of large bubbles, or the under-segmentation of regions containing smaller bubbles (Forbes and de Jager, 2004).

Forbes and de Jager (2004) developed a method which uses the classification of segmented regions to improve the watershed performance under conditions where large and small bubbles exist within the same image.

Histogram equalisation

An image histogram illustrates the dynamic range and amount of contrast that an image has. A histogram refers to the number of occurrences of the each pixel value within the image, as shown in C.7. The image histogram can be used to normalise the dynamic range of an image, to more consistent images to subsequent algorithms across changes in lighting and camera exposure conditions.

Histogram equalisation, or contrast stretching, is performed to maximise the contrast in an image, which normalises the illumination of an image before further processing. This is performed by stretching the histogram linearly, such that a specified, percentage of pixels are at the white (255) and black (0) pixel values.

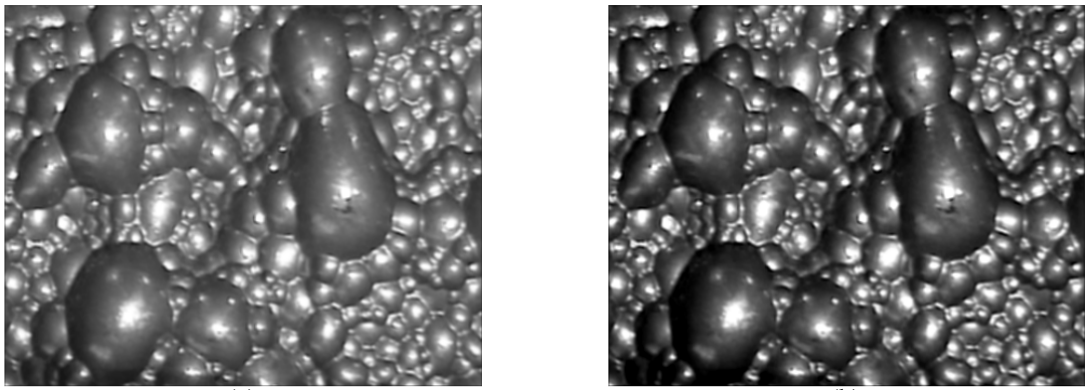

(a) (b)

Figure C.6.: (a) A froth surface image before histogram equalisation. (b) The same image after histogram equalisation. (Source: Forbes (2007))

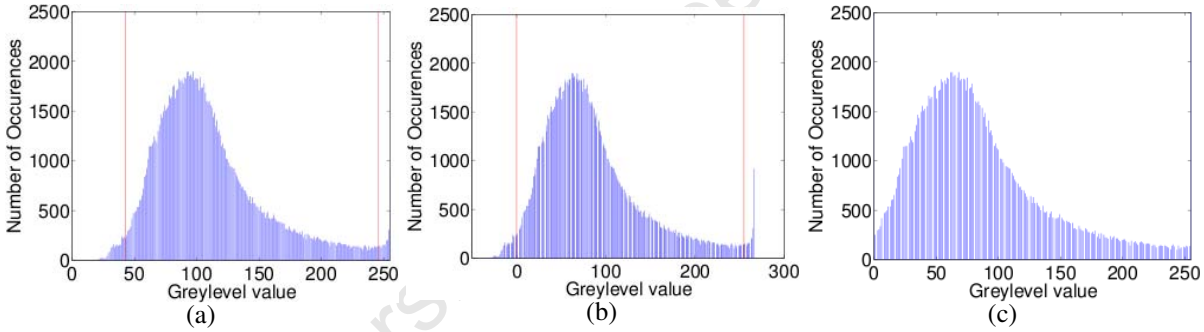

Figure C.7.: (a) Histogram corresponding to the image on the left in C.6. (b) Intermediate stage during histogram equalisation. (c) Final histogram after equalisation, corresponding to the image on the right in C.6. The red line indicates the points corresponding to the user-specified percentage of white and black pixels. (Source: Forbes (2007))

This result of this process is illustrated in Figure C.6, where the image histogram has been modified as shown in Figure C.7.

Low pass filtering

A low pass filter is performed on the input image to reduce the amount of noise present. An image with high frequency noise tends to cause the segmentation to over-segment, and is good for images with small bubbles present. However, under these conditions, larger bubbles tend to be over-segmented. Thus, the size of the low pass filter can be used to determine which bubbles are segmented.

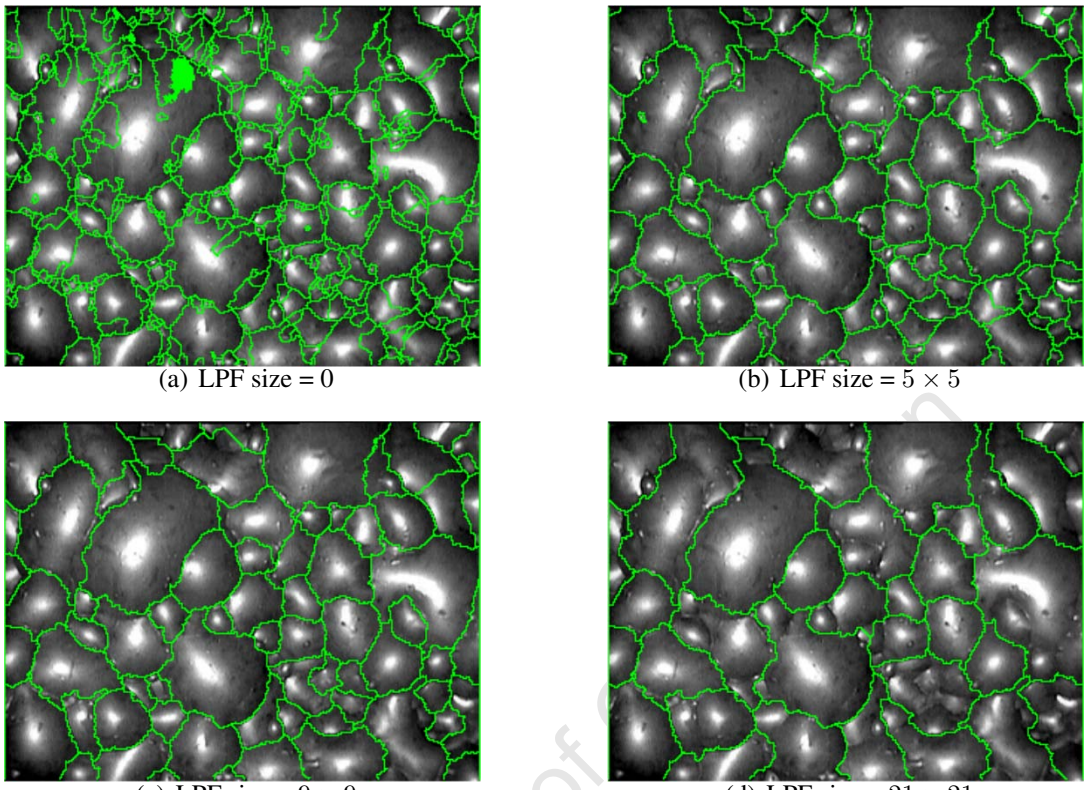

(a) LPF size = 0 (b) LPF size = 5×5

(c) LPF size = 9×9 (d) LPF size = 21×21

Figure C.8.: Outputs of the watershed algorithm for different levels of low pass filtering. (Source: Forbes (2007))

The low pass filter is implemented as a simple $n \times n$ box filter, with values of $\frac{1}{n^2}$ in each element.

Figure C.8 shows the effect of different low pass filter size on the final watershed segmentation output.

Watershed segmentation

The watershed algorithm finds local watersheds, or maximum values within an image. The watershed algorithm is commonly used for segmentation, where the maximum values within the image are identified as the boundaries to the segmented regions.

For a froth image, the identification of the local minima is required, as the minima are located at the bubble boundaries, which the darker regions within the image. Due to the nature of a froth surface, structured lighting can be used to form highlights, which define a local maxima

at the centre of each bubble. Thus, froth images need to be inverted to ensure that the highlights become minima points.

Vincent and Soille (1991) describe the algorithm using an analogy where the image is a topographical surface. If holes are pierced at the location of the local minima, as the surface is lowered into water, the water level within the topographical surface rises within each catchment basement (Figure C.10). When the water from two basins are about to merge, a 'dam wall' is built to prevent this (Figure C.11). On completion, separate regions are defined, bordered by 'dam walls'.

Markers are required to denote the minimal regions. While the application of various thresholding techniques may work, this is not reliable. Thus, Vincent describes a method for determining the *h*-dome image (D_h) of an image (I), which can then be used for marker extraction. The *h*-dome image is determined from

$$D_h(I) = I - \rho_I(I - h)$$

where $\rho_I(J)$ is the greyscale reconstruction (Vincent, 1993) of I from J, which is illustrated in Figure C.9.

A threshold is then applied to the *h*-dome image to generate a binary marker image M.

A homotopic transform is then used to combine the marker image by calculating a modified image I' using a greyscale reconstruction

$$I' = \rho^*_{min(I+1,(m+1)M)}((m+1)M) \tag{C.1}$$

where M is the binary marker image and m is the maximal value of pixels in I. The result is an image where the markers occur where the original image had minima.

The watershed algorithm can then be applied to the inverse of the image I', which will result in the final segmentation of bubbles.

The output from the watershed segmentation with various levels of low pass filtering applied can be seen in Figure C.8.

Texture classification of poorly segmented regions

Figure C.8 shows that when the size of a low pass filter is changed, the level of segmentation in an image is altered. At smaller low pass filter levels, smaller bubbles are segmented correctly,

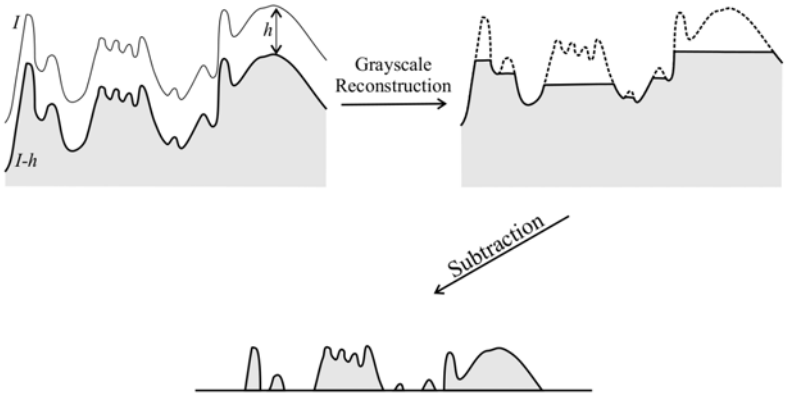

Figure C.9.: Determining the *h*-domes from image *I* (Source: Vincent (1993))

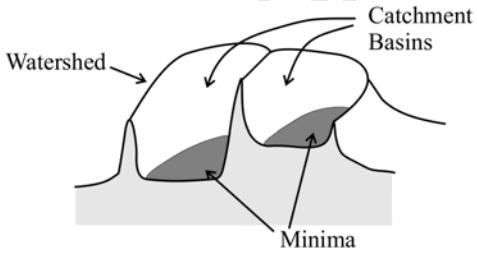

Figure C.10.: Minima, catchment basins and watersheds (Source: Vincent and Soille (1991))

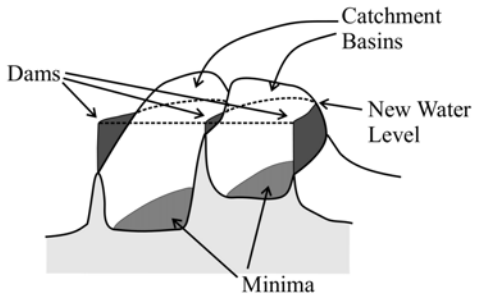

Figure C.11.: Building dams as the water level rises (Source: Vincent and Soille (1991))

at the expense of over-segmentation in larger bubbles, whereas the converse is true at larger low pass filter levels.

Forbes and de Jager (2004) describe an algorithm where large, correctly segmented bubbles are identified, by classification, from the segmentation performed on an input image that has had a large low pass filter applied. These identified bubbles are then masked out and a subsequent segmentation is performed on a modified input image obtained with smaller low pass filter value. The result is a segmentation that is more accurate. This algorithm is illustrated in Figure C.12.

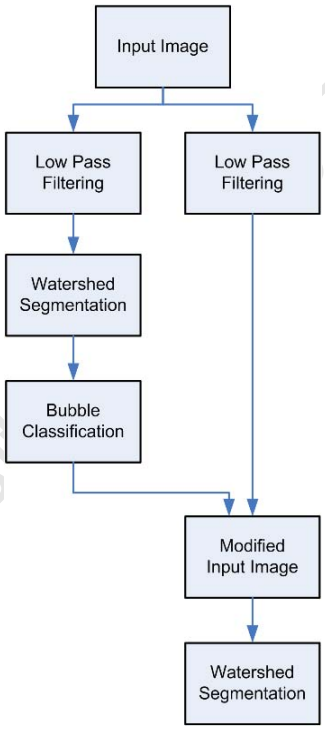

Figure C.12.: Flow sheet of the two-pass watershed algorithm, incorporating texture based classification. (Source: Forbes (2007))

Classification is performed to determine whether segmented regions are single bubbles, or clusters of small bubbles using a texture method involving greyscale co-occurrence matrix (GSCOM) for each segmented region. Greyscale co-occurrence matrices describe the probability of neighbouring pixels having certain grey level values (Gotlieb and Kreysig, 1990).

The greyscale co-occurrence matrix, $P_{i,j}$, is an $n \times n$ matrix which can be determined from

$$P_{i,j} = \sum_{a} \sum_{b} u(a,b) \tag{C.2}$$

where

$$u(a,b) = \begin{cases} 1 & \text{if } s(a,b) = t(a-d_1, b-d_2) \\ 0 & \text{otherwise} \end{cases}$$

and

$$s(a,b) = \begin{cases} 1 & \text{if } im(a,b) = i \\ 0 & \text{otherwise} \end{cases}$$

$$t(a,b) = \begin{cases} 1 & \text{if } im(a,b) = j \\ 0 & \text{otherwise} \end{cases}$$

and (d_1, d_2) is the user-specified distance vector and im is the input image with n grey levels.

The GSCOM for two segmented regions can be seen in Figure C.13. This figure shows that the larger the spread of values away from the diagonal within the GSCOM, the greater the contrast. As illustrated in Figure C.13 a segmented region which consists of a single bubble will have a GSCOM values closely neighbouring the diagonal through the matrix. A segmented region with multiple bubbles have a GSCOM where values are further spread out from the matrix diagonal.

Greyscale co-occurrence matrices can be used to determine textural features, of which, fourteen have been proposed by Haralick (1979). The particular feature used for the classification of multiple bubbles is the contrast measure, which can be given by:

$$\text{Contrast} = \sum_{i,j} (i-j)^2 P_{i,j} \tag{C.3}$$

Using this measure, the contrast value will be higher in a GSCOM with values spread away from the diagonal. Thus, a threshold contrast value can be used to separate out regions which are single bubbles from regions which contain multiple bubbles.

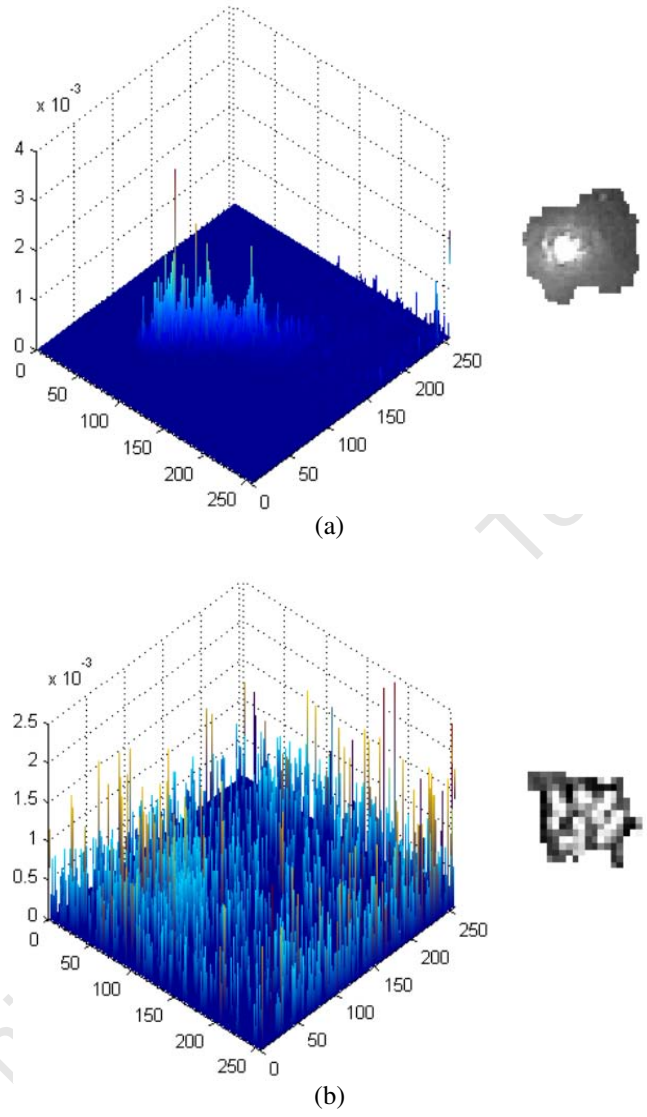

Figure C.13.: (a) Typical surface plot of a GSCOM for a single bubble and the image from which it was generated. (b) Typical surface plot of a GSCOM for a collection of tiny bubbles and the image from which it was generated. (Source: Forbes (2007))

Once both of the watersheds are complete, the resulting image can be combined with the larger bubble segmentation to produce a more better quality segmentation than can be obtained from a single pass.

This algorithm can be extended to include more classification stages by classifying the segmentation results from watersheds which have been determined from input images applied with decreasing low pass filters.

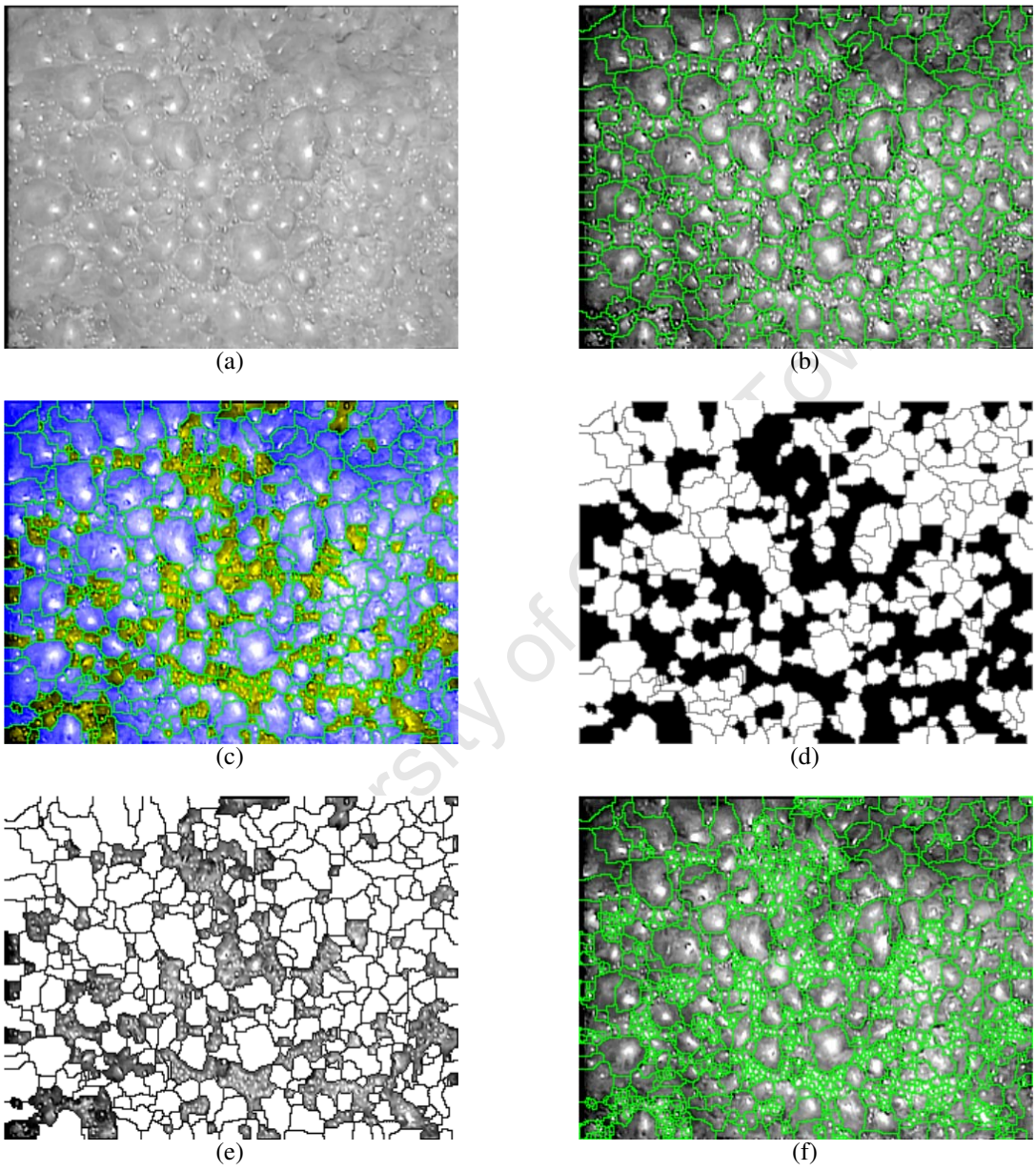

Figure C.14.: (a) Input image for segmentation. (b) First pass of watershed algorithm resulting in over-segmentation. (c) Results of classification according to GSCOM contrast. Blue indicates single bubbles and yellow, collections of tiny bubbles. (d) Classification mask generated from (c). (e) Input image to second watershed stage after it has been low pass filtered and had the mask applied to it. (f) Final watershed segmentation. (Source: Forbes (2007))

Bubble size

The area of the segmented regions, which consist of isolated bubbles can be determined by counting the pixels within each region. The bubble size distribution is calculated by sorting the bubbles in a frame by bubble area. A cumulative area distribution is determined from the sorted bubble areas, which are binned into a histogram at intervals of 10% of the total area. The bubble area at the interval boundaries are output as the bubble size distribution. Resulting values are represented in $pixels^2$ or mm^2 if an appropriate conversion factor has been applied.

The resulting values may not be the actual bubble size distribution, but is more correctly the surface film size distribution. Wang and Neethling (2007) have shown that as the froth surface has a more poly-disperse bubble size distribution, the surface film size distribution approaches the actual bubble size distribution.

Once segmented regions have been isolated estimates for other measurements are easily possible such as the Sauter mean bubble diameter, bubble film circularity or ellipticity.

C.2.3. Measurement of froth stability

Froth stability is a difficult concept to define and parameter to measure. Little consensus between stability measurements has been found in the literature (Aveyard *et al.*, 1994, Bikerman, 1953, Hatfield, 2006, Ventura-Medina *et al.*, 2003, Woodburn *et al.*, 1994). Many stability measurements are measurable parameters[1], and others relate to immeasurable, but modelled froth structure.

On the froth surface, an aspect of froth stability is visually apparent. This aspect is characterised by the extent and rate of bursting of the froth surface films.

Hatfield (2006) describes a measurement of froth stability based upon the examination of consecutive frames (Figure C.15) after image registration has taken place. Image registration refers to the alignment correction of two images relative to each other.

The image registration method used is a well known technique, referred to as cross correlation. Cross correlation is performed by taking a Fourier transform of both images, as shown in Figure C.17. Typically, a sub-region of 256×128 pixels is analysed[2], as shown in Figure C.16. The Fourier transform of the first image is multiplied by the complex conjugate of the Fourier

[1] The range of measurable parameters developed span two and three-phase systems, laboratory measurements and on-site measurements.

[2] This is the largest area that is a power of two that can be selected from a 320×240 pixel image.

transform of the second image. The result is then transformed into the spacial domain, and normalised by the average energy of the two images, as shown in Figure C.18. The result of this operation is a matrix which has a peak, the cross correlation peak, at the spacial offset between the two images.

Cross correlation peak

The cross correlation peak is a measure of the similarity between the two images. As such, this measurement can be used to determine the amount of change that has occurred between consecutive images. Generally, two types of changes occur in consecutive froth images; deformation, which is caused by bubbles moving at different rates to each other, which may be a function of froth mobility, and surface film or lamella bursting. As surface film bursting causes a large change in correlation peak value, the correlation peak can be used to infer froth stability.

Froth surface burst fraction

Once the images are registered, the second frame is subtracted from the first. The absolute mean difference between the two frames can then be determined and forms another measure of froth stability. Alternatively, a user defined threshold can be applied to the resulting difference map between the two images to determine the regions of greatest change, which can be calculated as a fraction of the total image. Figure C.19 shows the result of this algorithm, where the red areas represent the regions of greatest change in the consecutive images.

C.2.4. Measurement of froth surface velocity

Froth surface velocity is calculated using three methods. The performance of each method is acceptable for a certain range of froth speeds, however block matching performs well consistently over the widest range of froth velocities. The watershed blob tracking method performs well with slow moving froths, particularly where froth is moving at speeds that result in subpixel motion per frame. The stability method performs well with very fast moving froths, and is more robust in regimes where slight motion blur occurs.

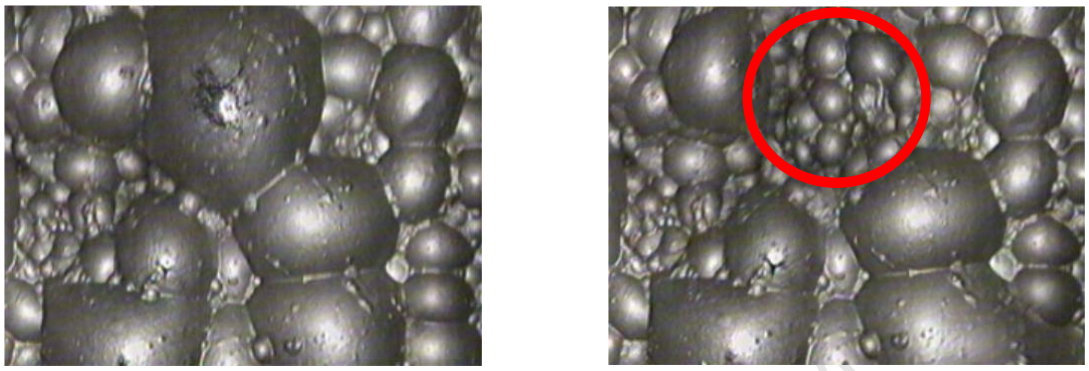

Figure C.15.: Two consecutive frames of video footage. Note the bubble that has burst. (Source: Forbes (2007))

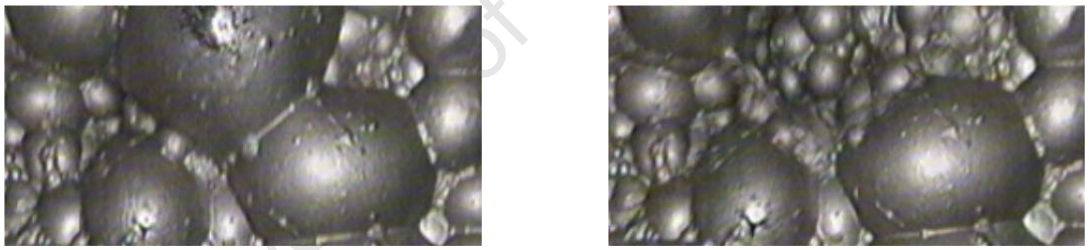

Figure C.16.: Cropped areas of size 256×128 on which the Fourier transform can be easily calculated. (Source: Forbes (2007))

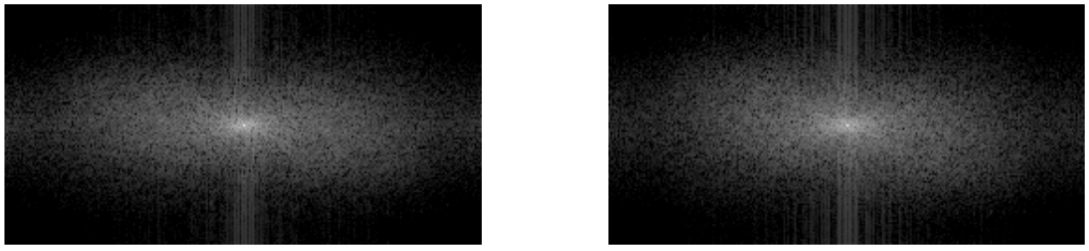

Figure C.17.: Fourier transforms of corresponding images in Figure C.16. (Source: Forbes (2007))

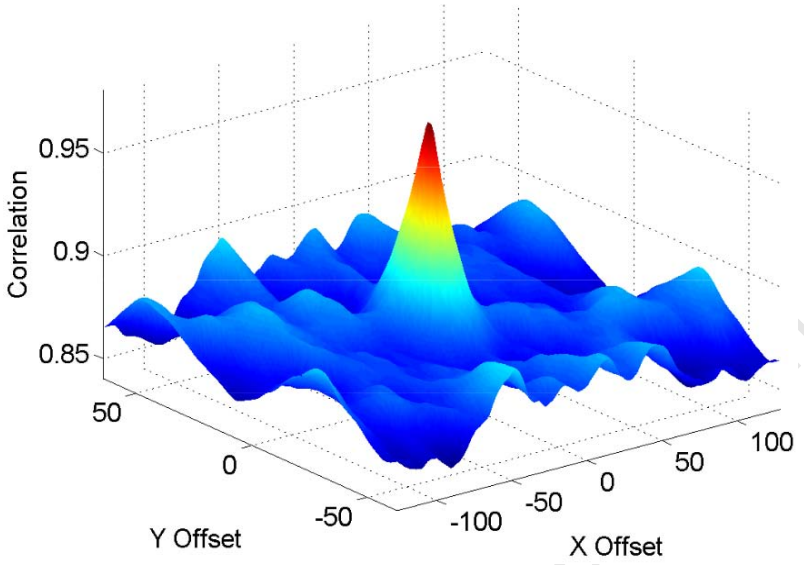

Figure C.18.: Space domain correlation peak. (Source: Forbes (2007))

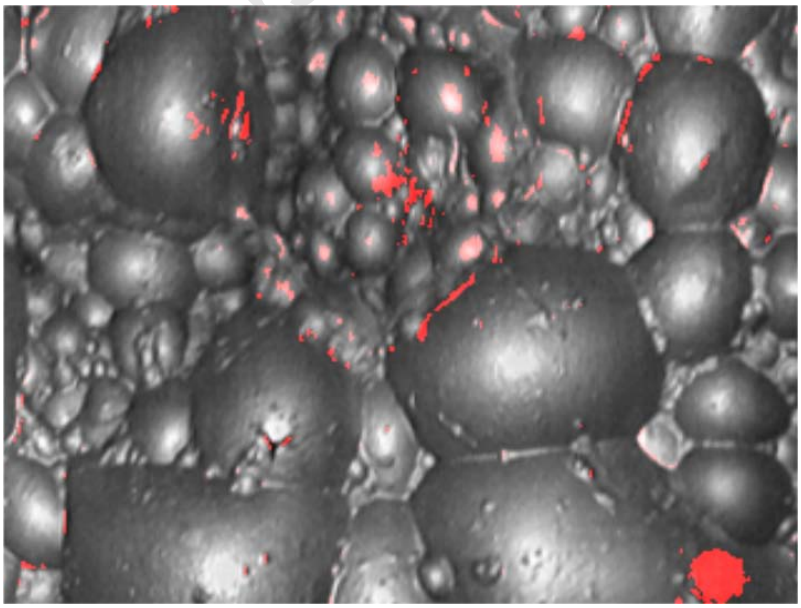

Figure C.19.: Original image with red areas indicating the areas of change. (Source: Forbes (2007))

Typically froth velocity is calculated by comparing pairs of frames or user specified batches ranging from two to five frames in length. Where multiple measurements are obtained per frame pair, the mean velocity is determined.

Block matching

Block matching is performed where the first frame within a frame pair is subdivided into a user specified number of blocks. Cross correlation, similar to that described in section C.2.3, is used to search the best match within a sub-region of the consecutive frame for each block from the first frame. This process results in a motion vector field, as shown in Figure C.20, which is then used to calculate the final mean velocity for the frame pair.

Bubble tracking

The watershed segmentation algorithm segments individual bubbles within each frame. The bubble tracking algorithm then uses this information to track the movement of each bubble through the frames.

The bubble centres are tracked over multiple frames using the bubble size to ensure that correct bubbles are matched. Only bubbles that are matched through all of the frames are used in the final velocity calculation. This process produces a motion vector field, as shown in Figure C.21, which is then used to calculate the final mean velocity measure.

Stability

As mentioned in section C.2.3, the froth stability measurement requires an image registration step. This step is performed using a single block match within the image, and results in a single coarse velocity measure for each frame pair.

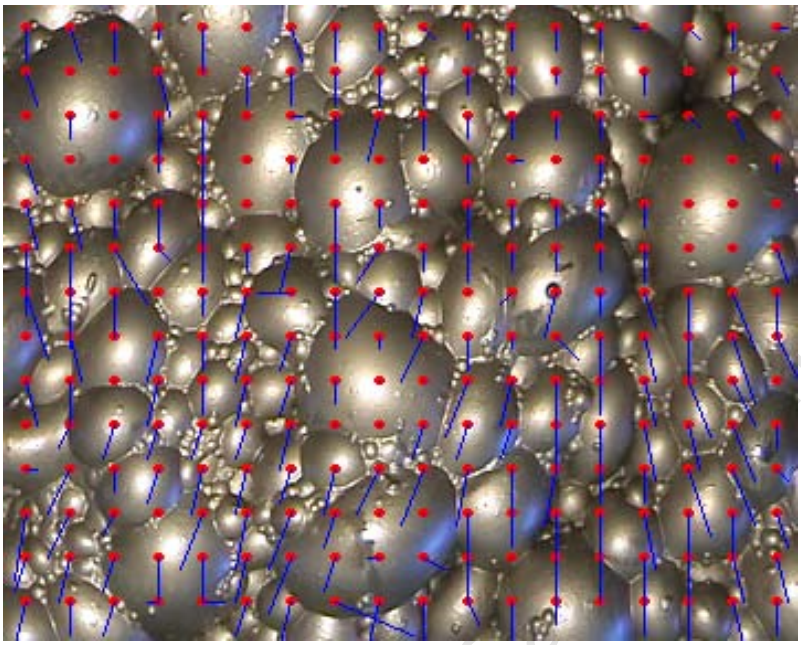

Figure C.20.: Resulting motion vector field from the block matching velocity algorithm.

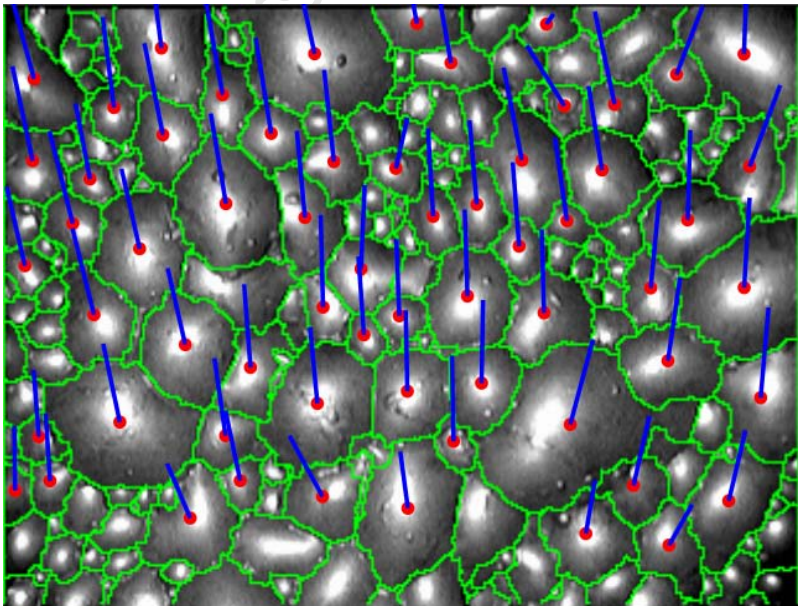

Figure C.21.: Resulting motion vector field from the bubble matching velocity algorithm. (Source: Forbes (2007))